



UiT The Arctic University of Norway

Department of Arctic and Marine Biology

Tundra vegetation ecology from the sky

Aerial images and photogrammetry as tools to monitor landscape change

Isabell Eischeid

A dissertation for the degree of Philosophiae Doctor - March 2022



Tundra vegetation ecology from the sky

Aerial images and photogrammetry as tools to
monitor landscape change

Isabell Eischeid



A dissertation for the degree of Philosophiae Doctor (PhD)
at UiT The Arctic University of Norway

March 2022

Cover:
Drone image, Svalbard, I.Eischeid, 2019.

Acknowledgements

This PhD project was made possible by a grant from Aarhus University (and Jesper Madsen who decided to give it to me) as well as Tromsø Forskningsstiftelse and funding from SIOS. The Norwegian Polar Institute financed and provided logistics for field work and office space. The Arctic University of Norway (UiT) provided a workspace, an administrative staff that made me feel very welcome and financed two months of “Corona extension”.

I would like to thank my six! supervisors! Eeva, Virve, Åshild, Jesper, Nigel and Rolf. It truly was a privilege to be surrounded by such a great group of resourceful and nice people that always wanted the best for me. You have successfully falsified the quantity vs. quality hypothesis. There was always an open office (or Teams channel) and never any doubt that this thesis can be finished even when a virus changed most of our plans. Special thanks to Virve for being so positive when I sent her an email many years ago that pretty much only just said, “I know some people you have been working with, I like GIS and soils and you should employ me.” Already then, you said that you had a feeling that I would get “stuck” in Tromsø. I guess you were right, thanks for giving me that opportunity.

None of this work would have been possible with all the technical support I got. Jakob, thanks for quite literally taking me under your wings! Francesco, thanks for inviting me to Italy and introducing me to the world of photogrammetry and random forests. Anne and Harald from the mapping section at NP for helping with everything that had to do with the GPSes and David for tirelessly processing drone and satellite images for me. I also want to express my gratitude to Rolf Andersen at UiT who went out of his way many times to help me find the right processing servers and workflows.

It is wonderful to be surrounded by people at work that give you the feeling that you belong. I am very lucky to be part of the COAT family and the Biodiversity section at NP. Here is a collective thank you to all of you, for inspiring conversations and coffee break chats. Thank you to the NP Longyearbyen staff, especially Sofia and Stein Tore for welcoming me with open arms, it almost felt like an all-inclusive holiday.

The NorPop Fun team at UiT deserves a special mention here. It’s wonderful to have you guys around. Little did I know that the last months of my PhD would become some of the nicest. Julia, thank you for stumbling into our office last year and being so much more than just a rubber duck. And Yin, thanks for being my comma police and our entertaining breaks.

To all my Tromsø friends, thank you for making life outside of work so much more interesting! Ingrid, thank you for your positive energy, emotional and scientific support and the many fun hours in the field and our wonderful other adventures on land and water! Linda, thanks for 7 years of friendship, the fantastic field season, that you keep on visiting me and sharing my sense of humor. Maeve, I will forever be grateful for sharing this PhD journey with you, the ski tours, the early morning swims and multivariate stats discussion in a hot tub overlooking Kvaløya. The last years wouldn’t have been the same without you.

Last but not least, I would like to thank my family. My parents for being such nice and interesting people, sharing the fascination for Biology (it’s all your fault!) and accepting that I found a home in the North. Torgeir for sticking around and always encouraging me, building a home for us, joining for fieldwork, being the best home office buddy I could ask for and showing so much understanding throughout this PhD journey. Takk!

Supervisors

Eeva Marjatta Soininen // Department for Arctic and Marine Biology at UiT The Arctic University of Norway in Tromsø, Norway

Rolf Anker Ims // Department for Arctic and Marine Biology at UiT The Arctic University of Norway in Tromsø, Norway

Jesper Madsen // Department for Ecoscience at Aarhus University in Rønde, Denmark

Åshild Ønvik Pedersen // Norwegian Polar Institute in Tromsø, Norway

Virve Tuulia Ravolainen // Norwegian Polar Institute in Tromsø, Norway

Nigel Gilles Yoccoz // Department for Arctic and Marine Biology at UiT The Arctic University of Norway in Tromsø, Norway

Author contributions

	Paper I	Paper II	Paper III	Paper IV
Concept and idea	VR, ES, IS, IE, MF, RW, ÅP	IE, RI, JM, ÅP, ES, VR	IE, JM, RI, ÅP, ES, VR	FP
Study design and methods	VR, ES, IS, IE, MF, RW, ÅP	IE, JA, FP, VR	IE, JM, ÅP, ES, NY, VR	HB, NB, IE, AH, SH, MH, AK, TV, FP
Data gathering and interpretation	-	IE, FP, VR	IE, JM, BN, KS, VR	HB, NB, IE, AH, SH, MH, AK, TV, FP
Manuscript preparation	VR, ES, IS, IE, MF, RW, ÅP	IE, ES, JA, RI, JM, ÅP, NY, VR	IE, JM, RI, BN, ÅP, KS, ES, NY, VR	HB, NB, IE, AH, SH, MH, AK, TV, FP

Abbreviations for authors

Alexandra Hamer (AH)

Andreas Kollert (AK)

Bart. A. Nolet (BN)

Eeva M. Soininen (ES)

Francesco Pirotti (FP)

Heidemarie Bernsteiner (HB)

Inga Svala Jónsdóttir (IS)

Isabell Eischeid (IE)

Jakob J. Assmann (JA)

Kees H.T. Schreven (KS)

Mads Forchhammer (MF)

Marius Huber (MH)

Natalie Brožová (NB)

Nigel G. Yoccoz (NY)

René van der Wal (RW)

Rolf A. Ims (RI)

Stefan Haselberger (SH)

Tom M. Vandyk (TV)

Virve T. Ravolainen (VR)

Åshild Ø. Pedersen (ÅP)

List of Papers

Paper I: Ravolainen, V., Soininen, E. M., Jónsdóttir, I. S., Eischeid, I., Forchhammer, M., van der Wal, R., & Pedersen, Å. Ø. (2020). High Arctic ecosystem states: Conceptual models of vegetation change to guide long-term monitoring and research. *Ambio*, 49(3), 666-677. doi:10.1007/s13280-019-01310-x

Paper II: Eischeid I., Soininen, E. M., Assmann, J.J., Ims, R.A., Madsen, J., Pedersen, Å.Ø., Pirotti, F., Yoccoz, N.G. & Ravolainen, V.T. (2021). Disturbance Mapping in Arctic Tundra Improved by a Planning Workflow for Drone Studies: Advancing Tools for Future Ecosystem Monitoring. *Remote Sensing*, 13(21), 4466. doi:10.3390/rs13214466

Paper III: Eischeid I., Soininen, E. M., Keeves, K., Madsen, J., Nolet, B., Pedersen, Å.Ø., Yoccoz, N.G. & Ravolainen, V.T. Snowmelt progression drives spring habitat selection and vegetation disturbance by an Arctic avian herbivore at multiple scales. (advanced manuscript)

Paper IV: Bernsteiner, H., Brožová, N., Eischeid, I., Hamer, A., Haselberger, S., Huber, M., Kollert, A., Vandyk, T.M. & Pirotti, F. (2020). Machine learning for classification of an eroding scarp surface using terrestrial photogrammetry with NIR and RGB imagery. *ISPRS Ann. Photogramm. Remote Sens. Spatial Inf. Sci.*, V-3-2020, 431–437. doi:10.5194/isprs-annals-V-3-2020-431-2020 (the first eight authors contributed equally)

Table of Contents

List of Abbreviations.....	1
1 Summary	2
2 Introduction	4
2.1 Background information.....	4
2.2 Thesis objectives.....	7
3 Methods.....	10
3.1 Study system.....	10
3.2 Data collection.....	15
3.3 Data processing and analysis.....	22
4 Key findings	25
4.1 Paper I - High Arctic ecosystem states: Conceptual models of vegetation change to guide long-term monitoring and research	25
4.2 Paper II - Disturbance Mapping in Arctic Tundra Improved by a Planning Workflow for Drone Studies: Advancing Tools for Future Ecosystem Monitoring.....	26
4.3 Paper III - Snowmelt progression drives spring habitat selection and vegetation disturbance by an Arctic avian herbivore at multiple scales.....	27
4.4 Paper IV - Machine learning for classification of an eroding scarp surface using terrestrial photogrammetry with NIR and RGB imagery.....	28
5 Results and discussion.....	29
5.1 Which vegetation states and drivers are likely important for shaping Svalbard’s moss tundra habitats in the future?.....	29
5.2 How do the presented conceptual models define the monitoring goals for moss tundra ecosystems in Svalbard and how can this thesis contribute?	31
5.3 Can we detect the habitat types described for Svalbard’s tundra ecosystem using drone images?.....	31
5.4 Can we use drone images to detect abiotic and biotic habitat disturbances?	32
5.5 Can we quantify the role multiple drivers play in steering goose grubbing distribution and intensity?.....	34
5.6 How do random forests classifiers perform in tundra environments?.....	36
5.7 What have I learned from using photogrammetry and drones in tundra environments in the context of adaptive monitoring?.....	37
5.8 Limitations and outlook.....	39
6 Conclusion.....	43
7 References	44

List of Abbreviations

COAT	Climate-ecological Observatory for Arctic Tundra
DSM	Digital surface model
GCP	Ground control point
GEE	Google earth engine
GLCM	Gray level co-occurrence matrix
GPS	Global positioning system
GSD	Ground sampling distance (“pixel size”)
NDVI	Normalized difference vegetation index
NIR	Near-infrared
OOB	Out-of-bag error
PPK	Post processed kinematic
RF	Random forest
RGB	Red-green-blue
RPAS	Remotely piloted aircraft system
SfM	Structure from motion
STM	State and transition model
UAS	Unmanned aerial system
UAV	Unmanned aerial vehicle

1 Summary

Arctic tundra ecosystems are vulnerable to the direct and indirect effects of climate change. Long-term temperature increases, higher frequencies of extreme weather events and changes in food web structures will all affect the state of Arctic tundra ecosystems at different temporal and spatial scales. As ecologists, we are asked to understand these biotic and abiotic interactions and find methods to measure them. This thesis applies new technology and methods within the principles of adaptive monitoring to achieve four overarching goals: 1) Design a conceptual model for Svalbard's moss tundra ecosystem and define the vegetation monitoring needs of high Arctic tundra systems in the context of climate change and herbivore management. 2) Design new monitoring approaches that help quantify habitat types and drivers of future vegetation state changes. 3) Evaluate the practical implications of using drones, drone imagery, photogrammetry, and image classification-based approaches for monitoring and 4) Evaluate how the findings of the thesis can contribute to future adaptive monitoring of Svalbard's moss tundra and provide suggestions for future drone and photogrammetry-based studies.

We proposed that Svalbard's moss tundra habitat currently has three stable states, a graminoid, moss and bare patch state. Transitions between these states can be caused through slow long-term changes e.g., temperature increases and grazing pressure, or through short-term disturbance events such as local erosion, freezing, trampling or herbivory. Remote sensing approaches using photogrammetry as well as drone and satellite images were tested to quantify state variables useful for long-term monitoring of Arctic tundra ecosystems: extent of vegetation types and bare ground, biotic and abiotic disturbances (winter damage and pink-footed goose grubbing) and snowmelt progression as a driver for pink-footed goose abundances within the landscape.

Drone images and random forest classifiers (RF) were reliably able to distinguish up to 15 different tundra ground cover classes, including those that represent disturbances such as winter damage from extreme weather events, pink-footed goose grubbing and bare ground. Disturbance classes were generally overestimated; additional more precise ground truthing point collection can likely help to produce locally precise RF classifiers in the future. Normalized difference vegetation index (NDVI) values for disturbed areas (pink-footed goose grubbing or winter damage) were lower than undisturbed areas and higher than those covered in bare ground or gravel. Time-series analyses of drone images are therefore likely suitable tools to detect newly emerging disturbances in the future.

During spring, snowmelt progression was mapped using drone and satellite images to enable analysis of pink-footed goose habitat selection, habitat use and vegetation disturbance likelihood via grubbing. It revealed that both habitat use and grubbing likelihood were driven by vegetation class and snowmelt date. Moss tundra habitats that were free of snow during the first two weeks of the pre-breeding period had highest grubbing likelihoods. The study led to an estimation of approximately 23% of moss tundra and 10% of dwarf-shrub heath habitats within a pre-breeding site to be affected by pink-footed goose grubbing in a single season. This study was conducted in a late snowmelt year and one season is not enough to generalize the

findings. However, it demonstrated successful mapping of snowmelt progression using drones and satellite images. Future work should focus on studying interannual variation of snowmelt patterns and how this affects habitat use and disturbance by pink-footed geese.

Drone-based remote sensing, photogrammetry and RF classifiers were useful tools in detecting nuanced differences in ground cover types. Successful ground cover type classifications were mostly dependent on optical variables, especially near-infrared, but terrain-related variables generally improved the classifiers. Transfer of RF classifiers between study sites was not possible but could be improved through simplifications of the classifier or other machine learning approaches. Drones that are used in Arctic conditions should be tolerant to strong winds and cold temperatures. Precise geometric and spectral calibrations are especially important when using drone images in the context of long-term monitoring. Satellite-based remote sensing studies generally lack enough ground truthing data from Arctic regions and drone images collected in different Arctic regions will therefore be especially valuable in closing this gap.

The ground cover vegetation classifications conducted through this thesis can provide baseline data to detect future state changes, for example an increase in bare ground or the expansion of species such as *Equisetum* spp. or *Carex subspathacea*. This thesis has shown that it is possible to map the extent of pink-footed goose grubbing by means of drones. Studying the long-term consequences of grubbing on tundra ecosystems will require a closer integration of drone images and detailed field surveys that span over multiple seasons. The snow cover maps that were generated from drone images could be analyzed in more detail and provide valuable information for optimizing satellite-based snow cover classifications. Combining drone NDVI maps and already existing plot-based biomass estimates could be used to upscale these to larger spatial extents.

This thesis has shown examples of several stages of adaptive monitoring. Defining conceptual models of Arctic moss tundra has helped to develop hypotheses and specifying targets for monitoring goals and the consecutive studies presented in this thesis. It has shown that drones can be useful tools to detect and quantify the extent of vegetation classes as well as abiotic and biotic disturbances. This thesis presents a novel approach of studying the effect of snowmelt timing on the extent of pink-footed goose vegetation disturbance by combining field and remote sensed data from drones and satellites and helped to elevate studies of causal ecological relationships into a spatial context. This thesis shows that approaches of studying biotic and abiotic interactions in tundra ecosystems with help of drone and satellite images can be successful and expands our toolset to study a rapidly changing Arctic.

2 Introduction

2.1 Background information

2.1.1 Tundra ecosystem and climate change

The Arctic tundra is the northernmost terrestrial biome. Here, cold temperatures prevent tree growth and the ground is frozen for most parts of the year. Herbivores play an important role in shaping vegetation productivity and plant community compositions of Arctic tundra ecosystems (Bråthen et al. 2007, Ims et al. 2013). Amplification processes cause climate change to proceed exceptionally fast in the Arctic region (Arrhenius 1896, Serreze and Barry 2011). Changes in sea ice cover significantly alter the thermal balance of the Arctic (Holland and Bitz 2003) and temperatures have increased in all seasons (IPPC 2019). Thawing permafrost releases large quantities of greenhouse gases, which further accelerates the rate of climate change and Arctic warming (Schuur et al. 2015). The tundra ecosystem is not only experiencing progressive warming but is also expected to face an increasing frequency and intensity of extreme weather events (Maxwell et al. 2019). Whilst warm summer temperatures favor increases in plant biomass, especially fast-growing forbs, graminoids or shrubs (Elmendorf et al. 2012, Myers-Smith et al. 2015), short-term extreme events such as fires, icing events and insect outbreaks can reduce biomass or create spaces of bare ground (e.g. Jepsen et al. 2013, Hu et al. 2015, Milner et al. 2016). Annual Arctic precipitation is predicted to increase with up to 60% throughout the 21st century (Bintanja 2018). Because precipitation can be in the form of either rain or snow, even small temperature differences can significantly change the duration and physical properties of the snowpack (Bintanja 2018, Peeters et al. 2019). The extent, depth and physical properties of snow plays an important role in shaping tundra ecosystems (Bokhorst et al. 2016). Snow can provide habitats, e.g., for small mammals (Reid et al. 2012, Domine et al. 2018) and it can restrict habitats, e.g., for grazing muskoxen or reindeer (Klein et al. 1993, Hansen and Aanes 2012). Climate change likely increases the complexity of future biotic and abiotic interactions as well as long term and short responses of tundra ecosystems (Hastings et al. 2007, Ims et al. 2013, Post et al. 2019). Studying these interactions requires robust conceptual models and methods that define and capture key ecosystem processes (Bentley and Anandhi 2020).

2.1.2 Adaptive monitoring

Adaptive monitoring aims to improve the quality of long-term ecological monitoring programs by the guidance of tractable scientific questions and hypotheses (Lindenmayer and Likens 2009, 2010). Good adaptive monitoring, as defined by (Lindenmayer and Likens 2010), is based on three pillars: well defined questions, rigorous statistical design, and a management-driven need to know more about the ecosystem. Successful long-term monitoring programs need to be able to include new scientific questions and methods to stay relevant and adapt to changing ecosystems and altered management needs over time (Burt 1994, Overton and Stehman 1996, Porzig et al. 2011). Conceptual models are therefore key to most adaptive monitoring programs, as they outline the hypothesized causal relationships between the components of the study system (Lindenmayer and Likens 2009, 2010, Ims et al. 2013). Thus, they provide the base for

scientific questions, hypotheses for measurable drivers of change and focal points for discussion. (Lindenmayer and Likens 2009) provided a workflow framed as an iterative loop that builds on scientific questions or conceptual models and a study design that is able to answer these questions or quantify the components of the conceptual model. After data collection, analysis and interpretation, the chosen methods should enter a re-evaluation phase. In this phase, the questions and models can be updated based on the new knowledge gained, or more appropriate analytical methods can be suggested. At this stage, new technology can also be included. Examples of successful adaptive monitoring programs can be found across the world in both terrestrial and aquatic environments (Lindenmayer 2012, Ims et al. 2013, Fölster et al. 2014, Perryman et al. 2018, Hubbard Brook 2022). The work of this thesis was conducted within the Climate-ecological Observatory for Arctic Tundra (COAT) long-term adaptive monitoring program (Ims et al. 2013).

2.1.3 State and transition models

One method to describe the complexity of an ecosystem is through state and transition models (STMs). The concept of STMs was first defined by (Westoby et al. 1989) and born out of the need to describe rangeland plant communities that were not developing towards a final state of equilibrium or climax, but instead, shifting between multi-directional stable states. Typical drivers of ecosystem state changes can be climatic variations, alterations in grazing pressure or major stochastic events (Westoby et al. 1989, Scheffer et al. 2001, Creutzburg et al. 2015, Oliva et al. 2016). State and transition model theory has been tested in many ecosystems. Several studies have pointed out, that disturbances can be so severe, or the system little resistant, that new stable states are not reversible (Jones 1992), or only partly reversible (Asefa et al. 2003), for example through changes in soil properties. Or, on the contrary, that alternate states can vary in function and diversity but are transient and do not reach any stable equilibrium (Fukami and Nakajima 2011). In tundra ecosystems, state changes have been linked to several biotic and abiotic processes. Shrub expansion that occurs in some Arctic regions can be attributed to a feedback loop of warmer summer temperatures and thicker, more insulating snow-cover (trapped by the shrubs) and thus warmer soil temperatures during winter (Sturm et al. 2005, Myers-Smith et al. 2015). In contrast, on Hudson Bay, an increased population of lesser snow geese (*Chen caerulescens caerulescens*) has pushed a wetland into a new, overgrazed, stable state with hyper-saline soils (Jefferies et al. 2004b). In Iceland STMs have been used to identify restoration goals for regions with long-term overgrazing by sheep (Barrio et al. 2018). In high Arctic Svalbard, Wal (2006) argued that reindeer densities can move tundra vegetation into three alternate stable states that are either lichen-, moss- or graminoid-dominated. Using STMs as a tool in management as opposed to purely as a conceptual model requires a thorough understanding of the system and descriptions of e.g., threshold values (Bestelmeyer 2006, Twidwell et al. 2013), quantifiable state variables (Suding and Hobbs 2009) and timeframe estimates for state transitions (Sato and Lindenmayer 2021).

2.1.4 Drones in ecology

Lightweight drones are an increasingly popular tool in ecological research (Tang and Shao 2015). Praised as a new tool that will revolutionize ecological research dating back in 2012/2013 (Koh and Wich 2012, Anderson and Gaston 2013), drones have since been used in ecological studies across all continents and many landscape types, e.g., to map European forests (Torresan et al. 2017), to detect landscape types in Antarctica (Miranda et al. 2020), or chimpanzee nests in Tanzania (Bonnin et al. 2018). Drones come in all forms and shapes (Vergouw et al. 2016) and commonly also are referred to as UAVs (Unmanned Aerial Vehicles), or UAS (Unmanned Aerial Systems), or RPAS (Remotely Piloted Aircraft Systems). Here, I will use the word drone because it is short and gender-neutral (Joyce et al. 2021). Within the field of ecology, the most popular type of drones are multirotor drones, that can often be bought off the shelf, and small fixed wing planes that are specialized for mapping flights (Sun et al. 2021). Drones can be equipped with a range of sensors, such as “normal” RGB (red, green, blue) cameras, multi- and hyperspectral cameras, thermal sensors, LiDAR and trackers that can follow individual animals, (e.g. Liu et al. 2017, Maes et al. 2017, Bagaram et al. 2018, Saarinen et al. 2018, Díaz-Delgado et al. 2019, Muller et al. 2019). Drone-based measurements can complement smaller scale field measurements and provide detailed information across the ecological scales from individual species to monitoring entire ecosystems (Sun et al. 2021). Some of the practical advantages of using drones versus satellites are the possibility of quick and location specific deployment (Mangewa et al. 2019) especially of lightweight drones, to obtain data even on cloudy days (Dash et al. 2018) and self-determined temporal survey intervals (Tang and Shao 2015). Probably, the main advantage of drones is scale-appropriate measurements (Huylenbroeck et al. 2020) that can capture spatial-temporal variation in vegetation cover such as single shrubs (Cunliffe et al. 2016), terrain (e.g., thaw slump progression (Van der Sluijs et al. 2018)) and micro-climate heterogeneity (Duffy et al. 2021) that generally would not be possible with (non-military) satellites or planes (Sun et al. 2021). Drones haven proven to be especially useful as a ground truthing and upscaling tool in combination with satellite images (Dash et al. 2018, Karami et al. 2018, Rossi et al. 2018, Daryaei et al. 2020, Miranda et al. 2020) which can inform regional conservation management (Stark et al. 2018) and improve our ability to interpret satellite images (Siewert and Olofsson 2020, Assmann et al. 2020). This high diversity of drone applications has led to an equally high diversity of methods and reporting standards. Therefore, there has been a need for more standardized field and data processing protocols to reduce sources of error (Morgan et al. 2010) and improve replication opportunities (Barnas et al. 2020). Recent landscape mapping protocols include items such flight planning, geometric and radiometric calibrations, image processing and how to report these steps and results (Aasen et al. 2018, Assmann et al. 2019, Tmušić et al. 2020). With the right methods and rigorous scientific protocols drones could therefore become an important tool in effective monitoring of natural resources (Anderson and Gaston 2013, Tmušić et al. 2020). With this thesis I am planning to test the suitability of using drones (with RGB and multispectral sensors) in the context of long-term Arctic tundra monitoring and actively use and build upon recommended guidelines for drone-based landscape mapping.

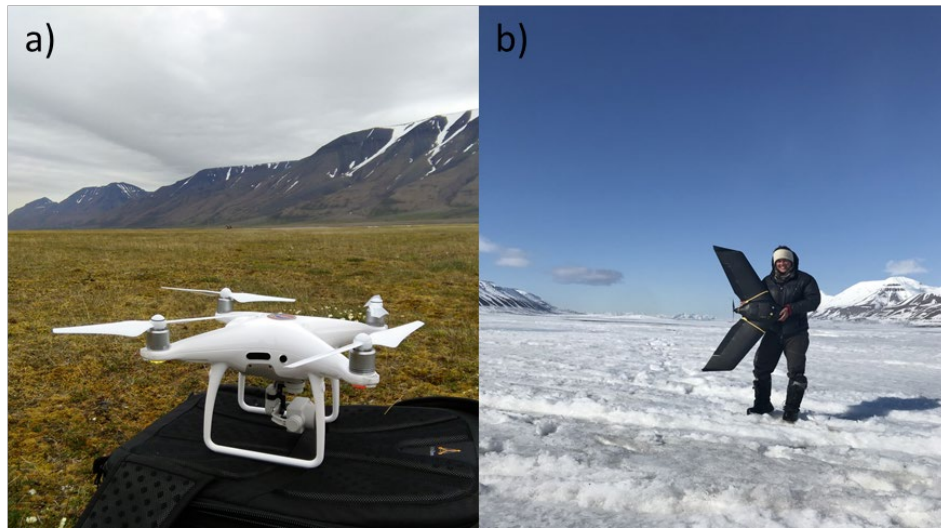


Figure 1: Examples for two of the most common drone types used in ecological research. a) A multi-rotor drone and b) a small, fixed wing drone. Pictures taken in Svalbard, by a) I.Eischeid and b) L. Ársælsdóttir

2.2 Thesis objectives

2.2.1 COAT Tools+

This thesis was carried out in the context of COAT Tools+ which was funded by Tromsø Research Foundation. COAT, short for Climate-ecological Observatory of Arctic Tundra, is a long-term, ecosystem-based, and adaptive observation system. Its mission is to resolve how Arctic tundra food webs are impacted by climate change and provide science-based management advice. The Tools+ project is a method development initiative to integrate and evaluate new technology and enhance the scientific observation capacities of COAT (Ims et al. 2013).

2.2.2 Aims

The overall aim of this thesis was to apply principles of adaptive monitoring to understand causal relationships of biotic and abiotic interactions in a high Arctic tundra ecosystem. Specifically, I used components of an adaptive monitoring framework (Figure 2) to achieve the following four goals.

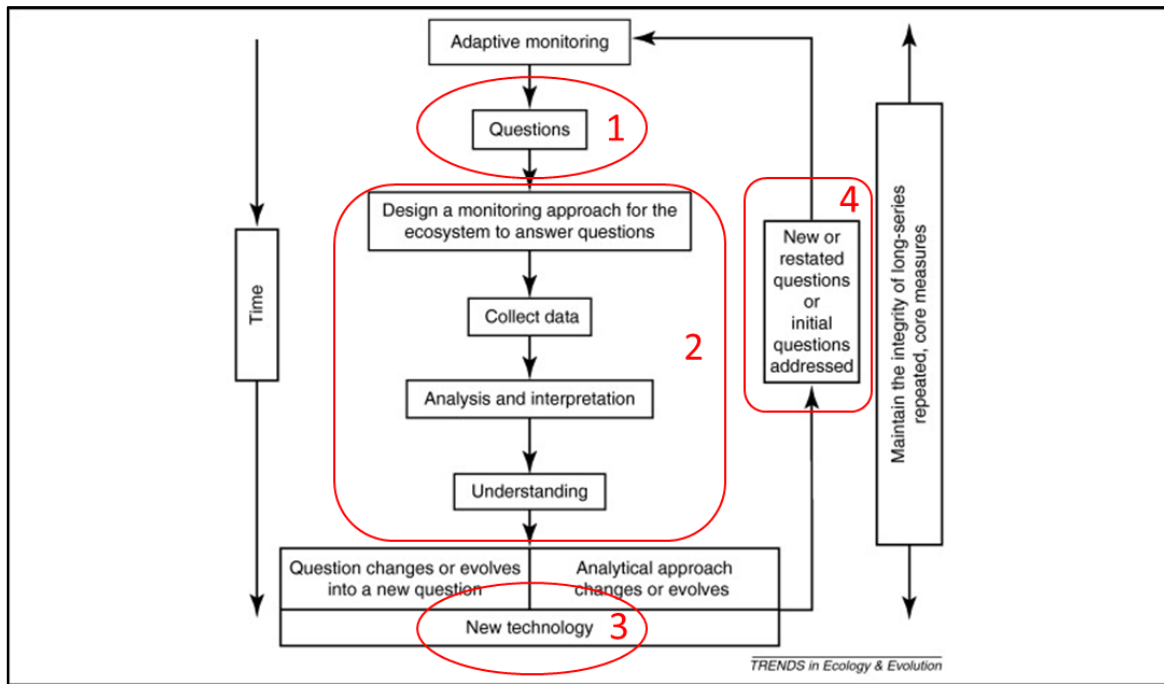


Figure 2: Conceptual model for an iterative approach to adaptive monitoring. This figure was first published in Lindenmayer and Likens (2009) and is shared here with permission from the journal. It highlights important steps in time of an adaptive monitoring program: The monitoring is designed to answer specific questions and after data collection and data analysis, a re-evaluation can answer or alter these original scientific questions. It also allows for the inclusion of new technology to better answer the scientific questions and monitoring needs. The red circles highlight aspects of the adaptive monitoring framework that I apply in this thesis to specify the research questions.

1) The first goal of this thesis was to design conceptual models for Svalbard’s moss tundra ecosystem and define the vegetation monitoring needs of high Arctic tundra systems in the context of climate change and herbivore management. I would like to answer the following questions (Paper I):

1a) Which vegetation states and drivers are likely important at shaping Svalbard’s tundra ecosystem in the future?

1b) How do the presented conceptual models define the monitoring goals for moss tundra ecosystems in Svalbard and how can this thesis contribute?

2) The second goal was to design new monitoring approaches that help quantify habitat types and drivers of vegetation state change in the future by exploring the following questions within the context of long-term adaptive monitoring (Paper II, III).

2a) Can we detect the habitat types described for Svalbard’s tundra ecosystem using drone images?

2b) Can we use drone images to detect abiotic and biotic habitat disturbances?

2c) Can we quantify the role multiple drivers play in steering goose grubbing distribution and intensity?

3) The third goal was to evaluate the practical implications of using drones, drone imagery, photogrammetry and image classification-based approaches for monitoring tundra or alpine environments (Paper II-IV).

3a) How do random forests classifiers perform in tundra environments?

3b) What have I learned from using photogrammetry and drones in tundra environments in the context of adaptive monitoring?

4) The final aim was to evaluate how the findings of the thesis (Paper I-IV) can contribute to monitoring programs like COAT in the future.

3 Methods

3.1 Study system

3.1.1 Thesis framework

The studies in this thesis are interrelated by sharing scientific questions, methods and data (Figure 3). Paper I was a conceptual study that defines the research framework for Paper II and III. In Paper II we mapped ground-cover types, including habitat disturbances in three sites Svalbard during summer. Paper III was a study conducted in spring, situated at one of study sites that we also investigated for Paper II. We are using the maps and methods developed in Paper II but expand the study by integrating snowmelt progression, timing of disturbances and pink-footed goose movement data. Paper IV was situated in the Alps but shared a large proportion of methodology with Paper II and III. This allowed me to draw some wider-scale methodical conclusions.

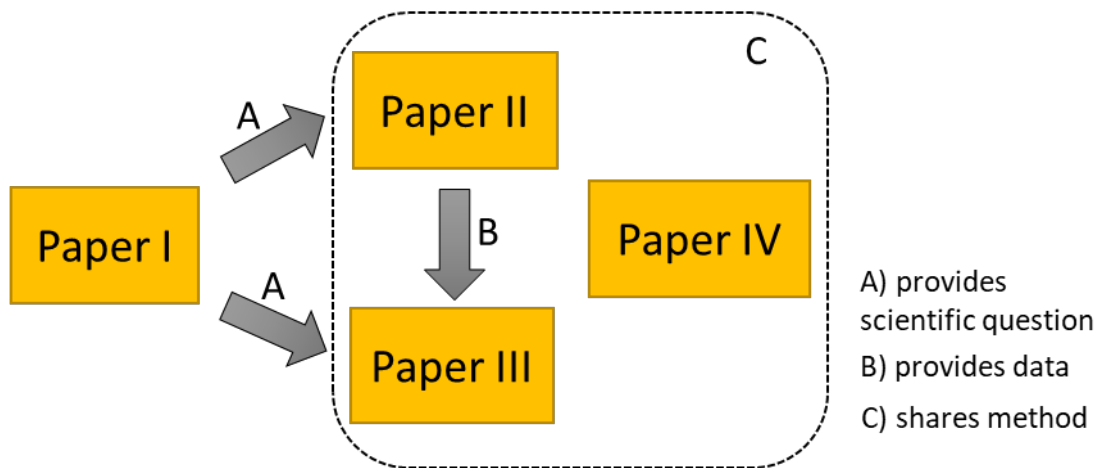


Figure 3: Conceptual framework on how the Papers in this study are linked to one another. Paper I: High Arctic ecosystem states: Conceptual models of vegetation change to guide long-term monitoring and research, Paper II: Disturbance Mapping in Arctic Tundra Improved by a Planning Workflow for Drone Studies: Advancing Tools for Future Ecosystem Monitoring, Paper III: Snowmelt progression drives spring habitat selection and vegetation disturbance by an Arctic avian herbivore at multiple scales, Paper IV: Machine learning for classification of an eroding scarp surface using terrestrial photogrammetry with NIR and RGB imagery.

3.1.2 Study area

All four studies were conducted in tundra ecosystems (Figure 4). Paper I was a conceptual paper for high Arctic tundra and is relying on the tundra ecosystem of Svalbard as a case study. The studies of Paper II and III were conducted in the same ecological context, in Svalbard (74°- 81° N-10°- 35° E). The Svalbard archipelago is located in the high Arctic zone of the Circumpolar Arctic Vegetation Map (Walker et al. 2003). The archipelago is strongly influenced by the Gulf stream and has average winter temperatures up to 20°C higher than other places at the same latitude (Ims et al. 2013). The bioclimatic zones range from polar deserts, Northern Arctic tundra to middle Arctic tundra (Jónsdóttir 2005). Annual precipitation is low, around 190 mm (Lawrimore et al. 2021) and the growing season lasts for one to three months (Jónsdóttir 2005). Glaciers cover approximately 60% of the land surface and only approximately 16% is vegetated

(Johansen et al. 2012). The periglacial landscape is characterized by U-shaped valleys (Figure 5) and the vegetated areas are mostly confined to elevations below 200 m above sea level (Elvebakk 2005). The study of Paper IV was conducted in Rotmoos Valley in the Austrian Alps ($46^{\circ}50'24''\text{N}$, $11^{\circ}01'59''\text{E}$). This area is characterized by an inner alpine climate and a mean annual precipitation of 819 mm (Bernsteiner et al. 2020). The area was shaped by glacial erosion with 40 m of accumulated sediments and local peat deposits of 2.65 m (Patzelt, 1995 and Bortenschlager, 2010 in Bernsteiner et al. (2020)).

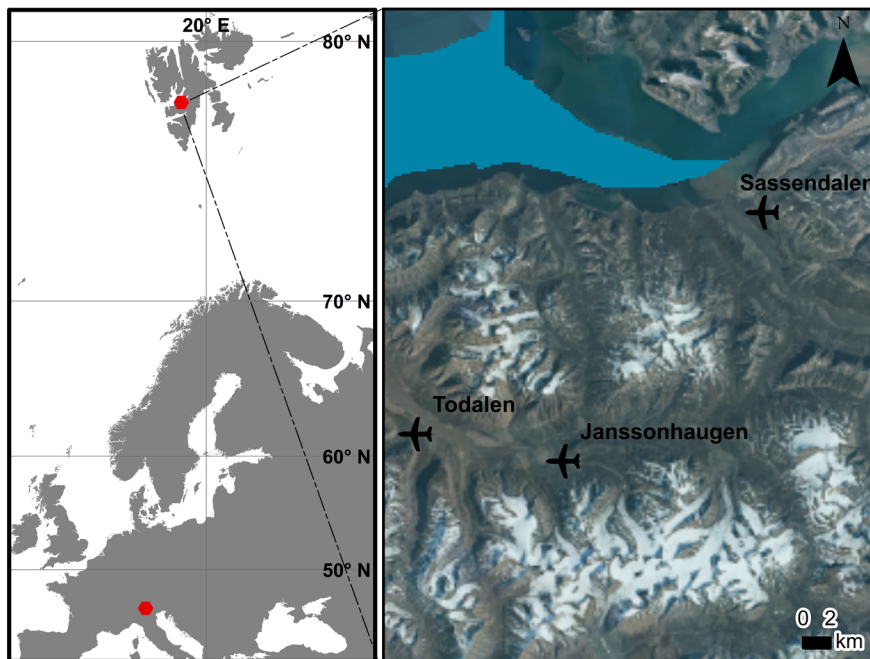


Figure 4: Locations for the studies included in this thesis indicated by red dots. Rotmoos valley in the Austrian Alps in the South ($46^{\circ}50'24''\text{N}$, $11^{\circ}01'59''\text{E}$) and Svalbard in the North (74° - 81°N , 10° - 35°E). The core study sites for Paper II and IV are shown in the zoomed map, Janssonhaugen ($78^{\circ}10'11.85''\text{N}$, $16^{\circ}18' 2.47''\text{E}$), Sassendalen ($78^{\circ}19'53.08''\text{N}$, $16^{\circ}58'28.33''\text{E}$) and Todalen ($78^{\circ}11'19.54''\text{N}$, $15^{\circ}49'24.06''\text{E}$).



Figure 5: Aerial images of Arctic tundra field sites in Svalbard. From left to right: Janssonhaugen ($78^{\circ}10'11.85''\text{N}$, $16^{\circ}18' 2.47''\text{E}$), Sassendalen ($78^{\circ}19'53.08''\text{N}$, $16^{\circ}58'28.33''\text{E}$) and Todalen ($78^{\circ}11'19.54''\text{N}$, $15^{\circ}49'24.06''\text{E}$). Pictures taken in July-August 2019 with a dji phantom 4 pro drone by I.Eischeid.

3.1.3 Habitat disturbances

In Paper II and III, we investigated the extent and timing of biotic and abiotic disturbances as part of ground-cover mapping and an analysis of snowmelt progression on the extent of herbivory. In general terms, disturbance is “any relatively discrete event in time that disrupts the ecosystem, community, or population structure and changes resources, substrate availability, or the physical environment” (White 1985). Disturbance can thus be understood as a force that influences landscape heterogeneity and diversity. It can cause open spaces and create unique structural change and patterns in the landscape with a mosaic of areas with various disturbance intensity and unaffected regions (Turner 2005). Examples of biotic disturbances in a high Arctic ecosystem are those caused by herbivores, e.g., through extensive grazing (Wal 2006), trampling (Tuomi et al. 2021) or grubbing (Speed et al. 2010b). Abiotic disturbances are often caused by either increases in temperature, temperature fluctuation, precipitation or a combination thereof: Plants that get damaged because of temperature changes during the spring and soil destabilization because of permafrost thaw (Lantuit et al. 2012, Milner et al. 2016). In this thesis I am focusing on the biotic disturbance, goose grubbing, and the abiotic disturbance, winter damage of plants, as two drivers of state change (see below).

3.1.3.1 Goose grubbing

The Svalbard population of breeding pink-footed geese has increased substantially the last decades (Madsen et al. 2016). Pink-footed geese overwinter in the Netherlands, Belgium and Denmark and migrate to the High Arctic for the breeding season (Madsen et al. 2009). Their numbers have increased from c. 40,000 in the 1980s to c. 80,000 in 2015-2019 (Heldbjerg et al. 2021). This has mainly been attributed to improved protection from hunting, intensified agricultural production and milder temperatures at their overwintering sites that improved their physical condition and survival rates (Van Eerden et al. 2005). During their pre-nesting stage, pink-footed geese concentrate their feeding on plant roots and rhizomes, this is commonly termed grubbing. While grubbing, geese often remove large amounts of moss in order to access the desired plant parts and open up bare ground (Fox et al. 2006). The recovery rate of grubbed areas depends on grubbing intensity, ground-cover type and weather conditions (Handa et al. 2002, Jefferies and Rockwell 2002, Jefferies et al. 2004a, Speed et al. 2010a). The rapid increase of grubbing geese has therefore been proposed as one of the drivers of tundra vegetation degradation on Svalbard (Speed et al. 2009, Pedersen et al. 2013a). Grubbing activity can vary in intensity and form. In dry areas without significant moss cover, geese often aim directly for single rhizomes which leaves behind distinct holes, often visible many years after (Wal et al. 2020). In moist and mesic areas with a thick moss carpet, they can remove large areas of moss while they search for rhizomes. The different “types” of grubbing are illustrated in Figure 6.

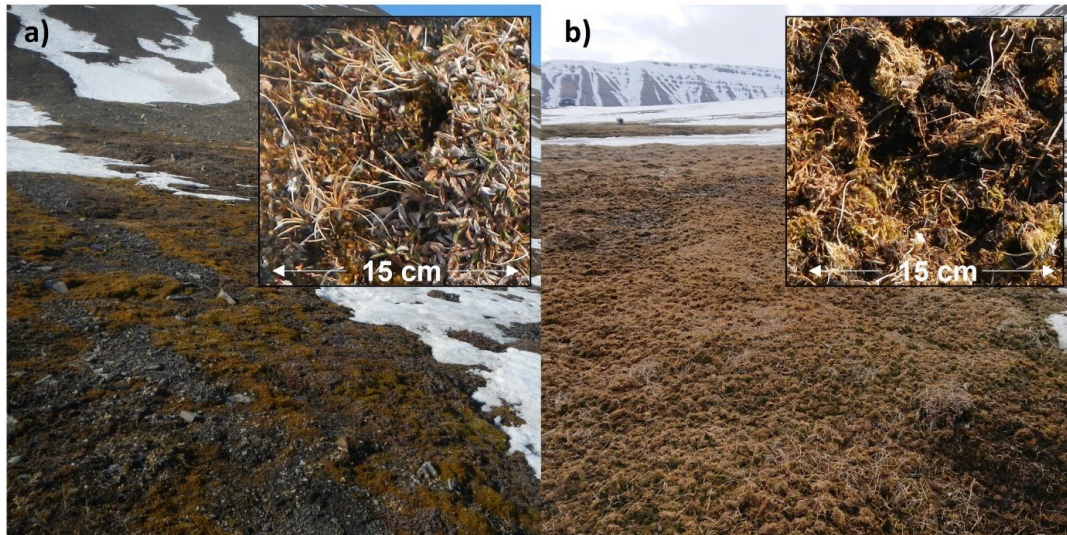


Figure 6: a) Dwarf-shrub heath and b) Moss tundra vegetation class in late May 2019. Inserts show the habitat disturbances typical for the two vegetation classes: Single, isolated grubbing holes in dwarf-shrub heath (left) and continuous grubbing removing the moss carpet in moss tundra vegetation class. Pictures taken in Svalbard, by I.Eischeid

3.1.3.2 Winter damage

Winter rain events have increased over recent years in Svalbard (Peeters et al. 2019). Such events often cause basal ice, which blocks grazing grounds for herbivores, and have wide impacts on population dynamics of the entire vertebrate community (Hansen et al. 2013, Albon et al. 2017, Hansen et al. 2019a, Hansen et al. 2019b, Pedersen et al. 2021). Continuously higher winter temperatures have increased the frequency of winter days with temperatures above 0°C and thus the frequency of rain on snow events (Førland et al. 2011, Hansen et al. 2014). Periodic warm periods during winter and sequential freezing damages plant tissue, and coupled with rain, it encapsulates plants in an ice coat (Le Moullec et al. 2021). In addition, extreme winter warming can lead to desiccation when plants leave hibernation but cannot access water due to frozen soils (Bjerke et al. 2017). Freezing temperatures after snow melt can damage plant tissues and decrease flowering success (Milner et al. 2016). During the summer it is not always possible to determine what has caused the die-offs. In this thesis, I collectively refer to icing, desiccation or other damage that may occur during winter as ‘winter damage’. Dwarf shrub tissues that were damaged due to frost and died typically turn grey; mosses can turn white in their tips or be exposed to “freeze burns” and turn black (Figure 7).

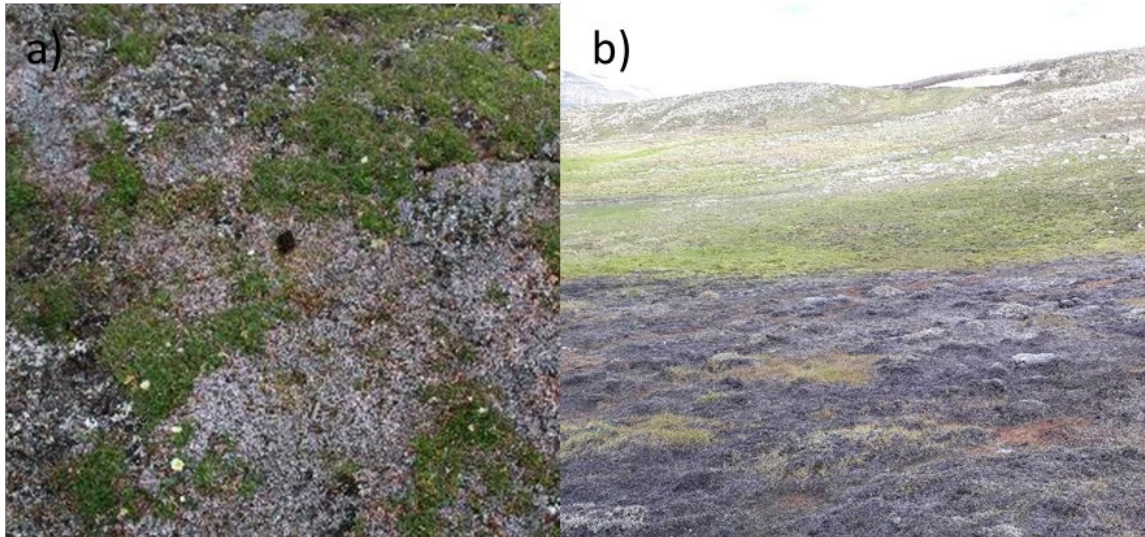


Figure 7: Examples of winter damaged vegetation. a) Dead *Dryas octopetala* stems and leaves surrounded by healthy vegetation. b) Damaged and dead? moss carpet, the ecological process behind this damage is not fully understood. Pictures taken in Svalbard, by a) C. Jaspers and b) V. Ravolainen.

3.1.4 Ground cover classes

In each of the four papers included in this thesis, we grouped the ground into different, yet similar, ground cover classes. Svalbard's tundra vegetation has been classified previously (e.g. Jónsdóttir 2005, Elvebakk 2005, Walker et al. 2005, Johansen et al. 2012) with varying degree of detail and purpose. We were particularly interested to find ground cover classes that would provide useful information for monitoring, such as disturbance classes, and were visually detectable.

Paper I focused on moss tundra habitats and thereby has the most detailed descriptions within this habitat type. We used the habitat types in Paper I as the baseline to define the ground cover classes for Paper II and III but customized them to fit with the specific goals of each study. In the conceptual paper of this study (Paper I), we defined four main habitat types: Cryptogram barrens, Dwarf-shrub heath, Moss-graminoid tundra and Wetlands. These overarching classes are a product of climate, topography, substrate, hydrology and herbivory (Ravolainen et al. 2020).

In Paper II, we used more detailed subclasses of these general habitat types to describe the study system (Figure 8). Ground cover class selection was driven by finding a compromise between ecologically relevant classes and the visual detectability of these. Within the "Dwarf-shrub heath" habitat type, were the classes of *heath moss*, *heath graminoid*, *dryas*, *cassiope* and *winter damage woody*. Within the habitat type "Moss-graminoid tundra" were the ground cover class *moss graminoid* and *winter-damage moss*. The ground cover classes *moss equisetum*, *Carex subspathacea* and *grubbing*, could be assigned to either the "Moss-graminoid tundra" or "Wetland" habitat type. The ground cover types *wetland*, *moss-brown wetland* were within the "Wetland" habitat type. The ground cover classes *bare ground*, *biological crust* and *gravel* could be assigned to multiple habitat types. Detailed descriptions of these ground cover classes can be found in (Appendix A in Paper II).

The ground cover classes chosen in Paper III were generally in accordance with the four major habitat types described in Paper I. With the exception that we made a general, non-vegetated or sparsely vegetated class that included the “Cryptogam barrens” habitat type, but also areas that were covered in bare ground, biological crust and water. The “moss tundra” class in Paper III included predominantly areas within the Moss-graminoid tundra and Wetland habitat type. In

Paper IV, the main goal was to describe classes that give an indication of active erosion sites in a peat scarp. These classes were rock, dry grass, green grass, peat and snow.

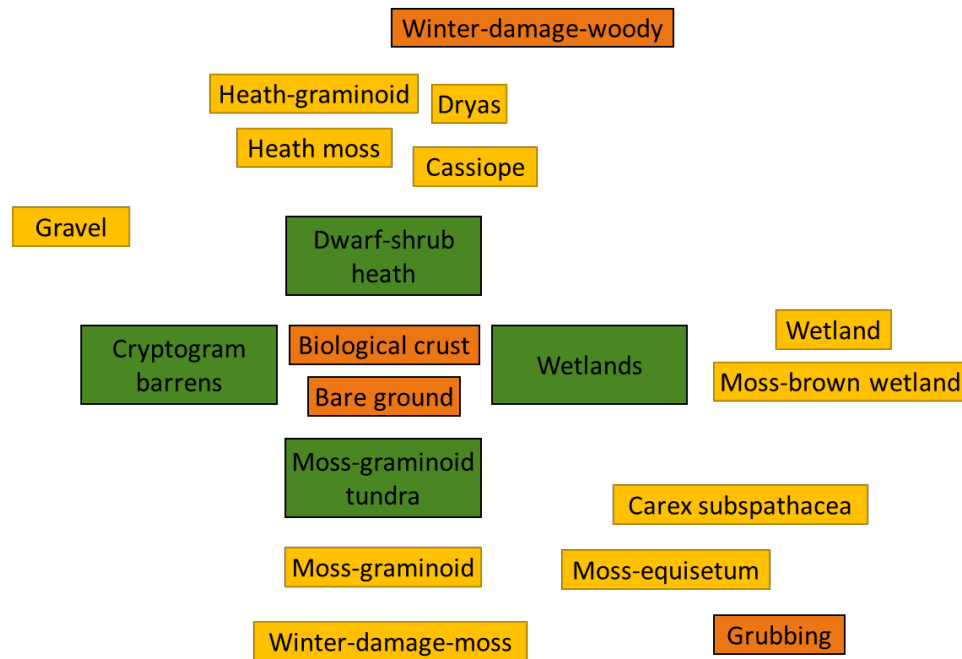


Figure 8: Habitat types in green (Paper I) and their associated ground cover types in yellow and orange (Paper II). The positions of yellow and orange boxes indicate which habitat type they are closest associated with. The classes colored in orange can be associated to habitat disturbances and were investigated more closely (Figure 5 in Paper II). More detailed descriptions about the ground cover classes can be found in Appendix A -Paper II.

3.2 Data collection

3.2.1 Geometric accuracy

The field-based studies of this thesis (Paper II-IV) focused on centimeter scale difference in terrain and snow cover as well as in the highly heterogenous plant communities. Therefore, it was essential that measurements were conducted with appropriate spatial accuracies.

3.2.1.1 Handheld GPS

Handheld GPS (Global Positioning System) units have accuracies at meter scales. The Garmin device we used had reported accuracy of three meters about 95% of the time, pending clear skies and low magnetic activity (Garmin). The GPS location received is based on a triangulation between multiple position readings received from all satellites that are within the field of view of the GPS. Because of the inaccuracies of a normal hand-held GPS, we only used this unit to

register spatial positions for the observers during pink-footed goose surveys (Paper III). Driving and moving in and out of the car made it not possible to use more advanced equipment.

3.2.1.2 Base stations

To obtain more accurate positions that would be possible with a handheld GPS, we relied on base stations situated at previously measured locations (Paper II-IV). In less remote places, mapping authorities often provide a network of permanent base stations that can be used as reference points. In Svalbard, there is only a small number of official base stations and none of them were close enough to the study sites so that we could use them directly. Therefore, we used mobile base stations and established a new network of “known locations” to create our own reference points. We used equipment from Leica Geosystems, GS10 and CS10 (<https://leica-geosystems.com>) for all high precision GPS work. As reference point, we used a marker that had been measured and marked by the local governing body (Figure 9), hereafter called “flagpost location” and was close (500 m) to the study site Todalen. To establish new “known locations” in Janssonhaugen and Sassendalen, we set up one base station at the “flagpost location” and a second base station at each of the two study sites. We then let both stations log their positions for several days and used GNSS processing to calculate the position of the new “known location” in Janssonhaugen and Sassendalen. During GNSS processing the deviations/offset of measured GPS locations of the established “known location” are used to estimate a similar offset (by matching time intervals every 15 seconds) at the new “known location” and calculate a corrected mean over time. The closer the two base stations are, and the longer they run in parallel, the more the increase in accuracy. Our reports revealed a 3D accuracy of approximately one millimeter. We marked the new “known locations” with aluminum pipes in ground so that they can be used as reference points in long-term monitoring.



Figure 9: Leica GS10 Basestations at four locations in Svalbard used as reference point for drone flights and ground truthing. From left to right: “flagpost location”, Janssonhaugen, Sassendalen, Todalen. Pictures taken by I.Eischeid (1,2,4) and T.Blæsterdalen (3).

3.2.1.3 Real time kinematic positioning (RTK)

The core of the high precision GPS work for this thesis was done via real time kinematic links (RTK). With RTK, a mobile GPS unit (the rover) is communicating with a GPS base station that is located at a “known location” via a radio-link. The base station (because it is at a known point) can continuously compute the error/spatial offset at its location. The rover receives information about its position from the triangulation based on the positions received from

satellites (like a hand-held GPS), but it then corrects the position by “talking in real time” with the base station to receive information about the spatial errors/offset at any given point in time. This results in accuracies of approximately 2 cm. We used the RTK approach for several applications. We established a new “known location” at the Todalen site, as it was close enough to the “flagpost location” so that we did not have to use two base stations in parallel. Further, we used the RTK link system to measure ground-control points (GCP), which were targets visible in the drone images and used for georeferencing. All ground truthing points (for ground-cover classes) were also collected using the RTK system. The drone used in Paper II and III was taking advantage of the same RTK system. The drone replaces the rover as the mobile unit but utilizes the same technology to obtain position errors in real time during flight.

3.2.1.4 Total station

In the study of Paper IV we used a total station instead of base station (Leica TC1100). The total station uses the distance and angle to calculate spatial positions in the terrain. We placed the total station approximately 20 meters from the peat scarp erosion site. From this place, we measured the angle and distance from two already “known points” in the landscape, thus calculating the coordinate and orientation of the total station. We then used the total station to geolocate the GCPs that were placed across in the peat scarp.

3.2.1.5 Ground control points (GCPs)

For the drone-based studies in Paper II and III, we used GCPs solely as a backup. Because the drone we had available had RTK capacities, where GCPs theoretically not necessary. As GCPs we used white canvass (1 x 1 m) with two black diagonal squares (checkerboard) that were clearly visible on the drone images. After each flight we measured the location of the GCPs using the GPS rover/base RTK setup (Figure 10).

In the study of Paper IV, we had eleven GCPs placed across the study area of the peat scarp. As GCPs we used white cardboard (0.5 x 0.5 m) with black circular coded targets that could automatically be recognized by the image processing software (Figure 10). In front of the peat scarp landscape feature, we had an available “known location” that had previously been measured. At this “known location” we placed a total station and from there we could measure the exact location of each of the GCPs. This method was especially useful for an almost vertical wall like the peat scarp feature, where the highest elevated areas easily can obstruct the features in the lowest part of scarp.

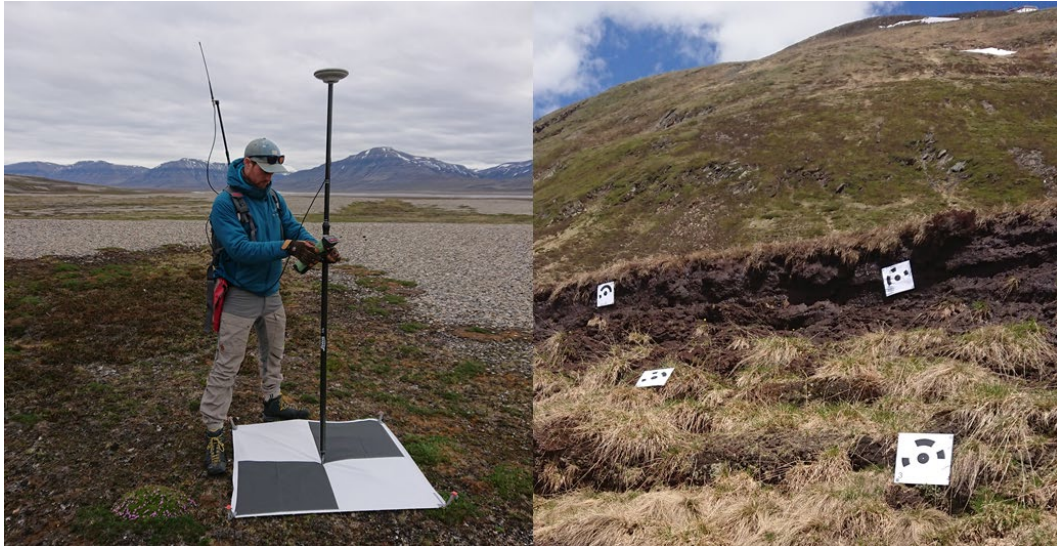


Figure 10: Ground control points (GCP) used for georeferencing of drone and hand-held camera images. On the left, 1 x 1 m canvass, measured with the Leica GS10 rover, Svalbard, July 2019. On the right, cardboard targets, 0.5 x 0.5 m, with black circular coded targets for automatic recognition, Obergurgl, June 2019. Pictures taken by I.Eischeid

3.2.2 Cameras

3.2.2.1 Drone cameras

The two drone cameras that we had available for Paper II and III were a “regular” RGB (red, green, blue) camera (model AeriaX - sensefly) and a multispectral camera (Sequoia+ - sensefly). The RGB camera has a resolution of 6,000 x 4,000 pixels (3:2), which resulted in ground sampling distances (GSD) of approximately 2 cm at 100 m altitude. The Sequoia+ camera had four spectral bands, green, red, near infrared (NIR) and red edge and a GSD of approx.. 10 cm at 100 m altitude. It had an inbuilt light sensor and was radiometrically pre-calibrated (Cubero-Castan et al. 2018). Therefore, similar to the GCPs, we only took spectral calibration images as backup. We used both grey-canvasses (1 x 1 m) of which we had a known spectral signature (measured in the lab) and a grey-card (A4 size) where the spectral signature was provided (Zenith Lite – SphereOptics).

3.2.2.2 Handheld cameras

In the study for Paper IV, we used two different cameras to take images of an eroding peat scarp. We used a consumer grade Canon EOS 450D (27mm) camera to take RGB images and a modified NIKON D-200 to take NIR images. The NIR range had wavelengths between 750-1500 nm. To be able to take NIR images, we first removed the original filter, which blocks radiation above 720 nm and then installed a HOYA R72 filter. The filter allowed the camera to take images in the wavelength between 750 nm and 950 nm (the camera sensors maximum capacity).

3.2.3 Drone mapping

3.2.3.1 Drone system

The drone that I used for this thesis (Paper II, III) was a fixed-wing RTK drone (eBeeX) produced by Sensefly (www.sensefly.com). The drone has a weight of 1.6 kg and is therefore light enough to not require special certification outside of the general European pilot registration requirements. The drone can be transported in three pieces (core and two wings) and is therefore suitable (yet large in volume) for long hikes to remote field sites. The eBeeX is a drone especially equipped for flying mapping missions. It flies at pre-programmed flight lines with specified flight height and image overlap. A laptop and a radio antenna are used to monitor and control the drone during the flight. During the summer flights, (Paper II) we used a direct RTK link to the drone. To do so, we connected the laptop with a serial port cable to the Leica base station (Figure 11) so that the base station could give RTK corrections to the drone, this resulted in accuracies around 2 cm. In spring (Paper III) the necessary cable was not available, therefore we used post-processing-kinematics (PPK) to correctly georeference the drone images. The PPK workflow requires a base station that is logging its position (and therefore spatial offset) in vicinity to the flight area. We used the “flagpost known location” and logged the position at one second intervals. Afterwards we could match the drone images and logged base station positions based on the time and correct the image positions, this resulted in accuracies around 5 cm.



Figure 11: left: Leica GS16 basestation connected to PC (with installed eMotion (sensefly) flying software) via Leica GEV 269 cable, picture taken by I.Eischeid. Fixed wing drone (eBeeX) launch by an eager PhD student, picture by V.Ravolainen, Svalbard 2019.

3.2.3.2 Drone flights

For all flights (Paper II, III), we tried to fly as close as possible to noon (earliest 10:00, latest 15:00) to avoid shadowing (during sunny days) and have as stable light conditions as possible. We did not fly on days where light conditions were unstable, with so called “popcorn” clouds that produced shadows on the study sites. The eBeeX drone can handle wind speeds of up to 14 m/s, but that results in very fast flying speeds when the drone is experiencing tail winds and is faster than the shutter speeds the cameras usually can confidently handle (Zhou et al. 2020). In

addition, start and landing procedures were difficult at these conditions. Therefore, we flew at wind speeds of 7 m/s and under. During summer we were able to conduct all planned flights. During spring, wind and light conditions prevented flights on two of the planned sampling days. Flight heights and image overlap varied between days and projects, mostly balancing the desire to obtain as low ground sampling distance (GSD) and high image overlap as possible but short enough flight times to have stable light conditions. During spring, cold temperatures also restricted flight times because the laptop batteries drained quickly.

3.2.4 Habitat type and disturbance assessments (ground truthing)

Field based habitat type and disturbance assessments were major components for the studies in Paper II and III. For both studies, we collected ground truthing data of the ground-cover classes included in each of the studies. We used the rover/base RTK system to obtain ground truthing data at 2 cm accuracy (Figure 12). Ground cover class detail varied between the studies, but the general procedure was the same. We spread ground truthing points out across the extent of the study area to reduce spatial autocorrelations as much as possible. A stratified random approach would have been best (Roberts et al. 2017), but because we did not have any previous maps from the sites, it would have been difficult to plan a more standardized approach whilst also covering all the ground truthing classes. During the summer survey (Paper II), we used several days at each study site to collect detailed ground truthing data. During spring (Paper III), as the landscape was constantly changing, we collected ground truthing data on the same days we were flying, but only for a limited number of classes (snow, no snow, disturbed vegetation). Additionally, in spring, we surveyed the progression of snowmelt and pink-footed goose disturbance in 320 plots that were spaced out in clusters across the study site. These plots were marked with small nails so that we could find them throughout the season. We also determined the exact location of all the plots by measuring two corners of each of the plots using the rover/base RTK system.



Figure 12: Super-field assistants ground truthing during spring and summer. Left: Linda surveying a plot for snowmelt timing and goose grubbing. Middle: Torgeir taking a ground truthing point of the grubbing class. Right: Ingrid happily mapping a patch of graminoid heath. Pictures taken in May and July in Svalbard, 2019 by I.Eischeid.

3.2.5 Satellite images

In the study of Paper III, we extrapolated the drone-based study onto a larger area using satellite images. We took advantage of the freely available Sentinel 2 images, provided by ESA. The Sentinel 2 mission is comprised of two satellites that orbit at a 180° phase in a polar orbit (ESA 2022). This results in highly frequent revisit times in the polar regions, at least once a day. The satellite is equipped with 13 spectral bands, four of these at ten-meter resolution (red, green, blue, NIR), which are the ones we used for the study. We retrieved the satellite images using Google Earth Engine (GEE - <https://earthengine.google.com>), which is a free platform for universities and researchers. To obtain satellite images within the study period and study area, we used a shapefile to filter for images within the area, selected the time frame of the study and applied a cloud detection mask. Because the mask was not 100% reliable, we manually checked that the images were free of clouds in the study area. The biggest advantage with GEE is that all filtering and processing can be done online without downloading all the images that were not suitable.

3.2.6 Pink-footed goose surveys

For Paper III, we conducted goose surveys and used GPS collared birds (Figure 13) to track their movement. I was not involved in the GPS collaring field work but were given access to the data (www.movebank.org), see Paper III, Clausen et al. (2020) and Schreven et al. (2021) for more information on tagging procedures and bird handling. During spring 2019, we conducted manual goose census surveys by driving (by car) along the same route throughout the pink-footed goose pre-breeding period. For each observation we recorded the observer's position (handheld GPS), measuring the distance (laser-beam on binocular) and angle (compass) to the goose. This made it possible to calculate their spatial position.



Figure 13: Pink-footed goose survey during Spring 2019. Left: Super-field assistant Linda waiting for the first geese to arrive. Right: Pink-footed goose equipped with solar powered GPS tracking device – kindly using one of the monitoring sites in Todalen. Grubbing visible on the ground. Pictures taken in May, 2019 in Svalbard by I.Eischeid.

3.3 Data processing and analysis

3.3.1 Photogrammetry

In the studies of Paper II-IV, we relied heavily on modern photogrammetric methods to stitch images together and create three-dimensional (3D) point clouds. Traditional photogrammetry relied on detailed, manual 3D position reference point measurements of each image to match pixels and objects of multiple images into one. Higher computing capacities have led to the emergence of more effective tool: Structure-from-Motion (SfM), which recognizes matching features on overlapping images and detects camera position, orientation and terrain geometry simultaneously (Westoby et al. 2012). This can be used to create two-dimensional (2D) orthomosaics to generate one large (averaged) image of all the small images. And, because overlapping images have slightly different camera angles, it is possible to generate 3D point clouds. The principles of SfM were already developed in the 1990s but experienced a sort of renaissance with the rise of drone-based mapping (Westoby et al. 2012, Anderson et al. 2019). We used two different software programs (Paper II, III -Pix4D Mapper (www.pix4d.com), Paper IV Agisoft Metashape (www.agisoft.com), but the general SfM method was very similar for both. First, features (key points) on each of the images were matched with the same features on the other images. In the next step, camera positions and angles were used to calculate 3D point clouds with an associated RGB and NIR value for each point in space. In Paper II and III, we continued to generate 2D orthomosaics and digital surface models (DSM) out of the point clouds (using Pix4D Mapper) to use them for analysis. In Paper IV, we used the 3D point clouds directly and imported them into CloudCompare (www.cloudcompare.org) to generate training data. Joining many hundreds of drone images into a single point cloud requires computers with good processing powers. These computers do not need to be specialized but need to have more capacity than an average PC given to an ecologist in a research institute. Because we only needed processing capacities a few times throughout the year, I joined a pilot project by the IT section at Tromsø's Arctic University. Together, we set up a temporary server that I could log into via a Remote Desktop. The specifications were: Microsoft Azure sky, Virtual Machine size NV12 (12 cores, 112 GB RAM, Nvidia GPU).

3.3.2 Spatial layers

In addition to the primary spatial layers that were obtained through the handheld cameras (RGB + NIR, 3D point cloud) and the drone cameras (RGB + multispectral (green, red, red-edge, NIR), DSM), we computed a secondary set of variables for both optical layers and terrain descriptors. The most important ones are described below.

3.3.2.1 Normalized difference vegetation index (NDVI)

From the drone orthomosaics and satellite images we calculated the normalized difference vegetation index ($NDVI = (NIR-red)/(NIR+red)$). We included it as a predictor variable in the ground-cover classifications and as an estimator for general plant biomass density to detect disturbed areas (Schinasi et al. 2018). In Pix4D mapper, it is possible to calculate NDVI within the final processing steps. And in GEE, we calculated the NDVI using the satellite bands within the platform and then downloaded the final layer.

3.3.2.2 Gray level co-occurrence matrix (GLCM)

In Paper II, to help distinguish between ground-cover classes of similar color, we calculated the neighborhood characteristics for each pixel in the green, red-edge and NDVI orthomosaics using gray level co-occurrence matrices (GLCM). It is a method that describes the structural characteristics within a chosen neighborhood of the central point or pixel (Haralick et al. 1973). We calculated seven different GLCMs, variance, homogeneity, contrast, dissimilarity, entropy and second moment using the GLCM R package (Zvoleff 2020). Because neighborhood size influences the values for each GLCM, we used the example of (Fan 2013) and tested predictive ability of multiple neighborhood sizes.

3.3.2.3 Terrain

In Paper II and IV, we used terrain variables as predictors within the classifier. In Paper II, we calculated habitat ruggedness and dissection at multiple neighborhood sizes from the DSM using the spatialEco R package (Evans 2020). In Paper IV, we calculated the terrain variables directly from the 3D point cloud using CloudCompare. We analyzed the predictive abilities of 18 different terrain descriptors (such as roughness, verticality and mean curvature) with three different neighborhood sizes.

3.3.2.4 Training data

In addition to the ground truthing data collected in the field, we also generated manual training data of ground-cover classes (Paper II-IV). In ArcGIS (Paper II, III) or CloudCompare (Paper IV) we opened the point clouds/RBG orthomosaics/RGB satellite images and drew polygons to delineate areas that could be used as training data. In Paper II, we only used this method for ground-cover classes where we did not have enough data from the field (water, winter damaged heath and snow). For the studies in Paper III and IV, delineating polygons was the main method to obtain training data. In Paper III, we delineated polygons for a snow/no snow classification using GEE. To classify habitat classes (moss tundra, dwarf-shrub heath, not vegetated) with satellite images, we used the drone-based classification from Paper II as the training dataset. In Paper IV, we trained the classifier on six ground cover classes (such as grass, peat, rocks) from the 3D point cloud.

3.3.3 Random forest classifier

The studies of Paper II-IV relied heavily on random forests classifiers to detect ground cover types and snowmelt progression. The random forest (RF) classifier, sometimes also referred to as “quasi-machine learning”, is a classification approach that combines the results of multiple decision trees (using random subsets of the data) to generate a final, combined “decision forest” (Breiman 2001). The reason we chose to conduct the studies using RFs was because they can efficiently handle many predictor variables and classes without overfitting and because it provides a ranking of variable importance (Breiman 2001, Cutler et al. 2012, Belgiu and Drăguț 2016). This allowed us to test many predictive spatial layers and select and obtain information on which of these will most likely be important for monitoring in the future. The overall predictive accuracy of a RF can be evaluated using the Out-of-Bag (OOB) error (Breiman 2001). It has, however, been shown that with autocorrelated training data, the OOB can be

overoptimistic, and it is therefore recommended to use independent validation datasets that are not used to build the RF (Mascaro 2014, Millard and Richardson 2015). This can either be a K-fold mechanism where the RF assembly is repeated a defined number of times (Hastie et al. 2009) or splitting the dataset manually (e.g. Mascaro 2014). In this thesis (Paper II-IV) we split training and validation datasets manually. This was, in part, for practical reasons, because the classifier outputs using manual splits were more detailed than using the K-fold mechanism. In addition, the manual approach allowed us to specify the distance between the training and validation points to reduce chances of autocorrelation. For the snow classifications in Paper III and in Paper IV, we only constructed one RF for each dataset, with 500 trees each. For the vegetation classifications in Paper II and III, because the classes were more complex, we used multiple runs (n=30), i.e. created 30 RFs, with a new training and validation dataset split for each (See Figure 4 in Paper II). This provided us with information about the variance around the mean and allowed us to assess the robustness of the classifier. We used r-miner (Cortez 2020), a package in R (R Team 2013) for building and testing the RF classifiers. To predict the results of the classifier over the study area to create classified maps, we used the “predict” function in the R raster package (Hijmans 2020). Because RFs are suitable for parallel processing (Cutler et al. 2012), we used the Cluster R package to speed up processing (Mouselimis 2020).

4 Key findings

4.1 Paper I - High Arctic ecosystem states: Conceptual models of vegetation change to guide long-term monitoring and research

We addressed the importance of adaptive monitoring and creating conceptual models to guide research questions and data collection. We stressed the need to find a balance in monitoring vegetation's response to warming by obtaining a more general understanding of tundra vegetation changes as well as increasing knowledge of ecosystem-specific responses. Therefore, we recommended the use of conceptual models of vegetation change in High Arctic ecosystems to guide long-term monitoring and research. Using Svalbard as a case study, we suggested three conceptual models for different purposes and levels of detail.

First, we defined a general ecological conceptual model for the main habitat types in Svalbard: cryptogam barrens, dwarf-shrub heath, wetlands and moss-graminoid tundra (Figure 1a in Paper I). Long term-changes and extreme events are needed for a habitat type at these levels to change into another. Examples of such drivers are changes in hydrology, soil movement, establishment or loss of sea bird colonies and long-term changes in herbivore densities.

We then developed a more detailed ecological conceptual model for moss-graminoid tundra, a key habitat for many terrestrial animals in Svalbard (Figure 1b in Paper I). We proposed a three-state system: moss state, herbaceous state and bare patch state. Transitions between the moss state and herbaceous state were previously described by Wal (2006) with long-term herbivore density variations and temperature as key drivers for state change. We suggested that short-term disturbance events (pulses) such as heavy rainfall, active layer detachments or intensive goose grubbing can cause the system to shift to a bare patch state. Depending on succeeding conditions, such as the frequency of disturbance events, summer temperatures and grazing intensities, the system can move back to a moss or herbaceous state.

Finally, we proposed a monitoring-oriented conceptual model that describes the ecosystem components that can influence the state of moss-graminoid tundra habitat (Figure 14). Using the conceptual model, we defined a set measurable *state variables* that help quantify these predictors and the effect they have (Table 1 in Paper I).

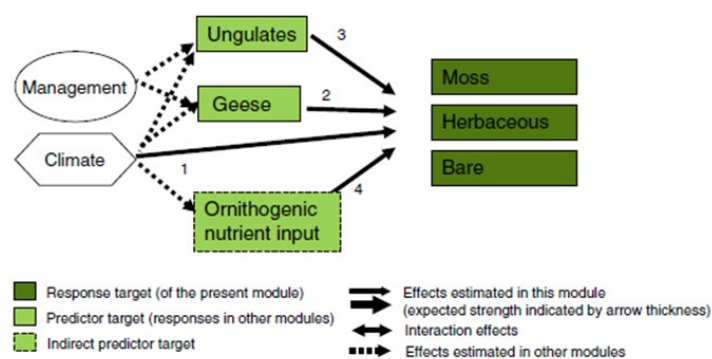


Figure 14: Published in Ravolainen et al. (2020). A detailed conceptual model for moss tundra on Svalbard implemented within the monitoring program Climate-ecological Observatory for Arctic Tundra—COAT. The included drivers are expected to have direct impact on the state shifts. Indirect impacts (dashed lines) and effects the vegetation can have on the herbivores have been outlined earlier (Ims et al. 2013). Climate (pathway 1) can act as a 'press' via gradually warming temperature, or as a 'pulse driver' through, for example, abrupt extreme winter weather events. Likewise, the impact of herbivores can happen as an abrupt pulse event, as in the case of goose grubbing driving vegetation patches from vegetated to the bare patch state (pathway 2), or as press herbivory by reindeer gradually causing a shift from the moss to the herbaceous state (pathway 3). Fertilization by seabirds is an important driver of state shifts on the coast (pathway 4).

4.2 Paper II - Disturbance Mapping in Arctic Tundra Improved by a Planning Workflow for Drone Studies: Advancing Tools for Future Ecosystem Monitoring

We developed a method planning workflow that was aimed at ecologists that wish to include drone imagery-based methods into their monitoring programs. It reviews topics such as the selection of predictor variables, layer resolutions, selection and optimization of ground-cover classes and the development and validation of models (See Table 1 in Paper II).

We applied this workflow in a case study, producing ground cover maps at three study sites (Janssonhaugen, Sassendalen, Todalen) in Svalbard. For each site, we generated a high-resolution map of tundra vegetation using drone images and a random forest classifier.

First, we compared NDVI values of disturbed areas (state variables: goose grubbing and winter damage) with undisturbed areas within the same habitat class. Areas classified as goose grubbing, winter damage or biological crust had lower NDVI values than their undisturbed counterparts but higher values than bare ground (Figure 5 in Paper II).

Second, we trained the RF classifier based on our ground-cover classes. The classification was based on four spectral bands, the normalized difference vegetation index (NDVI) and three types of terrain variables. After optimizing our class selection (Figure 3 in Paper II), we were able to distinguish up to 15 ground cover classes, including goose grubbing and a mixed class for winter damage and biological crust. We created classified maps of the three study sites (Figures 7-9 in Paper II). The overall predictive ability of the optimized classifier had macro-F1 between 84.4% - 88.5% and class-specific F1 scores were generally high (Table 1). However, we detected a consistent overestimation of the disturbance classes. Classifiers that included optical and terrain-based predictor variables performed better than those only using optical variables.

Finally, we tested the transferability of each locally trained RF to the other two study sites. Transferability was low, 50% or less (Figure 10 in Paper II). Transfer between the sites Janssonhaugen and Sassendalen was highest and shared a greater number of high importance predictor variables.

Table 1: F1- scores of ground-cover classifications at the three study sites on Svalbard using the optimized classes and all predictor variables (optical and terrain). Class names in order from left to right: moss-graminoid, moss-equisetum, wetland, moss-brown-wetland, Carex subspathacea, heath, dryas, cassiope, winter-damage-woody/biological crust, grubbing, bare ground, gravel, water, snow.

site	Class													
	mgr	meq	wet	mbw	csu	hea	dry	cas	wdc	gru	bgr	gra	wat	sno
JAN	85.2	89.3	92.3	-	-	76.5	94.9	80.7	83.1	90.5	92.8	91.3	89.3	100
SAS	70.5	83.8	92.8	-	-	77.3	80.2	92.0	88.7	86.1	75.0	84.0	93.4	-
TOD	84.7	85.9	80.8	86.4	97.7	95.6	80.7	74.7	77.5	78.3	88.9	74.0	98.9	-

4.3 Paper III - Snowmelt progression drives spring habitat selection and vegetation disturbance by an Arctic avian herbivore at multiple scales

In this study we assessed how snowmelt timing and vegetation influence habitat selection, habitat use and vegetation disturbance likelihoods via grubbing by pink-footed geese during spring (Figure 15).

First, we analyzed how snowmelt timing and vegetation type influence pink-footed goose habitat selection and habitat by using GPS telemetry and field-based observations. Second, we used field measurements of snowmelt, vegetation class and goose grubbing to make a predictive grubbing likelihood maps. And third, we tested whether habitat use estimates correlated with predicted grubbing likelihoods.

We conducted the study at two spatial scales. A fine-scale analysis (5cm resolution) using drone images at the Todalen site of Paper II. The smaller site was nested within a larger, “valley-scale”, study area (~30 km²) which we studied using Sentinel 2 satellite images (10 m resolution). We used vegetation class and snowmelt date as predictors and retrieved them from field assessments as well as drone and satellite images. The vegetation maps we used were generated from a simplified version of the ground cover classification map using drones presented in Paper II. We generated snow cover maps from drone repeat flights and cloud-free satellite images.

The results of this study showed that at both spatial scales, snowmelt timing and vegetation type were important predictors for habitat selection and use as well as for vegetation habitat disturbance from pink-footed geese. Moss tundra habitats were preferred over dwarf-shrub heath habitats throughout the spring season. Habitat selection for earlier and later snow free areas was similar, therefore higher habitat selection ratios for early snow free areas was a result of that these habitats were available longest. Estimated habitat use and grubbing likelihoods were positively correlated at both spatial scales. We predicted that 23.1% of the moss tundra habitat and 10.1% of dwarf-shrub heath habitat were affected by pink-footed goose grubbing in the valley study area.



Figure 15: A conceptual model for the interaction of snow, vegetation class and goose behavior. Snow cover and snowmelt timing influence pink footed goose feeding behavior because it restricts access to food resources (pathway 1). The vegetation class influences the food quality for the geese (pathway 2). The resulting goose habitat selection in turn influences the vegetation disturbance intensity and spatial distribution (pathway 3).

4.4 Paper IV - Machine learning for classification of an eroding scarp surface using terrestrial photogrammetry with NIR and RGB imagery

As part of a summer school, we evaluated the capacities of a random forests (RF) to create a classified three-dimensional (3D) model of an eroding peat scarp in Rotmoos valley near Obergurgl, Austria. We were taking advantage of increasingly advanced and affordable close-range sensing techniques and processing powers which allows the use of advanced photogrammetry and the computation of RFs (Figure 16).

We used conventional RGB camera and a near-infrared (NIR) filter to take overlapping pictures of a 20 m long eroding peat scarp. We merged the RGB and NIR images into a single 3D point cloud and extracted 18 geometric features using three different radii (0.02, 0.05 and 0.1m) totaling 58 variables. Using the point cloud, we created a training dataset for five different ground cover classes, rock, dry grass, green grass, peat and snow. We used 50% of the training dataset to create the RF and evaluated its performance with the remaining 50% of the dataset.

The overall classification accuracy was 98%. Rock and snow had the highest observation and prediction accuracies. The largest source of error was caused by mixing between the dry and the green grass classes with observation and prediction error rates of 1.9 – 5.6%. The spectral predictor variables (NIR, R, G, B) had higher importance rankings than the terrain derived variables. Terrain variables calculated at 0.1 m radius were higher ranked than those at 0.02 m and 0.05 m radius. NIR had the highest variable importance ranking of the spectral variables and verticality (at 0.1 m radius) was the most important terrain feature.

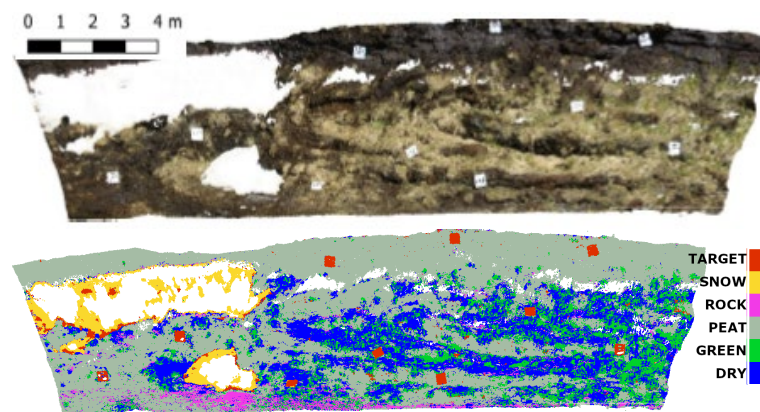


Figure 16: Eroding peatscape presented as a RGB point cloud (top) and the classified point cloud with five ground cover classes (rock, dry grass, green grass, peat, snow) using a random forest classifier and 58 predictors (bottom).

5 Results and discussion

5.1 Which vegetation states and drivers are likely important for shaping Svalbard's moss tundra habitats in the future?

Based on satellite monitoring, on a global scale, the Arctic tundra has become greener over recent decades (Tucker et al. 2001, Keenan and Riley 2018). On a local scale, this trend is, however, highly heterogenous (Berner et al. 2020), and many areas have not significantly changed or even had a reduction of greenness because of e.g., erosion, winter damage, overgrazing or land use change (Walker et al. 2009, Lara et al. 2018). Ecological causes of greening can be attributed to rising temperatures (Keenan and Riley 2018) that change growing conditions to increased biomass production of existing plants (Hudson and Henry 2009), colonization of previously barren land or by new, more productive species (Elmendorf et al. 2012). Browning can be linked to disturbance events such as fires (Hu et al. 2015), insect outbreaks (Jepsen et al. 2013) or long-term trends such as permafrost degradation (Grosse et al. 2016) or increases in herbivore densities (Barrio et al. 2017). Both greening and browning trends can likely be observed within the same ecosystem, especially in heterogenous tundra environments, typical for Svalbard. The conceptual model for moss-graminoid moss tundra (Figure 1b in Paper I) recognized the monitoring need for greening-browning dynamics of Arctic tundra ecosystems. Therefore, we suggest adding a “bare patch” state as an alternative to the “moss” or “herbaceous” state described by Wal (2006) for Svalbard's moss tundra ecosystems.

Adjusting the conceptual models to integrate new knowledge is one of the key principles of adaptive monitoring (Lindenmayer and Likens 2009). When developing the conceptual models, using Svalbard as a case study, we were challenged to find the balance of describing locally meaningful examples which were generic enough to provide valuable information for researchers and managers working in other High Arctic ecosystems (or elsewhere). For this thesis, I would like to suggest and discuss some Svalbard specific additions to the conceptual model because they define some of the research questions in Paper II and III (Figure 17)

A recent (field-plot based) revisit study (Wal et al. 2020) in certain valleys in Nordenskjöld Land has documented a striking increase of *Equisetum* ssp. and *Carex subspathacea* in previously disturbed plots in moist and wet habitats. These species appear to replace *Dupontia* ssp. and *Eriophorum scheuchzeri*. In addition, *Carex subspathacea* is occupying drier habitats than it did 20 years ago. The herbaceous moss state described in Paper I, could be described in more detail as three substates: 1) graminoid (eg. *Dupontia* ssp, *E. scheuchzeri*, *Poa* spp., *Festuca* spp.), 2) *Carex subspathacea* or 3) dominated by *Equisetum* ssp.. My personal observations have shown that *Equisetum* spp. can also establish in moss dominated moss tundra with few other graminoids.

The conceptual model did not include biological crusts as part of potential moss tundra states. These crusts consist of a mixture of cyanobacteria and can form on instable loamy soils (Migala et al. 2014) and can act as ecosystem engineers by weathering the substrate underneath making

it available for plant colonization (Agnelli et al. 2021). More research is needed on the succession pathways that involve biological crusts. In the field, we have observed that these crusts also form around winter damaged plants, but this has not been studied in detail. Therefore, I suggest including them in the conceptual model as they may play a role in shaping new plant communities.

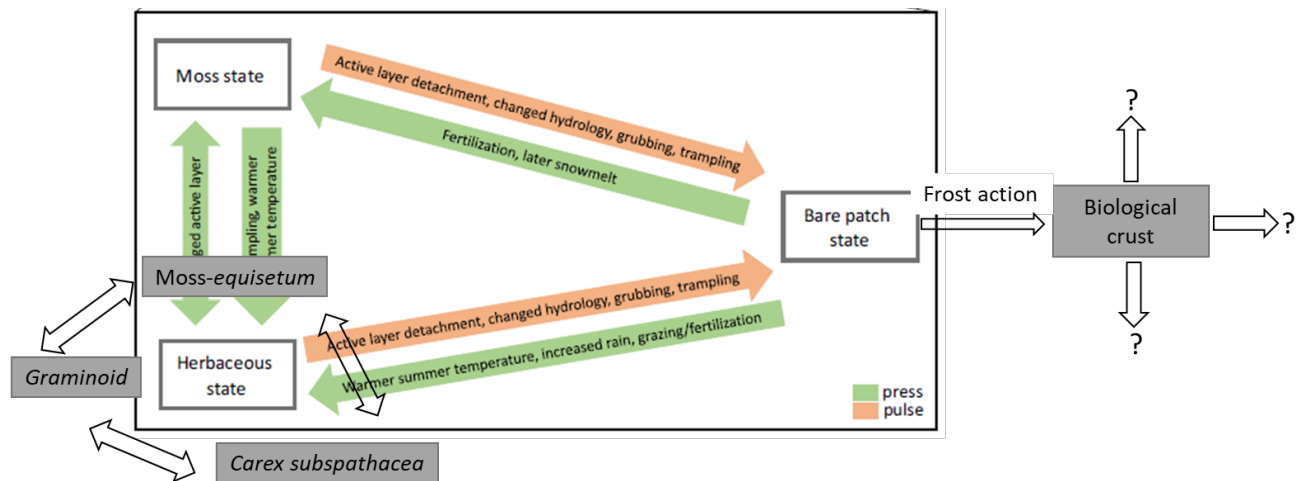


Figure 17: Refined version (gray boxes) of conceptual model presented in Figure 1b in Paper I to account for three possible sub-states of herbaceous moss tundra and a possible pathway of biological crust development after the bare patch state. *Original figure caption:* We suggest the moss-graminoid tundra can be found in a (i) moss, (ii) herbaceous, (iii) or bare patch characterized state. The drivers that cause shifts between these states can be characterized as those that gradually change their impact ('press'), and those whose impact is a sudden event ('pulse'). Both biotic and abiotic drivers can push the moss-graminoid tundra in the same direction, e.g. both sudden active layer detachments and high abundance of herbivores trampling or grubbing can cause the shift from the vegetated to the bare patch state. *Suggested elaborations:* The herbaceous state can be very diverse and could be described by (at least) three sub-states with either Graminoid, Moss-equisetum or Carex subspathacea dominance. In recent years regrowth after the bare patch has often been followed by the Moss-equisetum or Carex subspathacea. They can evolve into the Graminoid sub-state or Moss state over time. Bare patches can be regrown by biological crust and depending on terrain and frost-action these areas could develop to any moss state or another habitat class such as dwarf-shrub heath.

Paper I focused on moss-graminoid tundra as a key habitat and described it in detail. It is important to keep in mind that the other habitat types can have equally diverse states and state changes. For example, dwarf-shrub heath habitat types can often be found on ridges and convex landscapes and can be free from snow during the winter or early in spring (Bjune 2000). This makes them especially prone to geological-cryospheric processes such as frost heave and cryoturbation and at the same time an attractive habitat to herbivores when snow covers other parts of the landscape (Pedersen et al. 2013a). This thesis therefore also focuses on dwarf-shrub heath habitats although they are not discussed in as much detail in Paper I. It is important to note that the conceptual models presented are ongoing work and that vegetation states are not fully understood and described. These models will therefore change over time when being tested in the field (through studies like Paper II, III of thesis) and updated when we have a better understanding of the system.

5.2 How do the presented conceptual models define the monitoring goals for moss tundra ecosystems in Svalbard and how can this thesis contribute?

Defining good questions is a core component of successful adaptive monitoring programs (Lindenmayer and Likens 2010). In Paper I, we used the ecological moss-graminoid tundra model to frame a monitoring-oriented conceptual model that can help with the practical implementation of ecosystem-based monitoring. The conceptual model follows the principles of the Climate-ecological Observatory for Arctic Tundra (COAT) long-term adaptive monitoring program (Ims et al. 2013). It outlined general dependencies between biotic and abiotic drivers within the terrestrial moss tundra food web on Svalbard (Figure 14). Moss tundra states can be directly influenced by ungulates, geese and seabirds and the abiotic driver, climate. Both climate and management can also indirectly affect the moss tundra state, e.g., by changing the abundance or behavior of herbivores and predators.

With the help of the conceptual model, we defined measurable *state variables* that can help to quantify the effect of different drivers within the ecosystem. A complete list of the proposed state variables can be found in Paper I, page 670. Path numbers correspond with labels in Figure 14. The state variables that I proceeded to focus on in this thesis were “ice damage” (path nr. 1), “extent of vegetation types/bare ground” (path nr. 1-3), “abundance of herbivores” (path nr. 2 only) and “grubbing impact” (path nr. 2). This thesis therefore aims to “put some numbers on the arrows” and provide information that can be integrated into ecosystem-based assessments on Svalbard and give new insights into plant-herbivore interactions in general.

5.3 Can we detect the habitat types described for Svalbard’s tundra ecosystem using drone images?

After the class optimization procedure, we were able to distinguish up to 15 ground cover classes and the overall classification results (macro-F1 scores 84.4% - 88.5%) in Paper II were promising. Macro-F1 at this level can be considered high, taking into account the number of ground-cover classes and a strict spatial separation of training and validation data. Although difficult to compare because ground cover detail was different, the level of accuracies was similar to other drone-based tundra classifications (Siewert and Olofsson 2020, Thomson et al. 2021).

The class specific F1-scores varied from 76.5% (heath in Janssonhaugen) to 100% (snow in Janssonhaugen), but, from a monitoring perspective, prediction and observation accuracies and confusion matrices may be more informative because they provide information about which classes tend to mix and if a consistent over- or underestimation can be observed. In other words, how good a classification is depends largely on the goals and monitoring needs. In this study, class mixing was largely restricted to ecologically similar ground cover classes, i.e., within the same habitat type. For example, grouping the ground-cover classes into a dry-mesic dwarf-

shrub heath and a mesic-wet graminoid moss tundra-wetland complex would have resulted in observation and prediction accuracies of mostly over 90% at all three study sites.

The great advantage with drone-based mapping is that it provides information at larger spatial extent than possible with plot or transect based studies. As suggested by Wal et al. (2020) we included *Equisetum* spp. and *Carex subspathacea* as ground-cover classes in our maps. The moss-equisetum class was detectable as its own ground cover class across all three study sites, with F1 scores over 80%. This suggests that drone images and RF classifications are promising tools to monitor *Equisetum* expansion in Svalbard and possibly elsewhere. *Carex subspathacea* was present at all three sites, but we decided too late to include it as its own ground cover class at the first two sites. Therefore, we only collected ground truthing data for *C. subspathacea* within a small area at the Todalen site. The high F1-score of 97.7% may be an artifact of spatial autocorrelation, because the ground truthing points were very close to one another, but it also suggests great potential for studying *C. subspathacea* via drone images in the future.

Two sets of classes that we struggled with, were the distinction between the herbaceous and moss state, and more generally, finding a clear distinction between moss tundra and wetland habitats. We observed that these classes follow a moisture or terrain gradient, but we had difficulties drawing clear-cut borders between these classes. Because NDVI values are sensitive to water content (Hennessy et al. 2020), high water content in the moss can challenge classification robustness through seasonal variation of moisture levels. Forcing ecological diversity into distinct vegetation classes will always remain to be a challenge.

Overall, with its mentioned limitations, the classification results of the study in Paper II suggest that drone image-based mapping can be a useful method to detect some of the most important ground cover classes of importance to monitor future changes in Svalbard's tundra ecosystem (Ims et al. 2013). It can help to detect the mentioned COAT state variables "extent of vegetation types/bare ground" as described in Paper I, Table 1.

5.4 Can we use drone images to detect abiotic and biotic habitat disturbances?

Ecology has long recognized the importance of biotic and abiotic disturbance to alter the state of the ecosystem (Grime 1979, White 1985). Disturbance effects to the ecosystem can be highly scale dependent (Adler et al. 2001). But, for example, although we have detailed knowledge of herbivore-plant interactions, we still have little knowledge about the consequences of these interactions at larger spatial scales (Siewert and Olofsson 2021).

One of the main goals of this thesis was to improve estimations of spatial and temporal occurrences of biotic and abiotic disturbances that can cause vegetation state changes. I focused on winter damage (abiotic) and goose grubbing (biotic) because these disturbances have been very prevalent in Svalbard in recent years (Pedersen et al. 2013b, Bjerke et al. 2017, Peeters et al. 2019, Wal et al. 2020). The spatial distribution of winter damage and goose grubbing, in centimeter to meter scale patches, irregularly spread across the landscape, makes it difficult to

study solely using plots or transects that cover only a small percentage of the landscape (Bjerke et al. 2017, Wal et al. 2020). We used three methodical approaches to estimate the spatial extent of disturbances. Two direct approaches, by identifying disturbance in images 1) disturbance detection based on NDVI and 2) treating disturbances as stand-alone ground cover classes in a random forest (RF) classifier (Paper II). And a third approach, estimating disturbances indirectly by using snowmelt timing and vegetation types to predict habitat selection and grubbing intensities by pink-footed geese during spring (Paper III). The third approach is discussed in section 5.5.

The NDVI index is commonly used for change or disturbance detection in satellite-based timeseries to e.g., monitor windthrows or clearcuts in forests, fires, or moth outbreaks (Spruce et al. 2011, Lambert et al. 2015, Tian et al. 2018, Gao et al. 2021). Within the timeframe of this thesis, we could not collect drone-based time series data that span multiple years. Therefore, we used a space for time substitute to compare NDVI values of disturbed and undisturbed plots within the same habitat type. We showed that pixels (10 cm) recorded as winter damage, biological crust and grubbing had lower NDVI than undisturbed areas within the same habitat class.

This poses great potential for future time-series-based detection of disturbance emergence or regrowth in Svalbard and similar ecosystems. The advantage of using NDVI as a single predictor for disturbance occurrence is that it is methodologically and computationally relatively simple. The challenge with this method is that it requires repeat measurements over multiple years, is dependent on spectral calibrations, exact georeferencing and previous knowledge of the ground cover classes. Because several of the ground cover classes were not distinguishable based on NDVI values alone, we tested the possibility of including disturbances as ground cover classes into the random forest classifier.

The results of Paper II showed that the RF classifier was able to detect disturbances as stand-alone ground cover classes (F1 scores between 77.5-90.5%). We registered a slight but consistent overestimation of the disturbance-related classes, grubbing, winter damage and biological crust. Inconsistencies within the grubbing class can most likely be corrected by adding additional ground cover classes for disturbed (e.g., reindeer trampling) terrain and brown, senescent *Cassiope*. In the process of optimizing the RF classifier, we grouped the woody winter damage and biological crust classes together because they were difficult to distinguish from one another. Improvements in the precision of ground truthing data collection may make it possible to treat them as two separate ground cover classes in the future. The biological crust class was a very broad class that included any coat of biological film, cyanobacteria and crust. Paying more attention to the diverse forms of biological crust in the ground truthing protocol could help to distinguish at least some of the crust covered areas from winter damage. Instead of mapping many hundred square meters, it may be more appropriate to focus on high resolution mapping within a smaller area to find key variables that help distinguish between biological crust and winter damage.

Especially for goose grubbing, there has long been stated a need for more spatially explicit disturbance monitoring (Fox et al. 2006, Wal et al. 2020). The results of this study have shown

that drone imagery-based detection of abiotic and biotic disturbances such as winter damage and goose grubbing is possible. Which of the two above discussed methods is most appropriate for monitoring will depend on multiple factors, such as the main monitoring goal, if extensive ground truthing is possible or if annual repeat flights are feasible and thus allowing the construction of a time-series. The results of this study have shown that drone image-based methods open up new possibilities for monitoring biotic and abiotic disturbances in Arctic tundra ecosystems. It provides tools to detect and better study the COAT state variables “ice (winter) damage” and “grubbing impact”, as described in Paper I, Table 1.

5.5 Can we quantify the role multiple drivers play in steering goose grubbing distribution and intensity?

Both approaches presented above are based on visual detection of grubbing extents and hence relied mainly on distinguishing color differences. Therefore, best detection results can be expected in peak biomass season when visual differences between healthy and disturbed areas are largest. These methods could not distinguish between new and old grubbing from previous years. Nor did it capture early season grubbing where the vegetation cover already has regrown in summer (I. Eischeid, unpublished field data). Grubbing also occurs in drier dwarf-shrub heath habitats, but because it is less intense and does not accompany moss mat removal (Figure 6), it was not possible to detect these areas using drone images alone (I. Eischeid, unpublished field data). Finally, these detection-based methods did not provide any causal information on the spatial distribution of grubbing and its intensity.

In Paper III, we tried a different approach, using landscape predictors to estimate goose grubbing extent. Through previous studies we knew that vegetation class is a strong predictor for goose habitat use and habitat disturbance (Pedersen et al. 2013a, Pedersen et al. 2013b). We also expected that snow cover plays a role in determining suitable habitats although this had not quantitatively been shown (Wisiz et al. 2008, Speed et al. 2009, Pedersen et al. 2013a, Anderson et al. 2016). Therefore, we assessed if we could map the relevant vegetation classes and snowmelt progression using drones and satellites. This would allow us to extrapolate predictive modelling of goose grubbing to larger spatial extents. We used a simplified version of the ground cover classification map presented in Paper II and generated snow cover maps from repeat drone flights and satellite images.

We conducted the study at two spatial scales, using drone images at the Todalen site (also used in Paper II) and Sentinel 2 satellite images to test if we can upscale our findings to a larger spatial extent (~30 km²). The results of this study showed that snowmelt timing and vegetation class were important predictors for habitat use and, at both scales, this correlated well with habitat disturbance.

From a monitoring perspective, this opens new opportunities of integrating remote sensing-based methods to derive important predictors for future goose grubbing assessments. In years when no field work is possible, GPS telemetry-based data could be used to determine annual grubbing hotspots within the pre-breeding sites. The disadvantage of only using telemetry is that it will not provide information about the entire extent of the habitat use and disturbance.

Thus, I recommend conducting an annual goose grubbing field survey at the end of the pre-breeding period with plots that are measured with a differential GPS. Field assessment could then be used to make an annual predictive grubbing likelihood map. GPS telemetry data could be used to validate the findings by testing the correlation between grubbing predictions and habitat use.

This study has shown that it was possible to quantify two drivers (vegetation class and snowmelt date) and that these are important determinants of pink-footed goose habitat use and vegetation disturbance. Further, it provided information on grubbing for habitats where it is not very visible. It is also better (compared to the methods in Paper II) suited to provide temporally explicit grubbing estimates. Because we cannot detect grubbing on satellite images, a prediction-based approach is better suited for landscape-wide estimates. This, for example, would allow identification of important pre-breeding habitats and estimate annual carbon emissions caused by grubbing.

We showed that overall, the patterns measured at the drone and satellite scales were similar. By moving from a drone-based (5 cm) to a satellite-based (10 m) resolution, information on landscape heterogeneity is inherently lost (Siewert and Olofsson 2020, Assmann et al. 2020). Many small patches that were free early from snow in the drone images were not visible in the satellite images (I. Eischeid, unpublished field data). A systematic study about the loss of information would be necessary to better understand the limitations of only using satellite images.

This analysis of habitat selection and grubbing likelihood was dependent on snow maps at high temporal resolution. Drone-based assessments are sensitive to strong winds (common in the area), require fieldwork and are spatially limited. Optical satellite data is great for upscaling to larger areas but dependent on cloud free days. In 2019, we were lucky with the number of cloud-free days, in years before and after there were fewer images available (Sentinel 2A in GEE). Moving forward, I suggest further studies that analyze the temporal resolution requirements of snow maps needed to adequately predict goose grubbing. For example, a single mid spring-season image may be enough to at least predict most likely grubbing hotspots for the season. Although satellite data may not be equally available each year, we showed that snowmelt timing is an important driver for habitat disturbance and that it is possible to study it at management relevant spatial scales. This will provide a better understanding about interannual variations in habitat use and disturbance. It can help predicting the consequences that changes of spring temperatures and snow cover will have on pink-footed geese and tundra habitats.

Although this study was limited to a specific ecosystem, the results and methodical approach may be applicable in other systems, e.g., goose disturbances elsewhere (Abraham et al. 2005) or systems where snow cover drives spatial and temporal habitat use herbivores (Ohashi et al. 2016). This study helps to better understand the causal relationships of the COAT state variables “grubbing impact” and “herbivore abundances” as described in Paper I, Table 1.

5.6 How do random forests classifiers perform in tundra environments?

For all the analytical papers included in this thesis (Paper II-IV), we used random forest (RF) classifiers as the main tool to distinguish ground cover classes. This provided a basis to gain a better understanding for optimization opportunities and transferability of RF classifiers, as well as to understand which optical and terrain-based predictor variables are likely most essential in tundra environments.

We chose the RF classifier because it was reported to provide good results in similar ecosystems or datasets (Fan 2013, Mascaro 2014, Karami et al. 2018). Instead of testing multiple classifiers, this allowed us to have more time to develop our ecological questions and test multiple types of predictor variables. Whether other classifiers would have performed better is highly speculative, but a recently published study that compared five classifiers using a very similar dataset as in Paper II, showed that RFs outperformed bayes, K-nearest neighbor, support vector machine and decision tree classifiers in classifying wetlands using drone images (Zhou et al. 2021). Although RF classifiers can handle many input variables, (Hastie et al. 2009) has shown that reducing the number of input variables and “branches” (mtry) in the prediction tree can improve classifications. In future, I would therefore pay more attention to optimizing the RF by trying variable selection functions (Saeys et al. 2007, Ehrlinger 2016) or testing parameter optimization functions to tune the decision trees (Kulkarni and Sinha 2012, Probst et al. 2019).

Better knowledge of what kind of predictor variables are best suited for distinguishing ground cover classes in a RF classifier can help to reduce overfitting (Saeys et al. 2007), improve transferability (Tuanmu et al. 2011) and limit time-consuming computations (Laliberte and Rango 2009). A comparison of variable importance values across the three sites in Paper II and the study of Paper IV (both tundra environments), suggests that optical variables were more important than terrain variables to distinguish between classes. Of the optical variables NIR related layers (NIR or NDVI) were of great importance in both papers. Although terrain related variables were overall less important, their inclusion improved the RF performance in both studies. This corresponds with the findings of other drone and satellite-based RF classification studies (e.g. Dubeau et al. 2017, Díaz-Delgado et al. 2019). In both Paper II and IV, we tested a variation of neighborhood sizes because it has been shown that neighborhood size can be of great importance for the value of the predictor variable (Fan 2013, Wang et al. 2015). Common for both studies was that larger neighborhoods generally had higher variable importance values than those with smaller neighborhoods. Small scale terrain characteristics like ruggedness were either not unique descriptors for particular ground cover classes, or noise due to gaps and shadows distorted the differences (Lu and He 2018). Careful evaluation of the variable importance values can give an indication on which spatial layers to collect in future field campaigns.

Our results suggest that the most promising results for future drone-based classification surveys in similar environments can be expected from high resolution images that include a NIR band. This is not surprising as NIR and NDVI are often used for plant biomass estimates e.g., (Wessels et al. 2006, Zhu and Liu 2015) or detecting landcover changes, e.g., (Lunetta et al.

2006, Jung and Chang 2015). Hennessy et al. (2020), however, point out that the NIR spectra is vulnerable to variations in moisture content and highlights the importance to red edge wavelengths for discrimination of vegetation classes. Because terrain feature layers improved the classifiers, they should be included, but it is not likely that spatial resolutions of one to two centimeters will provide better information than coarser resolutions of a few tenths of centimeters (Lu and He 2018). The most appropriate scales will depend on the targeted ground cover classes and ecosystem properties.

In Paper II, we tested the transferability of RF classifiers across different locations within the same type of environment and using the same drone. We applied the RF from each study site (Janssonhaugen, Sassendalen, Todalen) at the other two study sites. Transferability of the RFs was low with macro-F1 scores of 50% or less (Paper II, Figure 10). Low transferability rates could be attributed to local overfitting of the RF classifier, or that plant communities between study sites differed too much, and a classifier transfer thus would not be appropriate (Jin et al. 2018). The data of the study in Paper II suggests that both hypotheses were true. Transferability between Janssonhaugen and Sassendalen was best. More similar highly ranked importance values for these sites suggests these two sites had more similar plant communities. My personal observation was that the ground cover classes in Todalen were more diffuse and blended and thus more difficult to detect and compare across sites. This is supported by the fact that several of the highest variable importance scores for the Todalen RF were terrain derived variables with large neighborhood sizes and not picking up local variations. Larger neighborhood sizes can increase the risk for spatial autocorrelation and overfitting because nearby training and validation points will more likely have the same values. Low transferability of RFs has been documented elsewhere (Juel et al. 2015, Maxwell et al. 2016, Jin et al. 2018), but can be improved by applying transformation matrices (Segev et al. 2015) or reducing the number of classes (Miranda et al. 2020). Alternative classifiers or deep learning approaches should also be tested (Zhang et al. 2019, Tong et al. 2020). How much attention should be placed on temporal and/or spatial transferability of the classifier will essentially depend on the monitoring goals and available resources.

5.7 What have I learned from using photogrammetry and drones in tundra environments in the context of adaptive monitoring?

The use of drones in ecology has markedly increased during the past five years. The fact that most of the drone-related articles referred to in this thesis were published after I started my PhD in late 2018, I think, illustrates the point quite well. In Norway non-commercial drone airspace regulations were very vague (a colleague described it as the “wild west era”) but more harmonized European regulations have been implemented at the start of 2021 (<https://luftfartstilsynet.no>). Technological advancements, cheaper equipment and ecologists that have pushed the industry to provide products suitable for scientific work has led to a quick growth of the field of drone ecology (Crutsinger et al. 2016). Similarly, the use of drone images in science has evolved from “taking images from the air” to methodically robust procedures and a range of guidelines to standardize data collection and processing, (e.g. Aasen et al. 2018,

Assmann et al. 2019, Tmušić et al. 2020). With the workflow we presented in Paper II, we contributed to the process of fully integrating drones as a tool in ecology. We emphasized, like with other scientific methods, the importance of documenting and reflecting how methodological decisions will affect the study's outcome. I think there is a risk in remote sensing that research is driven by visual detectability. Drones are a great tool in ecology but decisions on pixel sizes and ground-cover class detail should be based on an ecological understanding and documented in hypotheses like we present in Paper II, Table 1.

5.7.1 The hardware

Calibrated data and methods that can easily be repeated are key assets in adaptive long-term monitoring (Lindenmayer and Likens 2010). Therefore, I tried to find a drone and post-processing procedures that can be easily repeated and do not require extensive specialized training. Throughout the time of my thesis, I used both a small multi-copter drone (Figure 1a) and the fixed wing (Figure 1b). The multi-copter drone (dji – phantom 4 pro) would have been suitable for long-term monitoring because it is easy to fly, quite light and comparably cheap. Using it under Arctic conditions has, however, proven to be difficult. Our drone did not have the ability to use GLONASS satellites, so positioning was less accurate, high soil iron content was probably disturbing the compass, and strong winds made it often not possible to fly the drone. We also struggled to cover enough area on a single flight day as we wanted to cover the full extent of the COAT vegetation/goose monitoring sites. The dji phantom 4 pro drone can be rigged to have a multispectral camera as payload, but we did not explore that route further. Instead, we added a single band, additional NIR camera (<https://sentera.com/>) onto the drone but we battled with extracting standardized NIR values that were not readily processed into a NDVI value. The RGB images we obtained from this drone were however of excellent quality and with better spectral calibration routines I would not out-rule this drone for future assessments. The fixed wing drone (eBeeX - sensefly) with the real-time kinematic (RTK) link and pre-calibrated camera required more up-front learning and preparation time. RGB image quality was comparable to the multi-copter drone but post-processing of the images was much easier. Although the fixed wing drone and processing software (Pix4D Mapper) are more expensive, it seems like a good solution for monitoring programs such as COAT, where a lot of data has to be collected within a very short summer season and image processing will be in the hands of technicians (as opposed to students with time and interest to explore new avenues). Personally, I would like to spend more time to explore the world of home-built drones and open-source photogrammetry software to tailor the tool to the state variables of interest, but this would be an unlikely avenue in long-term monitoring programs that depend on steady tools and robust data.

5.7.2 Photogrammetry

The structure-from-motion (SfM) method uses image angles and pixel color signatures to generate three-dimensional surface models. These point clouds can be ten times denser than those generated from airborne lidar (Cunliffe et al. 2016, Fraser et al. 2016). Structure-from-motion has even been used to generate an Arctic-wide terrain model at two-meter resolution from overlapping satellite images (www.pgc.umn.edu/data/arcticdem). This terrain model was

good enough that I used it for all of my flight planning when using the fixed wing drone. Because SfM creates a 3D model of the surface, we need to make a big distinction between using photogrammetry in treeless environments and those covered in trees or bushes. In high-Arctic tundra and alpine environments we were able to create surface models that were similar to the terrain because maximum vegetation heights were around 20 cm. In other systems or seasons, SfM will detect bushes (Alonzo et al. 2020, Cunliffe et al. 2020) or snow heights (Goetz and Brenning 2019). Beyond shrub-less tundra, our methods and findings are likely most similar to arid savanna regions with little erect vegetation (Koci et al. 2017). The processing powers needed to join hundreds of drone images is usually more than that of an average laptop given to an ecologist. Processing power limitations and considerations are often mentioned in scientific articles within the field, (e.g. Koci et al. 2017, Assmann et al. 2019) and need to be considered before data is collected. I used a temporary server to process my data. This was useful because I did not need the processing capacities all year round and saved cost for buying a more powerful computer. But it took several months to find the right resources at the University, and I was dependent on the IT department to make changes to the server. In a project with long-term perspective like COAT, a stable processing platform (physical or server) will be essential for effective data management.

5.7.3 Upscaling

I think one of the biggest advantages with drone images is that it improves the quality of information we obtain from satellite images. Most research institutes without specialized personnel are limited to fly drones within “line of sight”. This restricts the area that can be effectively mapped on a single field day to a few square kilometers (small fixed wing). Drone technology as a tool in ecology will therefore likely be restricted to areas of a few km² and not to map entire valley systems. Many Arctic regions are difficult to access and regular “line of sight” flights with drones is an unlikely scenario. Climatic conditions make it especially challenging to operate drones in many Arctic regions (Kramar 2019). Satellite-based observation technologies are therefore important tools to detect and document environmental change in Arctic tundra ecosystems (Beamish et al. 2020). One of the biggest challenges with Arctic remote sensing is accessibility to proficient ground truthing information and this is where drone images can contribute substantially (Beamish et al. 2020). Drone images can help with spectral unmixing and provide information about spatial heterogeneity otherwise lost in satellite images. For example, a decline in NDVI is caused by overall reduction in biomass or a larger percentage of bare ground and otherwise changed vegetation (Assmann et al. 2020). I do not think that drone images will replace satellite-based monitoring programs. But I see them as an essential tool to increase the type and quality of information we can obtain from satellites. In the context of COAT, in the future, they can help with upscaling ground-cover classifications, disturbance detections and improve snow cover maps.

5.8 Limitations and outlook

One of the goals with this thesis was to “put numbers” on some of the arrows and boxes of the moss tundra conceptual model presented in Paper I and quantify the state variables stated as COAT monitoring goals (Table 1 in Paper I). In the paragraphs below, I will evaluate and

discuss which of these state variables we were able to measure and provide suggestions for future studies and monitoring approaches. This includes the vegetation module state variables that were studied in this thesis (ice damage, vegetation type/bare ground, abundance of herbivores, grubbing impact) and two state variables that were listed as monitoring goals for drones (productivity at peak-season /phenology) or are closely related (snow cover) but not quantified in this thesis.

5.8.1 Ice damage (winter damage)

One COAT state variable is the monitoring of the temporal and spatial changes in the occurrence of ice damage. In this thesis and in Paper II, we used a broader term “winter damage” to acknowledge that besides icing events, also other factors can cause plants to be damaged/die during the winter: for example, through late season freezing or general exposure to extremely cold temperatures. It was possible to detect winter damage in the landscape using drones as a mixed class with biological crust, rather than an independent class. Detecting winter damage as its own unique class will therefore be a challenge in the future. Separation between winter damage and biological crust was best in Todalen (compared to the other two sites) and a more detailed analysis to understand why they were better distinguished there, as well as more detailed ground truthing data, may improve the classifications. Detecting newly occurring winter damage in previously healthy vegetation through annual repeat measurements via drone images will likely be a suitable tool. This could yield estimates on the area and type of terrain affected. With additional data on snow and weather conditions, this may even help to reveal some causal relationships on winter damage occurrences. In future, I would recommend to compare the drone winter damage maps with annual field transects (2016 - 2021) that document winter damage in selected sites. These transects could act as additional ground truthing datapoints to make better maps. Or the winter damage maps can give an indication of how representative these transects are to characterize winter damage occurrences within the area.

5.8.2 Vegetation types/bare ground

The drone-based and simplified satellite-based image classifications showed promising results regarding monitoring of the most important vegetation types and the extent of bare ground. Some visually similar vegetation classes will be difficult to detect with drone images and I would suggest not to rely on drone images alone. Of the expected vegetation changes, the expansion of *Equisetum* spp. and *Carex subspathacea* are likely the easiest to detect because of their distinct coloration. Our results suggest that bare ground within the moss tundra habitats can be successfully monitored using drone images. This will be especially useful information for upscaling and biomass estimate comparisons with satellite images. The limitation with the drone-based bare ground mapping is that this detects the state but not the drivers that cause it (biological, physical or combination thereof). Knowledge about the terrain and goose densities will, however, help to attribute bare ground emergence to some of the most likely causes.

5.8.3 Abundance of herbivores

My original plan was to count geese using drones. Pink-footed geese are known to be very shy during breeding season (Madsen et al. 2009) but preliminary tests at a staging area in Finland has shown that it is possible take drone images of resting flocks (Jesper Madsen, personal communication). During the pre-breeding period in Svalbard, pink-footed geese showed behavior more similar to that of the breeding season and just like planes and helicopters they noticed the drone in the air. Therefore, I could not assume that they show natural behavior when approaching them with a drone, and instead, counted geese and located their spatial positions manually. This provided information on where the highest goose densities were. This approach was time consuming, and I would not recommend it as a regular survey method. Previous goose counts in the area were conducted by noting the number of geese in several corridors (Anderson et al. 2015). I would recommend a corridor approach but decrease the size (to e.g. 0.5 km²) of these corridors to have more spatially explicit information on high or low goose densities to estimate disturbance likelihoods. These goose density estimates could be linked to changes in NDVI to assess whether high interannual variability in goose densities is detectible using satellite images.

5.8.4 Grubbing impact

Through the work conducted in this thesis I have learned a lot about detectability and predictors of grubbing extent and intensity (Paper II, III), but less so on the impact of grubbing on tundra landscapes. This thesis has thus prepared the tools to better monitor grubbing impact in the future. Two topics that should be considered when studying the impacts of grubbing are vegetation recovery and terrain changes induced by geese. I had planned to include a recovery study in this thesis but due to travelling restrictions in 2020 this was not possible.

A preliminary analysis of data (NDVI values in drone images), collected in 2021, suggests that regrowth of grubbed areas after two years was high. I assume that drones will therefore be a useful tool to track vegetation regrowth after grubbing. Tracking detailed changes in plant community composition using drone images alone will be difficult. Therefore, I would suggest a form of hybrid monitoring where drone images can be used to assist field-based assessments by delineating areas that have been impacted. The biggest challenge with studying habitat regrowth is that we do not know where the new disturbances will occur. Drone images can therefore help to match similar areas that have been generally undisturbed to those that have recently been regrown. Field-assessments could then be used to compare these areas with one another and included into long-term recovery study.

One of the most pressing questions about pink-footed goose grubbing is on how much they change the terrain and modify vegetation and soil properties with their specialized feeding technique. The timeframe of this thesis unfortunately did not allow me to study this in detail. I (and others) have observed that previously grubbed areas often are located in slightly lower areas than the surrounding terrain. Terrain changes could also be studied using a hybrid field and drone approach. High resolution 3D point clouds or DSMs and NDVI maps of at least three consecutive years would be necessary to assess this hypothesis using drones. The NDVI maps would help to identify areas that were undisturbed in year 1, disturbed in year 2 and regrown in

year 3. These areas could then be analyzed in the field and compared to areas that remained undisturbed throughout the three years. Using drone-based terrain models and snow depth estimates in combination with field assessments could then be used to assess if goose grubbing has caused changes in hydrology or snow accumulation. Alternatively, automatic cameras could be used to monitor snowmelt at selected “disturbance recovery sites” to assess if snowmelt patterns are impacted by grubbing. The challenge with surface model-based terrain monitoring approaches is that they measure the surface and do not distinguish between vegetation or water. Thus, if newly grubbed areas fill up with water, no terrain changes would be detected. Again, a hybrid version of using drone images to detect disturbance hotspots and detailed field assessments and/or automatic camera-based monitoring would be a good approach to study how grubbing may lead to a change in hydrology.

5.8.5 Productivity at peak-season/phenology

Both productivity at peak-season and phenology are listed as state variables that could be monitored using drones (Table 1 in Paper I). We did not study productivity at peak-season in any of the studies published through this thesis. We did, however, collect the information needed to estimate productivity. The drone images provided reliable NDVI measurements and were collected at peak-season. Unfortunately, we did not have time to collect repeat images within the same area to determine the seasonal maximum NDVI. Estimating productivity in very wet moss areas is difficult because NDVI is sensitive to moisture which leads to overestimations. A possible method to overcome this problem is to use the classified maps and first distinguish the major ground cover types and then only compare changes in NDVI with the classes. Further, I suggest using the COAT point framing monitoring plots to calibrate the drone NDVI measurements to actual biomass estimates and/or test if other vegetation indices (e.g., red edge-based ones) would be better estimators in wet moss tundra. Similarly, would phenology measurements generally be possible with the types of images that we collected but a higher temporal resolution of both flights and field plots would be necessary to obtain robust indicators of phenology.

5.8.6 Snow cover

Although snow cover mapping was not listed as any of the state variables directly linked to the moss tundra module (Table 1 in Paper I) this kind of information is of general interest to COAT monitoring and a key driver in other monitoring modules (Ims et al. 2013). During the spring season field work we collected drone images on several days that match a cloud-free satellite image. This data could be analyzed to get a better understanding on how information loss occurs when upscaling from centimeter to ten-meter scale. It would be possible to calculate how high the percentage of snow-free area on the ground has to be before it is detected as snow-free in a satellite image. This could possibly be used to perform spectral unmixing. The good quality of the drone images would also help to detect areas with dirty or wet snow and help to improve snow-no snow classifications of satellite images.

6 Conclusion

This thesis, as also shown by others, has demonstrated that defining conceptual models can help developing hypotheses and specifying targets for monitoring goals. With our conceptual models of Svalbard's moss tundra, we emphasized the need to detect both long-term trends and short-term disturbance events and the necessity of quantifiable state variables that can describe changes to the ecosystem at relevant spatial and temporal scales. We further highlight that a full understanding of states and state drivers of Svalbard's (and other Arctic) terrestrial ecosystems requires more work. We showed that drone images can be useful tools to quantify several state variables, such as the distribution of vegetation types, bare ground, snow cover extent and disturbances, such as winter damage and pink-footed goose grubbing. Further, we were able to use drone images, satellite images and field surveys as a tool to map snowmelt progression, and link this to pink-footed grubbing likelihoods in the landscape. Successful ground cover type classifications using random forests were mostly dependent on optical variables, especially near-infrared, but terrain-related variables generally improved the classifiers. The timeframe of the thesis did not allow me to evaluate how well drone images will perform in long-term monitoring (i.e., repeated measures on, for instance, seasonal or annual scales), but the data collected will provide a baseline for monitoring and state-change studies on Svalbard's tundra ecosystem in the future. We are just at the beginning of exploring the potential that drone images offer to ecology. Our studies have shown that collecting ground truthing data in the field requires a good understanding of focal ecosystem components and their interactions with both abiotic and biotic factors, to not only detect visually distinctive, but also ecologically relevant ground cover classes. A close integration of detailed field-based assessments and drone images can elevate studies of causal ecological relationships into a spatial context. In addition, drone images will continue to improve the quality of information we gain from satellite-based remote sensing. For these reasons, I encourage closer collaboration between photogrammetrists, remote sensors and ecologists to take advantage of the full potential remote sensing technologies offer to the field of ecology and perhaps to remote sensing as well. This thesis has expanded our toolset to study a rapidly changing Arctic by showing that approaches of studying biotic and abiotic interactions can be successful. It has therefore served as an attempt to merge the fields of Arctic tundra ecology and remote sensing, and its results will hopefully encourage future interdisciplinary studies and cooperation.

7 References

- Aasen, H., E. Honkavaara, A. Lucieer, and P. J. Zarco-Tejada. 2018. Quantitative remote sensing at ultra-high resolution with UAV spectroscopy: A review of sensor technology, measurement procedures, and data correction workflows. *Remote Sensing* 10.
- Abraham, K. F., R. L. Jefferies, and R. T. Alisauskas. 2005. The dynamics of landscape change and snow geese in mid-continent north america. *Global Change Biology* 11:841–855.
- Adler, P., D. Raff, and W. Lauenroth. 2001. The effect of grazing on the spatial heterogeneity of vegetation. *Oecologia* 128:465–479.
- Agnelli, A., G. Corti, L. Massaccesi, S. Ventura, and L. P. D’Acqui. 2021. Impact of biological crusts on soil formation in polar ecosystems. *Geoderma* 401:115340.
- Albon, S. D., R. J. Irvine, O. Halvorsen, R. Langvatn, L. E. Loe, E. Ropstad, V. Veiberg, R. Van Der Wal, E. M. Bjørkvoll, E. I. Duff, and others. 2017. Contrasting effects of summer and winter warming on body mass explain population dynamics in a food-limited arctic herbivore. *Global change biology* 23:1374–1389.
- Alonzo, M., R. J. Dial, B. K. Schulz, H.-E. Andersen, E. Lewis-Clark, B. D. Cook, and D. C. Morton. 2020. Mapping tall shrub biomass in alaska at landscape scale using structure-from-motion photogrammetry and lidar. *Remote Sensing of Environment* 245:111841.
- Anderson, H. B., C. E. Hübner, J. D. M. Speed, J. Madsen, and R. van der Wal. 2015. Biding time before breeding: Flexible use of the arctic landscape by migratory geese during spring. *Polar Research* 34.
- Anderson, H. B., J. D. M. Speed, J. Madsen, Å. Ø. Pedersen, I. M. Tombre, and R. van der Wal. 2016. Late snow melt moderates herbivore disturbance of the arctic tundra. *Écoscience* 23:29–39.
- Anderson, K., and K. J. Gaston. 2013. Lightweight unmanned aerial vehicles will revolutionize spatial ecology. *Frontiers in Ecology and the Environment* 11:138–146.
- Anderson, K., M. J. Westoby, and M. R. James. 2019. Low-budget topographic surveying comes of age: Structure from motion photogrammetry in geography and the geosciences. *Progress in Physical Geography: Earth and Environment* 43:163–173.
- Arrhenius, S. 1896. XXXI. On the influence of carbonic acid in the air upon the temperature of the ground. *The London, Edinburgh, and Dublin Philosophical Magazine and Journal of Science* 41:237–276.
- Asefa, D., G. Oba, R. Weladji, and J. Colman. 2003. An assessment of restoration of biodiversity in degraded high mountain grazing lands in northern ethiopia. *Land degradation & development* 14:25–38.
- Assmann, J. J., J. T. Kerby, A. M. Cunliffe, and I. H. Myers-Smith. 2019. Vegetation monitoring using multispectral sensors — best practices and lessons learned from high latitudes. *Journal of Unmanned Vehicle Systems* 7:54–75.
- Assmann, J. J., I. H. Myers-Smith, J. T. Kerby, A. M. Cunliffe, and G. N. Daskalova. 2020. Drone data reveal heterogeneity in tundra greenness and phenology not captured by satellites. *Environmental Research Letters* 15:125002.
- Bagaram, M. B., D. Giuliarelli, G. Chirici, F. Giannetti, and A. Barbati. 2018. UAV remote sensing for biodiversity monitoring: Are forest canopy gaps good covariates? *Remote Sensing* 10.
- Barnas, A. F., D. Chabot, A. J. Hodgson, D. W. Johnston, D. M. Bird, and S. N. Ellis-Felege. 2020. A standardized protocol for reporting methods when using drones for wildlife research. *Journal of Unmanned Vehicle Systems* 8:89–98.
- Barrio, I. C., D. S. Hik, J. Þórsson, K. Svavarsdóttir, B. Marteinsdóttir, and I. S. Jónsdóttir. 2018. The sheep in wolf’s clothing? Recognizing threats for land degradation in iceland using state-and-transition models. *Land Degradation & Development* 29:1714–1725.

- Barrio, I. C., E. Lindén, M. Te Beest, J. Olofsson, A. Rocha, E. M. Soininen, J. M. Alatalo, T. Andersson, A. Asmus, J. Boike, and others. 2017. Background invertebrate herbivory on dwarf birch (*Betula glandulosa-nana* complex) increases with temperature and precipitation across the tundra biome. *Polar Biology* 40:2265–2278.
- Beamish, A., M. K. Reynolds, H. Epstein, G. V. Frost, M. J. Macander, H. Bergstedt, A. Bartsch, S. Kruse, V. Miles, C. M. Tanis, and others. 2020. Recent trends and remaining challenges for optical remote sensing of arctic tundra vegetation: A review and outlook. *Remote Sensing of Environment* 246:111872.
- Belgiu, M., and L. Drăguț. 2016. Random forest in remote sensing: A review of applications and future directions. *ISPRS Journal of Photogrammetry and Remote Sensing* 114:24–31.
- Bentley, C., and A. Anandhi. 2020. Representing driver-response complexity in ecosystems using an improved conceptual model. *Ecological Modelling* 437:109320.
- Berner, L. T., R. Massey, P. Jantz, B. C. Forbes, M. Macias-Fauria, I. Myers-Smith, T. Kumpula, G. Gauthier, L. Andreu-Hayles, B. V. Gaglioti, and others. 2020. Summer warming explains widespread but not uniform greening in the arctic tundra biome. *Nature Communications* 11:1–12.
- Bernsteiner, H., N. Brožová, I. Eischeid, A. Hamer, S. Haselberger, M. Huber, A. Kollert, T. Vandyk, and F. Pirotti. 2020. MACHINE LEARNING FOR CLASSIFICATION OF AN ERODING SCARP SURFACE USING TERRESTRIAL PHOTOGRAMMETRY WITH NIR AND RGB IMAGERY. *ISPRS Annals of Photogrammetry, Remote Sensing & Spatial Information Sciences* 5.
- Bestelmeyer, B. T. 2006. Threshold concepts and their use in rangeland management and restoration: The good, the bad, and the insidious. Wiley Online Library.
- Bintanja, R. 2018. The impact of arctic warming on increased rainfall. *Scientific Reports* 8.
- Bjerke, J. W., R. Treharne, D. Vikhamar-Schuler, S. R. Karlsen, V. Ravolainen, S. Bokhorst, G. K. Phoenix, Z. Bochenek, and H. Tømmervik. 2017. Understanding the drivers of extensive plant damage in boreal and arctic ecosystems: Insights from field surveys in the aftermath of damage. *Science of The Total Environment* 599-600:1965–1976.
- Bjune, A. E. 2000. Pollen analysis of faeces as a method of demonstrating seasonal variations in the diet of svalbard reindeer (*rangifer tarandus platyrhynchus*). *Polar Research* 19:183–192.
- Bokhorst, S., S. Pedersen, L. Brucker, O. Anisimov, J. Bjerke, R. Brown, D. Ehrlich, R. Essery, A. Heilig, S. Ingvander, C. Johansson, M. Johansson, I. Jónsdóttir, N. Inga, K. Luojus, G. Macelloni, H. Mariash, D. McLennan, G. Rosqvist, and T. Callaghan. 2016. Changing arctic snow cover: A review of recent developments and assessment of future needs for observations, modelling, and impacts. *Ambio* 45.
- Bonnin, N., A. C. Van Andel, J. T. Kerby, A. K. Piel, L. Pintea, and S. A. Wich. 2018. Assessment of chimpanzee nest detectability in drone-acquired images. *Drones* 2.
- Bråthen, K. A., R. A. Ims, N. G. Yoccoz, P. Fauchald, T. Tveraa, and V. H. Hausner. 2007. Induced shift in ecosystem productivity? Extensive scale effects of abundant large herbivores. *Ecosystems* 10:773–789.
- Breiman, L. 2001. Random forests. *Machine learning* 45:5–32.
- Burt, T. 1994. Long-term study of the natural environment-perceptive science or mindless monitoring? *Progress in Physical Geography* 18:475–496.
- Clausen, K., K. Schreven, and J. Madsen. 2020. Effects of capture and marking on the behaviour of moulting pink-footed geese *anser brachyrhynchus* on svalbard. *Wildfowl* 70:13–29.
- Cortez, P. 2020. Rminer: Data mining classification and regression methods.
- Creutzburg, M. K., J. E. Halofsky, J. S. Halofsky, and T. A. Christopher. 2015. Climate change and land management in the rangelands of central oregon. *Environmental Management* 55:43–55.
- Crutsinger, G. M., J. Short, and R. Sollenberger. 2016. The future of UAVs in ecology: An insider perspective from the silicon valley drone industry. *Journal of Unmanned Vehicle Systems* 4:161–168.

- Cubero-Castan, M., K. Schneider-Zapp, M. Bellomo, D. Shi, M. Rehak, and C. Strecha. 2018. Assessment of the radiometric accuracy in a target less work flow using Pix4D software. Pages 1–4 2018 9th workshop on hyperspectral image and signal processing: Evolution in remote sensing (WHISPERS).
- Cunliffe, A. M., R. E. Brazier, and K. Anderson. 2016. Ultra-fine grain landscape-scale quantification of dryland vegetation structure with drone-acquired structure-from-motion photogrammetry. *Remote Sensing of Environment* 183:129–143.
- Cunliffe, A. M., C. D. McIntire, F. Boschetti, K. J. Sauer, M. Litvak, K. Anderson, and R. E. Brazier. 2020. Allometric relationships for predicting aboveground biomass and sapwood area of oneseed juniper (*Juniperus monosperma*) trees. *Frontiers in plant science* 11:94.
- Cutler, A., D. R. Cutler, and J. R. Stevens. 2012. Random forests. Pages 157–175 in C. Zhang and Y. Ma, editors. *Ensemble machine learning: Methods and applications*. Springer US, Boston, MA.
- Daryaei, A., H. Sohrabi, C. Atzberger, and M. Immitzer. 2020. Fine-scale detection of vegetation in semi-arid mountainous areas with focus on riparian landscapes using sentinel-2 and UAV data. *Computers and Electronics in Agriculture* 177:105686.
- Dash, J. P., G. D. Pearse, and M. S. Watt. 2018. UAV multispectral imagery can complement satellite data for monitoring forest health. *Remote Sensing* 10.
- Díaz-Delgado, R., C. Cazacu, and M. Adamescu. 2019. Rapid assessment of ecological integrity for LTER wetland sites by using UAV multispectral mapping. *Drones* 3:3.
- Domine, F., G. Gauthier, V. Vionnet, D. Fauteux, M. Dumont, and M. Barrere. 2018. Snow physical properties may be a significant determinant of lemming population dynamics in the high arctic. *Arctic Science* 4:813–826.
- Dubeau, P., D. J. King, D. G. Unbushe, and L.-M. Rebelo. 2017. Mapping the dabus wetlands, ethiopia, using random forest classification of landsat, PALSAR and topographic data. *Remote Sensing* 9:1056.
- Duffy, J. P., K. Anderson, D. Fawcett, R. J. Curtis, and I. M. Maclean. 2021. Drones provide spatial and volumetric data to deliver new insights into microclimate modelling. *Landscape Ecology*:1–18.
- Ehrlinger, J. 2016. ggRandomForests: Exploring random forest survival. arXiv preprint arXiv:1612.08974.
- Elmendorf, S. C., G. H. Henry, R. D. Hollister, R. G. Björk, N. Boulanger-Lapointe, E. J. Cooper, J. H. Cornelissen, T. A. Day, E. Dorrepaal, T. G. Elumeeva, and others. 2012. Plot-scale evidence of tundra vegetation change and links to recent summer warming. *Nature climate change* 2:453–457.
- Elvebakk, A. 2005. A vegetation map of svalbard on the scale 1:3.5 mill. *Phytocoenologia* 35:951–967.
- ESA. 2022. https://www.esa.int/Enabling_Support/Operations/Sentinel-2_operations
- Evans, J. S. 2020. spatialEco: Spatial analysis and modelling utilities.
- Fan, H. 2013. Land-cover mapping in the nujiang grand canyon: Integrating spectral, textural, and topographic data in a random forest classifier. *International Journal of Remote Sensing* 34:7545–7567.
- Fölster, J., R. K. Johnson, M. N. Futter, and A. Wilander. 2014. The swedish monitoring of surface waters: 50 years of adaptive monitoring. *AMBIO* 43:3–18.
- Førland, E. J., R. Benestad, I. Hanssen-Bauer, J. E. Haugen, and T. E. Skaugen. 2011. Temperature and precipitation development at svalbard 1900–2100. *Advances in Meteorology* 2011.
- Fox, A., I. S. Francis, and E. Bergersen. 2006. Diet and habitat use of svalbard pink-footed geese *Anser brachyrhynchus* during arrival and pre-breeding periods in adventdalen. *Ardea* 94:691–699.
- Fraser, R. H., I. Olthof, T. C. Lantz, and C. Schmitt. 2016. UAV photogrammetry for mapping vegetation in the low-arctic. *Arctic Science* 2:79–102.
- Fukami, T., and M. Nakajima. 2011. Community assembly: Alternative stable states or alternative transient states? *Ecology Letters* 14:973–984.
- Gao, Y., A. Quevedo, Z. Szantoi, and M. Skutsch. 2021. Monitoring forest disturbance using time-series MODIS NDVI in michoacán, mexico. *Geocarto International* 36:1768–1784.

- Garmin. 2022. . Garmin US. - <https://support.garmin.com/en-US/?faq=z0n0KE1XVF0Pe4Su8QiZgA>
- Goetz, J., and A. Brenning. 2019. Quantifying uncertainties in snow depth mapping from structure from motion photogrammetry in an alpine area. *Water Resources Research* 55:7772–7783.
- Grime, J. 1979. *Plant strategies and vegetation processes* John Wiley. New York.
- Grosse, G., S. Goetz, A. D. McGuire, V. E. Romanovsky, and E. A. Schuur. 2016. Changing permafrost in a warming world and feedbacks to the earth system. *Environmental Research Letters* 11:040201.
- Handa, I. T., R. Harmsen, and R. L. Jefferies. 2002. Patterns of vegetation change and the recovery potential of degraded areas in a coastal marsh system of the hudson bay lowlands. *Journal of Ecology* 90:86–99.
- Hansen, B. B., M. Gamelon, S. D. Albon, A. M. Lee, A. Stien, R. J. Irvine, B.-E. Sæther, L. E. Loe, E. Ropstad, V. Veiberg, and others. 2019a. More frequent extreme climate events stabilize reindeer population dynamics. *Nature Communications* 10:1–8.
- Hansen, B. B., V. Grøtan, R. Aanes, B.-E. Sæther, A. Stien, E. Fuglei, R. A. Ims, N. G. Yoccoz, and Å. Ø. Pedersen. 2013. Climate events synchronize the dynamics of a resident vertebrate community in the high arctic. *Science* 339:313–315.
- Hansen, B. B., K. Isaksen, R. E. Benestad, J. Kohler, Å. Ø. Pedersen, L. E. Loe, S. J. Coulson, J. O. Larsen, and Ø. Varpe. 2014. Warmer and wetter winters: Characteristics and implications of an extreme weather event in the high arctic. *Environmental Research Letters* 9:114021.
- Hansen, B. B., Å. Ø. Pedersen, B. Peeters, M. Le Moullec, S. D. Albon, I. Herfindal, B.-E. Sæther, V. Grøtan, and R. Aanes. 2019b. Spatial heterogeneity in climate change effects decouples the long-term dynamics of wild reindeer populations in the high arctic. *Global Change Biology* 25:3656–3668.
- Hansen, B., and R. Aanes. 2012. Kelp and seaweed feeding by high-arctic wild reindeer under extreme winter conditions. *Polar Research* 31:17258.
- Haralick, R. M., K. Shanmugam, and I. H. Dinstein. 1973. Textural features for image classification. *IEEE Transactions on systems, man, and cybernetics*:610–621.
- Hastie, T., R. Tibshirani, and J. Friedman. 2009. *The elements of statistical learning: Data mining, inference and prediction*. Second edition. Springer.
- Hastings, A., J. E. Byers, J. A. Crooks, K. Cuddington, C. G. Jones, J. G. Lambrinos, T. S. Talley, and W. G. Wilson. 2007. Ecosystem engineering in space and time. *Ecology Letters* 10:153–164.
- Heldbjerg, H., F. Johnson, K. Koffijberg, R. McKenzie, S. Nagy, G. Jensen, J. Madsen, and J. Baveco. 2021. EGMP population status and assessment report. 6th meeting of the AEWA european goose management international working group.
- Hennessy, A., K. Clarke, and M. Lewis. 2020. Hyperspectral classification of plants: A review of waveband selection generalisability. *Remote Sensing* 12:113.
- Hijmans, R. J. 2020. *Raster: Geographic data analysis and modeling*.
- Holland, M. M., and C. M. Bitz. 2003. Polar amplification of climate change in coupled models. *Climate Dynamics* 21:221–232.
- Hu, F. S., P. E. Higuera, P. Duffy, M. L. Chipman, A. V. Rocha, A. M. Young, R. Kelly, and M. C. Dietze. 2015. Arctic tundra fires: Natural variability and responses to climate change. *Frontiers in Ecology and the Environment* 13:369–377.
- Hubbard Brook ecosystem study. 2022. <https://hubbardbrook.org/>.
- Hudson, J. M., and G. Henry. 2009. Increased plant biomass in a high arctic heath community from 1981 to 2008. *Ecology* 90:2657–2663.
- Huylbroeck, L., M. Laslier, S. Dufour, B. Georges, P. Lejeune, and A. Michez. 2020. Using remote sensing to characterize riparian vegetation: A review of available tools and perspectives for managers. *Journal of Environmental Management* 267:110652.

- Ims, R. I., U. Jepsen J., A. Stien, and N. G. Yoccoz. 2013. Science plan for COAT: Climate-ecological observatory for arctic tundra. Fram Centre, Norway.
- IPPC - M., M., S. M., C. S., D. C., E. A., H. A., K. G., M. A., M.-T. J., M. M. M. C., O. G., P. H., and S. E. A. G. 2019. Polar regions. Pages 203–320 in H.-O. Pörtner, D. C. Roberts, V. Masson-Delmotte, P. Zhai, M. Tignor, E. Poloczanska, K. Mintenbeck, A. Alegría, M. Nicolai, A. Okem, J. Petzold, B. Rama, and N. M. Weyer, editors. The ocean and cryosphere in a changing climate. A special report of the intergovernmental panel on climate change. Book Section, IPCC, Geneva.
- Jefferies, R. L., and R. F. Rockwell. 2002. Foraging geese, vegetation loss and soil degradation in an arctic salt marsh. *Applied Vegetation Science* 5:7–16.
- Jefferies, R. L., R. F. Rockwell, and K. F. Abraham. 2004a. The embarrassment of riches: Agricultural food subsidies, high goose numbers, and loss of arctic wetlands, a continuing saga. *Environmental Reviews* 11:193–232.
- Jefferies, R. L., R. F. Rockwell, and K. F. Abraham. 2004b. Agricultural Food Subsidies, Migratory Connectivity and Large-Scale Disturbance in Arctic Coastal Systems: A Case Study1. *Integrative and Comparative Biology* 44:130–139.
- Jepsen, J. U., M. Biuw, R. A. Ims, L. Kapari, T. Schott, O. P. L. Vindstad, and S. B. Hagen. 2013. Ecosystem impacts of a range expanding forest defoliator at the forest-tundra ecotone. *Ecosystems* 16:561–575.
- Jin, S., Y. Su, S. Gao, T. Hu, J. Liu, and Q. Guo. 2018. The transferability of random forest in canopy height estimation from multi-source remote sensing data. *Remote Sensing* 10:1183.
- Johansen, B. E., S. R. Karlsen, and H. Tømmervik. 2012. Vegetation mapping of svalbard utilising landsat TM/ETM data. *Polar Record* 48:47–63.
- Jones, R. 1992. Resting from grazing to reverse changes in sown pasture composition: Application of the. *Tropical Grasslands* 26:97–99.
- Jónsdóttir, I. S. 2005. Terrestrial ecosystems on svalbard: Heterogeneity, complexity and fragility from an arctic island perspective. Pages 155–165 *Biology and environment: Proceedings of the royal irish academy*. JSTOR.
- Joyce, K. E., K. Anderson, and R. E. Bartolo. 2021. Of course we fly unmanned—we’re women! *Drones* 5(1), 21.
- Juel, A., G. B. Groom, J.-C. Svenning, and R. Ejrnæs. 2015. Spatial application of random forest models for fine-scale coastal vegetation classification using object based analysis of aerial orthophoto and DEM data. *International Journal of Applied Earth Observation and Geoinformation* 42:106–114.
- Jung, M., and E. Chang. 2015. NDVI-based land-cover change detection using harmonic analysis. *International Journal of Remote Sensing* 36:1097–1113.
- Karami, M., A. Westergaard-Nielsen, S. Normand, U. A. Treier, B. Elberling, and B. U. Hansen. 2018. A phenology-based approach to the classification of arctic tundra ecosystems in greenland. *ISPRS Journal of Photogrammetry and Remote Sensing* 146:518–529.
- Keenan, T., and W. Riley. 2018. Greening of the land surface in the world’s cold regions consistent with recent warming. *Nature climate change* 8:825–828.
- Klein, D. R., G. D. Yakushkin, and E. B. Pospelova. 1993. Comparative habitat selection by muskoxen introduced to northeastern alaska and the taimyr peninsula, russia. *Rangifer* 13:21–25.
- Koci, J., J. X. Leon, B. Jarihani, R. C. Sidle, S. N. Wilkinson, and R. Bartley. 2017. Strengths and limitations of UAV and ground-based structure from motion photogrammetry in a gullied savanna catchment. University of the Sunshine Coast, Queensland.
- Koh, L. P., and S. A. Wich. 2012. Dawn of drone ecology: Low-cost autonomous aerial vehicles for conservation. *Tropical conservation science* 5:121–132.
- Kramar, V. 2019. UAS (drone) arctic challenges: Next steps. Proceedings of the FRUCT’25, Helsinki, Finland, 5-8 November 2019.

- Kulkarni, V. Y., and P. K. Sinha. 2012. Pruning of random forest classifiers: A survey and future directions. Pages 64–68 2012 international conference on data science & engineering (ICDSE). IEEE.
- Laliberte, A. S., and A. Rango. 2009. Texture and scale in object-based analysis of subdecimeter resolution unmanned aerial vehicle (UAV) imagery. *IEEE Transactions on Geoscience and Remote Sensing* 47:761–770.
- Lambert, J., J.-P. Denux, J. Verbesselt, G. Balent, and V. Cheret. 2015. Detecting clear-cuts and decreases in forest vitality using MODIS NDVI time series. *Remote Sensing* 7:3588–3612.
- Lantuit, H., W. Pollard, N. Couture, M. Fritz, L. Schirrmeister, H. Meyer, and H.-W. Hubberten. 2012. Modern and late holocene retrogressive thaw slump activity on the yukon coastal plain and herschel island, yukon territory, canada. *Permafrost and Periglacial Processes* 23:39–51.
- Lara, M. J., I. Nitze, G. Grosse, P. Martin, and A. D. McGuire. 2018. Reduced arctic tundra productivity linked with landform and climate change interactions. *Scientific Reports* 8:1–10.
- Lawrimore, J., R. Ray, S. Applequist, B. Korzeniewski, and M. Menne. 2021. Global summary of the month (GSOM), version 1. NOAA National Centers for Environmental Information.
- Le Moullec, M., A.-L. Hendel, M. P. Bon, I. S. Jonsdottir, O. Varpe, R. van der Wal, L. Beumer, K. Layton-Matthews, K. Isaksen, and B. B. Hansen. 2021. Towards rainy arctic winters: Experimental icing impacts tundra plant productivity and reproduction. pre print.
- Lindenmayer, C. A. A., David B. AND Zammit. 2012. A novel and cost-effective monitoring approach for outcomes in an australian biodiversity conservation incentive program. *PLOS ONE* 7:1–11.
- Lindenmayer, D. B., and G. E. Likens. 2009. Adaptive monitoring: A new paradigm for long-term research and monitoring. *Trends in Ecology & Evolution* 24:482–486.
- Lindenmayer, D. B., and G. E. Likens. 2010. The science and application of ecological monitoring. *Biological Conservation* 143:1317–1328.
- Liu, Q., S. Li, Z. Li, L. Fu, K. Hu, and others. 2017. Review on the applications of UAV-based LiDAR and photogrammetry in forestry. *Scientia Silvae Sinicae* 53:134–148.
- Lu, B., and Y. He. 2018. Optimal spatial resolution of unmanned aerial vehicle (UAV)-acquired imagery for species classification in a heterogeneous grassland ecosystem. *GIScience & Remote Sensing* 55:205–220.
- Lunetta, R. S., J. F. Knight, J. Ediriwickrema, J. G. Lyon, and L. D. Worthy. 2006. Land-cover change detection using multi-temporal MODIS NDVI data. *Remote Sensing of Environment* 105:142–154.
- Madsen, J., K. K. Clausen, T. K. Christensen, and F. A. Johnson. 2016. Regulation of the hunting season as a tool for adaptive harvest management — first results for pink-footed geese *Anser brachyrhynchus*. *Wildlife Biology* 22:204–208.
- Madsen, J., I. Tombre, and N. E. Eide. 2009. Effects of disturbance on geese in svalbard: Implications for regulating increasing tourism. *Polar Research* 28:376–389.
- Maes, W. H., A. R. Huete, and K. Steppe. 2017. Optimizing the processing of UAV-based thermal imagery. *Remote Sensing* 9.
- Mangewa, L. J., P. A. Ndakidemi, and L. K. Munishi. 2019. Integrating UAV technology in an ecological monitoring system for community wildlife management areas in tanzania. *Sustainability* 11.
- Mascaro, G. P. A. K., Joseph AND Asner. 2014. A tale of two “forests”: Random forest machine learning aids tropical forest carbon mapping. *PLOS ONE* 9:1–9.
- Maxwell, A. E., T. A. Warner, and M. P. Strager. 2016. Predicting palustrine wetland probability using random forest machine learning and digital elevation data-derived terrain variables. *Photogrammetric Engineering & Remote Sensing* 82:437–447.
- Maxwell, S. L., N. Butt, M. Maron, C. A. McAlpine, S. Chapman, A. Ullmann, D. B. Segan, and J. E. Watson. 2019. Conservation implications of ecological responses to extreme weather and climate events. *Diversity and Distributions* 25:613–625.

- Migala, K., B. Wojtuń, W. Szymański, and P. Muskała. 2014. Soil moisture and temperature variation under different types of tundra vegetation during the growing season: A case study from the faglebekken catchment, SW spitsbergen. *CATENA* 116:10–18.
- Millard, K., and M. Richardson. 2015. On the importance of training data sample selection in random forest image classification: A case study in peatland ecosystem mapping. *Remote sensing* 7:8489–8515.
- Milner, J. M., Ø. Varpe, R. van der Wal, and B. B. Hansen. 2016. Experimental icing affects growth, mortality, and flowering in a high arctic dwarf shrub. *Ecology and evolution* 6:2139–2148.
- Miranda, V., P. Pina, S. Heleno, G. Vieira, C. Mora, and C. E.G.R. Schaefer. 2020. Monitoring recent changes of vegetation in fildes peninsula (king george island, antarctica) through satellite imagery guided by UAV surveys. *Science of The Total Environment* 704:135295.
- Morgan, J. L., S. E. Gergel, and N. C. Coops. 2010. Aerial Photography: A Rapidly Evolving Tool for Ecological Management. *BioScience* 60:47–59.
- Mouselimis, L. 2020. ClusterR: Gaussian mixture models, k-means, mini-batch-kmeans, k-medoids and affinity propagation clustering.
- Muller, C. G., B. L. Chilvers, Z. Barker, K. P. Barnsdale, P. F. Battley, R. K. French, J. McCullough, and F. Samandari. 2019. Aerial VHF tracking of wildlife using an unmanned aerial vehicle (UAV): Comparing efficiency of yellow-eyed penguin (*megadyptes antipodes*) nest location methods. *Wildlife Research* 46:145–153.
- Myers-Smith, I. H., S. C. Elmendorf, P. S. Beck, M. Wilmking, M. Hallinger, D. Blok, K. D. Tape, S. A. Rayback, M. Macias-Fauria, B. C. Forbes, and others. 2015. Climate sensitivity of shrub growth across the tundra biome. *Nature Climate Change* 5:887–891.
- Ohashi, H., Y. Kominami, M. Higa, D. Koide, K. Nakao, I. Tsuyama, T. Matsui, and N. Tanaka. 2016. Land abandonment and changes in snow cover period accelerate range expansions of sika deer. *Ecology and evolution* 6:7763–7775.
- Oliva, G., D. Ferrante, P. Paredes, G. Humano, and A. Cesa. 2016. A conceptual model for changes in floristic diversity under grazing in semi-arid patagonia using the state and transition framework. *Journal of Arid Environments* 127:120–127.
- Overton, W. S., and S. V. Stehman. 1996. Desirable design characteristics for long-term monitoring of ecological variables. *Environmental and Ecological Statistics* 3:349–361.
- Pedersen, Å. Ø., L. T. Beumer, R. Aanes, and B. B. Hansen. 2021. Sea or summit? Wild reindeer spatial responses to changing high-arctic winters. *Ecosphere* 12:e03883.
- Pedersen, Å. Ø., I. Tombre, J. U. Jepsen, P. B. Eidesen, E. Fuglei, and A. Stien. 2013a. Spatial patterns of goose grubbing suggest elevated grubbing in dry habitats linked to early snowmelt. *Polar Research* 32:19719.
- Pedersen, Åshild Ønvik, J. D. M. Speed, and I. M. Tombre. 2013b. Prevalence of pink-footed goose grubbing in the arctic tundra increases with population expansion. *Polar Biology* 36:1569–1575.
- Peeters, B., Å. Pedersen, L. E. Loe, K. Isaksen, V. Veiberg, A. Stien, J. Kohler, J.-C. Gallet, R. Aanes, and B. Hansen. 2019. Spatiotemporal patterns of rain-on-snow and basal ice in high arctic svalbard: Detection of a climate-cryosphere regime shift. *Environmental Research Letters* 14:015002.
- Perryman, S. A. M., N. I. D. Castells-Brooke, M. J. Glendining, K. W. T. Goulding, M. J. Hawkesford, A. J. Macdonald, R. J. Ostler, P. R. Poulton, C. J. Rawlings, T. Scott, and P. J. Verrier. 2018. The electronic Rothamsted Archive (e-RA), an online resource for data from the Rothamsted long-term experiments. *SCIENTIFIC DATA* 5.
- Porzig, E. L., K. E. Dybala, T. Gardali, G. Ballard, G. R. Geupel, and J. A. Wiens. 2011. Forty-five years and counting: Reflections from the palomarin field station on the contribution of long-term monitoring and recommendations for the future. *The Condor* 113:713–723.
- Post, E., R. B. Alley, T. R. Christensen, M. Macias-Fauria, B. C. Forbes, M. N. Gooseff, A. Iler, J. T. Kerby, K. L. Laidre, M. E. Mann, J. Olofsson, J. C. Stroeve, F. Ulmer, R. A. Virginia, and M. Wang. 2019. The polar regions in a 2°C warmer world. *Science Advances* 5:eaaw9883.

- Probst, P., M. N. Wright, and A.-L. Boulesteix. 2019. Hyperparameters and tuning strategies for random forest. *Wiley Interdisciplinary Reviews: data mining and knowledge discovery* 9:e1301.
- Ravolainen, V., E. M. Soininen, I. S. Jónsdóttir, I. Eischeid, M. Forchhammer, R. van der Wal, and Å. Ø. Pedersen. 2020. High arctic ecosystem states: Conceptual models of vegetation change to guide long-term monitoring and research. *Ambio* 49:666–677.
- Reid, D. G., F. Bilodeau, C. J. Krebs, G. Gauthier, A. J. Kenney, B. S. Gilbert, M. C.-Y. Leung, D. Duchesne, and E. Hofer. 2012. Lemming winter habitat choice: A snow-fencing experiment. *Oecologia* 168:935–946.
- Roberts, D. R., V. Bahn, S. Ciuti, M. S. Boyce, J. Elith, G. Guillera-Arroita, S. Hauenstein, J. J. Lahoz-Monfort, B. Schröder, W. Thuiller, D. I. Warton, B. A. Wintle, F. Hartig, and C. F. Dormann. 2017. Cross-validation strategies for data with temporal, spatial, hierarchical, or phylogenetic structure. *Ecography* 40:913–929.
- Rossi, F. C., A. Fritz, and G. Becker. 2018. Combining satellite and UAV imagery to delineate forest cover and basal area after mixed-severity fires. *Sustainability* 10:2227.
- R Team. 2013. R: A language and environment for statistical computing. R Foundation for Statistical Computing, Vienna, Austria.
- Saarinen, N., M. Vastaranta, R. Näsi, T. Rosnell, T. Hakala, E. Honkavaara, M. A. Wulder, V. Luoma, A. M. Tommaselli, N. N. Imai, and others. 2018. Assessing biodiversity in boreal forests with UAV-based photogrammetric point clouds and hyperspectral imaging. *Remote Sensing* 10:338.
- Saeyns, Y., I. Inza, and P. Larrañaga. 2007. A review of feature selection techniques in bioinformatics. *Bioinformatics* 23:2507–2517.
- Sato, C. F., and D. B. Lindenmayer. 2021. The use of state-and-transition models in assessing management success. *Conservation Science and Practice* 3:e519.
- Scheffer, M., S. Carpenter, J. A. Foley, C. Folke, and B. Walker. 2001. Catastrophic shifts in ecosystems. *Nature* 413:591–596.
- Schinasi, L. H., T. Benmarhnia, and A. J. De Roos. 2018. Modification of the association between high ambient temperature and health by urban microclimate indicators: A systematic review and meta-analysis. *Environmental Research* 161:168–180.
- Schreven, K., C. Stolz, J. Madsen, and B. Nolet. 2021. Nesting attempts and success of arctic-breeding geese can be derived with high precision from accelerometry and GPS-tracking. *Animal Biotelemetry* 9.
- Schuur, E. A., A. D. McGuire, C. Schädel, G. Grosse, J. W. Harden, D. J. Hayes, G. Hugelius, C. D. Koven, P. Kuhry, D. M. Lawrence, and others. 2015. Climate change and the permafrost carbon feedback. *Nature* 520:171–179.
- Segev, N., M. Harel, S. Mannor, K. Crammer, and R. El-Yaniv. 2015. Learn on source, refine on target: a model transfer learning framework with random forests. *IEEE transactions on pattern analysis and machine intelligence* 39.
- Serreze, M. C., and R. G. Barry. 2011. Processes and impacts of arctic amplification: A research synthesis. *Global and planetary change* 77:85–96.
- Siewert, M. B., and J. Olofsson. 2020. Scale-dependency of arctic ecosystem properties revealed by UAV. *Environmental Research Letters* 15:094030.
- Siewert, M. B., and J. Olofsson. 2021. UAV reveals substantial but heterogeneous effects of herbivores on arctic vegetation. *Scientific reports* 11:1–10.
- Speed, J. D. M., E. J. Cooper, I. S. Jónsdóttir, R. Van Der Wal, and S. J. Woodin. 2010a. Plant community properties predict vegetation resilience to herbivore disturbance in the arctic. *Journal of Ecology* 98:1002–1013.
- Speed, J. D. M., S. J. Woodin, H. Tommervik, and R. van der Wal. 2010b. Extrapolating herbivore-induced carbon loss across an arctic landscape. *Polar Biology* 33:789–797.


- Speed, J. D. M., S. J. Woodin, H. Tømmervik, M. P. Tamstorf, and R. van der Wal. 2009. Predicting habitat utilization and extent of ecosystem disturbance by an increasing herbivore population. *Ecosystems* 12:349–359.
- Spruce, J. P., S. Sader, R. E. Ryan, J. Smoot, P. Kuper, K. Ross, D. Prados, J. Russell, G. Gasser, R. McKellip, and W. Hargrove. 2011. Assessment of MODIS NDVI time series data products for detecting forest defoliation by gypsy moth outbreaks. *Remote Sensing of Environment* 115:427–437.
- Stark, D. J., I. P. Vaughan, L. J. Evans, H. Kler, and B. Goossens. 2018. Combining drones and satellite tracking as an effective tool for informing policy change in riparian habitats: A proboscis monkey case study. *Remote Sensing in Ecology and Conservation* 4:44–52.
- Sturm, M., J. Schimel, G. Michaelson, J. M. Welker, S. F. Oberbauer, G. E. Liston, J. Fahnestock, and V. E. Romanovsky. 2005. Winter Biological Processes Could Help Convert Arctic Tundra to Shrubland. *BioScience* 55:17–26.
- Suding, K. N., and R. J. Hobbs. 2009. Models of ecosystem dynamics as frameworks for restoration ecology. *New models for ecosystem dynamics and restoration*:3–21.
- Sun, Z., X. Wang, Z. Wang, L. Yang, Y. Xie, and Y. Huang. 2021. UAVs as remote sensing platforms in plant ecology: review of applications and challenges. *Journal of Plant Ecology* 14:1003–1023.
- Tang, L., and G. Shao. 2015. Drone remote sensing for forestry research and practices. *Journal of Forestry Research* 26:791–797.
- Thomson, E., M. Spiegel, I. Althuisen, P. Bass, S. Chen, A. Chmurzynski, A. Halbritter, J. Henn, I. Jónsdóttir, K. Klanderud, Y. Li, B. Maitner, S. Michaletz, P. Niittynen, R. Roos, R. Telford, B. Enquist, V. Vandvik, M. Macias-Fauria, and Y. Malhi. 2021. Multiscale mapping of plant functional groups and plant traits in the high arctic using field spectroscopy, UAV imagery and sentinel-2A data. *Environmental Research Letters* 16:055006.
- Tian, L., J. Wang, H. Zhou, and J. Wang. 2018. Automatic detection of forest fire disturbance based on dynamic modelling from MODIS time-series observations. *International Journal of Remote Sensing* 39:3801–3815.
- Tmušić, G., S. Manfreda, H. Aasen, M. R. James, G. Gonçalves, E. Ben-Dor, A. Brook, M. Polinova, J. J. Arranz, J. Mészáros, R. Zhuang, K. Johansen, Y. Malbeteau, I. P. de Lima, C. Davids, S. Herban, and M. F. McCabe. 2020. Current practices in UAS-based environmental monitoring. *Remote Sensing* 12.
- Tong, X.-Y., G.-S. Xia, Q. Lu, H. Shen, S. Li, S. You, and L. Zhang. 2020. Land-cover classification with high-resolution remote sensing images using transferable deep models. *Remote Sensing of Environment* 237:111322.
- Torresan, C., A. Berton, F. Carotenuto, S. F. Di Gennaro, B. Gioli, A. Matese, F. Miglietta, C. Vagnoli, A. Zaldei, and L. Wallace. 2017. Forestry applications of UAVs in Europe: A review. *International Journal of Remote Sensing* 38:2427–2447.
- Tuanmu, M.-N., A. Viña, G. J. Roloff, W. Liu, Z. Ouyang, H. Zhang, and J. Liu. 2011. Temporal transferability of wildlife habitat models: Implications for habitat monitoring. *Journal of Biogeography* 38:1510–1523.
- Tucker, C. J., D. A. Slayback, J. E. Pinzon, S. O. Los, R. B. Myneni, and M. G. Taylor. 2001. Higher northern latitude normalized difference vegetation index and growing season trends from 1982 to 1999. *International journal of biometeorology* 45:184–190.
- Tuomi, M., M. Väisänen, H. Yläne, F. Q. Brearley, I. C. Barrio, K. Anne Bråthen, I. Eischeid, B. C. Forbes, I. S. Jónsdóttir, A. L. Kolstad, and others. 2021. Stomping in silence: Conceptualizing trampling effects on soils in polar tundra. *Functional Ecology* 35:306–317.
- Turner, M. G. 2005. Landscape ecology: What is the state of the science? *Annu. Rev. Ecol. Evol. Syst.* 36:319–344.
- Twidwell, D., S. D. Fuhlendorf, C. A. Taylor Jr, and W. E. Rogers. 2013. Refining thresholds in coupled fire–vegetation models to improve management of encroaching woody plants in grasslands. *Journal of Applied Ecology* 50:603–613.
- Van der Sluijs, J., S. V. Kokelj, R. H. Fraser, J. Tunnicliffe, and D. Lacelle. 2018. Permafrost terrain dynamics and infrastructure impacts revealed by UAV photogrammetry and thermal imaging. *Remote Sensing* 10.

- Van Eerden, M. R., R. H. Drent, J. Stahl, and J. P. Bakker. 2005. Connecting seas: Western palaeartic continental flyway for water birds in the perspective of changing land use and climate. *Global Change Biology* 11:894–908.
- Vergouw, B., H. Nagel, G. Bondt, and B. Custers. 2016. Drone technology: Types, payloads, applications, frequency spectrum issues and future developments. Pages 21–45 *The future of drone use*. Springer.
- Wal, R. van der. 2006. Do herbivores cause habitat degradation or vegetation state transition? Evidence from the tundra. *Oikos* 114:177–186.
- Wal, R. van der, H. Anderson, A. Stien, L. E. Loe, and J. Speed. 2020. Disturbance, recovery and tundra vegetation change final report project 17/92 -to svalbard environmental protection fund. Svalbard Environmental Protection Fund.
- Walker, D.A., Reynolds, M.K., Daniëls, F.J., Einarsson, E., Elvebakk, A., Gould, W.A., Katenin, A.E., Kholod, S.S., Markon, C.J., Melnikov, E.S., Moskalenko, N.G., Talbot, S.S., Yurtsev, B.A. and The other members of the CAVM Team, (2005), The Circumpolar Arctic vegetation map. *Journal of Vegetation Science*, 16: 267-282.
- Walker, D., M. Leibman, H. Epstein, B. Forbes, U. Bhatt, M. Reynolds, J. Comiso, A. Gubarkov, A. Khomutov, G. Jia, and others. 2009. Spatial and temporal patterns of greenness on the yamal peninsula, russia: Interactions of ecological and social factors affecting the arctic normalized difference vegetation index. *Environmental Research Letters* 4:045004.
- Wang, H., R. Pu, Q. Zhu, L. Ren, and Z. Zhang. 2015. Mapping health levels of robinia pseudoacacia forests in the yellow river delta, china, using IKONOS and landsat 8 OLI imagery. *International Journal of Remote Sensing* 36:1114–1135.
- Wessels, K. J., S. Prince, N. Zambatis, S. MacFadyen, P. Frost, and D. Van Zyl. 2006. Relationship between herbaceous biomass and 1-km² advanced very high resolution radiometer (AVHRR) NDVI in kruger national park, south africa. *International Journal of Remote Sensing* 27:951–973.
- Westoby, M. J., J. Brasington, N. F. Glasser, M. J. Hambrey, and J. M. Reynolds. 2012. “Structure-from-motion” photogrammetry: A low-cost, effective tool for geoscience applications. *Geomorphology* 179:300–314.
- Westoby, M., B. Walker, and I. Noy-Meir. 1989. Opportunistic management for rangelands not at equilibrium. *Rangeland Ecology & Management/Journal of Range Management Archives* 42:266–274.
- White, P. S. 1985. Natural disturbance and patch dynamics: An introduction. *Natural disturbance and patch dynamics*:3–13.
- Wisz, M., M. Tamstorf, J. Madsen, and M. Jespersen. 2008. Where might the western svalbard tundra be vulnerable to pink-footed goose (*anser brachyrhynchus*) population expansion? Clues from species distribution models. *Diversity and Distributions* 14:26–37.
- Zhang, C., I. Sargent, X. Pan, H. Li, A. Gardiner, J. Hare, and P. M. Atkinson. 2019. Joint deep learning for land cover and land use classification. *Remote Sensing of Environment* 221:173–187.
- Zhou, R., C. Yang, E. Li, X. Cai, J. Yang, and Y. Xia. 2021. Object-based wetland vegetation classification using multi-feature selection of unoccupied aerial vehicle RGB imagery. *Remote Sensing* 13:4910.
- Zhou, Y., M. Daakir, E. Rupnik, and M. Pierrot-Deseilligny. 2020. A two-step approach for the correction of rolling shutter distortion in UAV photogrammetry. *ISPRS Journal of Photogrammetry and Remote Sensing* 160:51–66.
- Zhu, X., and D. Liu. 2015. Improving forest aboveground biomass estimation using seasonal landsat NDVI time-series. *ISPRS Journal of Photogrammetry and Remote Sensing* 102:222–231.
- Zvoleff, A. 2020. Glcm: Calculate textures from grey-level co-occurrence matrices (GLCMs).

Paper I



High Arctic ecosystem states: Conceptual models of vegetation change to guide long-term monitoring and research

Virve Ravolainen , Eeva M. Soininen, Ingibjörg Svala Jónsdóttir, Isabell Eischeid, Mads Forchhammer, René van der Wal, Åshild Ø. Pedersen

Received: 25 June 2019/Revised: 3 December 2019/Accepted: 13 December 2019/Published online: 18 January 2020

Abstract Vegetation change has consequences for terrestrial ecosystem structure and functioning and may involve climate feedbacks. Hence, when monitoring ecosystem states and changes thereof, the vegetation is often a primary monitoring target. Here, we summarize current understanding of vegetation change in the High Arctic—the World’s most rapidly warming region—in the context of ecosystem monitoring. To foster development of deployable monitoring strategies, we categorize different kinds of drivers (disturbances or stresses) of vegetation change either as pulse (i.e. drivers that occur as sudden and short events, though their effects may be long lasting) or press (i.e. drivers where change in conditions remains in place for a prolonged period, or slowly increases in pressure). To account for the great heterogeneity in vegetation responses to climate change and other drivers, we stress the need for increased use of ecosystem-specific conceptual models to guide monitoring and ecological studies in the Arctic. We discuss a conceptual model with three hypothesized alternative vegetation states characterized by mosses, herbaceous plants, and bare ground patches, respectively. We use moss-graminoid tundra of Svalbard as a case study to discuss the documented and potential impacts of different drivers on the possible transitions between those states. Our current understanding points to likely additive effects of herbivores and a warming climate, driving this ecosystem from a moss-dominated state with cool soils, shallow active layer and slow nutrient cycling to an ecosystem with warmer soil, deeper permafrost thaw, and faster nutrient cycling. Herbaceous-dominated vegetation and (patchy) bare ground would present two states in response to those drivers. Conceptual models are an operational tool to focus monitoring efforts towards management needs and identify the most pressing scientific questions. We promote greater

use of conceptual models in conjunction with a state-and-transition framework in monitoring to ensure fit for purpose approaches. Defined expectations of the focal systems’ responses to different drivers also facilitate linking local and regional monitoring efforts to international initiatives, such as the Circumpolar Biodiversity Monitoring Program.

Keywords Arctic tundra · Climate change · Ecological monitoring · Ecosystem state · Press driver · Pulse driver

INTRODUCTION

Vegetation plays a key role in terrestrial ecosystem functioning, with its attributes such as species composition, structure, and productivity influencing soil carbon and nitrogen cycling and supporting associated biodiversity (Wookey et al. 2009). International assessments such as the Circumpolar Biodiversity Monitoring Plan (CBMP within CAFF—Conservation of Arctic Flora and Fauna) highlight the importance of monitoring vegetation (Christensen et al. 2013; Ims and Ehrich 2013). The CBMP has suggested four Focal Ecosystem Components for monitoring plants: (i) all plants (species, life-form groups and associated communities); (ii) rare species and species of concern; (iii) non-native species; and (iv) species that humans use as food. Abundance, productivity, composition, diversity, and phenology are attributes that further specify the monitoring of most of these Focal Ecosystem Components. These attributes describe vegetation characteristics that are commonly used to measure shifts in whole ecosystem structure and function, i.e. ecosystem state shifts (Scheffer and Carpenter 2003; Bråthen et al. 2017).

Adaptive monitoring is chosen as the paradigm to be used in CBMP initiatives (Christensen et al. 2013). In this framework, conceptual models form a basis for hypotheses and predictions about change. The process of describing the expected changes often allows for the identification of variables to monitor (Lindenmayer and Likens 2009). Conceptual models are therefore a useful tool to inform monitoring decisions. Establishment of adaptive monitoring programmes typically concerns (i) articulation of the monitoring targets set as questions or hypotheses about the system's change; (ii) designing a monitoring approach and deciding upon the variables; and (iii) performing data collection and analysis. Thereafter, interpretation of the results will reveal the need to re-visit the questions and adjustment of protocols. Adaptivity refers to the programmes possibility to adjust to new potentially important processes, while maintaining the integrity of core variable sets. Hence, adaptive monitoring is not at odds with maintaining long time-series, but rather articulates a way to adapt new protocols and measures as needed (Lindenmayer et al. 2011).

One way to conceptualize vegetation change is the 'state-and-transition' or 'alternative stable states' approach (Briske et al. 2008). The premise of the alternative states models—a term we prefer given that many states are transient rather than stable (Fukami and Nakajima 2011) is that a given location or habitat may occur in one or more different vegetation states depending on conditions (i.e. 'driver impacts'). Hypothesized alternative states models can hence be used as a tool in building conceptual models that guide monitoring. State transition models developed for rangelands are an example of this, with vegetation structural components and the drivers behind changes specified to produce comprehensive catalogues of alternative states and their transitions (Stringham et al. 2003; Briske et al. 2005; Barrio et al. 2018). In tundra ecosystems, some alternative state models have been proposed (Van der Wal 2006; Bråthen et al. 2017; Barrio et al. 2018), but the use of specific conceptual models in Arctic monitoring programmes has been very limited. However, the question "how does vegetation change" is put in the spotlight by on-going rapid climate change (Anisimov et al. 2007; Post et al. 2009; Christensen et al. 2013), and calls for increased attention to what suite of interacting biotic and abiotic drivers are key when developing vegetation monitoring strategies.

Vegetation change may happen gradually or abruptly. Drivers of vegetation change can likewise manifest themselves as a trend developing gradually over time, or as a sudden event that pushes the subject of interest over a threshold into another domain (Briske et al. 2008). Indeed, Arctic climate change provides examples of drivers that induce both gradual change (e.g. rising mean temperature)

and discrete events that occur suddenly (e.g. mild winters with rain-on-snow events or other weather extremes) (Anisimov et al. 2007). In other words, Arctic climate change generates disturbances or stresses that can manifest themselves as 'press driver' (i.e. disturbances or stresses that remain in place for a long time, or slowly increase in pressure) and those that act as 'pulse driver' (i.e. sudden and short events, though their effects may be long lasting). A press driver can be described as extensive, pervasive, or subtle and a pulse driver as infrequent, sudden or as an event (Collins et al. 2011; Ratajczak et al. 2017). Current understanding of what shapes Arctic vegetation acknowledges the influence of what can be termed press and pulse drivers (Walker et al. 2005; Zimov 2005; Van der Wal 2006; Wookey et al. 2009; Myers-Smith et al. 2011; Bråthen et al. 2017), but the last decades of rapid changes in climate warrant discussion of new conceptual models that express their distinction more clearly.

Arctic land areas are warming considerably and are at risk of experiencing ecosystem change and biome shifts at already relatively modest increases in global mean temperatures (Beck et al. 2011; Grimm et al. 2013; Warszwski et al. 2013). However, evidence is accumulating that vegetation change in the Arctic is highly spatially heterogeneous (Beck and Goetz 2011; Elmendorf et al. 2012a; Myers-Smith et al. 2015; Huang et al. 2017) and lagging behind temperature change (Huang et al. 2017). Indeed, a review of experimental warming studies and long-term monitoring in the Arctic showed that no change in plant abundance was the most common response (Bjorkman et al. 2020). High Arctic, *sensu* Christensen et al. (2020), vegetation abundance is characterized by no or weak trends in relation to experimental warming and ambient rising temperatures (Hudson and Henry 2010; Prach et al. 2010; Elmendorf et al. 2012a). This heterogeneity in vegetation responses to warming challenges monitoring to strike a balance between ecosystem-specific understanding and general understanding of tundra vegetation changes that can be applied more universally.

Here, we propose a general and a detailed conceptual model for vegetation change in Svalbard that can help guide and inspire vegetation monitoring and future research also in other High Arctic tundra ecosystems. Some of the impact pathways discussed below have been documented in previous research, while others are proposed as hypotheses to be tested in future research and through monitoring. For now, we take a pragmatic approach, and categorize drivers as 'press' when their pressure gradually increases, or remains in place, over multiple years and as 'pulse' when they change over less than annual timescales, acknowledging that the best definition may vary between subjects of interest. We discuss press and pulse drivers in moss-graminoid tundra habitats in three potential

alternative vegetation states characterized by (i) a thick moss layer, (ii) herbaceous plants, and (iii) bare patches. Because there is more monitoring knowledge from the Low Arctic than the High Arctic (Bjorkman et al. 2020), we build on insight from lower latitude but focus on the High Arctic. We hope our examples will spark a broader and more thorough discussion on the full range of High Arctic vegetation states and drivers of transitions between them.

DRIVERS OF ARCTIC VEGETATION CHANGE: CURRENT EXAMPLES OF PRESS AND PULSE DRIVERS

Average temperature rise is an example of a mainly press driver in the system. A number of studies have found that in the Low Arctic warmer temperatures over time influence plant growth and abundance, especially, shrubs have increased (Tape et al. 2006; Elmendorf et al. 2012b; Myers-Smith et al. 2015; Bråthen et al. 2017). Tall shrubs are a growth form that is lacking in the High Arctic where dwarf shrubs and herbaceous plants are the main constituents of vegetation. Yet, the biomass of High Arctic plants is also closely linked to summer temperatures (Schmidt et al. 2012; Van der Wal and Stien 2014; Myers-Smith et al. 2019). With a continued press from warmer summer temperatures, plant abundance of especially the relatively fast growing growth forms such as the herbaceous forbs and graminoids, as well as the woody, deciduous shrubs would be expected to increase (Elmendorf et al. 2012b).

Sudden or short-term pulse drivers can damage vegetation, creating bare ground in previously vegetated habitats. Contrary to boreal and temperate ecosystems where fire, drought and insect outbreaks cause sudden, large-scale state shifts (Scheffer and Carpenter 2003; Briske et al. 2005; Beck et al. 2011), Arctic tundra has not been characterized by such dramatic and spatially extensive responses to these pulse drivers. However, climate warming may potentially change this. Tundra fires (Mack et al. 2011) and variable winter weather causing basal ground-ice formation (Bokhorst et al. 2012; Milner et al. 2016; Peeters et al. 2019) are already documented examples of pulse events that are likely to play a more prominent role for tundra vegetation in the future. Small rodent population fluctuations and their impact when at high densities act as a pulse driver of vegetation composition in many Low Arctic ecosystems (Ravolainen et al. 2011; Olofsson et al. 2012), and in some High Arctic systems (Johnson et al. 2011; Bilodeau et al. 2014). Yet, documentation of their potential to create persistent bare ground patches is lacking.

The same factor, such as grazing, may act as a press or pulse driver depending on its temporal pattern of change. A

sudden decrease in grazing pressure could, for instance, shift herbaceous grassland to woody tundra. This has been documented in riparian Low Arctic tundra where cessation of grazing led to surprisingly fast increases in willow growth (Ravolainen et al. 2014), suggesting that here reindeer (*Rangifer tarandus*) grazing acted as a pulse driver. On the other hand, sustained grazing pressure—a press driver—in the same study system keeps willow shrub recruits restricted to a low height and restricts the altitudinal limit of tall willow shrubs (Bråthen et al. 2017).

SVALBARD VEGETATION STATES IN MOSS-GRAMINOID TUNDRA

Differences in topography, snow lie, hydrology, and substrate give rise to general habitat types such as wetland, dwarf-shrub heath, cryptogam-barren and moss-graminoid tundra in Svalbard (Fig. 1a). While dramatic environmental changes can ultimately drive shifts from one of these broad types to another, here we will focus mainly on examples from Svalbard moss-graminoid tundra which covers 8–24% of continuous vegetation in central Spitsbergen (Johansen et al. 2012) and is a key habitat for many terrestrial animals (Staaland et al. 1993; Speed et al. 2009).

We propose a generalized conceptual model with three hypothesized alternative states within moss-graminoid tundra (Fig. 1b). Biotic and abiotic drivers may act in concert and push moss-graminoid tundra towards similar state changes. For the transition between the moss state and the herbaceous state, we hypothesize mainly press driver impacts. A warmer climate, gradually increased active layer depth, and more available nutrients could push the moss state towards the herbaceous state, with the latter sustaining a greater number of herbivores (Fig. 1b). The same state transition, with increased graminoid dominance, is also likely to occur where large herbivores graze, trample, and fertilize vegetation, i.e. in response to increased herbivore numbers (Van der Wal 2006). The opposite transition, from the herbaceous state to the moss state, could potentially occur with reduced herbivore activity. Graminoids and forbs are already common in many High Arctic vegetation types (Walker et al. 2005). We hypothesize that the herbaceous, graminoid-dominated state, with relatively fast nutrient cycling and high tolerance to mechanical disturbance and grazing, would become more common given a press from longer, warmer, and wetter summers in the presence of a high number of herbivores, notably reindeer.

Abiotic events and biotic agents can act as pulse drivers to shift the moss or the herbaceous state to the state characterized by bare patches (typically from < 1 m² to covering a few 10 m², and often occurring over large areas)

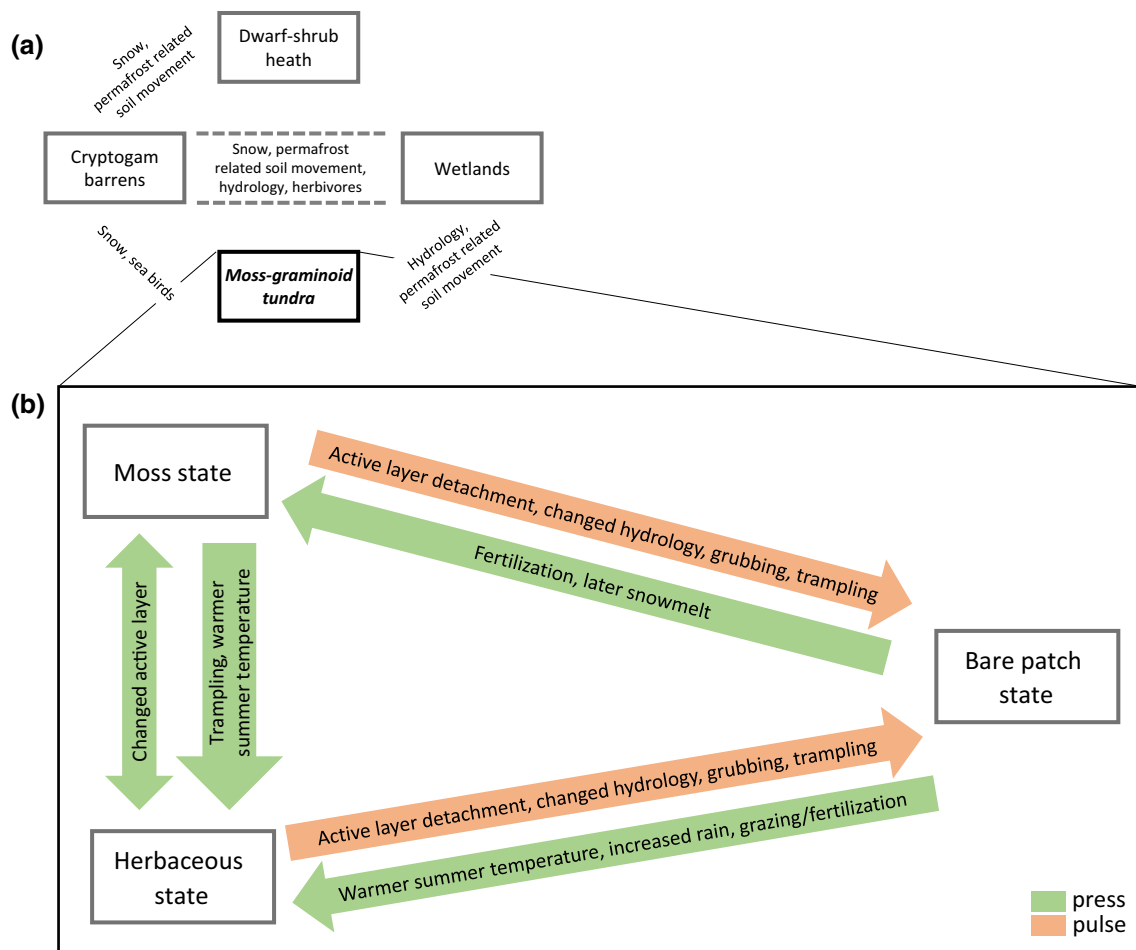


Fig. 1 Topography, snow cover, hydrology, herbivory, and substrate are general factors supplemental to climate that differentiate High Arctic habitat types on Svalbard: wetlands, dwarf-shrub heathlands, barrens with lichens or mosses, and moss-graminoid tundra (a). Within the context given by the general habitats, transitions between alternative states can happen (b). We suggest the moss-graminoid tundra can be found in a (i) moss, (ii) herbaceous, (iii) or bare patch characterized state. The drivers that cause shifts between these states can be characterized as those that gradually change their impact (‘press’), and those whose impact is a sudden event (‘pulse’). Both biotic and abiotic drivers can push the moss-graminoid tundra in the same direction, e.g. both sudden active layer detachments and high abundance of herbivores trampling or grubbing can cause the shift from the vegetated to the bare patch state. See main text for examples and references

(Fig. 1b). In the High Arctic, warm summers cause active layer deepening, thaw slumps and the opening up of bare soil (Anisimov et al. 2007; Lousada et al. 2018), and this can happen in the course of few weeks or during a single summer season (Ravolainen pers.obs.). In the Canadian Low Arctic, lesser and greater snow goose grubbing, i.e. foraging for below-ground plant parts, has caused local and large-scale shifts to a bare ground state in interaction with hydrology and salinity (Jefferies et al. 2006; Lefebvre et al. 2017). Goose foraging can remove nearly all vegetation within only a few years also in the High Arctic (pers. obs. authors). Hence, although goose populations may gradually increase, being a ‘press driver’, goose grubbing at a given location, due to an amplifying effect of saline sub-soil or other abiotic factors, may act as a pulse driver. We hypothesize that the abiotic and biotic pulse drivers could increase the number and size of bare patches, causing a

distinct bare ground state in landscapes that currently have continuous plant cover and hence changing the spatial patterning of vegetation.

While a general model such as presented in Fig. 1b is useful for clarifying which state transitions can be expected to occur, a monitoring programme is reliant on an integrated effort that specifies how to monitor both the vegetation state shifts and the drivers. In the following, we suggest a more detailed conceptual model that specifies expected climate- and management-driven impacts of herbivores and nutrients on vegetation state transitions in moss-graminoid tundra. In doing so, we illustrate the process from depicting conceptual models to implementing practical monitoring with the required set of variables (Fig. 2, Table 1). The model suggested here is a part of an ecosystem-based, adaptive monitoring programme in Norway (Ims et al. 2013).

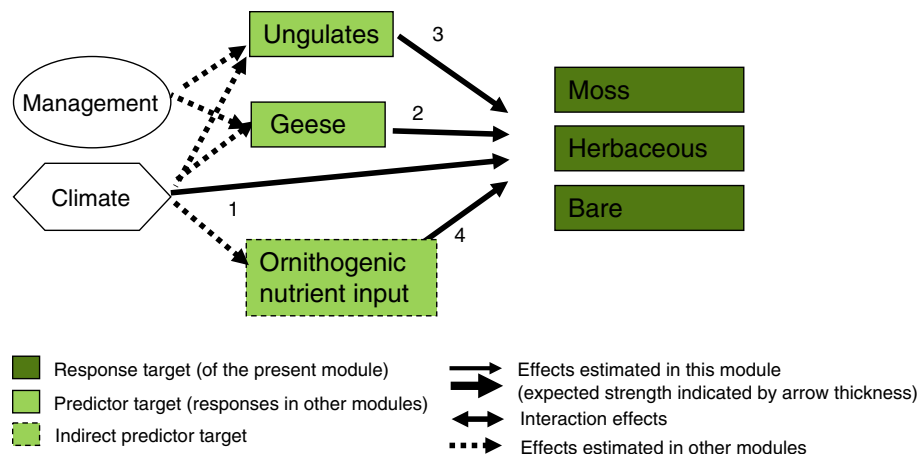


Fig. 2 A detailed conceptual model for moss tundra on Svalbard implemented within the monitoring programme Climate-ecological Observatory for Arctic Tundra—COAT. The included drivers are expected to have direct impact on the state shifts. Indirect impacts (dashed lines) and effects the vegetation can have on the herbivores have been outlined earlier (Ims et al. 2013). Climate (pathway 1) can act as a ‘press’ via gradually warming temperature, or as a ‘pulse driver’ through, for example, abrupt extreme winter weather events. Likewise, the impact of herbivores can happen as an abrupt pulse event, as in the case of goose grubbing driving vegetation patches from vegetated to the bare patch state (pathway 2), or as press herbivory by reindeer gradually causing a shift from the moss to the herbaceous state (pathway 3). Fertilization by seabirds is an important driver of state shifts on the coast (pathway 4). See main text for more examples and references

Table 1 The set of variables derived from the conceptual model for monitoring of vegetation state transitions in moss-graminoid tundra on Svalbard (Fig. 2). Path refers to the pathways outlined in Fig. 2. The relation to the Circumpolar Biodiversity Monitoring Program (CBMP) for terrestrial Arctic and the Focal Ecosystem Components (FEC), and their Attributes (Attr.) are indicated

State variable	Interval	Method	Path	FEC*	Attr.*
Moss layer thickness	1 year	Field measure			
Biomass of vascular plant species and functional groups	1 year	Point frequency		All plants	Diversity, composition, and abundance
Ice damage	1 year	Transect, drone and satellite imagery	1		
Extent of vegetation types, bare ground	5 years	Drone and satellite imagery	2, 3	All plants	Diversity, composition and abundance/diversity and spatial structure
Productivity at peak season	1 year	Drone and satellite imagery, NDVI	1	All plants	Productivity
Phenology	1 year	Drone and satellite imagery, time-integrated NDVI	1	All plants	Phenology
Air and soil temperatures	Multiple	Weather stations, medium-sized station, small, distributed loggers	1		
Permafrost thaw depth	1 year	Late summer maximum depth at bore hole	1		
Snow depth, duration, distribution	Multiple	Field measurement, modelling	1		
Soil moisture	Multiple	Weather stations, small loggers	1		
Abundance of herbivores	1 year	Pellet counts, camera traps, population census	2, 3		
Grubbing impact	1 year	Counts	2, 3		
Soil nutrient level	1 year	Near-infra red spectrometry	2, 3, 4		
Ground-ice formation	Multiple	Field measurement, modelling	1		
Permafrost-soil movement	5 year	Satellite and drone imagery	1		

*The attributes of the focal ecosystem component in the Circumpolar Biodiversity Monitoring Plan; “All plants (species, life-form groups and associational communities) include attributes “diversity, composition and abundance”, “diversity and spatial structure”, “productivity”, and “phenology”

Svalbard is a High Arctic archipelago with a relatively simple food web. Moist, potentially very productive habitats of Svalbard tundra harbour moss tundra (Vanderpuye et al. 2002; Walker et al. 2005) that we suggested can exist in three alternative states: (i) dominated by mosses; (ii) herbaceous vascular plants in a matrix of moss, or (iii) as bare ground (Figs. 1, 2). The suggested moss-dominated state has a relatively high productivity and capability to retain nutrients and moisture. A deep moss layer, often with species from the genera *Aulacomnium*, *Tomentypnum*, and *Sanionia*, (Eurola and Hakala 1977; Vanderpuye et al. 2002; Van der Wal and Brooker 2004) insulates the soil, keeping it cool and with shallow active layer (Gornall et al. 2007). The suggested herbaceous state has abundant graminoids, e.g. *Alopecurus magellanicus*, *Poa* spp., forbs, e.g. *Saxifraga* spp., *Bistorta vivipara*, and dwarf shrubs, particularly *Salix polaris*, growing in a moss matrix (Eurola and Hakala 1977; Vanderpuye et al. 2002). Soils tend to be warmer and the active layer is consequently deeper than in the moss-dominated state (Van der Wal and Brooker 2004). The critical functions of the vegetated states of moss tundra, supporting vertebrate communities and regulating ecosystem processes, depend on the level of grazing, manuring, and disturbance imposed by the herbivorous animals [Figs. 2, 3 (van der Wal et al. 2004; Van der Wal and Brooker 2004; Van der Wal 2006)], but also by fertilization from colony nesting birds (Eurola and Hakala 1977; Vanderpuye et al. 2002). The suggested bare ground state can be either exposed organic soil, including decomposing moss, or mineral soil (sandy, or silty); and bare areas can range from small (< 1 m²) to large (10's of m²). In this state, the soil organic carbon content is lower than in the other two alternative states, and erosion and leaching may cause nutrient depletion (Van der Wal et al. 2007).

Summer temperature and soil moisture are likely the most important abiotic press drivers that affect moss tundra vegetation (Fig. 2, pathway 1). In Svalbard, summers have warmed moderately over the last 50 years, while spring, autumn and particularly winter temperatures have had a stronger warming trend (winter 1.6°C/decade) (Vikhamar-Schuler et al. 2016). We hypothesize that the warmer summers in central Spitsbergen during the last 50 years (Van Pelt et al. 2016) can, in the future, exert a press impact in favour of the herbaceous state over the moss-dominated state.

A climate-related pulse driver that influences the terrestrial ecosystem on Svalbard are rain-on-snow events in winter, leading to ground-ice formation (Fig. 2, pathway 1). The effects of ground-ice on plant communities have been mostly studied in dwarf shrub species that have sensitive organs exposed above-ground, revealing high spatial variability in damage from winter weather (Milner et al.

2016; Bjerke et al. 2017). The spatial extent and longer-term effects of winter damage to shrubs remains a question for future research and monitoring. The extent of winter damage in herbaceous and mossy vegetation states is currently undocumented. The frequency of “rain-on-snow” events has increased and the precipitation and snow cover patterns are expected to change (Adakudlu et al. 2019; Peeters et al. 2019). We therefore hypothesize that also plants with all sensitive organs below or at the soil surface may suffer from winter climate events, and integrate measurements of winter damage and extreme winter weather into the vegetation monitoring (Table 1).

It is hardly possible to predict climate impacts on moss tundra without considering the activities of herbivores, whose populations are dynamic and changing. Resident herbivores (Svalbard reindeer, *Rangifer tarandus platyrhynchus* and Svalbard rock ptarmigan, *Lagopus muta hyperborea*) are affected by changes in winter climate (Hansen et al. 2013; Albon et al. 2017). Mild winter weather (pulse driver), leading to ground-ice formation, results in reduced reindeer population growth rates (Albon et al. 2017). By contrast, longer and warmer summers (press driver), given they result in higher primary production, appear to increase population growth rates (Hansen et al. 2013). Similar positive effects of longer summers in the Arctic likely will act on the migratory geese (Jensen et al. 2008), whose populations have increased dramatically during the last decades because of reduced hunting pressure and greatly improved food availability in the wintering areas (Fox et al. 2005; Fox and Madsen 2017).

A major way through which herbivores impact the vegetation is through physical disturbance (Fig. 2, pathways 2 and 3). Particularly, the moss-dominated state is sensitive to changes in disturbance by reindeer and geese (Van der Wal and Brooker 2004; Speed et al. 2009) (Fig. 2, pathway 2). In early spring and summer, pink-footed geese (*Anser brachyrhynchus*) grub for below-ground plant parts of particularly grasses (*Dupontia* spp.) and sedges (*Eriophorum scheuchzeri*), but also *Equisetum arvense* and *Bistorta vivipara*, disrupting the moss layer (Fox et al. 2006; Anderson et al. 2012). Pink-footed goose grubbing affects an increasing proportion of the vegetated ground, and the effect of their activities is found in nearly all vegetation and landscape types (Pedersen et al. 2013). Patches opened by the grubbing activity of geese are currently mostly small but highly frequent in the landscapes (nearly 50% of 20,000 m² of moss tundra transects surveyed in 2018 had signs of grubbing disturbance; Ravolainen et al. unpublished data). Re-growth of moss is slow relative to vascular plants, which makes the moss state more sensitive to trampling than the herbaceous state. Timing of snowmelt modulates the impact of pink-footed geese on tundra vegetation since it controls the spatial

distribution of feeding geese (Anderson et al. 2016). It is not known what degree of grubbing intensity leads to changes in hydrology and other local abiotic factors. Whether the extent of grubbing (see Speed et al. 2009 for spatial predictions) continues to increase, whether there is potential for it affecting food availability for the year-round resident herbivores, and how dynamic the different vegetation states are in their responses and recovery remain to be addressed in future work.

Thaw slumps, ice wedge polygon collapses, and active layer detachments are pulse driver disturbances related to permafrost processes occurring on Svalbard. Yet, their impacts on vegetation state shifts lack documentation. From other Arctic areas, we know that eroding gullies (Perreault et al. 2016) and permafrost thaw slumps (Sluijs et al. 2018) can influence landscape structure and vegetation as local pulse drivers. The bare ground created by permafrost-related processes differs from that opened by geese in one fundamental way: landslides, thaw slumps, and thermokarsts remove or move soils, while geese remove the vegetation while leaving the soil largely in place. Thus, the respective formation mechanism of the bare ground patches could lead to different plant recruitment potential. We therefore hypothesize that habitats disturbed by geese will in the future support different vegetation states than bare ground created by permafrost-related erosion.

Another press driver in moss tundra is increasing nutrient turnover (Fig. 2, pathways 2 and 3). Both geese and reindeer enhance nutrient turnover (Van der Wal and Hessen 2009; Sjøgersten et al. 2010), but direct comparisons of their relative effects are lacking. What level of nutrient availability is necessary to maintain the different tundra states remains to be investigated. At high levels of nutrient input by seabirds moss tundra shifts to the herbaceous state (Euroala and Hakala 1977) (Fig. 2, pathway 4). Given that more than three million pairs of altogether 20 species of seabird breed on Svalbard, their influence should be considerable, as they are a significant driver of nutrient transfer from the marine to the terrestrial realm (Zwolicki et al. 2013). Vegetation development under climate change scenarios in moss tundra can be expected to be inherently tied to trends in seabird populations—particularly in coastal areas—in addition to the above-mentioned effects by herbivores.

Proportions of plant biomass consumed by reindeer across larger units of vegetation are generally low, and likely not dissimilar to estimates obtained for muskoxen *Ovibos moschatus* in NE Greenland although effects on vegetation are measurable when muskoxen are excluded (Mosbacher et al. 2016). In line with this, the few short-term exclosure studies of Svalbard reindeer herbivory have not found strong impacts on plant biomass (Wegener and

Odasz-Albrigtsen 1998; Dormann et al. 2004). Studies on geese, on the other hand, have shown locally strong suppression of vascular plant biomass, which could ultimately drive the system to a moss-dominated state (for a review, see Van der Wal and Hessen 2009). Were intense grazing to cease, then the herbaceous state would re-emerge (Sjøgersten et al. 2011). Studies looking at the cumulative effects of these key herbivores at current population levels are lacking. The reindeer population in Svalbard has doubled since 1980's (Le Moullec et al. 2019) and the pink-footed goose population increased by 36% between 2007 and 2013 (Anderson et al. 2016). We can hypothesize that changing population sizes of reindeer and pink-footed geese, as they share spring and summer habitat and forage plants, may be an additive press driver, shifting the system from cryptogam to herbaceous state and potentially, if grazing pressure become high enough, to a bare ground state (Fig. 2 pathways 2 and 3).

ARCTIC VEGETATION STATES: ECOSYSTEM-SPECIFIC SHIFTS

Warmer summer temperature (Schmidt et al. 2012), extreme winter weather (Bjerke et al. 2017), disturbance from herbivores (Olofsson et al. 2012), and permafrost-related processes, such as deeper thaw and active layer detachment (Myers-Smith et al. 2019), can all lead to vegetation state shifts. On a general level, we suggest that these drivers are important, and transitions towards more deciduous shrubs or more herbaceous vegetation at the cost of cryptogams can happen across the Arctic. However, we hypothesize that habitat differences (notably terrain, water regime, substrate, and snow distribution), as well as the assemblage of herbivores—of different-sized species with distinct feeding modes—will continue to dictate which states are possible and which transitions happen. For instance, the impact of very large herbivores like muskoxen will likely manifest partly through their trampling effect on mosses. Muskoxen trampling of wet habitats has been documented to decrease soil temperatures (Mosbacher et al. 2016), which is opposite to what has been observed in drier habitats concerning reindeer (Van der Wal and Brooker 2004; Van der Wal 2006). Further, bare ground patches caused by e.g. permafrost thaw slumps will in moist habitats probably revegetate within the course of some years (Lantz et al. 2009). Yet, we hypothesize that in drier habitats re-colonization might take longer and potentially even be hampered by increased frequency of extreme winter events such as ice encasement. These examples highlight the need for habitat and region specific, ecosystem-based conceptual models to guide future monitoring and research on Arctic vegetation states.

INTEGRATION OF DRIVERS IN VEGETATION MONITORING

The implementation of monitoring following a conceptual model as outlined above requires establishment of integrated measures capturing vegetation ‘response variables’, as well as measurements of the respective drivers. The variables monitored in Svalbard moss tundra (Table 1) provide an example of how monitored variables link to the above-unfolded conceptual model (Fig. 2). The relative importance of grazing, trampling, grubbing, and abiotic disturbances as drivers of vegetation state shifts warranted the selection of variables to monitor. More work is needed before we fully understand what drivers are best categorized as pulse and press in the changing Arctic terrestrial ecosystems. Our focus here has been on climate and herbivores as drivers of vegetation state shifts, while impacts of vegetation change on the herbivores are described elsewhere in models focussed on reindeer and geese (Ims et al. 2013). While being specific to the focal ecosystem, the conceptual model and the variables presented here are at the same time in correspondence with the focal ecosystem components suggested for monitoring in the international Circumpolar Biodiversity Monitoring Plan within CAFF (Christensen et al. 2013). A difference between the concept models of the international plan and the models we outline here and in the Climate-ecological Observatory for Arctic Tundra—COAT (Ims et al. 2013) is that we explicitly describe expected directional impacts of individual drivers on tundra vegetation states and other ecosystem components such as the respective herbivores. This hopefully facilitates understanding of the linkages between the ecosystem components, in line with ambitions given in the CBMP plan (Christensen et al. 2013) and other international assessments (Ims and Ehrich 2013). Monitoring data that allow for directly linking the variables describing ecosystem state and drivers of state shifts can give insights into climate–ecosystem dynamics (Post et al. 2009; Ims et al. 2013).

Conceptual models should be re-visited at regular intervals to adapt them and the respective monitoring programme to new knowledge (Lindenmayer et al. 2011). For instance, changes in environmental conditions may suggest that new impact pathways have gained importance. Currently, the occurrence of alien plant species, identified as a Focal Ecosystem Component by CBMP (Christensen et al. 2013), is largely confined to Svalbard’s settlements (Alsos et al. 2015) similar to the situation in the circumpolar Arctic (Wasowicz et al. 2019). Should alien plant species become more frequent in natural habitats, then they and their drivers would be included in the monitoring. By contrast, variables that are central for monitoring climate change impacts on vegetation, such as weather variables

and peak season biomass, are continuing time-series. While adjustments to the sampling protocols of these time-series will need to be considered at regular intervals, any change should be made without risking the integrity of long-term time-series. For instance, changes to new methods should be calibrated against previously used methods. One of the strengths of relying on the adaptive monitoring paradigm is the active consideration of new elements in context with the established programme, while maintaining time-series of core variables (Lindenmayer et al. 2011). Currently, very few monitoring programmes use adaptive monitoring, and we suggest that more active usage of this approach is warranted given the rapid change of Arctic ecosystems.

KEY FINDINGS AND RECOMMENDATIONS FOR THE CIRCUMPOLAR BIODIVERSITY MONITORING PLAN

Based on known and expected vegetation state changes in High Arctic Svalbard, we propose the use of conceptual models as basis for monitoring tundra vegetation. Current understanding of our worked up, and implemented case, moss-graminoid tundra, suggests that additive effects of a warmer climate and increasing herbivore pressure are likely to drive this system from a moss-dominated state with cool soils towards either a herbaceous state or a bare ground state, both having warmer soils and deeper active layers. We developed an ecosystem-specific conceptual model to determine the variables currently included in the long-term adaptive ecosystem monitoring on Svalbard. The examples of possible vegetation state transitions described for Svalbard moss-graminoid tundra are intended to encourage discussion and development of a broader set of conceptual models and potential vegetation states for other rapidly changing Arctic regions. We propose that development of a comprehensive set of conceptual models, with built-in best estimates of potential shifts in vegetation states, should become a priority of international monitoring bodies as they would help to link local and regional monitoring efforts in a circumpolar context.

Acknowledgements Open Access funding provided by Norwegian Polar Institute. We are grateful to our colleagues in COAT—Climate-ecological Observatory for Arctic Tundra for discussions, and to the editor Niels Martin Schmidt and anonymous reviewers for their thoughtful and constructive comments on earlier versions of this paper.

Open Access This article is licensed under a Creative Commons Attribution 4.0 International License, which permits use, sharing, adaptation, distribution and reproduction in any medium or format, as long as you give appropriate credit to the original author(s) and the source, provide a link to the Creative Commons licence, and indicate if changes were made. The images or other third party material in this

article are included in the article's Creative Commons licence, unless indicated otherwise in a credit line to the material. If material is not included in the article's Creative Commons licence and your intended use is not permitted by statutory regulation or exceeds the permitted use, you will need to obtain permission directly from the copyright holder. To view a copy of this licence, visit <http://creativecommons.org/licenses/by/4.0/>.

REFERENCES

- Adakudlu, M., J. Andresen, J. Bakke, S. Beldring, R. E. Benestad, W. Bilt, J. Boden, C. Borstad, et al. 2019. Climate in Svalbard 2100—A knowledge base for climate adaptation.
- Albon, S.D., R.J. Irvine, O. Halvorsen, R. Langvatn, L.E. Loe, E. Ropstad, V. Veiberg, R. Van Der Wal, et al. 2017. Contrasting effects of summer and winter warming on body mass explain population dynamics in a food-limited Arctic herbivore. *Global Change Biology* 23: 1374–1389.
- Alsos, I.G., C. Ware, and R. Elven. 2015. Past Arctic aliens have passed away, current ones may stay. *Biological Invasions* 17: 3113–3123.
- Anderson, H.B., T.G. Godfrey, S.J. Woodin, and R. van der Wal. 2012. Finding food in a highly seasonal landscape: Where and how pink footed geese *Anser brachyrhynchus* forage during the Arctic spring. *Journal of Avian Biology* 43: 415–422.
- Anderson, H.B., J.D.M. Speed, J. Madsen, A.O. Pedersen, I.M. Tombre, and R. van der Wal. 2016. Late snow melt moderates herbivore disturbance of the Arctic tundra. *Ecoscience* 23: 29–39.
- Anisimov, O.A., D.G. Vaughan, T. Callaghan, C. Furgal, H. Marchant, T.D. Prowse, H. Vilhjalmsson, and J.E. Walsh. 2007. Polar regions (Arctic and Antarctic). In *Climate change 2007: Impacts, adaptation and vulnerability. Contribution of working group II to the fourth assessment report of the intergovernmental panel on climate change*, ed. M.L. Parry, O.F. Canziani, J.P. Palutikof, P.J. van der Linden, and C.E. Hanson, 683–685. Cambridge: Cambridge University Press.
- Barrio, I.C., D.S. Hik, J. Thorsson, K. Svavarsdottir, B. Marteinsdottir, and I.S. Jonsdottir. 2018. The sheep in wolf's clothing? Recognizing threats for land degradation in Iceland using state-and-transition models. *Land Degradation and Development* 29: 1714–1725.
- Beck, P.S.A., and S.J. Goetz. 2011. Satellite observations of high northern latitude vegetation productivity changes between 1982 and 2008: Ecological variability and regional differences. *Environmental Research Letters* 6: 045501.
- Beck, P.S.A., G.P. Juday, C. Alix, V.A. Barber, S.E. Winslow, E.E. Sousa, P. Heiser, J.D. Herriges, et al. 2011. Changes in forest productivity across Alaska consistent with biome shift. *Ecology Letters* 14: 373–379.
- Bilodeau, F., G. Gauthier, D. Fauteux, and D. Berteaux. 2014. Does lemming winter grazing impact vegetation in the Canadian Arctic? *Polar Biology* 37: 845–857.
- Bjerke, J.W., R. Treharne, D. Vikhamar-Schuler, S.R. Karlsen, V. Ravolainen, S. Bokhorst, G.K. Phoenix, Z. Bochenek, et al. 2017. Understanding the drivers of extensive plant damage in boreal and Arctic ecosystems: Insights from field surveys in the aftermath of damage. *Science of the Total Environment* 599: 1965–1976.
- Bjorkman, A.D., M.G. Criado, I. Myers-Smith, V. Ravolainen, I.S. Jonsdottir, K. Westergaard, J.P. Lawler, M. Aronsson, et al. 2020. Status and trends in Arctic vegetation: Evidence from experimental warming and long-term monitoring. *Ambio*. <https://doi.org/10.1007/s13280-019-01161-6>.
- Bokhorst, S., J.W. Bjerke, H. Tommervik, C. Preece, and G.K. Phoenix. 2012. Ecosystem response to climatic change: The importance of the cold season. *Ambio* 41: 246–255. <https://doi.org/10.1007/s13280-012-0310-5>.
- Bråthen, K.A., V.T. Ravolainen, A. Stien, T. Tveraa, and R.A. Ims. 2017. Rangifer management controls a climate-sensitive tundra state transition. *Ecological Applications* 27: 2416–2427.
- Briske, D.D., B.T. Bestelmeyer, T.K. Stringham, and P.L. Shaver. 2008. Recommendations for development of resilience-based state-and-transition models. *Rangeland Ecology & Management* 61: 359–367.
- Briske, D.D., S.D. Fuhlendorf, and F.E. Smeins. 2005. State-and-transition models, thresholds, and rangeland health: A synthesis of ecological concepts and perspectives. *Rangeland Ecology & Management* 58: 1–10.
- Christensen, T., T. Barry, J. Taylor, M. Doyle, M. Aronsson, J. Braa, C. Burns, C. Coon, et al. 2020. Developing a circumpolar programme for the monitoring of Arctic terrestrial biodiversity. *Ambio*. <https://doi.org/10.1007/s13280-019-01311-w>.
- Christensen, T., J. Payne, M. Doyle, G. Ibaguchi, J. Taylor, N.M. Schmidt, M. Gill, M. Svoboda, M. Aronsson, C. Behe, C. Buddle, C. Cuyler, A.M. Fosaa, A.D. Fox, S. Heidmarsson, P. Krogh Henning, J. Madsen, D. McLennan, J. Nymand, C. Rosa, J. Salmela, R. Scuchman, M. Soloviev, and M. Wedege. 2013. *The arctic terrestrial biodiversity monitoring plan*. Akureyri: CAFF international secretariat.
- Collins, S.L., S.R. Carpenter, S.M. Swinton, D.E. Orenstein, D.L. Childers, T.L. Gragson, N.B. Grimm, M. Grove, et al. 2011. An integrated conceptual framework for long-term social-ecological research. *Frontiers in Ecology and the Environment* 9: 351–357.
- Dormann, C.F., R. van der Wal, and S.J. Woodin. 2004. Neighbour identity modifies effects of elevated temperature on plant performance in the High Arctic. *Global Change Biology* 10: 1587–1598.
- Elmendorf, S.C., G.H. Henry, R.D. Hollister, R.G. Bjork, A.D. Bjorkman, T.V. Callaghan, L.S. Collier, E.J. Cooper, et al. 2012a. Global assessment of experimental climate warming on tundra vegetation: Heterogeneity over space and time. *Ecology Letters* 15: 164–175.
- Elmendorf, S.C., G.H.R. Henry, R.D. Hollister, R.G. Bjork, N. Boulanger-Lapointe, E.J. Cooper, J.H.C. Cornelissen, T.A. Day, et al. 2012b. Plot-scale evidence of tundra vegetation change and links to recent summer warming. *Nature Climate Change* 2: 453–457.
- Euroala, S., and A.V.K. Hakala. 1977. The bird cliff vegetation of Svalbard. *Aquilo/Seria botanica* 15: 1–18.
- Fox, T.A., I.S. Francis, and E. Bergersen. 2006. Diet and habitat use of Svalbard Pink-footed Geese *Anser brachyrhynchus* during arrival and pre-breeding periods in Adventdalen. *Ardea* 94: 691–699.
- Fox, A.D., and J. Madsen. 2017. Threatened species to superabundance: The unexpected international implications of successful goose conservation. *Ambio* 46: 179–187.
- Fox, A.D., J. Madsen, H. Boyd, E. Kuijken, D.W. Norriss, I.M. Tombre, and D.A. Stroud. 2005. Effects of agricultural change on abundance, fitness components and distribution of two arctic-nesting goose populations. *Global Change Biology* 11: 881–893.
- Fukami, T., and M. Nakajima. 2011. Community assembly: Alternative stable states or alternative transient states? *Ecology Letters* 14: 973–984.
- Gornall, J.L., I.S. Jonsdottir, S.J. Woodin, and R. Van der Wal. 2007. Arctic mosses govern below-ground environment and ecosystem processes. *Oecologia* 153: 931–941.

- Grimm, N.B., F.S. Chapin, B. Bierwagen, P. Gonzalez, P.M. Groffman, Y.Q. Luo, F. Melton, K. Nadelhoffer, et al. 2013. The impacts of climate change on ecosystem structure and function. *Frontiers in Ecology and the Environment* 11: 474–482.
- Hansen, B.B., V. Grotan, R. Aanes, B.E. Saether, A. Stien, E. Fuglei, R.A. Ims, N.G. Yoccoz, et al. 2013. Climate events synchronize the dynamics of a resident vertebrate community in the high arctic. *Science* 339: 313–315.
- Huang, M.T., S.L. Piao, I.A. Janssens, Z.C. Zhu, T. Wang, D.H. Wu, P. Ciais, R.B. Myneni, et al. 2017. Velocity of change in vegetation productivity over northern high latitudes. *Nature Ecology & Evolution* 1: 1649–1654.
- Hudson, J.M.G., and G.H.R. Henry. 2010. High Arctic plant community resists 15 years of experimental warming. *Journal of Ecology* 98: 1035–1041.
- Ims, R.A., and D. Ehrlich. 2013. Terrestrial ecosystems. In *Arctic biodiversity assessment. Status and trends in Arctic biodiversity*, ed. H. Meltofte, 384–440. Akureyri: Conservation of Arctic Flora and Fauna.
- Ims, R. A., J. U. Jepsen, A. Stien, and N. G. Yoccoz. 2013. Science plan for COAT: Climate-ecological Observatory for Arctic Tundra. 1, Fram Centre, Tromsø, Norway.
- Jefferies, R.L., A.P. Jano, and K.F. Abraham. 2006. A biotic agent promotes large-scale catastrophic change in the coastal marshes of Hudson Bay. *Journal of Ecology* 94: 234–242.
- Jensen, R.A., J. Madsen, M. O’Connell, M.S. Wisz, H. Tommervik, and F. Mehlum. 2008. Prediction of the distribution of Arctic-nesting pink-footed geese under a warmer climate scenario. *Global Change Biology* 14: 1–10.
- Johansen, B.E., S.R. Karlson, and H. Tommervik. 2012. Vegetation mapping of Svalbard utilising Landsat TM/ETM plus data. *Polar Record* 48: 47–63.
- Johnson, D.R., M.J. Lara, G.R. Shaver, G.O. Batzli, J.D. Shaw, and C.E. Tweedie. 2011. Exclusion of brown lemmings reduces vascular plant cover and biomass in Arctic coastal tundra: Resampling of a 50 + year herbivore exclosure experiment near Barrow. *Alaska. Environmental Research Letters* 6: 045507.
- Lantz, T.C., S.V. Kokelj, S.E. Gergel, and G.H.R. Henry. 2009. Relative impacts of disturbance and temperature: Persistent changes in microenvironment and vegetation in retrogressive thaw slumps. *Global Change Biology* 15: 1664–1675.
- Le Moullec, M., A. Ø. Pedersen, A. Stien, J. Rosvold, and B. B. Hansen. 2019. A century of conservation: The ongoing recovery of svalbard reindeer. *Journal of Wildlife Management*: 1–11.
- Lefebvre, J., G. Gauthier, J.F. Giroux, A. Reed, E.T. Reed, and L. Belanger. 2017. The greater snow goose *Anser caerulescens atlanticus*: Managing an overabundant population. *Ambio* 46: 262–274. <https://doi.org/10.1007/s13280-016-0887-1>.
- Lindenmayer, D.B., and G.E. Likens. 2009. Adaptive monitoring: a new paradigm for long-term research and monitoring. *Trends in Ecology & Evolution* 24: 482–486.
- Lindenmayer, D.B., G.E. Likens, A. Haywood, and L. Miezi. 2011. Adaptive monitoring in the real world: Proof of concept. *Trends in Ecology & Evolution* 26: 641–646.
- Lousada, M., P. Pina, G. Vieira, L. Bandeira, and C. Mora. 2018. Evaluation of the use of very high resolution aerial imagery for accurate ice-wedge polygon mapping (Adventdalen, Svalbard). *Science of the Total Environment* 615: 1574–1583.
- Mack, M.C., M.S. Bret-Harte, T.N. Hollingsworth, R.R. Jandt, E.A.G. Schuur, G.R. Shaver, and D.L. Verbyla. 2011. Carbon loss from an unprecedented Arctic tundra wildfire. *Nature* 475: 489–492.
- Milner, J.M., O. Varpe, R. van der Wal, and B.B. Hansen. 2016. Experimental icing affects growth, mortality, and flowering in a high Arctic dwarf shrub. *Ecology and Evolution* 6: 2139–2148.
- Mosbacher, J.B., D.K. Kristensen, A. Michelsen, M. Stelvig, and N.M. Schmidt. 2016. Quantifying muskox plant biomass removal and spatial relocation of nitrogen in a high arctic tundra ecosystem. *Arctic, Antarctic, and Alpine Research* 48: 229–240.
- Myers-Smith, I., M. Grabowski, H.J.D. Thomas, S. Angers-Blondin, G.N. Daskalova, A.D. Bjorkman, A.M. Cunliffe, J.J. Assmann, et al. 2019. Eighteen years of ecological monitoring reveals multiple lines of evidence for tundra vegetation change. *Ecological Monographs* 89: 1–21.
- Myers-Smith, I.H., S.C. Elmendorf, P.S.A. Beck, M. Wilmking, M. Hallinger, D. Blok, K.D. Tape, S.A. Rayback, et al. 2015. Climate sensitivity of shrub growth across the tundra biome. *Nature Climate Change* 5: 887.
- Myers-Smith, I.H., B.C. Forbes, M. Wilmking, M. Hallinger, T. Lantz, D. Blok, K.D. Tape, M. Macias-Fauria, et al. 2011. Shrub expansion in tundra ecosystems: dynamics, impacts and research priorities. *Environmental Research Letters* 6: 045509.
- Olofsson, J., H. Tommervik, and T.V. Callaghan. 2012. Vole and lemming activity observed from space. *Nature Climate Change* 2: 880–883.
- Pedersen, A.O., J.D.M. Speed, and I.M. Tombre. 2013. Prevalence of pink-footed goose grubbing in the arctic tundra increases with population expansion. *Polar Biology* 36: 1569–1575.
- Peeters, B., A.O. Pedersen, L.E. Loe, K. Isaksen, V. Veiberg, A. Stien, J. Kohler, J.C. Gallet, et al. 2019. Spatiotemporal patterns of rain-on-snow and basal ice in high Arctic Svalbard: Detection of a climate-cryosphere regime shift. *Environmental Research Letters* 14: 015002.
- Perreault, N., E. Levesque, D. Fortier, and L. J. Lamarque. 2016. Thermo-erosion gullies boost the transition from wet to mesic tundra vegetation. *Biogeosciences* 13: 1237–1253.
- Post, E., M.C. Forchhammer, M.S. Bret-Harte, T.V. Callaghan, T.R. Christensen, B. Elberling, A.D. Fox, O. Gilg, et al. 2009. Ecological dynamics across the arctic associated with recent climate change. *Science* 325: 1355–1358.
- Prach, K., J. Kosnar, J. Klimesova, and M. Hais. 2010. High Arctic vegetation after 70 years: A repeated analysis from Svalbard. *Polar Biology* 33: 635–639.
- Ratajczak, Z., P. D’Odorico, S.L. Collins, B.T. Bestelmeyer, F.I. Isbell, and J.B. Nippert. 2017. The interactive effects of press/pulse intensity and duration on regime shifts at multiple scales. *Ecological Monographs* 87: 198–218.
- Ravolainen, V.T., K.A. Brathen, R.A. Ims, N.G. Yoccoz, J.A. Henden, and S.T. Killengreen. 2011. Rapid, landscape scale responses in riparian tundra vegetation to exclusion of small and large mammalian herbivores. *Basic and Applied Ecology* 12: 643–653.
- Ravolainen, V.T., K.A. Brathen, N.G. Yoccoz, J.K. Nguyen, and R.A. Ims. 2014. Complementary impacts of small rodents and semi-domesticated ungulates limit tall shrub expansion in the tundra. *Journal of Applied Ecology* 51: 234–241.
- Scheffer, M., and S.R. Carpenter. 2003. Catastrophic regime shifts in ecosystems: Linking theory to observation. *Trends in Ecology & Evolution* 18: 648–656.
- Schmidt, N.M., D. Kristensen, A. Michelsen, and C. Bay. 2012. High Arctic plant community responses to a decade of ambient warming. *Biodiversity* 13: 191–199.
- Sjogersten, S., D.P.J. Kuijper, R. van der Wal, M.J.J.E. Loonen, A.H.L. Huiskes, and S.J. Woodin. 2010. Nitrogen transfer between herbivores and their forage species. *Polar Biology* 33: 1195–1203.
- Sjogersten, S., R. van der Wal, M.J.J.E. Loonen, and S.J. Woodin. 2011. Recovery of ecosystem carbon fluxes and storage from herbivory. *Biogeochemistry* 106: 357–370.

- Sluijs, J., S.V. Kokelj, R. Fraser, J. Tunnicliffe, and D. Lacelle. 2018. Permafrost terrain dynamics and infrastructure impacts revealed by UAV photogrammetry and thermal imaging. *Remote Sensing* 10: 1734.
- Speed, J.D.M., S.J. Woodin, H. Tømmervik, M.P. Tamstorf, and R. van der Wal. 2009. Predicting habitat utilization and extent of ecosystem disturbance by an increasing herbivore population. *Ecosystems* 12: 349–359.
- Staaland, H., J.O. Scheie, F.A. Grøndahl, E. Persen, A.B. Leifseth, and Ø. Holand. 1993. The introduction of reindeer to Brøggerhalvøya, Svalbard: Grazing preference and effect on vegetation. *Rangifer* 3: 15–19.
- Stringham, T.K., W.C. Krueger, and P.L. Shaver. 2003. State and transition modeling: An ecological process approach. *Journal of Range Management* 56: 106–113.
- Tape, K., M. Sturm, and C. Racine. 2006. The evidence for shrub expansion in Northern Alaska and the Pan-Arctic. *Global Change Biology* 12: 686–702.
- Van der Wal, R. 2006. Do herbivores cause habitat degradation or vegetation state transition? Evidence from the tundra. *Oikos* 114: 177–186.
- van der Wal, R., R.D. Bardgett, K.A. Harrison, and A. Stien. 2004. Vertebrate herbivores and ecosystem control: Cascading effects of faeces on tundra ecosystems. *Ecography* 27: 242–252.
- Van der Wal, R., and R.W. Brooker. 2004. Mosses mediate grazer impacts on grass abundance in arctic ecosystems. *Functional Ecology* 18: 77–86.
- Van der Wal, R., and D.O. Hessen. 2009. Analogous aquatic and terrestrial food webs in the high Arctic: The structuring force of a harsh climate. *Perspectives in Plant Ecology Evolution and Systematics* 11: 231–240.
- Van der Wal, R., S. Sjogersten, S.J. Woodin, E.J. Cooper, I.S. Jonsdottir, D. Kuijper, T.A.D. Fox, and A.D. Huiskes. 2007. Spring feeding by pink-footed geese reduces carbon stocks and sink strength in tundra ecosystems. *Global Change Biology* 13: 539–545.
- Van der Wal, R., and A. Stien. 2014. High-arctic plants like it hot: A long-term investigation of between-year variability in plant biomass. *Ecology* 95: 3414–3427.
- Van Pelt, W.J.J., J. Kohler, G.E. Liston, J.O. Hagen, B. Luks, C.H. Reijmer, and V.A. Pohjola. 2016. Multidecadal climate and seasonal snow conditions in Svalbard. *Journal of Geophysical Research-Earth Surface* 121: 2100–2117.
- Vanderpuye, A.W., A. Elvebakk, and L. Nilsen. 2002. Plant communities along environmental gradients of high-arctic mires in Sassendalen, Svalbard. *Journal of Vegetation Science* 13: 875–884.
- Vikhmar-Schuler, D., K. Isaksen, J. Haugen, H. Tømmervik, B. Luks, T. Schuler, and J. Bjerke. 2016. Changes in winter warming events in the Nordic Arctic Region. *Journal of Climate* 29: 6223–6244.
- Walker, D.A., M.K. Reynolds, F.J.A. Daniels, E. Einarsson, A. Elvebakk, W.A. Gould, A.E. Katenin, S.S. Kholod, et al. 2005. The Circumpolar Arctic vegetation map. *Journal of Vegetation Science* 16: 267–282.
- Warszawski, L., A. Friend, S. Ostberg, K. Frieler, W. Lucht, S. Schaphoff, D. Beerling, P. Cadule, et al. 2013. A multi-model analysis of risk of ecosystem shifts under climate change. *Environmental Research Letters* 8: 044018.
- Wasowicz, P., A.N. Sennikov, K.B. Westergaard, K. Spellman, M. Carlson, L.J. Gillespie, J.M. Saarela, S.S. Seefeldt, et al. 2019. Non-native vascular flora of the Arctic: Taxonomic richness, distribution and pathways. *Ambio* 1: 2. <https://doi.org/10.1007/s13280-019-01296-6>.
- Wegener, C., and A.M. Odasz-Albrigtsen. 1998. Do Svalbard reindeer regulate standing crop in the absence of predators? A test of the “exploitation ecosystems” model. *Oecologia* 116: 202–206.
- Wookey, P.A., R. Aerts, R.D. Bardgett, F. Baptist, K.A. Brathen, J.H.C. Cornelissen, L. Gough, I.P. Hartley, et al. 2009. Ecosystem feedbacks and cascade processes: Understanding their role in the responses of Arctic and alpine ecosystems to environmental change. *Global Change Biology* 15: 1153–1172.
- Zimov, S.A. 2005. Pleistocene park: Return of the mammoth’s ecosystem. *Science* 308: 796–798.
- Zwolicki, A., K.M. Zmudzynska-Skarbek, L. Iliszko, and L. Stempniewicz. 2013. Guano deposition and nutrient enrichment in the vicinity of planktivorous and piscivorous seabird colonies in Spitsbergen. *Polar Biology* 36: 363–372.

Publisher’s Note Springer Nature remains neutral with regard to jurisdictional claims in published maps and institutional affiliations.

AUTHOR BIOGRAPHIES

Virve Ravolainen (✉) is a researcher at the Norwegian Polar Institute and in the ecosystem-monitoring program “Climate-ecological Observatory for Arctic Tundra - COAT”. Her areas of research are vegetation ecology, climate–herbivore–vegetation interactions, and ecosystem monitoring in the Arctic.
Address: Norwegian Polar Institute, Fram Centre, 9296 Tromsø, Norway.
Address: Norwegian Polar Institute, Fram Centre, 9062 Tromsø, Norway.
e-mail: virve.ravolainen@npolar.no

Eeva M. Soininen is a researcher at UiT—The Arctic University of Norway, and a coordinator in “Climate-Ecological Observatory for Arctic Tundra—COAT”. Her research is focused on food web interactions in northern and Arctic ecosystems.
Address: UiT, The Arctic University of Norway, 9037 Tromsø, Norway.

Ingibjörg Svala Jónsdóttir is a Professor of ecology at University of Iceland. Her research interest are plant–herbivore interactions, biodiversity, and the effects of climate change and land use on terrestrial ecosystems at northern latitudes.
Address: University of Iceland, 101 Reykjavik, Iceland.
Address: The University Centre in Svalbard, 9171 Longyearbyen, Norway.

Isabell Eischeid is a Ph.D. student at UiT—The Arctic University of Norway and The Norwegian Polar Institute. Her research is focused on developing tools for efficient ecosystem-based monitoring of Arctic terrestrial ecosystems, focusing on image-based methods across spatial scales.
Address: Norwegian Polar Institute, Fram Centre, 9296 Tromsø, Norway.
Address: UiT, The Arctic University of Norway, 9037 Tromsø, Norway.

Mads Forchhammer is a Professor of terrestrial zoology at University Centre in Svalbard. His main areas of interest are population dynamics, ecological responses to climate change, and monitoring ungulate populations.
Address: The University Centre in Svalbard, 9171 Longyearbyen, Norway.
Address: The Centre for Macroecology, Evolution and Climate (CMEC) and Greenland Perspective (GP), Natural History Museum of Denmark, University of Copenhagen, Copenhagen, Denmark.

René van der Wal is a Professor at the Swedish University of Agricultural Sciences. His research interests are ecology in Society, interdisciplinary working, digital innovation in nature conservation, community ecology, plant–herbivore interactions, invasive species, and Arctic ecology.

Address: Department of Ecology, Swedish University of Agricultural Sciences (SLU), Ulls väg 16, 75651 Uppsala, Sweden.

Address: University of Aberdeen, AB24 3UU Aberdeen, Scotland.

Åshild Ø. Pedersen is a Reseacher at the Norwegian Polar Institute and in “Climate-ecological Observatory for Arctic Tundra - COAT”. Her research interests are terrestrial ecology, vertebrate herbivores, ecosystem interactions and climate change.

Address: Norwegian Polar Institute, Fram Centre, 9296 Tromsø, Norway.

Address: Norwegian Polar Institute, Fram Centre, 9062 Tromsø, Norway.

Paper II

In the processing of writing the introduction of this thesis I discovered a mistake that I made when reporting some of the classification results in the following study. In Figure 6, the value for the point JAN – optimized – optical and terrain has a higher F1-macro score than originally reported and is now at 88.5 %. The class specific F1 scores in Table 2 in the JAN row are also higher than originally reported (I had accidentally reported the values for the classifier using optical variables only). In the introduction section to this thesis, I have reported the correct values. I will also send these corrections to the journal. The online version of this paper should therefore have the correct values by the date of the defense. The confusion matrices (in supplementary materials) were and are correct.

F1- scores of ground-cover classifications at the three study sites on Svalbard using the optimized classes and all predictor variables (optical and terrain). Class names in order from left to right: moss-graminoid, moss-equisetum, wetland, moss-brown-wetland, Carex subspathacea, heath, dryas, cassiope, winter-damage-woody/biological crust, grubbing, bare ground, gravel, water, snow.

site	Class													
	mgr	meq	wet	mbw	csu	hea	dry	cas	wdc	gru	bgr	gra	wat	sno
JAN	85.2	89.3	92.3	-	-	76.5	94.9	80.7	83.1	90.5	92.8	91.3	89.3	100
SAS	70.5	83.8	92.8	-	-	77.3	80.2	92.0	88.7	86.1	75.0	84.0	93.4	-
TOD	84.7	85.9	80.8	86.4	97.7	95.6	80.7	74.7	77.5	78.3	88.9	74.0	98.9	-



Article

Disturbance Mapping in Arctic Tundra Improved by a Planning Workflow for Drone Studies: Advancing Tools for Future Ecosystem Monitoring

Isabell Eischeid ^{1,2,3,*}, Eeva M. Soininen ¹, Jakob J. Assmann ⁴, Rolf A. Ims ¹, Jesper Madsen ³, Åshild Ø. Pedersen ², Francesco Pirotti ⁵, Nigel G. Yoccoz ¹ and Virve T. Ravolainen ²

¹ Department of Arctic and Marine Biology, UiT The Arctic University of Norway, 9037 Tromsø, Norway; eeva.soininen@uit.no (E.M.S.); rolf.ims@uit.no (R.A.I.); nigel.yoccoz@uit.no (N.G.Y.)

² Fram Centre, Norwegian Polar Institute, 9296 Tromsø, Norway; ashild.pedersen@npolar.no (Å.Ø.P.); virve.ravolainen@npolar.no (V.T.R.)

³ Department of Ecoscience, Aarhus University, 8410 Rønde, Denmark; jm@ecos.au.dk

⁴ Department of Biology—Ecoinformatics and Biodiversity, Aarhus University, 8000 Aarhus C, Denmark; j.assmann@bios.au.dk

⁵ CIRGEO Interdepartmental Research Center of Geomatics, TESAF Department, University of Padova, Viale dell'Università 16, 35020 Legnaro, Italy; francesco.pirotti@unipd.it

* Correspondence: isabell.eischeid@uit.no



Citation: Eischeid, I.; Soininen, E.M.; Assmann, J.J.; Ims, R.A.; Madsen, J.; Pedersen, Å.Ø.; Pirotti, F.; Yoccoz, N.G.; Ravolainen, V.T. Disturbance Mapping in Arctic Tundra Improved by a Planning Workflow for Drone Studies: Advancing Tools for Future Ecosystem Monitoring. *Remote Sens.* **2021**, *13*, 4466. <https://doi.org/10.3390/rs13214466>

Academic Editor: Shridhar D. Jawak

Received: 23 September 2021

Accepted: 2 November 2021

Published: 6 November 2021

Publisher's Note: MDPI stays neutral with regard to jurisdictional claims in published maps and institutional affiliations.



Copyright: © 2021 by the authors. Licensee MDPI, Basel, Switzerland. This article is an open access article distributed under the terms and conditions of the Creative Commons Attribution (CC BY) license (<https://creativecommons.org/licenses/by/4.0/>).

Abstract: The Arctic is under great pressure due to climate change. Drones are increasingly used as a tool in ecology and may be especially valuable in rapidly changing and remote landscapes, as can be found in the Arctic. For effective applications of drones, decisions of both ecological and technical character are needed. Here, we provide our method planning workflow for generating ground-cover maps with drones for ecological monitoring purposes. The workflow includes the selection of variables, layer resolutions, ground-cover classes and the development and validation of models. We implemented this workflow in a case study of the Arctic tundra to develop vegetation maps, including disturbed vegetation, at three study sites in Svalbard. For each site, we generated a high-resolution map of tundra vegetation using supervised random forest (RF) classifiers based on four spectral bands, the normalized difference vegetation index (NDVI) and three types of terrain variables—all derived from drone imagery. Our classifiers distinguished up to 15 different ground-cover classes, including two classes that identify vegetation state changes due to disturbance caused by herbivory (i.e., goose grubbing) and winter damage (i.e., 'rain-on-snow' and thaw-freeze). Areas classified as goose grubbing or winter damage had lower NDVI values than their undisturbed counterparts. The predictive ability of site-specific RF models was good (macro-F1 scores between 83% and 85%), but the area of the grubbing class was overestimated in parts of the moss tundra. A direct transfer of the models between study sites was not possible (macro-F1 scores under 50%). We show that drone image analysis can be an asset for studying future vegetation state changes on local scales in Arctic tundra ecosystems and encourage ecologists to use our tailored workflow to integrate drone mapping into long-term monitoring programs.

Keywords: classifier; disturbance; drone; ecological monitoring; GLCM; herbivore; random forest; Svalbard; winter climate effect; grubbing

1. Introduction

Rapid climate change is altering abiotic and biotic disturbance processes in the Arctic and could therefore lead to ecosystem state changes in tundra ecosystems [1–4]. Abiotic disturbances to the Arctic tundra may increase due to summer warming, leading to, e.g., permafrost collapse and erosion, whereas changes in the winter climate cause, for instance, rain-on-snow events and ground ice, permafrost thaw and changes of hydrological regimes [2,5–11]. In addition, climate change can also modify the intensity and frequency

of biotic disturbances to tundra, e.g., via herbivore grazing [12,13]. The cumulative effect of changes in multiple drivers can thus alter the state of tundra ecosystems [14]. Ecosystem state changes can be detected by mapping vegetation or tundra surface types, quantifying, for example, increases in forest or shrub cover [15,16], or assessing variables such as vegetation type composition and percentage of bare ground-cover [17,18]. While these examples illustrate that some ecosystem state changes have happened in the Arctic, it remains to be documented by means of long-term monitoring, which ecosystem states continue to develop in an Arctic landscape that is facing rapid environmental change [14].

High Arctic tundra, such as in Svalbard, represents an ecosystem in high demand for monitoring [3,13], as new biotic and abiotic conditions are evolving fast with rapid climate change. In particular, the winter climate in Svalbard has, since the late 1990s, seen a regime shift towards more frequent rain-on-snow events due to mild temperatures and, consequently, more pronounced formation of basal ice [19] that encapsulates and damages plants [20]. This commonly occurs in low-land tundra with, e.g., dwarf shrub vegetation [21]. Additionally, increasing herbivore populations (e.g., goose and reindeer) can cause biotic disturbances [12,22]. In Svalbard, a mode of herbivory with particular importance to the tundra is pink-footed goose (*Anser brachyrhynchus*) grubbing, which disrupts the vegetation by removing plants and the moss layer [23–25]. The population of pink-footed geese has increased dramatically since the 1990s [26], and heavy grubbing can remove enough vegetation to cause patches of bare ground, potentially leading to soil erosion, destabilizing permafrost and changes in the soil-carbon cycle [14,27–29]. Warmer summers can destabilize the permafrost further but simultaneously also lead to higher primary production and above-ground biomass [30]. Effects of summer warming, changed winter climate and altered herbivory are expected to change the current state of this high Arctic ecosystem [14]. The disturbances described above commonly cover only small areas but occur frequently across the landscape, resulting in a heterogeneous tundra where the vegetation is interspersed with different types of disturbed patches. Detecting such disturbances at the landscape scale requires new, improved monitoring methods [14].

Drones have become more accessible in recent years and allow researchers to cover larger spatial extents at multiple temporal scales [31]. Drone images provide spatial grain sizes that allow studying ecological processes at local scales in highly heterogeneous landscapes. They can help transferring from local and detailed knowledge to broad-scale environments with more spatial and temporal complexity and can improve the interpretation of satellite imagery [32]. In the Arctic, drones have been used for vegetation mapping [33–35], measurements of cryosphere characteristics [36–45], observations of permafrost thaw [46,47] and to help bridge the gap between field- and satellite-derived data [32,35,48]. Long-term monitoring is stated as a goal in many recently published drone studies (e.g., [49,50]), but as the technology is quite new, few current studies have compared results from drone data between years or even within the same season [32,35].

Ecological monitoring is based on comparable, repeated measurements and requires robust methodology at all steps from data collection to statistical inference. Monitoring that is based on comparisons of drone images across time (seasons, years) or space (between different areas) faces methodological challenges for obtaining consistent and comparable data [51–53]. Recent studies have developed guidelines for drone data acquisition, geometric processing and radiometric calibrations [31,53,54]. This helps ecologists obtain high-quality images that would allow for temporal and spatial comparison. There has been less attention on how to systematically analyze these images to extract ecological variables relevant for monitoring an ecosystem state's changes resulting from environmental drivers. Arctic ecological monitoring programs (e.g., [55–58]), networks [59] and drone ecologists, in general, are tasked with finding the balance between their scientific interests and technical remote sensing abilities. The use of drones as a tool in ecology will therefore benefit from shared protocols that go beyond the first steps of image acquisition and processing. To better capture ecosystem changes, we need to include further steps

in the overall workflow, such as variable selection, layer resolution, ground-cover class selection and model development, including ground calibration and validation [31,53].

The overall aim of our study is to test ways of using drone imagery to collect variables that will be important to describe vegetation state changes resulting from abiotic and biotic disturbance factors that currently frequently occur at our study sites in Svalbard. For this purpose, we develop a method planning workflow with a focus on the steps after image acquisition (Table 1) to serve as guidance for the use of drone images in tundra ecological monitoring.

Table 1. Method planning workflow for drone flight campaigns and image classifications in a tundra landscape. Studies for the steps where guidance has been published are referenced. Asterisks indicate the steps we included in our study.

Topic	Solution
(1) Flight planning	
What to consider when planning field work?	<p>Choose appropriate image overlap and camera angles for desired final product. *</p> <p>Ensure that the type of the drone, the camera and flight speeds integrate well with one another to obtain high-quality images of suitable resolution and avoid blurring due to slow rolling shutter speeds [60]. *</p> <p>Follow appropriate radiometric calibration guidelines. See guidelines from Aasen et al. [31], Assmann et al. [54] and Tmušić et al. [53] with advice for choices of flight line, (image) overlap, camera type, drone type, weather and sun, radiometric calibration, geolocation, ground control points and ground truthing. *</p> <p>Ensure accurate geolocation of images and groundtruthing data. *</p>
(2) Variable selection	
Which variables to derive from the drone images?	A priori knowledge of the landscape is important to select appropriate data layers and resolutions that represent ecologically explainable heterogeneity in the terrain. *
How to assess which of the available variables to include in a classifier?	Variable importance can be ranked in a preliminary classifier using a subset of the available data [61,62]. *
Which variables best discriminate between ground-cover classes?	Exploratory data analysis via visual inspection of data via plotting to detect patterns important for the classification. *
What neighborhood size to select?	<p>Neighborhood size can be ranked in a preliminary classifier using a subset of the available data [61,62]. *</p> <p>Appropriate neighborhood sizes for secondary layers can be computationally derived using a minimum entropy approach [63].</p> <p>Computational limits may define the minimum resolution or maximum possible neighborhood sizes [64]. *</p>

Table 1. Cont.

Topic	Solution
(3) Ground-cover class selection	
How to define the first choice of ground-cover classes for the classifier?	Data-driven—Cluster analysis to see the separability of data without human input (unsupervised classification). Research-driven—Considering data-driven results define classes that are present in the area of interest for monitoring or expected to change over time (supervised classifications). *
How to choose between classifier robustness and ground-cover class detail?	Pre-define the ecological context of the ground-cover classes to determine which ones are meaningful to merge due to ecological similarities. *
How to increase transparency on class selection and its effects on classification accuracy?	Define documentation of how the final classes, explain class merges and the research consequences of mixing classes. *
(4) Classifier development and validation	
How to choose groundtruthing points?	Choose areas that are representative for the ground-cover classes and large enough sample sizes [65]. * Aim for a training data cover of approximately 0.25% of the study site [66] (recommendation based on medium-coarse grain satellite data). Avoid spatial autocorrelation of groundtruthing points by stratified random sampling in a blocked design [67]
How to avoid overfitting the classifier?	Split the dataset into training and validation datasets (such as K-fold mechanism or using random resampling) [64]. *
How to assess classifier robustness?	Use an independent validation dataset for external validation [68] If an independent dataset is not available, repeat runs of the classifier though multiple K-fold runs or repeat sampling of training and validation dataset [68]. * Additional map validation by local experts can help discover issues that go undetected by classifier evaluation statistics. This can be conducted, for example, by visually comparing the classified map with the drone images, pictures or revisits to the site. *
(5) Transferability of classifier	
How to assess the potential for transferability?	Exploratory data analysis via visual inspection of data via plotting to detect trends/shifts in values across sites or time intervals. *
How to test the transferability of the classifier?	Repetition of data collection in new area, creation of independent classifier and test in other area. *
How to improve the transferability of the classifier?	Tree pruning, simplification of the classifier, transferability functions [69,70]

2. Material and Methods

2.1. Study System

Svalbard is a high Arctic archipelago (74°–81°N, 10°–35°E), where only 15% of the land is vegetated [71,72]. Our three study sites (Janssonhaugen (JAN), Sassendalen (SAS) and Todalen (TOD)) are located in Nordenskiöld Land in the center of the main island, Spitsbergen (Figure 1). The area is characterized by glacial valleys with continuous vegetation at low elevations and sparse to no vegetation at higher elevations and on mountain slopes [73]. The study sites have similar plant community compositions, and each spans

a gradient from moist-mesic tundra mires to dry-mesic ridges [74]. More information on the plant communities can be found in Appendix A. Annual precipitation is around 190 mm [75], and soils range from hyperskeletal cryosols in the moist moss tundra, haplic cryosols in the dry ridges and turbic cryosols where thaw-freeze cycles perturbate the ground (based on descriptions of Migala et al. [76]).

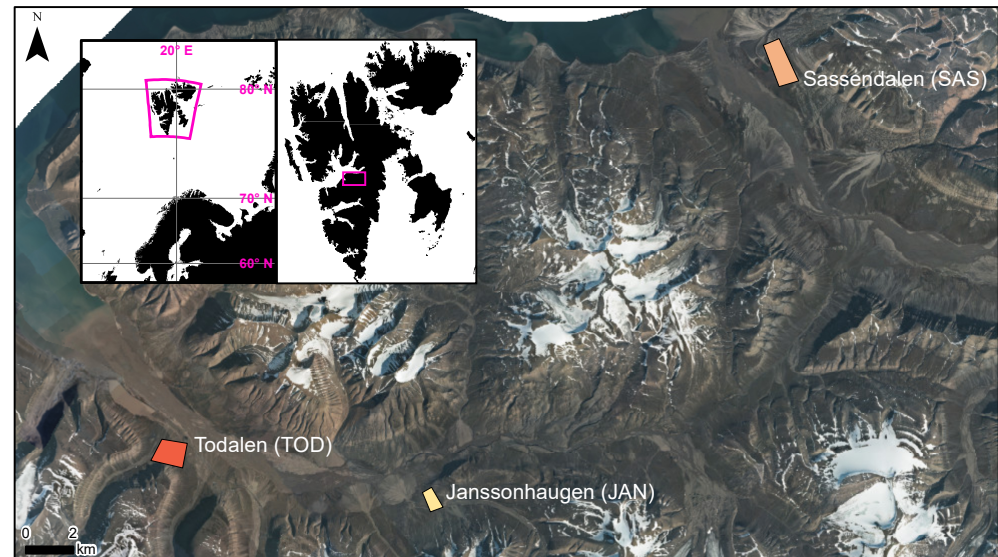


Figure 1. Location of drone flights of the case study in Central Spitsbergen, JAN: 78.16996°N, 16.300685°E, 0.3 km²; SAS: 78.331412°N, 16.974537°E, 1 km²; TOD: 78.188762°N, 15.82335°E, 1 km². Ground sampling distances (GSD) are listed for each site and camera (AeriaX RGB/Sequoia+ 4Band): JAN: 1.9 cm/9.8 cm; SAS: 2.2 cm/13.2 cm; TOD: 1.2 cm/10.3 cm. Aerial orthophoto provided by the Norwegian Polar Institute.

2.2. Study Preparation

We developed a workflow (see Table 1) to systematically plan the data collection and analysis steps of our study.

2.3. Data Collection

Our data collection choices are based on considerations presented in Table 1—(1) *Flight planning*. We captured aerial images during plant biomass peak season (20–28 July 2019) at the three study sites (Figure 1). We used a fixed wing drone (eBeeX by Sensefly) rigged with an AeriaX RGB camera and Sequoia+ four band camera (red, near infrared, red edge and green bands). As the Sequoia+ camera model is radiometrically calibrated automatically [77], we only took pictures of a spectral calibration target (Zenith Lite—SphereOptics) as backup. Image overlap was 70% or higher for the AeriaX RGB camera, while for the Sequoia+, side overlap was 60% and horizontal overlap 80%. We flew in perpendicular lines to the main slope of the terrain and kept a constant height over the ground (between 70 and 100 m above ground, depending on the camera and site) and speeds between 8–15 m/s).

Ground sampling distance (GSD) varied slightly between sites, see Figure 1. We flew around noon (earliest 10:00 latest 15:00) to have similar light conditions and avoid shadows on sunny days. We only flew on days with stable light conditions, such as blue skies (for study sites TOD, SAS) or continuous overcast (study site JAN), and wind speeds below 7 m/s. We used a Leica GS10 base station (Leica Geosystems) with an in-flight RTK (real time kinematic) link to the drone to obtain camera positions in real time and thus readily georeferenced images. We placed four ground control points (GCPs) in the area to validate spatial location accuracy, for which the maximum error was 5 cm.

We collected ground truth (GT) information, i.e., ground-cover class validation points, with the help of an accurate GPS system (Leica GS10 base station and rover) at 2 cm accuracy and real time correction. We aimed at collecting GT points spread throughout each of the study sites, with ca. 40 GT points per ground-cover class for each site, resulting in a total of 1782 GT points. We identified a total of 17 ground-cover classes, but not all classes were present at all sites. For each GT point, we noted the dominant ground-cover type in a ca. 7.5 cm radius around the point. Figure 2 illustrates the variation of the ground-cover classes. See Appendix A for detailed descriptions of each of the ground-cover classes.

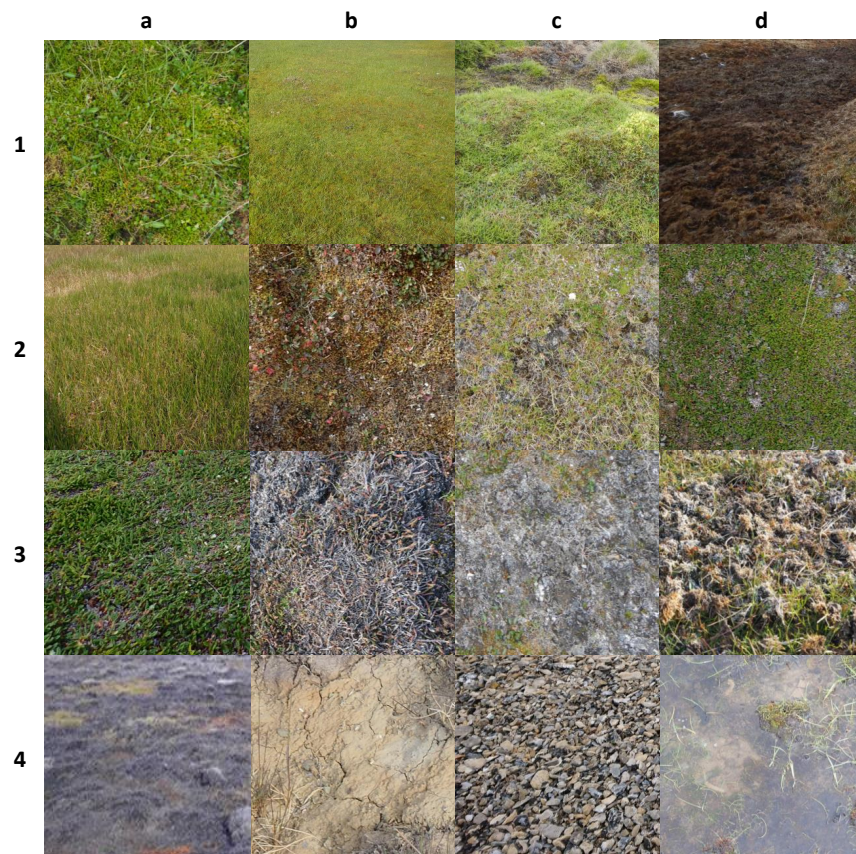


Figure 2. Images of 16 ground-cover classes that were included in the initial classification scheme. **row 1:** moss-graminoid, moss-equisetum, wetland, moss-brown-wetland; **row 2:** *Carex subspathacea*, heath-moss, heath-graminoid, dryas; **row 3:** cassiope, winter-damage-woody, biological crust, grubbing; **row 4:** winter-damage-moss, bare ground, gravel, water. The class snow is not shown in this graphic. Detailed information for each class can be found in the Appendix A.

2.4. Data Preparation

Using Pix4D Mapper [78], we generated five orthomosaics with images from the Sequoia+ sensor (four optical bands and the normalized difference vegetation index (NDVI)). With the same software, we created a digital surface model (DSM) using the 3D point cloud from the images of the AeriaX RGB camera. Our AeriaX RGB camera switched from manual to automatic settings during several instances and could therefore not be radiometrically calibrated. As a result, we used RGB images only to generate the DSM. We used the R (version 4.0.0.) software for all further analyses [79], and scripts can be found in the Supplementary Materials. To obtain textural information from our orthomosaics, we calculated gray level co-occurrence matrices (GLCMs), as conducted in Wang et al., 2015 [61], using the R package glcm [80]. We calculated seven types of GLCMs for the NDVI, green and red edge orthomosaics and using four different neighborhood sizes (0.3 m, 0.9 m, 1.5 m, 2 m) with equal offsets in all directions as we did not expect any specific directionality in our data. Larger neighborhood sizes for the GLCMs were not computationally feasible

with our setup, as processing times per variable reached multiple days. We did not include the DSM in our analysis because we found that the absolute height above sea level is not a useful predictor for generalizing across sites as it is too specific for each study site. Instead, we used it to calculate several of the terrain variables that were tested and discussed in [81]: slope at 1 m, 5 m and 10 m resolution, vector ruggedness, dissection, several curvature functions and terrain ruggedness (R package: SpatialEco [82]), all of the latter at 0.2 m and 1 m resolution using a range of neighborhoods sizes (0.6 m–2.2 m for the 0.2 m resolution, with 0.4 m intervals, and 3 m–131 m for the 1 m resolution, with 10 m intervals). We chose the smaller resolutions to capture the local heterogeneity of the terrain, such as tussocks and grubbing craters, and the larger resolutions to describe more general terrain positioning at the study sites.

2.5. Variable Selection

To reduce the number of drone-imagery-derived variables for further analyses, we used two exclusion criteria. First, we visually investigated the potential of the terrain variables to distinguish ground-cover classes by plotting maps and generating boxplots. This led us to exclude the curvature functions and terrain ruggedness and only continue with slope, vector ruggedness and dissection. Both GLCMs and terrain functions are dependent on the analysis window size (neighborhoods). For each site, we explored the GLCMs and terrain variable neighborhoods in preliminary models to assess their predictive ability for at least one of the ground-cover classes. This way we reduced the number of GLCMs from 84 to 39 and the terrain variables from 61 to 21. More detailed information on variable selection considerations can be found in Table 1—(2) *Variable selection*.

2.6. Ground-Cover Class Selection

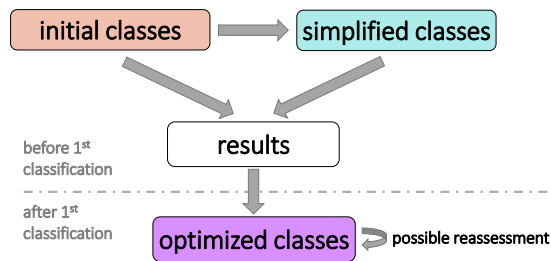
We used a research-driven class selection approach (see Table 1—(3) *Ground-cover class selection*). Since the final ground-cover classes were not pre-defined, we created a flowchart to guide our decision making on how to systematically test our ability to detect ground-cover classes (Figure 3a) at different levels of detail. As a starting point of selecting ground-cover classes, we created two lists of class detail (Figure 3b). Our scheme with *initial* classes included all the ground-cover classes that we identified as ecologically relevant to characterize the ground. We were mostly interested in detecting disturbance ground-cover classes, and our class selection is oriented towards that. We further created a *simplified* classes scheme that would fulfill our minimum requirements of detecting the disturbance-related classes (*bare ground*, *grubbing*, *winter damage*, *biological crust*) and merged all vegetated classes into one. After running the classification algorithm on both schemes and evaluating the results, we created a third, *optimized* classes list (Figure 3b). The *optimized* classes differ from initial classes in three ways: (i) *heath vegetation* is grouped into a single class, (ii) the *winter-damage-moss* class is excluded as it was a very localized phenomena and challenging to validate, and (iii) the *biological crust* and *winter damage classes* are grouped into a single (mixed) class.

2.7. Data Analysis

2.7.1. Disturbance Detection Based on NDVI

In an exploratory examination, we investigated our ability of using drone images and a GSD of approximately 10 cm to detect pink-footed goose grubbing, winter damage (i.e., grey areas of dead vegetation) and bare ground (open soil). We compared the NDVI value differences of the GT points in both disturbed and undisturbed areas within the same vegetation type: For dry-mesic habitats, we compared *cassiope* and *dryas* against *biological crust* and *winter damage*. For moist-mesic habitats, we compared *wetland* and *graminoid moss* against both *grubbing* and *bare ground*. We use box-and-whisker plots to show the range of NDVI values for each study site and ground-cover class.

(a) Class selection process



(b) Class selection Svalbard case study

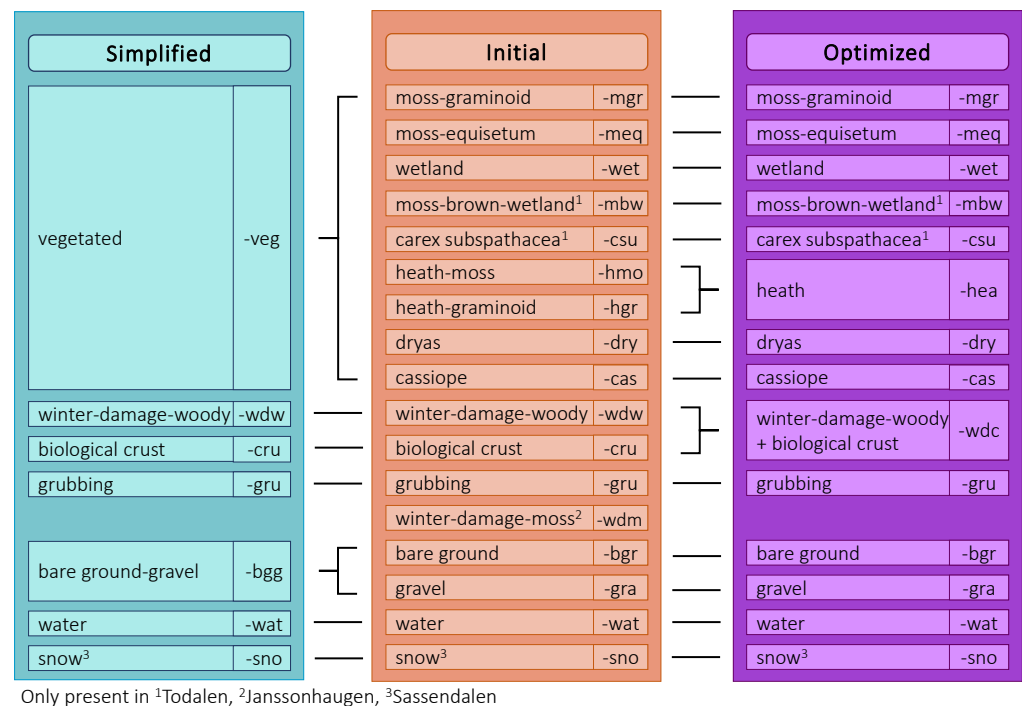


Figure 3. Ground-cover class selection schemes. (a) Stages to determine ground-cover classes balancing class detail and classification accuracy. The first stage includes testing two class schemes: one with the most possible detail and one with the minimum required class detail. In the second stage, the optimal classes are determined by merging the classes that improve the classification accuracy using the simplified class scheme as a guideline for meaningful merges. (b) The initial, simplified and optimized ground-cover classes and class abbreviations used in the case study to classify tundra vegetation on Svalbard.

2.7.2. Classifier Development and Validation

See Table 1 for considerations on (4) *Classifier development and validation*. We used a random forest (RF) classifier [83] to develop ground-cover classification models for each of the study sites. We selected the RF classifier as it has been shown to be successful for spatial vegetation data [84]. For each of the study sites, we generated six RF models using three levels of detail for output classes (*initial*, *simplified* and *optimized*) and two sets of input variables (*optical and terrain* and *optical only*). Note that the ground-cover classification schemes differed slightly between study sites as not all classes were present at each site (Figure 3b). We used our field ground truthing (GT) data as training data by extracting the pixel values for each layer that were within the 7.5 cm radius at each GT coordinate. For some classes (*snow*, *water*, *Carex subspathacea*, *dryas*, *cassiope*), we lacked sufficient GT points and therefore obtained additional training data from the drone imagery. To do this,

we drew polygons of the classes with insufficient training data using the RGB orthomosaics and field recordings and added all pixels within those polygons to our GT dataset.

Each RF model was developed as follows (Figure 4): we first split the extracted GT data 70–30% (stratified random, i.e., random 70–30% split within ground-cover class) into a training dataset and a validation dataset. As each GT coordinate encompassed several pixels, we reduced autocorrelation by not using any of the pixels from the same GT point for both training and validation. We then trained the RF model with the training dataset using the “fit” function (“rminer” package [85]) with $n_{tree} = 500$ and a default set of $m_{try} = 8$. We tested the classifier output on the independent validation dataset using the “predict” function in “rminer”. To assess the robustness of each RF model, we repeated the process (i.e., the dataset split, model fitting and validation) thirty times. We used F1 scores to compare model performances because this measure captures both observation accuracy (recall, i.e., proportion of correctly classified pixels of a ground-cover class among all pixels belonging to that class) and prediction accuracy (precision, i.e., proportion of correctly classified pixels of a ground-cover class among all pixels classified to of that class) in a single score ($F1 = 2 \cdot \frac{precision \cdot recall}{precision + recall}$). F1 scores range from 0 to 100%, with values close to 100% representing high observation and high prediction accuracy. We calculated mean F1 scores for each ground-cover class and the mean macro-F1 score (arithmetic mean of all ground-cover class F1 scores) to summarize the results of the 30 cross-validation runs. We used confusion matrices to assess in more detail where class mixing occurred. In addition, we assessed the selection of predictor variables by analyzing variable importance in each of the RF models.

We created classified maps for each site with the *optical and terrain* option with the *optimized* classes. We then computed maps from these model outputs for each site using the predict function (“raster package” [86]) with parallel processing to speed up the process (ClusterR package [87]). We validated the classification by comparing the classified maps with the drone orthomosaics and hand-held pictures taken in the field.

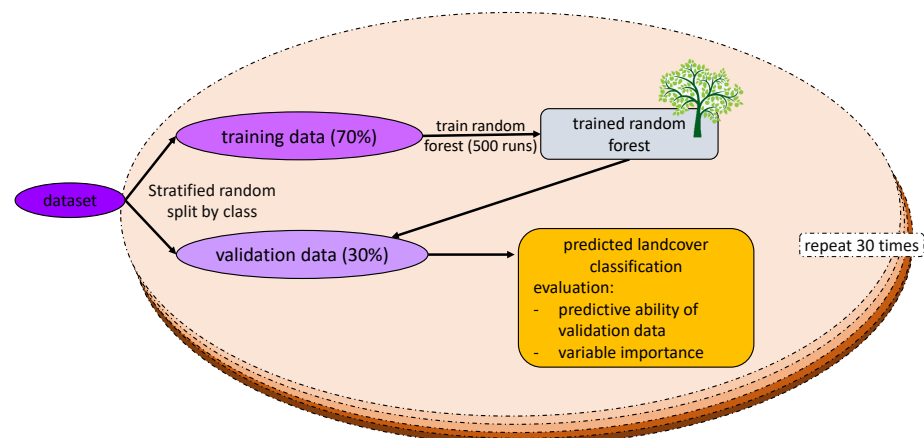


Figure 4. Data selection process, model validation and evaluation. The classifier was developed using 70% of the dataset as training data and 30% as validation data. The dataset split and classifier was run 30 times. Classifier performance mean and variance as well as variable importance values were calculated from the outputs.

2.7.3. Spatial Transferability

We tested how accurately a model, trained with the optimized classes developed for one study site, performed at the other two sites. First, we reduced the dataset to the ground-cover classes by excluding classes that were not present in all three sites. Then we ran the training on RF for each layer selection set (*optical and terrain* and *optical only*). Finally, we used these models to predict the ground-cover class for each pixel at the two other sites that were left out. We only tested the RF classifier transferability “as is” and did not adjust the RF trees by pruning or using transfer functions. See Table 1—(5) *Transferability of classifier*

for more information. We used macro-F1 scores to compare the prediction outputs with one another. To gain a better understanding of the similarities between the classifiers, we compared their variable importance rankings using the mean decrease accuracy measure.

3. Results

3.1. Disturbance Detection Based on NDVI

Disturbed and associated undisturbed ground-cover types differed in their median normalized difference vegetation index (NDVI) values but had overlapping interquartile ranges. This was consistent for the three study sites (Figure 5). Most of the *wetland* GT points had NDVI values of 0.75 or higher, and the median of registered *moss graminoid* points was around 0.7. Most grubbing GT points had NDVI values that were lower than the undisturbed classes and had median values between 0.53 and 0.58. The *bare ground* class had the lowest NDVI, and none of the values overlapped with the undisturbed classes except for the outliers (Figure 5a). Among the drier ground-cover classes, *dryas* and *cassiope* had NDVI value medians between 0.59 and 0.75 across the three sites, whereas the classes *winter damage* and *biological crust* had median values between 0.30 and 0.48 (Figure 5b). The difference in NDVI values between the undisturbed and disturbed classes in the dry-mesic habitat was less pronounced in TOD compared to JAN and SAS.

3.2. Class and Layer Selection

Comparisons of the RF classifier performances between the three classification schemes and two sets of variable selections at each site (Figure 6) showed that the ground-cover classifications based on both the terrain and optical layers had higher macro-F1 scores than the ones using only optical layers. The magnitude of the difference depended on the study site and chosen classification scheme. The classifiers using terrain and optical variables showed that: (i) the optimized classification schemes performed similarly (macro-F1 score 82–83%) in all three sites, and (ii) sites differed in terms of performance of the simplified and initial classification schemes. In site TOD, the simplified classification scheme performed better than in the sites JAN and SAS. The optimized classifier improved (compared to the initial and simplified) macro-F1 scores most in TOD.

3.3. Variable Importance

The order of importance values (measured as the mean decrease accuracy for each variable in the RF) varied between the three study sites. Among the optical variables, NDVI-based gray level co-occurrence matrices (GLCM) variables were important in all three sites. NDVI was the most important layer for SAS and JAN, but ranked 19th in TOD. The terrain variables that were most important were dissection (especially at large neighborhoods) for JAN and TOD and slope for SAS. Terrain variables that were calculated at 0.2 m resolution were among the least important for predicting ground-cover classes. Complete lists with all importance values can be found in the Supplementary Materials.

3.4. Ground-Cover Classification

Most ground-cover classes of the *optimized* classifier had F1 scores of 70% or higher, often over 80–90% (Table 2). The scores were generally highest for the classes *snow*, *Carex subspathacea*, *water* and *wetland*. The classes *heath* and *gravel* had the largest variation in F1 scores between study sites. There was no consistent bias in model-misclassification of the ground-cover classes in the three classifiers. Confusion matrices that show the ground-cover class distributions for each of the classifiers can be found in the Supplementary Materials. The two disturbance classes *grubbing* and *winter damage/crust* had higher observation accuracy (recall) than prediction accuracy (precision) in all three sites. Classification errors occurred mainly within the moist-mesic and the dry-mesic habitats: For example, in JAN, the most common example of misclassification was that *cassiope* (precision: 91.9%, recall: 72.1%) was classified as *heath* (precision: 67.1%, recall: 83.2%) or *winter damage/crust* (precision: 80.2%, recall: 87.1%). In TOD, *grubbing* (precision: 78.6%, recall: 78.3%) was

most commonly falsely misclassified (both directions) with the *wetland* (precision: 78.6%, recall: 83.0%) and *graminoid-moss* (precision: 88.8%, recall: 81.4%) classes.

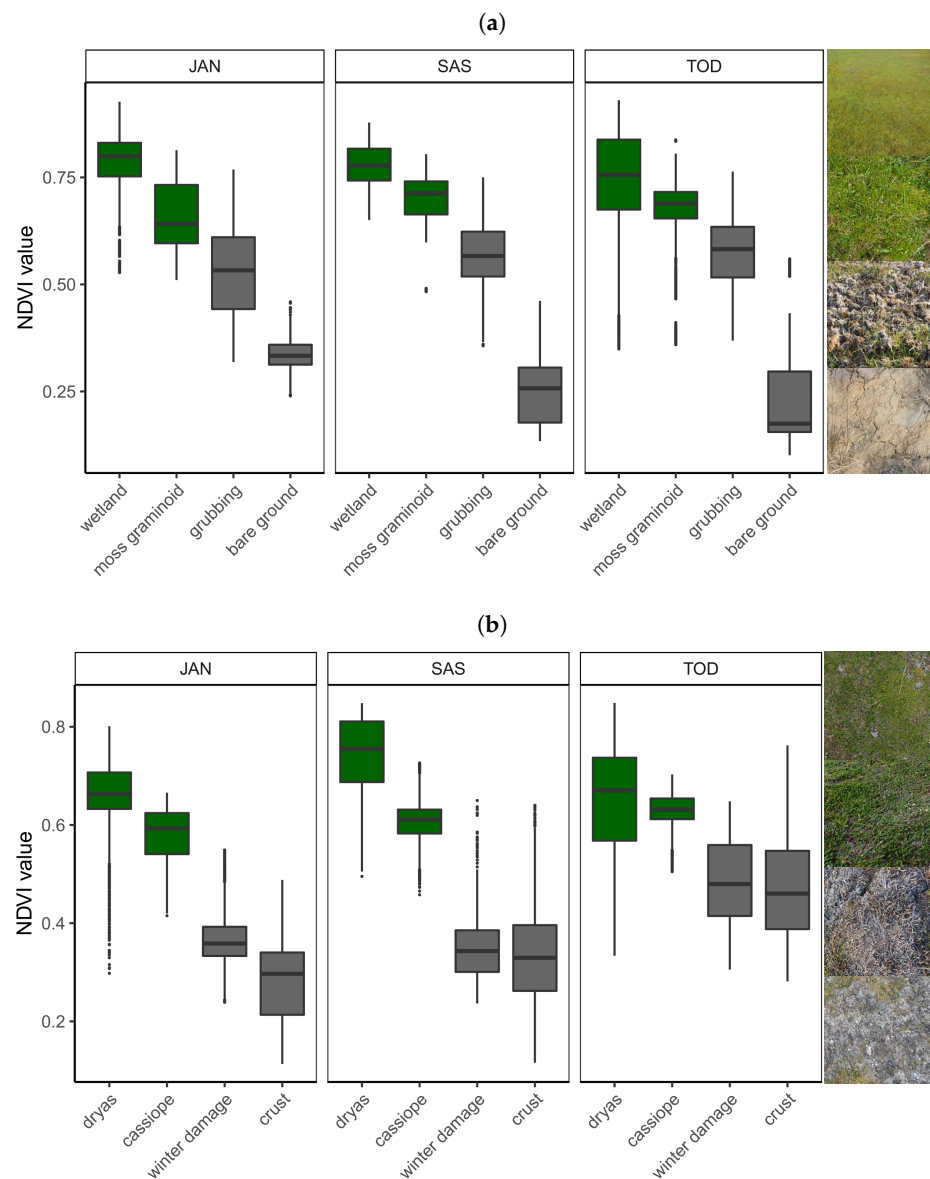


Figure 5. The distribution of NDVI values of selected ground-cover classes and their associated disturbances in the three study sites: The disturbed associates of classes *wetland* and *moss graminoid* are *grubbing* and *bare ground*, and the associated disturbed classes of *dryas* and *cassiope* are *winter damage* and *biological crust*. The boxes denote the interquartile ranges of NDVI values around the median for all registered ground-truthing pixels for each ground-cover class, and dots represent outliers. The order of the images (up-down) follows the x-axis from left to right for each plot. (a) Moist-mesic habitat; (b) Dry-mesic habitat.

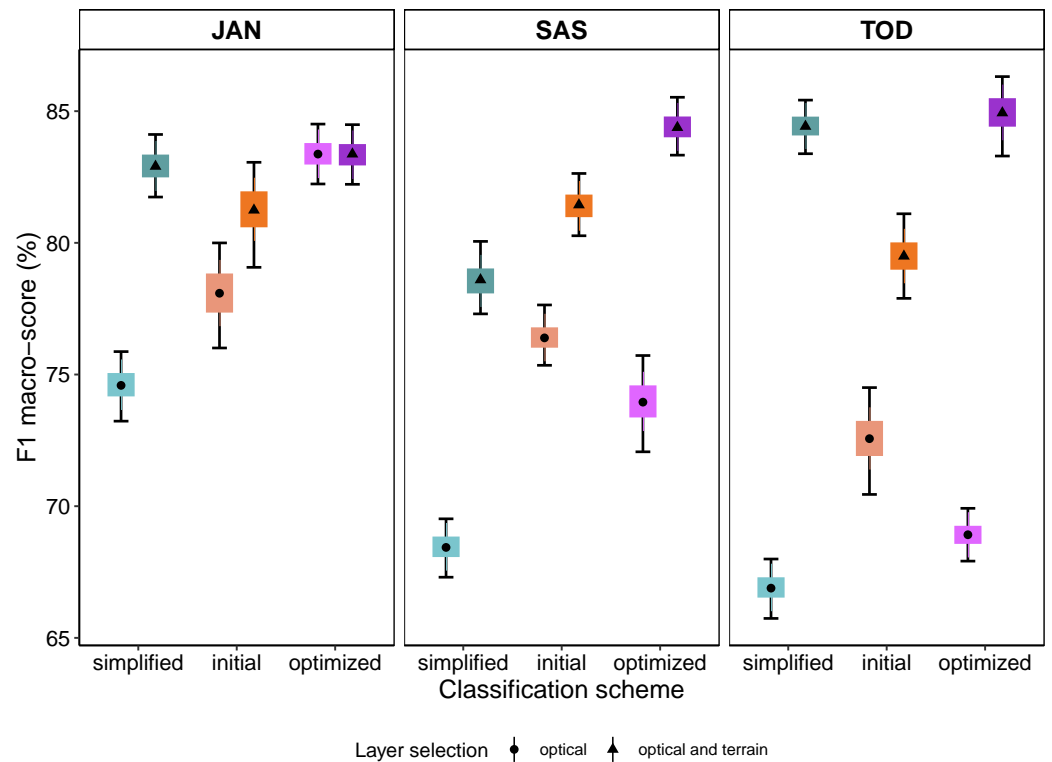


Figure 6. Comparison of site, classification scheme and layer selection. Black symbols represent mean macro-F1 scores after 30 runs, the colored boxes indicate confidence intervals of 0.5 and the bars represent the interval at 0.95.

Table 2. Macro-F1 scores of ground-cover classifications at the three study sites on Svalbard using the *optimized* classes and all variables (*optical and terrain*). Explanations to the class abbreviations can be found in Figure 3b.

site	Class													
	mgr	meq	wet	mbw	csu	hea	dry	cas	wdc	gru	bgr	gra	wat	sno
JAN	70.5	82.3	91.4	-	-	57.9	93.7	80.6	81.9	83.8	84.2	90.7	83.6	100
SAS	75.0	83.8	92.8	-	-	77.3	80.2	92.0	88.7	86.1	75.0	84.0	93.4	-
TOD	84.7	85.9	80.8	86.4	97.7	95.6	80.7	74.7	77.5	78.3	88.9	74.0	98.9	-

3.5. Visual Evaluation of Predicted Ground-Cover

Based on visual inspection, the classified maps (Figures 7–9) captured all ground-cover classes well. The *graminoid moss* tundra, the *wetlands* and the drier *Dryas* and *barren* classes were predicted as expected from our knowledge of the sites. Pink-footed goose grubbing was detected in *graminoid moss* tundra and in *wetland* vegetation (e.g., Figures 8b and 9b,d). *Winter damage/crust* was detected in dry ridges, within *Cassiope* belts and on top of polygonal moss tundra (e.g., Figures 8c and 9b). Based on our detailed in-field knowledge of the sites, there were site-specific misclassifications in “brown rugged terrain” (see discussion).

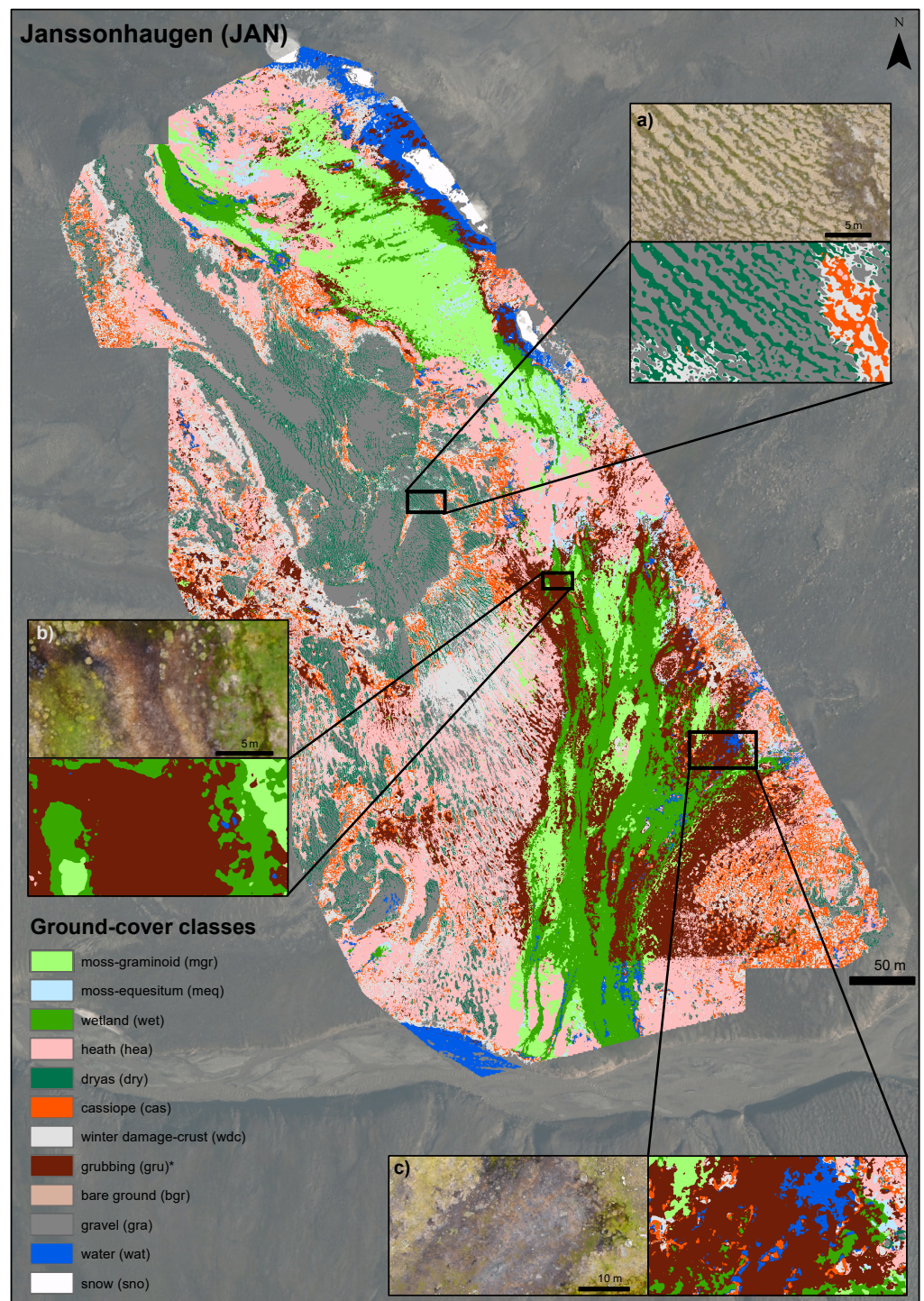


Figure 7. Classified map of Janssonhaugen (JAN). Zoomed areas highlight examples of classifications: (a) The classification of dry-mesic habitat with *dryas*, *cassiope*, *gravel* and *winter damage/crust*. (b) Wet, brown-colored mosses classified as *grubbing*. (c) Winter-damaged moss, classified as *grubbing* and *water*.

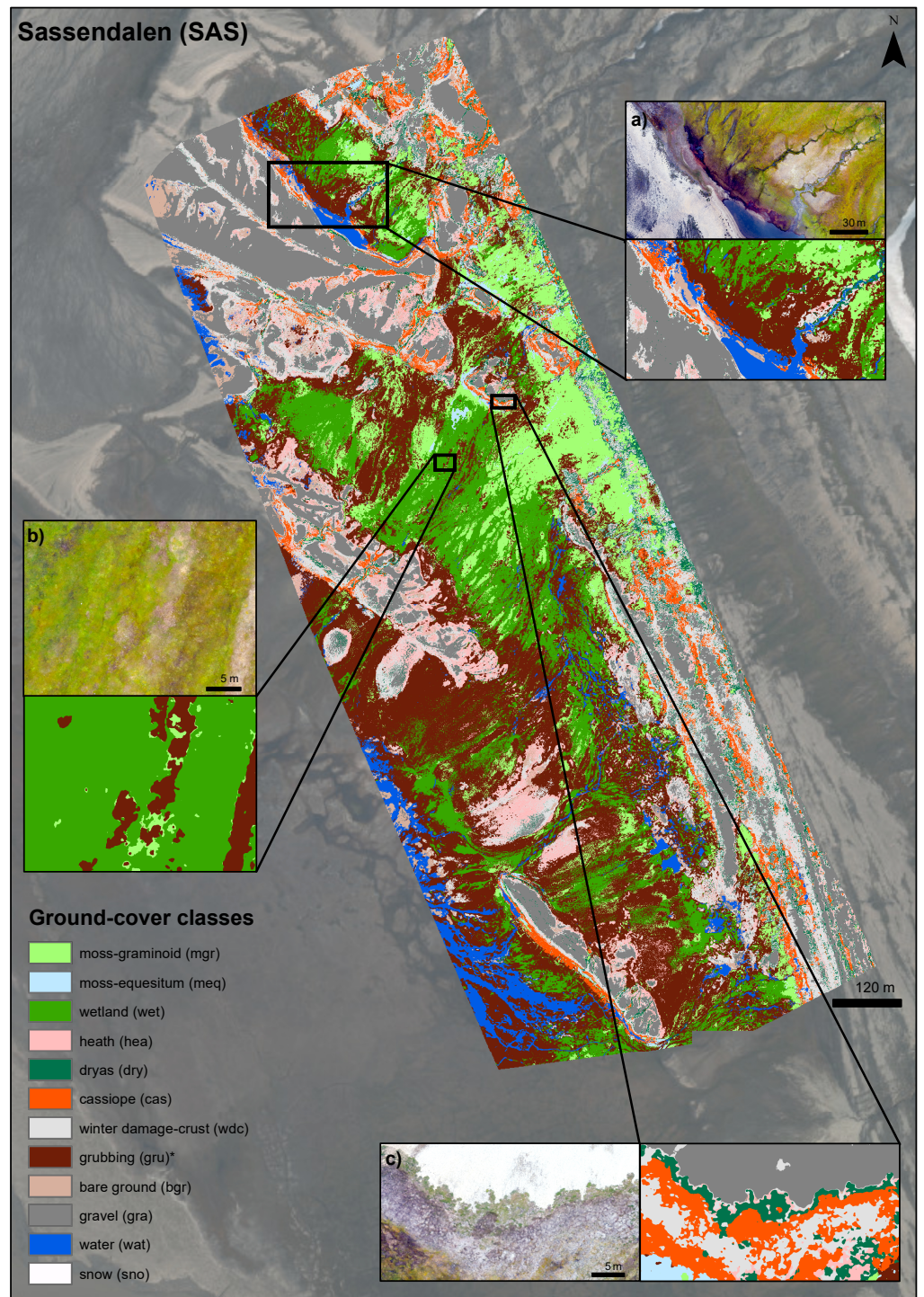


Figure 8. Classified map of Sassendalen (SAS). Zoomed areas highlight examples of classifications. (a) Dry and moist habitats: On the left, classification of dry-mesic habitat with *gravel* and a *cassiope belt*. On the right, moist habitat, classified as *wetland* and *moss-graminoid*, brown and rugged mosses classified as *grubbing*. (b) Grubbing detection in wetland area. (c) Zonation of dry-mesic ground-cover classes along a gravel ridge.

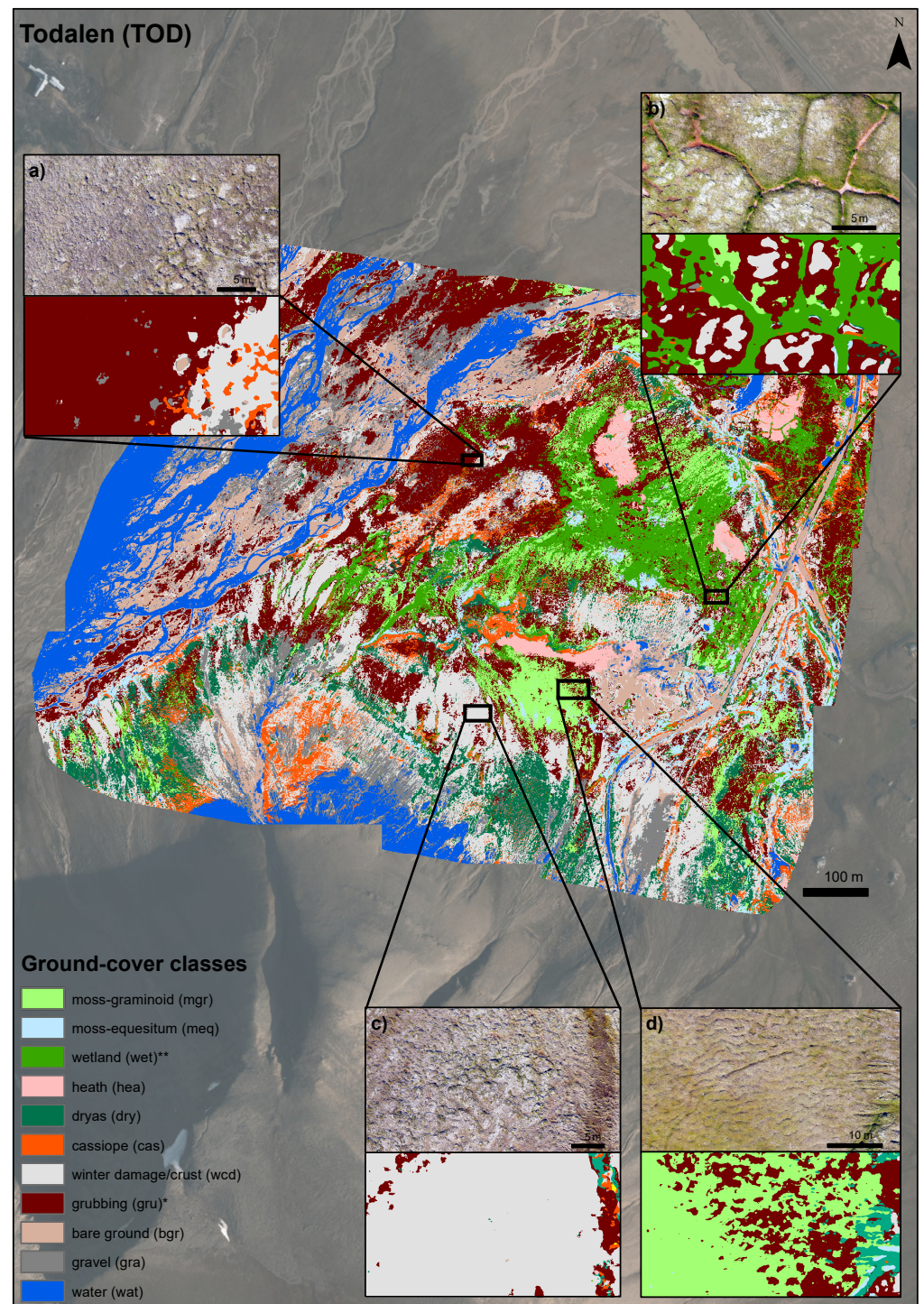


Figure 9. Classified map of Todalen (TOD). Zoomed areas highlight examples of classifications. (a) *Cassiope* classified as *grubbing*. (b) *Grubbing* and *winter damage/crust* on ice wedge polygons. (c) A dry-mesic habitat with *dryas*, *gravel* and *winter damage/crust* classified as *winter damage/crust*. (d) *Grubbing* in moss-graminoid habitat.

3.6. Spatial Transferability

In all cases, the models provided less accurate ground-cover classifications if trained in another site (transferred models (Figure 10)). Transferability was generally highest between the sites JAN and SAS, and using only optical variables was sufficient. The highest macro-F1 score was found when using the model developed for SAS (*optical* variables only) to

predict vegetation at JAN (macro-F1 score of 45.4%, Figure 10). Generally, transferability did not differ between using *optical and terrain* variables or using *optical* variables only. Ground-cover classes in TOD had the lowest prediction accuracy using models trained at the other study sites. Likewise, the model trained in TOD did not perform well in either of the other two study sites. The classifiers for JAN and SAS shared more of the top ten variable importance scores (see supplementary materials for details).

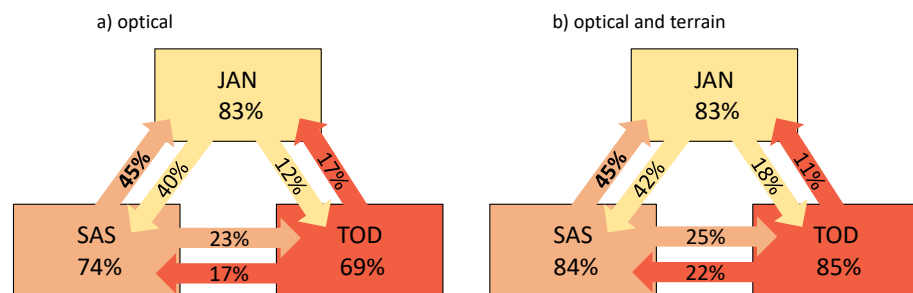


Figure 10. Classifier transferability between the three sites using the optimized classification scheme. Numbers inside the squares show the mean macro-F1 scores for in-site classifiers. The arrows indicate the direction and macro-F1 scores of using the classifier on the other sites. (a) Optical variables and (b) optical and terrain variables

4. Discussion

Our case study, using drone imagery in a high Arctic tundra landscape, showed that the classification of images can be reliably used to detect both vegetation types and small-scale disturbances from herbivory and winter weather events. The workflow we developed evaluates which combination of spatial variables and ground-cover classes yields random forest (RF) models with high predictive ability. Our suggested workflow emphasizes steps in drone image processing that have previously received less attention in ecological applications. The poor transferability of models between different sites highlights that RF models are spatially specific and degrade in accuracy when applied in different spatial contexts (sites). A point worth noting is that replicability is related to the method and that each of our RF models needs to be trained with site-specific data and care must be taken when using it in another context.

The lower normalized difference vegetation index (NDVI) values for the disturbed classes *winter damage/crust* and *grubbing* compared to their non-disturbed counterparts suggest that small-scale disturbances of tundra vegetation in Svalbard can be detected correctly using drone images. However, a range of NDVI values is commonly not exclusive to a certain vegetation class (see, e.g., Reynolds et al. [88]). This was also the case for the vegetation classes and their disturbed associates in our study that had partly overlapping ranges, especially in the site TOD. A classification approach is therefore needed to distinguish among the different classes, especially in cases where repeated NDVI measurements before and after the disturbance occurred are not available.

The F1 scores for the disturbed classes were generally high (77.5–88.7%), but reaching this classifier performance required merging *winter damage* and *biological crust* to one class. More work is thus needed to distinguish the different types of biological crust that have varied coloring from white to gray and dark brown/black from winter damage in the form of dead plants that make up a gray layer on the ground. Consistently higher recall than precision values for the disturbance classes *grubbing* and *winter damage/crust* suggest high detection rates coupled with slight but consistent overestimation of these classes. Field assessments supported these findings. We detected the following inconsistencies in the predicted map compared to knowledge from the field. We recognize that grubbing was overestimated in areas with brown-colored mosses where the surface of the tundra has

small-scale ruggedness due to soil movements, surface runoffs or reindeer trampling. The overestimation of grubbing also occurs in brown-colored, senescent *cassiope* areas and in patches of muddy water (e.g., Figures 7b,c, 8a and 9a, Eischeid, Ravolainen, personal observation). *Winter damage/crust* can be overestimated in areas with small, interspersed patches of healthy vegetation (e.g., Figure 9c, Eischeid, Ravolainen, personal observation). A mountain side shadow in the southern side of TOD was classified as water. These examples illustrate the need for additional ground-truthing and further fine-tuning of classification of the tundra vegetation types, particularly related to small-scale disturbances.

The overall high classification accuracy with macro-F1 values of over 80% for all three sites suggests that the classification performed well, comparable or better than other drone-based classifications in the high Arctic, such as Fraser et al. [89] and Thomson et al. [48]. We found no consistent bias in the misclassification of the ground-cover classes. Those misclassifications that occurred were between classes that are ecologically similar (e.g., within dry or wet habitats). The high detection of the classes *moss-graminoid*, *moss-equisetum*, *wetland*, *Carex subspathacea* and *grubbing* suggests that drone classification of tundra vegetation can be used to detect vegetation classes important to monitor future state changes in Svalbard's tundra ecosystem [14]. Increases in horsetails (*Equisetum* spp.) and *Carex subspathacea* abundances were recently reported from a revisit study in central Spitsbergen [90], highlighting the importance of developing image-based methods to support field-surveys to better obtain area estimates of such changes.

Our workflow (Table 1) builds on recent publications that aimed at systematizing the collection of drone images for research in natural systems. Review articles by Aasen et al. [31], Assmann et al. [54] and Tmušić et al. [53] focused on improving reproducibility and quality of drone-based surveys, including spectral calibration, standardized data collection and general quality control. With our workflow, we expanded this set of available guidelines, focusing on variable and class selection in an ecological context of Tundra ecosystems that can help researchers make decisions on drone data processing and image analysis. With our case study, we show how the workflow helped us to make systematic choices in planning our methods, as well as testing the limitations of our data, thereby ensuring ecologically sound research that is suitable for long-term monitoring.

Variable selection can be a very time-consuming process due to the large number of variables that can be retrieved from the original high-resolution layers and requires an understanding of the studied ecosystem to pre-select suitable variables. Relevant neighborhood sizes are an aspect of this process adding to selection/weight given to terrain and optical layers. We adapted the approach of Fan and Wang et al. [61,62], who systematically pre-tested different neighborhood sizes to find the most relevant ones. Analyzing three study sites simultaneously complicated the variable selection process and increased the total number of variables used for our analysis. Common systematic approaches to reducing the number of variables often rely on reruns with lower numbers of variables to find the smallest error rates [91]. These approaches were, however, not suitable when evaluating three classifiers (three study sites) simultaneously, and we, therefore, kept all the variables after the pre-test we determined to be important in at least one of the three study sites. Similarly, we kept the feature set size ($m_{\text{try}} = 8$) constant for all sites and classifiers to reduce the possible number of model outputs and comparisons. Further work on optimizing the site-specific models would allow us to find the most important predictor variables and optimized feature set.

As part of our workflow, we compared the RF classifier outputs that were based on optical and terrain variables or optical variables only. Using both terrain and optical variables improved in-site classifications compared to using only optical variables. In other contexts, different combinations of variables can lead to the best classification. For instance, drone surveys of structural landscape changes, such as landslides or river morphology, have achieved good results using terrain information only [92,93]. The optimal set of variables will depend on plant community composition, the ground-cover classification detail needed and the types of sensors available [89,94–96]. We therefore recommend future

drone-based ground-cover classification studies to include a wide range of variables and utilize our suggested selection procedures to find the most suitable ones for analysis.

Ground-cover classification maps have become a key resource in institutional, policy and law-making practice, but so far, there is a lack of conceptual frameworks and agreeable standards for map based monitoring [97]. Structuring ground-cover classes (i.e., in a hierarchical approach) can help with choosing appropriate class level detail and allow transferring across scales [97]. In our study, we found a structured selection approach, in line with adaptive monitoring goals [98], appropriate to find the optimal class level detail. It allowed us to focus on the ecological relevance of each of the ground-cover classes. We can therefore recommend our ground-cover class selection framework as a tool to create purpose-specific maps and find the balance between model accuracy and obtaining classes relevant for the monitoring goals.

Our results indicated low model transferability between study sites. Low regional transferability has also been reported in other RF classification studies [81,99]. Transferability can be improved by either reducing the number of classes [95], applying algorithm transfer functions, such as transformation matrices or tree pruning mechanism [69,70], or using different classifier types (e.g., [100,101]). Some deep learning approaches have recently been shown to provide classifications of drone and satellite data with reasonable transferability across space [102,103]. These approaches were outside the scope of our study as transferability was not the central goal. The right balance between a locally precise or transferable classifier will depend on the site-specific use-case, and a multi-approach framework may be needed to satisfy both local and regional monitoring requirements.

5. Conclusions

This study provides a planning workflow for generating vegetation cover maps with drones for ecological monitoring purposes in high Arctic tundra. Using random forest classifiers, we were able to successfully distinguish up to 15 different ground-cover classes, including two disturbance classes, goose grubbing and winter damage, which had lower NDVI values than their undisturbed counterparts. Although the models indicate a high predictive ability for the disturbance classes, field assessments have shown an overestimation of disturbances in parts of the moss tundra landscape. We show that a direct transfer of the models between study sites was not possible without further fine-tuning of methodologies. Future work might benefit from focusing separately on locally optimized maps and developing more generalized, transferable models. We have shown that it is possible to map the ground-cover classes that will likely be important to study state changes in Svalbard's tundra ecosystem. Future drone times-series are necessary to work on the detection of state transitions. We encourage closer interdisciplinary collaboration between experts of remote sensing, informatics and ecology to combine the knowledge-base and further improve the quality of map-based ecological monitoring.

Supplementary Materials: The following are available online at <https://www.mdpi.com/article/10.3390/rs13214466/s1>.

Author Contributions: The following authors contributed with the conceptualization, I.E., R.A.I., J.M., Å.Ø.P., E.M.S. and V.T.R.; methodology: I.E., J.J.A., F.P. and V.T.R.; investigation: I.E. and V.T.R.; formal analysis: I.E., F.P. and V.T.R.; visualization: I.E. and E.M.S.; writing—original draft preparation: I.E., E.M.S., Å.Ø.P. and V.T.R., writing—review and editing: I.E., E.M.S., J.J.A., R.A.I., J.M., Å.Ø.P., F.P., N.G.Y. and V.T.R.; funding acquisition: E.M.S., R.A.I., J.M., Å.Ø.P., N.G.Y. and V.T.R. All authors have read and agreed to the published version of the manuscript.

Funding: This research was funded by the Tromsø Research Foundation and made possible by a grant from the University of Aarhus, and the Norwegian Polar Institute provided personnel and field logistics.

Data Availability Statement: The data presented in this study are available on request from the corresponding author.

Acknowledgments: We thank Stein Tore Pedersen and the Norwegian Polar Institute for providing logistic support for our field work. We thank Ingrid G. Paulsen and Torgeir T. Blæsterdalen for support in the field. We thank the Governor of Svalbard and Hurtigruten for access to field accommodation. Anne Urset and Harald Faste Aas at the NPI mapping section provided valuable support with the GPS equipment. Furthermore, we thank Rolf Andersen at the Arctic University of Norway (UiT) for providing us processing services and support for using large datasets. This publication is a contribution from the Climate-Ecological Observatory for Arctic Tundra (COAT).

Conflicts of Interest: The authors declare no conflict of interest. The funders had no role in the design of the study; in the collection, analyses, or interpretation of data; in the writing of the manuscript; or in the decision to publish the results.

Appendix A. Ground-Cover Class Descriptions

The three sites for the drone flights were chosen so that they include ground-cover classes that are of high importance in tundra plant–herbivore interactions and have effects on plants from extreme winter weather events [14]. The meso-topography of mountainous tundra landscapes causes differentiation in vegetation types within relatively short distances (e.g., Mörsdorf et al. [104]), enabling study of dry, mesic, moist and wet ground-cover classes at the the same sites.

In the high Arctic Svalbard, the drier habitats of convex landscape forms are often dominated by *Dryas octopetala* heath [105] that is an available and important foraging habitat to the Svalbard reindeer and rock ptarmigan in the winter [106,107]. In a lower belt, below the ridges, in central parts of Spitsbergen, there is often *Cassiope tetragona* vegetation that is snow-covered during the winter. Winter extreme weather with rain-on-snow events have been shown to cause damage to these dwarf shrubs [20,21], although the area extent of such damage remains to be documented. Mountain sides and slightly sloping parts of the landscapes are often covered with a thick moss layer where herbaceous plants dominate alongside *Salix polaris*. In the lower parts of the landscapes, the moss tundra gradually changes to wetlands with cotton grasses and grasses adapted to wet conditions. The moss tundra and wetland parts of the landscapes are important summer foraging areas for all the vertebrate herbivores [14].

These landscapes encompass a selection of functionally important habitats with high potential for change due to climate change and the dynamic herbivore populations [14,58]. The expected trajectories of change differ between the dry, moist and wet habitats and between the disturbance types [14]. This highlights the importance of developing tools to quantify changes in areas of vegetation states and areas effected by the disturbances.

Vegetation types in Svalbard have been described in various sources earlier, including a vegetation map based on satellite data [72], plant sociological and classification studies [73,108] in Svalbard's flora [105] and in other research literature [22,30,109,110]. The previously defined vegetation state or type descriptions differ from each other depending on the purpose of the study. For our purpose of mapping especially the dwarf shrub vegetation types and the moss tundra, in combination with the most important disturbance to them (winter damage and herbivory by goose, respectively), we defined the following initial list of ground-cover classes so that it allowed us to work on vegetation and disturbances in combination.

(1a) Moss-graminoid

A common denominator for this class is a layer of mosses (typically 10–30 cm, or deeper) in moist terrain. Typical vascular plants are grasses in the genera *Poa*, *Festuca*, *Alopecurus* and *Dupontia*, the deciduous dwarf shrub *Salix polaris*, forbs in different genera such as *Ranunculus*, *Saxifraga*, *Micranthes* and *Pedicularis*, as well as some sedges (*Carex*). Moss flora is diverse, with dominant species from genera *Aulacomnium*, *Tomentypnum* and *Sanionia*.

(1b) Moss-equisetum

This class appears in habitats similar to the class moss-graminoid and in areas transitioning to wetland, but *Equisetum arvense* and *Equisetum scirpoides* dominate the vascular plant community.

(1c) Wetland

The wetlands in our study sites are located in slightly sloping areas and intermixed or downslope from the moist moss tundra. This class includes wetland dominated by mosses (such as *Drepanocladus* spp. and *Scorpidium* spp.) and graminoids such as *Eriophorum* spp. and *Dupontia fisheri*.

(1d) Moss-brown-wetland

This class is a specific type of wetland with less graminoids and mostly covered by wet, brown-colored mosses, giving the patches a potentially different spectral signature from 1c. This class was only mapped in TOD but also occurs in JAN and SAS, although less frequent there. These patches can be covered in water during wet years and dry out during drier years or seasons.

(2a) *Carex subspathacea*

This class occurs in habitats that otherwise would be classified as *wetland* but is characterized by a dense cover of *C. subspathacea*. It is one of the main arctic salt marsh plant species and has been documented to replace graminoids in areas of intensive pink-footed goose grubbing [90]. We only mapped this class in TOD, although it is also present in SAS and to a smaller extent in JAN.

(2b) Heath-moss

This class is typically found in slight depressions between ridges on the slopes and is characterized by a thin (approx. 1–5 cm) and drier moss layer often dominated by *Sanionia* spp. Vascular plants are usually sparse but include *Salix polaris*, *Saxifraga oppositifolia* or *Cerastium* spp.

(2c) Heath-graminoid

The heath-graminoid class is similar to the *heath-moss* class, with the difference that the moss layer is covered by graminoids, typically *Luzula confusa*, or in dry and convex terrain, such as *Carex* species.

(2d) Dryas

We assigned this class to ridges where open *Dryas octopetala* vegetation is found. The substrate in our *dryas* class is of gravel or thin silty soils on mainly alluvial deposits or terraces. *Dryas octopetala* occurs also in tussock tundra in Svalbard, but such *Dryas* areas were not common in the study sites.

(3a) Cassiope

We assigned this class if the dominant vegetation was *Cassiope tetragona*. This class is typically found downslope from the convex *Dryas* areas but above moss tundra and wetland areas where snow cover is stable in the winter.

(3b) Winter-damage-woody

This class is the disturbed counterpart to the *dryas* and *cassiope* classes. Periodic warm periods during winter result in sequential freezing that damages plant tissue, and coupled with rain, encapsulate plants with an ice coat. In addition, extreme winter warming can lead to desiccation when plants leave hibernation but cannot access water due to frozen soils [21]. Freezing temperatures after snow melt can damage plant tissues and decrease flowering success [20]. If the vegetation within a 15 cm circle was more than 80% damaged (gray), it was recorded for this class.

(3c) Biological crust

A layer of micro-organisms can cover bare soils, in which case, it is usually called biotic soil crust [111], but can also grow on damaged plants, in which case, it can be called biotic film. The biotic crust/film that is composed of a variety of bacteria, lichens and algae can grow over areas or that have been opened due to disturbances or over plants that were damaged. In our classification, we combined these two types of cryptogamic cover. The color of biotic crust can vary from almost white to gray or brown and black.

(3d) Grubbing

The grubbing class is the disturbed counterpart to the *moss tundra* and *wetland* classes. While grubbing, pink-footed geese often remove large amounts of moss in order to access the desired plant parts and opening up bare ground [27]. Grubbing can occur at different intensities. Our grubbing class describes areas where geese have removed enough moss to result in a continuous surface of dried moss interspersed with holes created by their beaks. We did not record singular holes (lighter intensity than our grubbing class). If grubbing has removed all vegetation and erosion processes have begun (higher intensity than our grubbing class), this would have been recorded as *bare ground* as it would not be possible to distinguish these patches from other bare areas that may have formed differently.

(4a) Winter-damage-moss

In one of our study sites, we recorded large patches of black/gray, previously moss-covered areas, probably disturbed by winter weather events. The most important process is not known but could include prolonged anaerobic conditions, freeze damage, perhaps combined with drought, but no apparent signs of fungal infections. This class was only recorded for JAN. These areas were black in color and different in appearance from the “winter-damage-woody” class.

(4b) Bare ground

This class encompasses all areas that are not covered with vegetation and have a soil substrate.

(4c) Gravel

This class describes gravel substrates, pebbles and up over in size. It also includes rocks.

(4d) Water

The class *water* includes lakes, rivers, streams and surface run-offs. The water can either be clear or (in most cases) enriched with sediments and brown in color.

Snow

A small snow field was only present in JAN.

References

- Bhatt, U.; Walker, D.; Raynolds, M.; Comiso, J.; Epstein, H.; Jia, G.; Gens, R.; Pinzon, J.; Tucker, C.; Tweedie, C.; et al. Circumpolar Arctic Tundra Vegetation Change Is Linked to Sea Ice Decline. *Earth Interact.* **2010**, *14*, 1–20. [[CrossRef](#)]
- Meredith, M.; Sommerkorn, M.; Cassota, S.; Derksen, C.; Ekaykin, A.; Hollowed, A.; Kofinas, G.; Mackintosh, A.; Melbourne-Thomas, J.; Muelbert, M.M.C.; et al. Polar regions. In *The Ocean and Cryosphere in a Changing Climate. A Special Report of the Intergovernmental Panel on Climate Change*; Pörtner, H.O., Roberts, D., Masson-Delmotte, V., Zhai, P., Tignor, M., Poloczanska, E., Mintenbeck, K., Alegría, A., Nicolai, M., Okem, A., et al., Eds.; IPCC: Geneva, Switzerland, 2019; pp. 203–320.
- Taylor, J.; Lawler, J.; Aronsson, M.; Barry, T.; Bjorkman, A.; Christensen, T.; Coulson, S.; Cuyler, C.; Ehrich, D.; Falk, K.; et al. Arctic terrestrial biodiversity status and trends: A synopsis of science supporting the CBMP State of Arctic Terrestrial Biodiversity Report. *Ambio* **2020**, *49*, 833–847. [[CrossRef](#)] [[PubMed](#)]
- Aronsson, M.; Heiðmarsson, S.; Jóhannesdóttir, H.; Barry, T.; Braa, J.; Burns, C.; Coulson, S.; Cuyler, C.; Falk, K.; Helgason, H.; et al. State of the Arctic Terrestrial Biodiversity Report; Conservation of Arctic Flora and Fauna International Secretariat: Akureyri, Iceland, 2021.
- AMAP. *Snow, Water, Ice and Permafrost. Summary for Policy-Makers. Arctic Monitoring and Assessment Programme (AMAP)*; AMAP: Oslo, Norway, 2017.
- Box, J.; Colgan, W.; Christensen, T.R.; Schmidt, N.; Lund, M.; Parmentier, F.J.; Brown, R.; Bhatt, U.; Euskirchen, E.; Romanovsky, V.; et al. Key indicators of Arctic climate change: 1971–2017. *Environ. Res. Lett.* **2019**, *14*, 045010. [[CrossRef](#)]
- Niittynen, P.; Heikkinen, R.K.; Aalto, J.; Guisan, A.; Kempainen, J.; Luoto, M. Fine-scale tundra vegetation patterns are strongly related to winter thermal conditions. *Nat. Clim. Chang.* **2020**, *10*, 1143–1148. [[CrossRef](#)]
- Wrona, F.J.; Johansson, M.; Culp, J.M.; Jenkins, A.; Mård, J.; Myers-Smith, I.H.; Prowse, T.D.; Vincent, W.F.; Wookey, P.A. Transitions in Arctic ecosystems: Ecological implications of a changing hydrological regime. *J. Geophys. Res. Biogeosci.* **2016**, *121*, 650–674. [[CrossRef](#)]
- Jorgenson, M.; Shur, Y.; Pullman, E. Abrupt increase in permafrost degradation in Arctic Alaska. *Geophys. Res. Lett.* **2006**, *33*, L02503. [[CrossRef](#)]
- Rennert, K.J.; Roe, G.; Putkonen, J.; Bitz, C.M. Soil Thermal and Ecological Impacts of Rain on Snow Events in the Circumpolar Arctic. *J. Clim.* **2009**, *22*, 2302–2315. [[CrossRef](#)]
- Biskaborn, B.; Smith, S.; Noetzel, J.; Matthes, H.; Vieira, G.; Streletskiy, D.; Schoeneich, P.; Romanovsky, V.; Lewkowicz, A.; Abramov, A.; et al. Permafrost is warming at a global scale. *Nat. Commun.* **2019**, *10*, 1–11. [[CrossRef](#)]

12. Kerbes, R.H.; Kotanen, P.M.; Jefferies, R.L. Destruction of Wetland Habitats by Lesser Snow Geese: A Keystone Species on the West Coast of Hudson Bay. *J. Appl. Ecol.* **1990**, *27*, 242–258. [[CrossRef](#)]
13. Hansen, B.B.; Grøtan, V.; Aanes, R.; Sæther, B.E.; Stien, A.; Fuglei, E.; Ims, R.A.; Yoccoz, N.G.; Pedersen, Å.Ø. Climate Events Synchronize the Dynamics of a Resident Vertebrate Community in the High Arctic. *Science* **2013**, *339*, 313–315. [[CrossRef](#)]
14. Ravolainen, V.; Soyninen, E.M.; Jónsdóttir, I.S.; Eischeid, I.; Forchhammer, M.; van der Wal, R.; Pedersen, Å.Ø. High Arctic ecosystem states: Conceptual models of vegetation change to guide long-term monitoring and research. *Ambio* **2020**, *49*, 666–677. [[CrossRef](#)]
15. Chapin, F.S., III; Woodwell, G.; Randerson, J.; Rastetter, E.; Lovett, G.; Baldocchi, D.; Clark, D.; Harmon, M.; Schimel, D.; Valentini, R.; et al. Reconciling Carbon-cycle Concepts, Terminology, and Methods. *Ecosystems* **2006**, *9*, 1041–1050. [[CrossRef](#)]
16. Scheffer, M.; Carpenter, S.; Lenton, T.; Bascompte, J.; Brock, W.; Dakos, V.; van de Koppel, J.; van de Leemput, I.; Levin, S.; Nes, E.; et al. Anticipating Critical Transitions. *Science* **2012**, *338*, 344–348. [[CrossRef](#)]
17. Jefferies, R.L.; Jano, A.P.; Abraham, K.F. A biotic agent promotes large-scale catastrophic change in the coastal marshes of Hudson Bay. *J. Ecol.* **2006**, *94*, 234–242. [[CrossRef](#)]
18. Van der Wal, R. Do herbivores cause habitat degradation or vegetation state transition? Evidence from the tundra. *Oikos* **2006**, *114*, 177–186. [[CrossRef](#)]
19. Peeters, B.; Pedersen, Å.; Loe, L.E.; Isaksen, K.; Veiberg, V.; Stien, A.; Kohler, J.; Gallet, J.C.; Aanes, R.; Hansen, B. Spatiotemporal patterns of rain-on-snow and basal ice in high Arctic Svalbard: Detection of a climate-cryosphere regime shift. *Environ. Res. Lett.* **2019**, *14*, 015002. [[CrossRef](#)]
20. Milner, J.M.; Varpe, Ø.; van der Wal, R.; Hansen, B.B. Experimental icing affects growth, mortality, and flowering in a high Arctic dwarf shrub. *Ecol. Evol.* **2016**, *6*, 2139–2148. [[CrossRef](#)] [[PubMed](#)]
21. Bjerke, J.W.; Treharne, R.; Vikhamar-Schuler, D.; Karlsen, S.R.; Ravolainen, V.; Bokhorst, S.; Phoenix, G.K.; Bochenek, Z.; Tømmervik, H. Understanding the drivers of extensive plant damage in boreal and Arctic ecosystems: Insights from field surveys in the aftermath of damage. *Sci. Total Environ.* **2017**, *599–600*, 1965–1976. [[CrossRef](#)]
22. Speed, J.D.; Woodin, S.; Tømmervik, H.; Tamstorf, M.; Wal, R. Predicting Habitat Utilization and Extent of Ecosystem Disturbance by an Increasing Herbivore Population. *Ecosystems* **2009**, *12*, 349–359. [[CrossRef](#)]
23. Speed, J.D.M.; Cooper, E.J.; Jónsdóttir, I.S.; Van Der Wal, R.; Woodin, S.J. Plant community properties predict vegetation resilience to herbivore disturbance in the Arctic. *J. Ecol.* **2010**, *98*, 1002–1013. [[CrossRef](#)]
24. Pedersen, Å.Ø.; Tombre, I.; Jepsen, J.U.; Eidesen, P.B.; Fuglei, E.; Stien, A. Spatial patterns of goose grubbing suggest elevated grubbing in dry habitats linked to early snowmelt. *Polar Res.* **2013**, *32*, 19719. [[CrossRef](#)]
25. Pedersen, A.S.; Speed, J.; Tombre, I. Prevalence of pink-footed goose grubbing in the arctic tundra increases with population expansion. *Polar Biol.* **2013**, *36*, 1569–1575. [[CrossRef](#)]
26. Madsen, J.; Williams, J.H.; Johnson, F.A.; Tombre, I.M.; Dereliev, S.; Kuijken, E. Implementation of the first adaptive management plan for a European migratory waterbird population: The case of the Svalbard pink-footed goose *Anser brachyrhynchus*. *Ambio* **2017**, *46*, 275–289. [[CrossRef](#)] [[PubMed](#)]
27. Fox, A.; Francis, I.; Bergersen, E. Diet and habitat use of Svalbard Pink-footed Geese *Anser brachyrhynchus* during arrival and pre-breeding periods in Adventdalen. *Ardea* **2006**, *94*, 691–699.
28. Van der Wal, R.; Sjögersten, S.; Woodin, S.J.; Cooper, E.J.; Jónsdóttir, I.S.; Kuijper, D.; Fox, T.A.D.; Huiskes, A.D. Spring feeding by pink-footed geese reduces carbon stocks and sink strength in tundra ecosystems. *Glob. Chang. Biol.* **2007**, *13*, 539–545. [[CrossRef](#)]
29. Speed, J.; Woodin, S.; Tømmervik, H.; van der Wal, R. Extrapolating herbivore-induced carbon loss across an arctic landscape. *Polar Biol.* **2010**, *33*, 789–797. [[CrossRef](#)]
30. Van der Wal, R.; Stien, A. High-arctic plants like it hot: A long-term investigation of between-year variability in plant biomass. *Ecology* **2014**, *95*, 3414–3427. [[CrossRef](#)]
31. Aasen, H.; Honkavaara, E.; Lucieer, A.; Zarco-Tejada, P.J. Quantitative Remote Sensing at Ultra-High Resolution with UAV Spectroscopy: A Review of Sensor Technology, Measurement Procedures, and Data Correction Workflows. *Remote Sens.* **2018**, *10*, 1091. [[CrossRef](#)]
32. Assmann, J.J.; Myers-Smith, I.H.; Kerby, J.T.; Cunliffe, A.M.; Daskalova, G.N. Drone data reveal heterogeneity in tundra greenness and phenology not captured by satellites. *Environ. Res. Lett.* **2020**, *15*, 125002. [[CrossRef](#)]
33. Lovitt, J.; Rahman, M.M.; McDermid, G.J. Assessing the Value of UAV Photogrammetry for Characterizing Terrain in Complex Peatlands. *Remote Sens.* **2017**, *9*, 715. [[CrossRef](#)]
34. Lousada, M.; Pina, P.; Vieira, G.; Bandeira, L.; Mora, C. Evaluation of the use of very high resolution aerial imagery for accurate ice-wedge polygon mapping (Adventdalen, Svalbard). *Sci. Total Environ.* **2018**, *615*, 1574–1583. [[CrossRef](#)]
35. Siewert, M.B.; Olofsson, J. Scale-dependency of Arctic ecosystem properties revealed by UAV. *Environ. Res. Lett.* **2020**, *15*, 094030. [[CrossRef](#)]
36. Harder, P.; Schirmer, M.; Pomeroy, J.; Helgason, W. Accuracy of snow depth estimation in mountain and prairie environments by an unmanned aerial vehicle. *Cryosphere* **2016**, *10*, 2559–2571. [[CrossRef](#)]
37. Pedersen, S.H.; Tamstorf, M.P.; Abermann, J.; Westergaard-Nielsen, A.; Lund, M.; Skov, K.; Sigsgaard, C.; Mylius, M.R.; Hansen, B.U.; Liston, G.E.; et al. Spatiotemporal Characteristics of Seasonal Snow Cover in Northeast Greenland from in Situ Observations. *Arct. Antarct. Alp. Res.* **2016**, *48*, 653–671. [[CrossRef](#)]

38. Cimoli, E.; Marcer, M.; Vandecrux, B.; Boggild, C.E.; Williams, G.; Simonsen, S.B. Application of Low-Cost UASs and Digital Photogrammetry for High-Resolution Snow Depth Mapping in the Arctic. *Remote Sens.* **2017**, *9*, 1144. [CrossRef]
39. Ewertowski, M.W.; Evans, D.J.A.; Roberts, D.H.; Tomczyk, A.M. Glacial geomorphology of the terrestrial margins of the tidewater glacier, Nordenskiöldbreen, Svalbard. *J. Maps* **2016**, *12*, 476–487. [CrossRef]
40. Tonkin, T.; Midgley, N.; Cook, S.; Graham, D. Ice-cored moraine degradation mapped and quantified using an unmanned aerial vehicle: A case study from a polythermal glacier in Svalbard. *Geomorphology* **2016**, *258*, 1–10. [CrossRef]
41. Phillips, E.; Everest, J.; Evans, D.J.; Finlayson, A.; Ewertowski, M.; Guild, A.; Jones, L. Concentrated, ‘pulsed’ axial glacier flow: Structural glaciological evidence from Kvíárjökull in SE Iceland. *Earth Surf. Process. Landforms* **2017**, *42*, 1901–1922. [CrossRef]
42. Nehyba, S.; Hanáček, M.; Engel, Z.; Stachoň, Z. Rise and fall of a small ice-dammed lake—Role of deglaciation processes and morphology. *Geomorphology* **2017**, *295*, 662–679. [CrossRef]
43. Jouvét, G.; Weidmann, Y.; Seguinot, J.; Funk, M.; Abe, T.; Sakakibara, D.; Seddik, H.; Sugiyama, S. Initiation of a major calving event on the Bowdoin Glacier captured by UAV photogrammetry. *Cryosphere* **2017**, *11*, 911–921. [CrossRef]
44. Jones, C.; Ryan, J.; Holt, T.; Hubbard, A. Structural glaciology of Isunguata Sermia, West Greenland. *J. Maps* **2018**, *14*, 517–527. [CrossRef]
45. Jouvét, G.; Weidmann, Y.; Kneib, M.; Detert, M.; Seguinot, J.; Sakakibara, D.; Sugiyama, S. Short-lived ice speed-up and plume water flow captured by a VTOL UAV give insights into subglacial hydrological system of Bowdoin Glacier. *Remote Sens. Environ.* **2018**, *217*, 389–399. [CrossRef]
46. Van der Sluijs, J.; Kokelj, S.V.; Fraser, R.H.; Tunnicliffe, J.; Lacelle, D. Permafrost Terrain Dynamics and Infrastructure Impacts Revealed by UAV Photogrammetry and Thermal Imaging. *Remote Sens.* **2018**, *10*, 1734. [CrossRef]
47. Cunliffe, A.M.; Tanski, G.; Radosavljevic, B.; Palmer, W.F.; Sachs, T.; Lantuit, H.; Kerby, J.T.; Myers-Smith, I.H. Rapid retreat of permafrost coastline observed with aerial drone photogrammetry. *Cryosphere* **2019**, *13*, 1513–1528. [CrossRef]
48. Thomson, E.; Spiegel, M.; Althuisen, I.; Bass, P.; Chen, S.; Chmurzynski, A.; Halbritter, A.; Henn, J.; Jónsdóttir, I.; Klanderud, K.; et al. Multiscale mapping of plant functional groups and plant traits in the High Arctic using field spectroscopy, UAV imagery and Sentinel-2A data. *Environ. Res. Lett.* **2021**, *16*, 055006. [CrossRef]
49. Turner, I.L.; Harley, M.D.; Drummond, C.D. UAVs for coastal surveying. *Coast. Eng.* **2016**, *114*, 19–24. [CrossRef]
50. Gillan, J.K.; Karl, J.W.; van Leeuwen, W.J.D. Integrating drone imagery with existing rangeland monitoring programs. *Environ. Monit. Assess.* **2020**, *192*, 1–20. [CrossRef]
51. Hoffmann, H.; Jensen, R.; Thomsen, A.; Nieto, H.; Rasmussen, J.; Friborg, T. Crop water stress maps for entire growing seasons from visible and thermal UAV imagery. *Biogeosci. Discuss.* **2016**, *13*, 6545–6563. [CrossRef]
52. Tirado, S.B.; Hirsch, C.N.; Springer, N.M. UAV-based imaging platform for monitoring maize growth throughout development. *Plant Direct* **2020**, *4*, e00230. [CrossRef] [PubMed]
53. Tmušić, G.; Manfreda, S.; Aasen, H.; James, M.R.; Gonçalves, G.; Ben-Dor, E.; Brook, A.; Polinova, M.; Arranz, J.J.; Mészáros, J.; et al. Current Practices in UAS-based Environmental Monitoring. *Remote Sens.* **2020**, *12*, 1001. [CrossRef]
54. Assmann, J.J.; Kerby, J.T.; Cunliffe, A.M.; Myers-Smith, I.H. Vegetation monitoring using multispectral sensors—Best practices and lessons learned from high latitudes. *J. Unmanned Veh. Syst.* **2019**, *7*, 54–75. [CrossRef]
55. Arctic Long-Term Ecological Research Site. Available online: <https://arc-lter.ecosystems.mbl.edu/> (accessed on 23 October 2020).
56. Bylot Island—Sirmilik National Park Long Term Monitoring Program. Available online: <http://www.cen.ulaval.ca/bylot/en/bylohistory.php> (accessed on 16 October 2020).
57. Zackenberg Ecological Research Operations. Available online: <https://g-e-m.dk/gem-localities/zackenberg-research-station/> (accessed on 23 October 2020).
58. Ims, R.; Jepsen, J.U.; Stien, A.; Yoccoz, N.G. *Science plan for COAT: Climate-ecological Observatory for Arctic Tundra*; Fram Centre Report Series 1; Fram Centre: Tromsø, Norway, 2013.
59. High-Latitude Drone Ecology Network (HiLDEN). Available online: <https://arcticdrones.org/> (accessed on 4 September 2020).
60. Zhou, Y.; Daakir, M.; Rupnik, E.; Pierrot-Deseilligny, M. A two-step approach for the correction of rolling shutter distortion in UAV photogrammetry. *ISPRS J. Photogramm. Remote Sens.* **2020**, *160*, 51–66. [CrossRef]
61. Wang, H.; Pu, R.; Zhu, Q.; Ren, L.; Zhang, Z. Mapping health levels of Robinia pseudoacacia forests in the Yellow River delta, China, using IKONOS and Landsat 8 OLI imagery. *Int. J. Remote Sens.* **2015**, *36*, 1114–1135. [CrossRef]
62. Fan, H. Land-cover mapping in the Nujiang Grand Canyon: Integrating spectral, textural, and topographic data in a random forest classifier. *Int. J. Remote Sens.* **2013**, *34*, 7545–7567. [CrossRef]
63. Weinmann, M.; Jutzi, B.; Hinz, S.; Mallet, C. Semantic point cloud interpretation based on optimal neighborhoods, relevant features and efficient classifiers. *ISPRS J. Photogramm. Remote Sens.* **2015**, *105*, 286–304. [CrossRef]
64. Mascaro, J.; Asner, G.P.; Knapp, D.E.; Kennedy-Bowdoin, T.; Martin, R.E.; Anderson, C.; Higgins, M.; Chadwick, K.D. A Tale of Two “Forests”: Random Forest Machine Learning Aids Tropical Forest Carbon Mapping. *PLoS ONE* **2014**, *9*, e85993. [CrossRef] [PubMed]
65. Belgiu, M.; Drăguț, L. Random forest in remote sensing: A review of applications and future directions. *ISPRS J. Photogramm. Remote Sens.* **2016**, *114*, 24–31. [CrossRef]
66. Colditz, R.R. An Evaluation of Different Training Sample Allocation Schemes for Discrete and Continuous Land Cover Classification Using Decision Tree-Based Algorithms. *Remote Sens.* **2015**, *7*, 9655–9681. [CrossRef]

67. Roberts, D.R.; Bahn, V.; Ciuti, S.; Boyce, M.S.; Elith, J.; Guillera-Aroita, G.; Hauenstein, S.; Lahoz-Monfort, J.J.; Schröder, B.; Thuiller, W.; et al. Cross-validation strategies for data with temporal, spatial, hierarchical, or phylogenetic structure. *Ecography* **2017**, *40*, 913–929. [CrossRef]
68. Hastie, T.; Tibshirani, R.; Friedman, J. *The Elements of Statistical Learning: Data Mining, Inference and Prediction*, 2nd ed.; Springer: Berlin/Heidelberg, Germany, 2009.
69. Segev, N.; Harel, M.; Mannor, S.; Crammer, K.; El-Yaniv, R. Learn on Source, Refine on Target: A Model Transfer Learning Framework with Random Forests. *IEEE Trans. Pattern Anal. Mach. Intell.* **2015**, *39*, 1811–1824. [CrossRef]
70. Sukhija, S.; Krishnan, N.C. Supervised heterogeneous feature transfer via random forests. *Artif. Intell.* **2019**, *268*, 30–53. [CrossRef]
71. Walker, D.; Raynolds, M.; Daniëls, F.; Einarsson, E.; Elvebakk, A.; Gould, W.; Katenin, A.; Kholod, S.; Markon, C.; Melnikov, E.; et al. The Circumpolar Arctic Vegetation Map. *J. Veg. Sci.* **2005**, *16*, 267–282. [CrossRef]
72. Johansen, B.E.; Karlsen, S.R.; Tømmervik, H. Vegetation mapping of Svalbard utilising Landsat TM/ETM data. *Polar Rec.* **2012**, *48*, 47–63. [CrossRef]
73. Elvebakk, A. A vegetation map of Svalbard on the scale 1:3.5 mill. *Phytocoenologia* **2005**, *35*, 951–967. [CrossRef]
74. Elvebakk, A. A survey of plant associations and alliances from Svalbard. *J. Veg. Sci.* **1994**, *5*, 791–802. [CrossRef]
75. Lawrimore, J.; Ray, R.; Applequist, S.; Korzeniewski, B.; Menne, M. Global Summary of the Month (GSOM), Version 1. In NOAA National Centers for Environmental Information. Available online: <https://www.ncei.noaa.gov/access/metadata/landing-page/bin/iso?id=gov.noaa.ncdc:C00946> (accessed on 10 September 2021).
76. Mięgała, K.; Wojtuń, B.; Szymański, W.; Muskała, P. Soil moisture and temperature variation under different types of tundra vegetation during the growing season: A case study from the Fuglebekken catchment, SW Spitsbergen. *Catena* **2014**, *116*, 10–18. [CrossRef]
77. Cubero-Castan, M.; Schneider-Zapp, K.; Bellomo, M.; Shi, D.; Rehak, M.; Strecha, C. Assessment Of The Radiometric Accuracy In A Target Less Work Flow Using Pix4D Software. In Proceedings of the 2018 9th Workshop on Hyperspectral Image and Signal Processing: Evolution in Remote Sensing (WHISPERS), Amsterdam, The Netherlands, 23–26 September 2018; pp. 1–4. [CrossRef]
78. Pix4Dmapper. Available online: <https://www.pix4d.com/product/pix4dmapper-photogrammetry-software> (accessed on 1 November 2021).
79. R Core Team. *R: A Language and Environment for Statistical Computing*; R Foundation for Statistical Computing: Vienna, Austria, 2013.
80. Zvloff, A. glcm: Calculate Textures from Grey-Level Co-Occurrence Matrices (GLCMs). R Package Version 1.6.5. Available online: <https://cran.r-project.org/web/packages/glcm/glcm.pdf> (accessed on 1 November 2021).
81. Maxwell, A.E.; Warner, T.A.; Strager, M.P. Predicting Palustrine Wetland Probability Using Random Forest Machine Learning and Digital Elevation Data-Derived Terrain Variables. *Photogramm. Eng. Remote Sens.* **2016**, *82*, 437–447. [CrossRef]
82. Evans, J.S. spatialEco: Spatial Analysis and Modelling Utilities. R Package Version 1.3-2. Available online: <https://cran.r-project.org/web/packages/spatialEco/spatialEco.pdf> (accessed on 1 November 2021).
83. Cutler, A.; Cutler, D.R.; Stevens, J.R. Random Forests. In *Ensemble Machine Learning: Methods and Applications*; Zhang, C., Ma, Y., Eds.; Springer: Boston, MA, USA, 2012; pp. 157–175. [CrossRef]
84. Karami, M.; Westergaard-Nielsen, A.; Normand, S.; Treier, U.A.; Elberling, B.; Hansen, B.U. A phenology-based approach to the classification of Arctic tundra ecosystems in Greenland. *ISPRS J. Photogramm. Remote Sens.* **2018**, *146*, 518–529. [CrossRef]
85. Cortez, P. rminer: Data Mining Classification and Regression Methods. R Package Version 1.4.6. Available online: <https://cran.r-project.org/web/packages/spatialEco/spatialEco.pdf> (accessed on 1 November 2021).
86. Hijmans, R.J. raster: Geographic Data Analysis and Modeling. R Package Version 3.3-13. Available online: <https://cran.r-project.org/web/packages/raster/raster.pdf> (accessed on 1 November 2021).
87. Mouselimis, L. ClusterR: Gaussian Mixture Models, K-Means, Mini-Batch-Kmeans, K-Medoids and Affinity Propagation Clustering. R Package Version 1.2.2. Available online: <https://cran.r-project.org/web/packages/ClusterR/ClusterR.pdf> (accessed on 1 November 2021).
88. Raynolds, M.K.; Comiso, J.C.; Walker, D.A.; Verbyla, D. Relationship between satellite-derived land surface temperatures, arctic vegetation types, and NDVI. *Remote Sens. Environ.* **2008**, *112*, 1884–1894.
89. Fraser, R.H.; Olthof, I.; Lantz, T.C.; Schmitt, C. UAV photogrammetry for mapping vegetation in the low-Arctic. *Arct. Sci.* **2016**, *2*, 79–102. [CrossRef]
90. Van der Wal, R.; Anderson, H.; Stien, A.; Loe, L.E.; Speed, J. Disturbance, Recovery and Tundra Vegetation Change Final Report project 17/92—to Svalbard Environmental Protection Fund. 2020. Available online: https://aura.abdn.ac.uk/bitstream/handle/2164/16573/SMF_Disturbance_recovery_veg_change.pdf;jsessionid=65802B34A907DB989FF65BD2D7FDB248?sequence=1 (accessed on 13 September 2021).
91. Hapfelmeier, A.; Ulm, K. A new variable selection approach using Random Forests. *Comput. Stat. Data Anal.* **2013**, *60*, 50–69. [CrossRef]
92. Rossi, G.; Tanteri, L.; Tofani, V.; Vannocci, P.; Moretti, S.; Casagli, N. Multitemporal UAV surveys for landslide mapping and characterization. *Landslides* **2018**, *15*, 1045–1052. [CrossRef]
93. Özcan, O.; Özcan, O. Multi-temporal UAV based repeat monitoring of rivers sensitive to flood. *J. Maps* **2021**, *17*, 163–170. [CrossRef]

94. Chen, J.; Yi, S.; Qin, Y.; Wang, X. Improving estimates of fractional vegetation cover based on UAV in alpine grassland on the Qinghai–Tibetan Plateau. *Int. J. Remote Sens.* **2016**, *37*, 1922–1936. [[CrossRef](#)]
95. Miranda, V.; Pina, P.; Heleno, S.; Vieira, G.; Mora, C.; Schaefer, C.E. Monitoring recent changes of vegetation in Fildes Peninsula (King George Island, Antarctica) through satellite imagery guided by UAV surveys. *Sci. Total Environ.* **2020**, *704*, 135295. [[CrossRef](#)] [[PubMed](#)]
96. Morgan, B.E.; Chipman, J.W.; Bolger, D.T.; Dietrich, J.T. Spatiotemporal Analysis of Vegetation Cover Change in a Large Ephemeral River: Multi-Sensor Fusion of Unmanned Aerial Vehicle (UAV) and Landsat Imagery. *Remote Sens.* **2021**, *13*, 51. [[CrossRef](#)]
97. Cullum, C.; Rogers, K.; Brierley, G.; Witkowski, E. Ecological classification and mapping for landscape management and science: Foundations for the description of patterns and processes. *Prog. Phys. Geogr.* **2015**, *40*, 38–65. [[CrossRef](#)]
98. Lindenmayer, D.B.; Likens, G.E. Adaptive monitoring: A new paradigm for long-term research and monitoring. *Trends Ecol. Evol.* **2009**, *24*, 482–486. [[CrossRef](#)] [[PubMed](#)]
99. Juel, A.; Groom, G.B.; Svenning, J.C.; Ejrnæs, R. Spatial application of Random Forest models for fine-scale coastal vegetation classification using object based analysis of aerial orthophoto and DEM data. *Int. J. Appl. Earth Obs. Geoinf.* **2015**, *42*, 106–114. [[CrossRef](#)]
100. Kalantar, B.; Mansor, S.B.; Sameen, M.I.; Pradhan, B.; Shafri, H.Z.M. Drone-based land-cover mapping using a fuzzy unordered rule induction algorithm integrated into object-based image analysis. *Int. J. Remote Sens.* **2017**, *38*, 2535–2556. [[CrossRef](#)]
101. Wessel, M.; Brandmeier, M.; Tiede, D. Evaluation of Different Machine Learning Algorithms for Scalable Classification of Tree Types and Tree Species Based on Sentinel-2 Data. *Remote Sens.* **2018**, *10*, 1419. [[CrossRef](#)]
102. Zhang, C.; Sargent, I.; Pan, X.; Li, H.; Gardiner, A.; Hare, J.; Atkinson, P.M. Joint Deep Learning for land cover and land use classification. *Remote Sens. Environ.* **2019**, *221*, 173–187. [[CrossRef](#)]
103. Tong, X.Y.; Xia, G.S.; Lu, Q.; Shen, H.; Li, S.; You, S.; Zhang, L. Land-cover classification with high-resolution remote sensing images using transferable deep models. *Remote Sens. Environ.* **2020**, *237*, 111322. [[CrossRef](#)]
104. Mörsdorf, M.A.; Ravolainen, V.T.; Yoccoz, N.G.; Thórhallsdóttir, T.E.; Jónsdóttir, I.S. Decades of Recovery From Sheep Grazing Reveal No Effects on Plant Diversity Patterns Within Icelandic Tundra Landscapes. *Front. Ecol. Evol.* **2021**, *8*, 502. [[CrossRef](#)]
105. Rønning, O.I. *Svalbards Flora*; Norsk Polarinstitut: Tromsø, Norway, 1996.
106. Pedersen, Å.Ø.; Overrein, Ø.; Unander, S.; Fuglei, E. *Svalbard Rock Ptarmigan (Lagopus Mutus Hyperboreus): A Status Report*; Norwegian Polar Institute (Norsk Polarinstitut): Tromsø, Norway, 2005.
107. Pedersen, Å.; Paulsen, I.; Albon, S.; Arntsen, G.L.; Hansen, B.; Langvatn, R.; Loe, L.E.; Le Moullec, M.; Overrein, Ø.; Peeters, B.; et al. *Svalbard Reindeer (Rangifer Tarandus Platyrhynchus): A Status Report*; Rapportserie—Norsk Polarinstitut, Norwegian Polar Institute: Tromsø, Norway, 2019.
108. Vanderpuye, A.W.; Elvebakk, A.; Nilsen, L. Plant communities along environmental gradients of high-arctic mires in Sassendalen, Svalbard. *J. Veg. Sci.* **2002**, *13*, 875–884. [[CrossRef](#)]
109. Euroala, S.; Hakala, A. The bird cliff vegetation of Svalbard. *Aquil. Ser. Bot* **1977**, *15*, 1–18.
110. Jónsdóttir, I.S. Terrestrial ecosystems on Svalbard: Heterogeneity, complexity and fragility from an Arctic island perspective. In *Biology and Environment: Proceedings of the Royal Irish Academy (JSTOR)*; Royal Irish Academy: Dublin, Ireland, 2005; pp. 155–165.
111. Agnelli, A.; Corti, G.; Massaccesi, L.; Ventura, S.; D’Acqui, L.P. Impact of biological crusts on soil formation in polar ecosystems. *Geoderma* **2021**, *401*, 115340. [[CrossRef](#)]

Supplementary Materials - Isabell Eischeid - Disturbance Mapping in Arctic
Tundra Improved by a Planning Workflow for Drone Studies: Advancing Tools
for Future Ecosystem Monitoring

1 Variable importance

Table 1: Variable importance values (0-1) for the optical variables in the optimized classification scheme. The numbers in the variable names indicate neighbourhood sizes: 03 (0.3m), 09 (0.9m), 1-5 (1.5m), 2 (2m)

Variable	JAN	SAS	TOD
green	0.029	0.048	0.018
green_glcm_03_mean	0.023	0.030	0.025
green_glcm_03_variance	0.025	0.037	0.025
green_glcm_09_mean	0.033	0.031	0.037
green_glcm_09_variance	0.027	0.028	0.026
green_glcm_1-5_mean	0.036	0.025	0.044
green_glcm_1-5_variance	0.038	0.026	0.033
green_glcm_2_contrast	0.007	0.006	0.036
green_glcm_2_dissimilarity	0.009	0.006	0.028
green_glcm_2_entropy	0.014	0.007	0.024
green_glcm_2_homogeneity	0.008	0.009	0.031
green_glcm_2_mean	0.041	0.024	0.030
green_glcm_2_second_moment	0.011	0.007	0.019
green_glcm_2_variance	0.037	0.023	0.029
ndvi	0.145	0.164	0.042
ndvi_glcm_03_mean	0.084	0.101	0.074
ndvi_glcm_03_variance	0.123	0.126	0.043
ndvi_glcm_09_mean	0.044	0.056	0.093
ndvi_glcm_09_variance	0.043	0.063	0.077
ndvi_glcm_1-5_mean	0.048	0.042	0.083
ndvi_glcm_1-5_variance	0.040	0.043	0.080
ndvi_glcm_2_contrast	0.054	0.038	0.019
ndvi_glcm_2_dissimilarity	0.046	0.047	0.018
ndvi_glcm_2_entropy	0.030	0.021	0.014
ndvi_glcm_2_homogeneity	0.032	0.034	0.020
ndvi_glcm_2_mean	0.078	0.045	0.071
ndvi_glcm_2_second_moment	0.026	0.013	0.012
ndvi_glcm_2_variance	0.069	0.049	0.064
near_infrared	0.074	0.068	0.011
red	0.034	0.084	0.040
red_edge	0.058	0.054	0.008
red_edge_glcm_03_mean	0.050	0.033	0.012
red_edge_glcm_03_variance	0.061	0.040	0.010
red_edge_glcm_09_mean	0.024	0.017	0.023
red_edge_glcm_09_variance	0.025	0.018	0.021
red_edge_glcm_1-5_mean	0.018	0.018	0.038
red_edge_glcm_1-5_variance	0.020	0.017	0.032
red_edge_glcm_2_contrast	0.010	0.012	0.017
red_edge_glcm_2_dissimilarity	0.009	0.010	0.015
red_edge_glcm_2_entropy	0.012	0.008	0.014
red_edge_glcm_2_homogeneity	0.008	0.009	0.016
red_edge_glcm_2_mean	0.020	0.015	0.039
red_edge_glcm_2_second_moment	0.011	0.007	0.015
red_edge_glcm_2_variance	0.019	0.019	0.031

Table 2: Variable importance values (0-1) for the terrain variables in the optimized classification scheme. The first numbers in the variable names indicate the pixels size: 02 (0.2m) and 1 (1m). The second numbers in the variable names indicate the neighbourhood sizes in meters.

Variable	JAN	SAS	TOD
dissection_02_1	0.004	0.004	0.013
dissection_02_1-8	0.010	0.005	0.013
dissection_02_2-2	0.013	0.005	0.016
dissection_1_11	0.017	0.021	0.022
dissection_1_121	0.065	0.016	0.087
dissection_1_131	0.093	0.020	0.100
dissection_1_21	0.022	0.040	0.068
rugged_02_1	0.005	0.011	0.010
rugged_02_1-4	0.006	0.016	0.014
rugged_02_1-8	0.006	0.014	0.021
rugged_02_2-2	0.007	0.013	0.022
rugged_1_101	0.052	0.027	0.035
rugged_1_11	0.014	0.051	0.048
rugged_1_131	0.056	0.022	0.027
rugged_1_21	0.028	0.035	0.054
rugged_1_31	0.031	0.041	0.061
rugged_1_41	0.021	0.046	0.051
rugged_1_51	0.021	0.058	0.035
slope_1	0.016	0.060	0.034
slope_10	0.015	0.052	0.047
slope_5	0.013	0.074	0.057

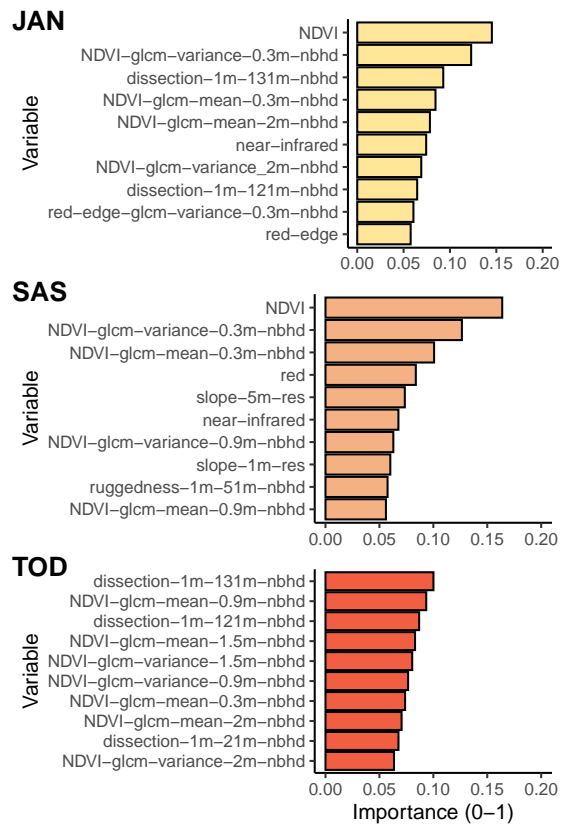


Figure 1: Variables importance, ten highest values for each site using the optimized classification scheme.

2 Ground-cover classification

2.1 Confusion matrices

a) Initial classification scheme

		predicted														observation accuracy (%)	
		bgr	cru	cas	dry	gra	hea	wdm	meq	hmo	sno	wat	gru	wdw	mgr		wet
observed	bgr	112	3	0	0	0	0	0	0	0	0	14	11	0	0	80.0	
	cru	0	283	5	0	121	0	0	0	3	0	7	21	60	0	56.6	
	cas	0	12	1469	0	0	240	0	0	49	0	17	29	164	0	74.2	
	dry	0	0	0	971	3	39	0	0	2	0	0	0	0	0	95.7	
	gra	0	51	0	2	1022	0	0	0	0	0	0	0	0	0	95.1	
	hea	0	6	4	44	1	502	0	0	0	0	0	0	0	0	90.1	
	wdm	0	6	0	0	3	0	429	0	0	0	0	29	0	0	91.9	
	meq	0	0	0	0	0	0	0	377	0	0	0	0	0	32	15	88.9
	hmo	0	0	14	6	0	31	0	0	170	0	0	16	30	14	0	60.5
	sno	0	0	0	0	0	0	0	0	0	113	0	0	0	0	0	100
	wat	1	0	12	0	18	0	5	0	0	1078	35	0	0	0	9	93.1
	gru	0	29	0	0	0	3	11	0	0	0	1132	0	44	32	90.5	
	wdw	0	465	112	0	0	0	0	0	82	0	3	3	1089	0	0	62.1
	mgr	0	0	0	0	0	1	0	43	0	0	0	18	0	622	60	83.6
	wet	0	0	0	0	0	0	0	0	0	0	0	58	0	21	1094	93.3
prediction accuracy (%)		99.1	33.1	90.9	94.9	87.5	61.5	96.4	89.8	55.6	100	96.3	83.7	81.1	84.9	90.4	

b) Simplified classification scheme

		predicted							observation accuracy (%)
		cru	sno	wat	veg	bgg	gru	wdc	
observed	cru	272	0	2	11	112	33	59	55.6
	sno	0	132	0	0	0	0	0	100
	wat	7	0	933	86	35	27	71	80.5
	veg	1	0	2	5984	18	21	115	97.4
	bgg	65	0	5	4	1133	11	0	93
	gru	16	0	2	94	2	1138	0	90.9
	wdc	445	0	8	230	0	8	941	57.7
prediction accuracy (%)		33.7	100	98	93.4	87.2	91.9	79.3	

c) Optimized classification scheme

		predicted											observation accuracy (%)	
		bgr	cas	dry	gra	meq	sno	wat	gru	wdc	hea	mgr		wet
observed	bgr	131	0	0	0	0	0	5	0	4	0	0	0	93.6
	cas	0	1443	0	0	0	0	24	39	216	279	0	0	72.1
	dry	0	0	1015	8	0	0	0	0	0	32	0	0	96.2
	gra	0	0	4	1024	0	0	0	0	49	1	0	0	95.0
	meq	0	0	0	0	383	0	0	0	0	0	22	17	90.8
	sno	0	0	0	0	0	116	0	0	0	0	0	0	100
	wat	7	4	0	14	0	0	913	6	130	0	0	8	84.4
	gru	0	0	0	0	1	0	4	1144	28	0	45	32	91.2
	wdc	0	108	0	118	0	0	16	16	1936	29	0	0	87.1
	hea	0	16	62	0	0	0	0	7	50	698	6	0	83.2
	mgr	0	0	0	0	50	0	0	16	2	2	623	50	83.8
	wet	3	0	0	0	1	0	0	50	0	0	22	1096	93.5
	prediction accuracy (%)		92.9	91.9	93.9	88.0	88.0	100	94.9	89.5	80.2	67.1	86.8	91.1

Figure 2: Confusion matrices for JAN with all variables (optical and terrain) using the a) initial, b) simplified and c) optimized classification scheme

a) Initial classification scheme

		predicted													observation accuracy (%)
		bgr	cru	cas	dry	gra	hea	meq	hmo	wat	gru	wdw	mgr	wet	
observed	bgr	149	25	0	0	18	0	0	0	1	9	7	0	0	71.3
	cru	2	178	6	1	23	8	0	2	0	25	142	0	0	46.0
	cas	0	1	587	4	0	0	7	21	0	57	6	4	0	85.4
	dry	0	1	4	258	3	6	14	1	0	8	7	17	0	80.9
	gra	18	36	0	0	380	2	0	0	0	0	12	0	0	84.8
	hea	0	3	9	9	0	222	0	25	0	0	16	0	0	78.2
	meq	0	0	1	3	0	0	152	2	0	0	0	7	11	86.4
	hmo	0	0	28	0	0	17	2	96	0	42	10	14	0	45.9
	wat	8	0	0	0	5	0	0	0	228	11	0	0	0	90.5
	gru	0	21	1	4	0	2	0	0	0	820	2	34	15	91.2
	wdw	2	120	24	9	5	26	0	0	0	0	895	0	0	82.8
	mgr	0	1	0	7	0	0	15	0	0	40	0	264	19	76.3
	wet	0	0	0	0	0	0	1	0	0	14	0	18	456	93.3
prediction accuracy (%)		83.2	46.1	88.9	87.5	87.6	78.4	79.6	65.3	99.6	79.9	81.6	73.7	91.0	

b) Simplified classification scheme

		predicted						observation accuracy (%)
		bgg	cru	wat	gru	wdw	veg	
observed	bgg	546	51	3	6	14	1	87.9
	cru	60	149	0	17	122	39	38.5
	wat	13	0	240	8	0	1	91.6
	gru	2	22	0	775	0	103	85.9
	wdw	16	128	0	0	980	58	82.9
	veg	0	0	0	38	28	2474	97.4
prediction accuracy (%)		85.7	42.6	98.8	91.8	85.7	92.5	

c) Optimized classification scheme

		predicted											observation accuracy (%)
		bgr	cas	dry	gra	meq	wat	gru	wdc	hea	mgr	wet	
observed	bgr	143	0	0	17	0	2	5	41	0	0	0	68.8
	cas	0	614	10	0	1	0	30	9	5	3	0	91.4
	dry	0	4	235	2	11	0	13	14	7	8	4	78.9
	gra	17	0	0	370	0	0	0	57	1	0	0	83.1
	meq	0	2	5	0	151	0	0	0	1	8	8	86.3
	wat	4	0	0	8	0	219	15	0	0	0	0	89.0
	gru	0	1	9	0	0	0	824	28	6	19	11	91.8
	wdc	9	20	8	37	0	0	21	1340	25	0	0	91.8
	hea	0	22	8	0	4	0	46	52	339	20	0	69.0
	mgr	0	0	7	0	12	0	52	8	0	253	15	72.9
	wet	0	0	0	0	4	0	12	0	0	16	455	93.4
	prediction accuracy (%)		82.7	92.6	83.3	85.3	82.5	99.1	80.9	86.5	88.3	77.4	92.3

Figure 3: Confusion matrices for SAS with all variables (optical and terrain) using the a) initial, b) simplified and c) optimized classification scheme

a) Initial classification scheme

		predicted															
		bgr	cru	cas	csu	dry	gra	hea	mbr	meq	hmo	gru	wdw	mgr	wet	wat	observation accuracy (%)
observed	bgr	709	27	6	0	0	11	0	0	0	6	25	14	0	0	8	88.0
	cru	0	1138	2	0	1	46	59	0	0	5	22	64	1	42	0	82.5
	cas	0	17	974	0	26	1	0	0	0	0	23	222	0	33	17	74.2
	csu	0	0	0	534	0	0	0	0	0	0	0	0	0	0	0	100
	dry	0	8	4	0	973	22	0	0	0	0	21	109	6	70	0	80.2
	gra	7	65	0	0	16	411	2	0	0	0	44	13	17	0	0	71.5
	hea	0	4	0	0	0	0	1406	0	0	59	0	0	0	23	0	94.2
	mbr	0	0	25	0	0	0	0	242	0	0	6	0	0	72	0	70.1
	meq	0	0	16	0	3	0	0	0	1079	0	30	8	90	41	0	85.2
	hmo	0	0	8	0	0	0	8	0	0	832	14	15	0	45	0	90.2
	gru	12	31	21	25	32	0	7	0	71	0	2071	47	85	242	0	78.3
	wdw	0	100	204	0	44	0	0	0	0	0	24	1153	0	5	0	75.4
	mgr	0	0	34	0	21	19	0	0	40	1	132	12	1662	149	0	80.3
	wet	0	12	0	0	0	0	0	0	29	14	240	19	25	2308	0	87.2
	wat	1	0	1	0	0	0	0	3	0	0	0	22	0	0	2593	99.0
	prediction accuracy (%)		97.3	81.2	75.2	95.5	87.2	80.6	94.9	98.8	88.5	90.7	78.1	67.9	88.1	76.2	99.0

b) Simplified classification scheme

		predicted						
		cru	veg	bgg	wat	gru	wdw	observation accuracy (%)
observed	cru	709	27	6	0	0	11	74.3
	veg	0	1138	2	0	1	46	96.1
	bgg	0	17	974	0	26	1	80.6
	wat	0	0	0	534	0	0	97.5
	gru	0	8	4	0	973	22	66.8
	wdw	7	65	0	0	16	411	51.9
prediction accuracy (%)		78.4	87.3	78.0	99.7	86.2	73.0	

c) Optimized classification scheme

		predicted														
		bgr	cas	csu	dry	gra	mbr	meq	gru	wdc	mgr	wet	hea	wat	observation accuracy (%)	
observed	bgr	695	0	0	0	19	0	0	44	32	0	3	11	3	86.1	
	cas	0	1020	0	29	0	0	0	26	198	0	19	3	10	78.2	
	csu	0	0	534	0	0	0	0	0	0	0	0	0	0	100	
	dry	0	11	0	976	12	0	4	16	184	2	49	0	0	77.8	
	gra	15	0	0	25	409	0	0	11	112	3	0	0	0	71.1	
	mbr	0	9	0	0	0	284	0	1	0	0	50	1	0	82.3	
	meq	0	14	0	11	0	0	1071	19	10	105	37	0	0	84.5	
	gru	18	28	30	33	8	0	85	2073	102	71	183	15	0	78.3	
	wdc	19	348	0	44	43	0	2	44	2420	1	40	49	0	80.4	
	mgr	0	19	0	11	22	0	17	104	69	1685	138	6	0	81.4	
	wet	0	0	0	0	0	1	49	286	64	31	2198	18	0	83.0	
	hea	0	0	0	11	0	1	0	13	2	0	80	2307	0	95.6	
	wat	4	2	0	0	0	0	0	0	17	0	0	0	2708	99.2	
	prediction accuracy (%)		92.5	70.3	94.7	85.6	79.7	99.3	87.2	78.6	75.4	88.8	78.6	95.7	99.5	

Figure 4: Confusion matrices for TOD with all variables (optical and terrain) using the a) initial, b) simplified and c) optimized classification scheme


```

###DATA EXTRACTION

# Load libraries (not sure if all are needed)
library(raster)
library(rgdal)
library(rlcm)
library(rgeos)
library(snow)
library(rminer)
library(splitstackshape)
library(data.table)

#Stack all the raster files
sas_image_map<-stack(sas_4band, sas_4band_qlcm, sas_slope, sas_dis_vrm1,
sas_dis_vrm02)

###Extract data

#set directory name

shp.dir <- "shapefile"

#Load ground truthing data point shapefile
gt2019sas <- readOGR(dsn = shp.dir,layer="gt_sas_2019")

#Create buffer to extract data around ground truthing points
gt2019sas_15cm<-gBuffer(gt2019sas,width=0.075, byid = TRUE)
gtpts_sas<-gt2019sas_15cm ## Change name for more general code, so that the buffer
size can be changed

#Load ground truthing data
sas_gt <- read.delim("gt_sassendalen_summer2019_2020_02_06.txt")
#add unique ID
sas_gt$ID<-1:nrow(sas_gt)

#Extract values at buffer locations (cluster number needs to be adjusted)
beginCluster(50)
gtpts_value_sas=extract(x=sas_image_stack_all, y=gtpts_sas, df=TRUE)
endCluster()
extracted_data_sas<-merge(gtpts_value_sas, sas_gt, by="ID", sort = TRUE)

```

Figure 5: R script: data extraction from raster stack with buffers around point

```

### RANDOM FOREST

#make a simple dataset to reduce to one entry per ground truth point (ID column and
class column)
sas_sub_data<-sas_data[,c(1,78)]
sas_sub_data$class<-as.factor(sas_sub_data$class)
sas_sub_data<-unique(sas_sub_data)

#Split dataset into training set (in this case 70%), here you need
#to adjust for splitting you want to do, depending on the class
#number you need to change the matrix size. And adjust the columns
#used for the random forest, in this example I only used the optical
#layers and not terrain for example.
sas_output<-list()
sas_all_scores<-c()
sas_c_matrix = matrix(0, 11, 11)
sas_all_cm<-c()

for(run.int in 1:30 ){
  run<-as.character(run.int)
  out_sas <- stratified(sas_sub_data, c("class"), 0.7)

  #create training dataset from the "out dataframe"
  sas_training.data<-sas_data[sas_data$ID %in% out_sas$ID,]

  #create validation dataset from the remaining data
  sas_validation.data<-sas_data[!sas_data$ID %in% out_sas$ID,]
  sas_validation.data<-sas_validation.data[,c(5:48,78)]

  #remove rows not to be included
  sas_training.data<-sas_training.data[,c(5:48,78)]
  sas_training.data$class<-as.factor(sas_training.data$class)

  #Run random forest model
  M_sas=rminer::fit(class~,sas_training.data,model="randomForest", task = "class")
  sas_output[[run]]<-list(model=M_sas)
  #create dataframe whilst extracting the descriptor
  sas_table_res <- as.data.frame(M_sas@object$importance)

  #change order of values in column from highest to lowest
  sas_table_res_s <- sas_table_res[order(sas_table_res$MeanDecreaseAccuracy),]

  sas_output[[run]][["importance"]]<-sas_table_res_s

  # use the model to predict the classes in the validation dataset
  sas_validation.data$pred.class=rminer::predict(M_sas,sas_validation.data)

  sas_validation.data$class<-as.factor(sas_validation.data$class)

  # compare predicted versus observed data
  sas_c.m<-rminer::mmetric(sas_validation.data$class,
sas_validation.data$pred.class, metric=c("ALL"))
  sas_c.m1<-rminer::mmetric(sas_validation.data$class,
sas_validation.data$pred.class, metric=c("CONF"))

  # add all metrics to outputs and make table
  sas_output[[run]][["accuracy"]]<-sas_c.m
  sas_all_scores<-rbind(sas_all_scores, sas_c.m)

  # make a extra output for confusion matrix and total summed confusion matrix
  sas_output[[run]][["cfm"]]<-sas_c.m1$conf
  sas_c_matrix<-sas_c_matrix + sas_c.m1$conf

  # make a long table with all confusion matrices
  sas_all_cm<-rbind(sas_all_cm, sas_c.m1$conf)
}
dev.off()

```

Figure 6: R script: Random forest as loop (30 repeats) with a new dataset split for each loop

```

### RF MODEL WITH ALL DATA (not splitting and therefore no loop necessary
#change the class values from numbers to being factors
sas_rf_data<-sas_data[,c(5:69,78)]
M_sas=rminer::fit(class~.,sas_rf_data,model="randomForest", task = "class")
savemodel(M_sas,"model_name") # saves to file

### Creating a map from the model
#load model
M_sas_reload<-loadmodel("model_name")
#load the raster stack you want to use (in this case sas image map), be careful the
raster stack and model use the same column names

closeAllConnections()
beginCluster()
sas_preds_rf <- clusterR(sas_image_map, raster::predict, args = list(model =
M_sas_reload))
endCluster()

#save the output
writeRaster(sas_preds_rf, "sas_result_optimized.tif", overwrite=TRUE)

```

Figure 7: R script: basic random forest without dataset split and mapping model predictions

```

###DATA EXTRACTION

# Load libraries (not sure if all are needed)
library(raster)
library(rgdal)
library(glcm)
library(rgeos)
library(snow)
library(rmineral)
library(splitstackshape)
library(data.table)

#Stack all the raster files
sas_image_map<-stack(sas_4band, sas_4band_glcm, sas_slope, sas_dis_vrm1,
sas_dis_vrm02)

###Extract data

#set directory name

shp.dir <- "shapefile"

#Load ground truthing data point shapefile
gt2019sas <- readOGR(dsn = shp.dir,layer="gt_sas_2019")

#Create buffer to extract data around ground truthing points
gt2019sas_15cm<-gBuffer(gt2019sas,width=0.075, byid = TRUE)
gtpts_sas<-gt2019sas_15cm ## Change name for more general code, so that the buffer
size can be changed

#Load ground truthing data
sas_gt <- read.delim("gt_sassendalen_summer2019_2020_02_06.txt")
#add unique ID
sas_gt$ID<-1:nrow(sas_gt)

#Extract values at buffer locations (cluster number needs to be adjusted)
beginCluster(50)
gtpts_value_sas=extract(x=sas_image_stack_all, y=gtpts_sas, df=TRUE)
endCluster()
extracted_data_sas<-merge(gtpts_value_sas, sas_gt, by="ID", sort = TRUE)

```

```

### RANDOM FOREST

#make a simple dataset to reduce to one entry per ground truth point (ID column and
class column)
sas_sub_data<-sas_data[,c(1,78)]
sas_sub_data$class<-as.factor(sas_sub_data$class)
sas_sub_data<-unique(sas_sub_data)

#Split dataset into training set (in this case 70%), here you need
#to adjust for splitting you want to do, depending on the class
#number you need to change the matrix size. And adjust the columns
#used for the random forest, in this example I only used the optical
#layers and not terrain for example.
sas_output<-list()
sas_all.scores<-c()
sas_c_matrix = matrix(0, 11, 11)
sas_all_cm<-c()

for(run.int in 1:30 ){
  run<-as.character(run.int)
  out_sas <- stratified(sas_sub_data, c("class"), 0.7)

  #create training dataset from the "out dataframe"
  sas_training.data<-sas_data[sas_data$ID %in% out_sas$ID,]

  #create validation dataset from the remaining data
  sas_validation.data<-sas_data[!sas_data$ID %in% out_sas$ID,]
  sas_validation.data<-sas_validation.data[,c(5:48,78)]

  #remove rows not to be included
  sas_training.data<-sas_training.data[,c(5:48,78)]
  sas_training.data$class<-as.factor(sas_training.data$class)

  #Run random forest model
  M_sas=rminer::fit(class~.,sas_training.data,model="randomForest", task = "class")
  sas_output[[run]]<-list(model=M_sas)
  #create dataframe whilst extracting the descriptor
  sas_table_res <- as.data.frame(M_sas@object$importance)

  #change order of values in column from highest to lowest
  sas_table_res_S <- sas_table_res[order(sas_table_res$MeanDecreaseAccuracy),]

  sas_output[[run]][["importance"]]<-sas_table_res_S

  # use the model to predict the classes in the validation dataset
  sas_validation.data$pred.class=rminer::predict(M_sas,sas_validation.data)

  sas_validation.data$class<-as.factor(sas_validation.data$class)

  # compare predicted versus observed data
  sas_c.m<-rminer::mmetric(sas_validation.data$class,
sas_validation.data$pred.class,metric=c("ALL"))
  sas_c.m1<-rminer::mmetric(sas_validation.data$class,
sas_validation.data$pred.class,metric=c("CONF"))

  # add all metrics to outputs and make table
  sas_output[[run]][["accuracy"]]<-sas_c.m
  sas_all.scores<-rbind(sas_all.scores, sas_c.m)

  # make a extra output for confusion matrix and total summed confusion matrix
  sas_output[[run]][["cfm"]]<-sas_c.m1$conf
  sas_c_matrix<-sas_c_matrix + sas_c.m1$conf

  # make a long table with all confusion matrices
  sas_all_cm<-rbind(sas_all_cm, sas_c.m1$conf)
}
dev.off()

```

```
### RF MODEL WITH ALL DATA (not splitting and therefore no loop necessary)
#change the class values from numbers to being factors
sas_rf_data<-sas_data[,c(5:69,78)]
M_sas=rminer::fit(class~.,sas_rf_data,model="randomForest", task = "class")
savemodel(M_sas,"model_name") # saves to file

### Creating a map from the model
#load model
M_sas_reload<-loadmodel("model_name")

#load the raster stack you want to use (in this case sas image map), be careful the
raster stack and model use the same column names

closeAllConnections()
beginCluster()
sas_preds_rf <- clusterR(sas_image_map, raster::predict, args = list(model =
M_sas_reload))
endCluster()

#save the output
writeRaster(sas_preds_rf, "sas_result_optimized.tif", overwrite=TRUE)
```

Paper III

1 **Snowmelt progression drives spring habitat selection and vegetation disturbance by an**
2 **Arctic avian herbivore at multiple scales**

3

4

5 Isabell Eischeid^{1,2,3*}, Jesper Madsen³, Rolf. A. Ims¹, Bart A. Nolet^{4,5}, Åshild Ø. Pedersen²,
6 Kees H.T. Schreven⁴, Eeva M. Soininen¹, Nigel G. Yoccoz¹, Virve T. Ravolainen²

7

8 ¹ Department of Arctic and Marine Biology, UiT The Arctic University of Norway, 9037
9 Tromsø, Norway

10 ² Fram Centre, Norwegian Polar Institute, 9296 Tromsø, Norway

11 ³ Department of Ecoscience, Aarhus University, 8410 Rønde, Denmark

12 ⁴ Department of Animal Ecology, Netherlands Institute of Ecology (NIOO-KNAW),
13 Droevendaalsesteeg 10, 6708 PB, Wageningen, The Netherlands

14 ⁵ Department of Theoretical and Computational Ecology, Institute for Biodiversity and
15 Ecosystem Dynamics, University of Amsterdam, Science Park 904, 1098 XH Amsterdam,
16 The Netherlands

17

18 *Corresponding author: Isabell Eischeid (isabell.eischeid@uit.no)

19

20

21

22

23 Abstract

24 Arctic tundra vegetation is affected both by rapid climatic change and fluctuations in
25 herbivore population sizes. Geese, such as pink-footed goose (*Anser brachyrhynchus*), are
26 major herbivores in high Arctic Svalbard. After arrival in spring, they feed intensively, using
27 a specialized technique called grubbing, on belowground rhizomes, causing soil erosion and
28 disturbances to vegetation. Moss tundra is preferred over dwarf-shrub vegetation, but to
29 predict future Arctic vegetation development, it is important to also understand how snowmelt
30 timing drives habitat selection, use and vegetation disturbance likelihoods. Here we analyzed
31 habitat selection and habitat use of geese using GPS telemetry data (n=12 geese) and field
32 observations by applying predictors on vegetation (moss tundra and dwarf shrub heath) and
33 snow melt progression derived from drone and satellite images at two spatial scales (fine
34 scale: 5 cm, 0.3 km²; valley scale: 10 m, 30 km²) during a three-week period in 2019. We
35 confirmed that habitat selection, use and disturbance was higher for moss tundra than dwarf-
36 shrub heath vegetation. Habitat selection did not differ between areas that were free from
37 snow early or late in the season, therefore habitat use was highest for the areas that were free
38 of snow earliest. Vegetation disturbances were also highest for early snow-free areas so that
39 habitat use and vegetation disturbance were positively correlated for both vegetation types.
40 The disturbance patterns we observed at the fine and valley-scale level corresponded well
41 with one another and led to an estimate of 23% moss tundra and 10% of dwarf-shrub heath
42 vegetation in the valley being disturbed by pink-footed geese. This study shows that both
43 vegetation class and snowmelt date are important predictors for habitat use and disturbance.
44 With the uncertainty around how snowmelt timing will develop, this provides us with better
45 tools to study and predict goose behavior and habitat disturbances in the future. Pending local
46 calibration with field assessments and drones, using satellite images and telemetry data can
47 provide a tool to detect disturbance hotspots caused by avian Arctic herbivores.

48

49 **Keywords:** *Anser brachyrhynchus*, drone, grubbing, moss tundra, Pink-footed goose, satellite,
50 Sentinel 2, snowmelt, UAV

51 1. Introduction

52 The Arctic is one of the regions on Earth that is most rapidly changing, with warmer
53 temperatures, greater levels of precipitation, and a general increase in variability and
54 unpredictability of weather (Bintanja 2018, IPCC 2019). Climate change affects herbivores
55 and their habitats, through direct and indirect effects, such as changes in plant biomass or
56 predator abundances (Hastings et al. 2007, Mysterud and Sæther 2011, Ims et al. 2013). In
57 turn, impact herbivores their bio-physical environment, e.g., through grazing (Peth and Horn
58 2006), trampling (Tuomi et al. 2021) and fertilization (Stark and Grellmann 2002). To better
59 understand and predict how Arctic ecosystems develop in the future we need to quantify both
60 the climatic drivers of landscape change and how this changes herbivore behavior and their
61 impact on the landscape (Jones et al. 1994, Wilby et al. 2001, Hastings et al. 2007, Smit and
62 Putman 2011). Studying landscape-herbivore interactions in rapidly changing and
63 heterogenous landscapes, demands monitoring methods at appropriate spatial and temporal
64 extent and resolution (Post et al. 2009, Ims et al. 2013, Ims and Yoccoz 2017, Ravolainen et
65 al. 2020, Eischeid et al. 2021).

66

67 One of the many climate-related variables that are currently changing is snow, which is an
68 important driver of availability and quality of habitat for herbivores in several ways (Rixen et
69 al. 2002). It is expected that precipitation in the Arctic will increase by 50-60% during the
70 21st century (Bintanja 2018). Small regional and interannual temperature fluctuations around
71 the freezing point can therefore have large consequences on the duration, physical properties
72 and distribution of the snow cover (Bokhorst et al. 2016). Changes in snow cover can have
73 large consequences for herbivore spring ecology, including vulnerability to trophic mismatch
74 between food availability (Gauthier et al. 2013, Doiron et al. 2015, Lameris et al. 2017) and
75 increased reproductive success when breeding habitats become available earlier (Madsen et
76 al. 2007, Tveraa et al. 2013, Jensen et al. 2014). Long distance migratory herbivores, such as
77 geese, cannot time their departure from spring staging areas in the temperate zone based on
78 environmental conditions at their destination (Fox et al. 2006, Kölzsch et al. 2015) and snow
79 cover in the spring therefore shapes habitat availability and the impact these herbivores exert
80 on the ecosystem during that time.

81

82 Several species of Arctic-breeding geese have increased in numbers, benefitting from
83 favorable overwintering conditions in recent decades (Abraham et al. 2005, Fox et al. 2018,

84 Heldbjerg et al. 2021). In the Arctic some of the larger-billed species can impact the state of
85 the vegetation of their Arctic summer habitats. Their beaks are strong enough to remove
86 below ground plant parts when above ground biomass is not available (Fox and Bergersen
87 2005). This behavior (termed grubbing) leads to vegetation loss and moss removal which
88 increases exposure for erosion and can alter carbon pools in both moist and dry tundra
89 habitats (Wal 2006, Speed et al. 2010a, Petit Bon et al. 2021). For instance, increases in lesser
90 snow geese populations (*Chen caerulescens caerulescens*) have caused severe habitat
91 degradation and changing the long-term ecological state of salt marsh wetlands by
92 significantly reducing graminoid and shrub cover (Jefferies et al. 2003, Abraham et al. 2005,
93 Peterson et al. 2013). In dry Arctic tundra habitats, goose disturbances can cause long lasting
94 ecosystem impacts because vegetation growth and recovery generally are slow (Forbes et al.
95 2001, Jefferies et al. 2003, Wal 2006, Speed et al. 2009). Selective feeding for preferred
96 vegetation (Speed et al. 2009) and variations in snow cover will therefore play a role in
97 determining which parts of the tundra will be most exposed to goose disturbances (Anderson
98 et al. 2015), but explicit documentation of snow cover impact on habitat use, selection and
99 vegetation disturbance are as of yet lacking.

100

101 The numbers of Svalbard breeding pink-footed geese have tripled during the last four decades
102 (Heldbjerg et al. 2021). They leave their last staging areas, on mainland Norway, without the
103 possibility to predict the snow cover extent at their destination on Svalbard but utilize pre-
104 breeding sites to wait and feed until their breeding grounds are free from snow (Fox et al.
105 2006, Duriez et al. 2009, Hübner et al. 2010, Anderson et al. 2015). Upon arrival, low lying
106 moist and wet habitats are preferred feeding grounds for this species, but extensive snow
107 cover can often prevent access to forage in these areas (Pedersen et al. 2013b, Anderson et al.
108 2016). Population increases and early snowmelt in south-west exposed dry habitats are
109 thought to favor feeding in habitats other than moist or wet moss tundra (Pedersen et al.
110 2013a, Pedersen et al. 2013b). Although several studies have addressed the importance of
111 snow in habitat selection and grubbing intensity (Wisz et al. 2008, Speed et al. 2009, Pedersen
112 et al. 2013a), have previous studies not investigated how changes in snow cover across the
113 snowmelt season influence habitat selection and vegetation disturbance. As changing habitat
114 availability across different spatial and temporal scales is expected to elicit dynamical pattern
115 of habitat use and selection (Myserud and Ims 1998, Holbrook et al. 2019), it is important
116 also use methods for mapping habitat availability that take into account relevant spatial scales
117 and temporal dynamics.

118 Recent studies have shown promising results of measuring Arctic herbivore disturbances with
119 drone images (Barnas et al. 2019, Eischeid et al. 2021, Siewert and Olofsson 2021) but rely
120 on differences in reflection values (e.g. NDVI) between disturbed and undisturbed parts of the
121 vegetation. This method is not suitable to detect pink-footed goose grubbing early in the
122 vegetative season or in dry habitats where disturbances are less visible (Eischeid et al. 2021)
123 but nevertheless frequent (Pedersen et al. 2013a, Pedersen et al. 2013b). The dynamic nature
124 of spring snow-herbivore interactions requires data both on herbivores and their habitat that
125 appropriately capture these dynamics in time and space. During spring, pink-footed geese
126 spend a large proportion of the day feeding, therefore it is likely that telemetry positions that
127 have thus far been used for studying for instance migratory patterns (Glahder et al. 2006), can
128 be used to not only infer their nesting habitat selection (Schreven et al. 2021) but also where
129 they cause disturbance. Drones can be used to map characteristics of snow (Schirmer and
130 Pomeroy 2020, Masný et al. 2021) including snow melt progression (Niedzielski et al. 2018)
131 and satellite images can help to upscale results to larger spatial scales (Dash et al. 2018,
132 Miranda et al. 2020, Assmann et al. 2020). Mapping snowmelt progression and goose habitat
133 selection by combining field data with remote sensing solutions at multiple scales will likely
134 provide new insights into the dynamic nature of snow-geese interactions during spring.

135
136 In this study, spanning snowmelt during the pre-breeding period of 2019, we used detailed
137 GPS-tracking data and visual observations of pink-footed goose combined with remote sensed
138 data (drone and satellite imagery) to assess goose habitat selection and vegetation disturbance
139 two spatial scales. We used remote sensing to quantify the availability of two major tundra
140 habitats and date of snowmelt through the spring snowmelt season, because we expected both
141 to be the drivers of pink-footed goose habitat use and vegetation disturbance at their pre-
142 breeding site. Specifically, we aimed at 1) combining field observations with remotely sensed
143 data at two spatial scales in order to estimate how habitat selection, use and vegetation
144 disturbance are driven by the progression of spring snowmelt, and then 2) use these estimates
145 to produce a fine-scale and a valley-wide vegetation disturbance likelihood map, and 3) assess
146 whether our estimates of habitat use correspond to estimates of vegetation disturbance rates.

147 2. Methods

148 2.1 Study system

149 2.1.1 Study area

150 We conducted our study in the southern side of Adventdalen, one of the largest valleys in
151 Nordenskiöld land in Svalbard (Figure 1), in the snow melting period (10 May – 03 June) in
152 2019. This area is one of the major pre-breeding sites that pink-footed geese use as a staging
153 and feeding area before their nesting grounds become free of snow (Hübner et al. 2010,
154 Anderson et al. 2012). The study area (valley-scale) covered 30 km² (78.19°N, 15.85°E) and
155 was accessible via gravel roads.

156

157 Adventdalen is a u-shaped glacial valley with different habitat types, situated along an
158 elevation gradient: A river and wetlands in the bottom of the valley, moist moss tundra in the
159 lower slopes and drier habitat types with species such as *Dryas octopetala* interspersed with
160 gravel in the upper ranges of the slopes. Rocks and gravel dominate steeper slopes and
161 elevations above (Elvebakk 1994, 2005). Annual precipitation is around 190 mm (Lawrimore
162 et al. 2021) and snowmelt timing varies between years and stretches through the months of
163 May and June (Anderson et al. 2015). In the study year (2019), snow melted out late and by
164 the beginning of June still 50 % of the study area was snow covered. Svalbard's terrestrial
165 ecosystem is characterized by low vertebrate biodiversity but is supplemented by large
166 populations of migratory birds such as pink-footed geese during the summer months (Ims and
167 Fuglei 2005, Ims et al. 2013, Descamps et al. 2017).

168

169 2.1.2 Study species - pink-footed geese

170 The pink-footed goose is the most numerous goose species on Svalbard (Fox et al. 2010). The
171 population has increased from c. 40,000 in the 1980s to c. 80,000 in 2015-2019 (Heldbjerg et
172 al. 2021). They migrate from wintering grounds in Belgium, the Netherlands and Denmark
173 via Norway and Finland to breed in Svalbard. The first individuals arrive around in the second
174 week of May and by the fourth week of May most birds have arrived (Glahder et al. 2006).
175 Geese mate in late May - early June, and shortly after incubate for approximately four weeks
176 (Madsen et al. 2007). During the pre-breeding period, there is little available above-ground
177 forage and pink-footed geese therefore use their beaks to access plant rhizomes below the
178 ground, a foraging mode called grubbing (Fox and Bergersen 2005, Anderson et al. 2012). In
179 dry areas, geese target rhizomes directly, leaving distinct holes that can still be visible many

180 years later, whereas in wet areas, geese simultaneously remove large areas of the moss layer
181 (Wal et al. 2020) (Figure 2). In the following, we refer to pink-footed geese as ‘geese’ and
182 grubbing activity as ‘disturbance’.

183 2.2 Study design

184 We applied a multi-method, spatially nested approach to obtain data for the analyses of
185 habitat selection, habitat use and vegetation disturbance of pink-footed goose in the pre-
186 breeding period (Figure 3,4). The data was gathered during the spring thaw from 10 May to
187 03 June in 2019. Drone and satellite images as well as field plots were used to obtain
188 predictor variables on snowmelt date and vegetation class. A habitat was defined by the
189 combination of vegetation class (i.e., moss tundra and dwarf-shrub heaths) and the date of
190 snowmelt. A fine scale study site (0.3 km² extent, 5 cm resolution) was nested within the
191 “valley scale” (30 km², 10 m resolution) study area (Figure 1). The two major vegetation
192 classes (i.e., moss tundra and dwarf-shrub heath) here were well represented both at the fine-
193 scale site and valley scale study area. We applied two methods for obtaining data on goose
194 habitat selection and habitat use that covered both spatial scales. A number of birds that
195 previously have used the area of Adventdalen valley were equipped with GPS collars and
196 provided data with high temporal resolution. The number of collared geese was limited
197 (n=12) and because these local resident birds do not necessarily represent the full range of
198 behaviors, we also conducted field-based observations. These observations yielded a second,
199 less temporally resolved data set based on census counts and positioning of geese multiple
200 times throughout the pre-breeding period. We generated a vegetation disturbance model from
201 field plots assessments and combined it with the remote sensed predictor variables to generate
202 vegetation disturbance maps. Finally, we compared the results of the habitat use assessment
203 and the vegetation disturbance maps.

204 2.3 Data collection and processing

205 2.3.1 Field plots (vegetation class, snowmelt date, disturbance)

206 We marked 320 field plots on 18 May 2019 (Julian day 138) at the fine-scale study site
207 (Figure 1, 3) to assess vegetation disturbance and snowmelt progression. Plots were placed in
208 20 groups of 16 plots each. Twelve of these groups were in moss tundra vegetation, and four
209 in the dwarf shrub heath vegetation, four covered both vegetation types. The minimum
210 distance between groups was approximately ten meters. To capture differences in snow melt
211 timing, we placed the groups in snow free terrain (n= 6), along the snow edge (n= 5) and on

212 ground that was still covered in snow (n= 9). Within each group, the plots were placed in a
213 perpendicular cross with four plots in each direction. This minimized the number of markers
214 we needed to establish in the frozen ground. For each of the plots we registered the vegetation
215 class (moss tundra, dwarf-shrub or barren), and every fourth day, we noted the status of the
216 snow cover in the plot (snow or snow-free) and presence of goose disturbance (none or
217 disturbed). Disturbed plots had to have at least one clearly identifiable grubbing hole.
218 Prior to analysis, we removed the plots that either were placed on barren ground or still
219 covered in snow by the end of the pre-breeding period. As a result, we had 285 plots, 211 in
220 moss tundra and 74 in dwarf-shrub heath used for further analysis. We started the field survey
221 on 18 May but because we had already a drone images available for 14 May, we used the
222 images to distinguish which of the plots that were snow free on 18 May were already snow
223 free on 14 May.

224

225 2.3.2 Goose telemetry

226 We used goose telemetry data, obtained from a mark-recapture campaign in 2018-2019, to
227 investigate the migration ecology of pink-footed geese, a total of 56 adult geese, primarily
228 adult females, have been caught and marked with GPS-GSM transmitter neckbands (Ornitela
229 UAB, Lithuania). Captures took place on a spring staging site in Tyrnävä, Oulu, Finland in
230 April-May 2018 and 2019, and during molt on brood rearing sites Daudmannsøyra, western
231 Spitsbergen, and on Isdammen in Adventdalen in July-August 2018 (Schreven et al. 2021). Of
232 these geese, 42 geese were present on Svalbard during 10 May to 03 June 2019, of which we
233 selected only include GPS positions that were within the range of the fine-scale and valley-
234 scale study sites. To exclude geese that were moving too fast to be feeding, we excluded GPS
235 positions with accelerometer speeds of over 1 km/h. In the fine-scale site, a total of seven
236 tagged individuals (GPS positions n= 36934) and in the valley-scale site, twelve tagged
237 individuals (GPS positions n= 142158) were available for further analyses. These were 11
238 females and 1 male (1 from Oulu, 1 from Daudmannsøyra, 10 from Isdammen). Of these, two
239 bred in Adventdalen and adjacent side valleys, while one bred in Sauriedalen (35 km NNW)
240 and others did not attempt to breed in 2019. Inferred from the movement of GPS-tagged geese
241 (Schreven 2021), the egg-laying commenced on 1 June on average (range: 29 May-4 June).
242 The collars recorded a GPS position (and speed) every 10 minutes, with an accuracy of 24%
243 within 5 m, 47% within 10 m, 74% within 20 m and 96% within 50 m. For more details on
244 handling procedures of geese and the GPS transmitters, see (Clausen et al. 2020, Schreven et
245 al. 2021).

246 2.3.3 Visual goose observations

247 We counted goose numbers along the roads in the Adventdalen valley in May 2019. After the
248 first small groups of pink-footed geese were observed on the 10 May, we counted them
249 systematically from Julian day 131 (11 May) until day 151 (31 May) (daily until 16 May and
250 every 2-3 days thereafter). For each counting day, two observers slowly drove along the same
251 route and stopped every time a goose or a group of geese was observed. We counted geese
252 within a maximum distance of 600m. For each observation we noted: 1) The number of geese,
253 2) their activity according to three categories (feeding = grazing or grubbing if identifiable,
254 sitting or walking) and 3) snow cover at the observation site according to three coarse classes
255 (on snow, snow-free or at snow-edge) and 4) a GPS position of the observer, a compass
256 course and measured distance, using distance binoculars. We calculated the positions of each
257 goose (or group of geese), using the observer's position as well as distance and angle to the
258 goose. We excluded observations where the geese were walking without feeding or were on a
259 snow-covered area. This resulted in 1300 observations and a total of 6676 geese available for
260 further analysis.

261

262 2.3.4 Developing and extracting environmental predictors from drone and satellite data

263 2.3.4.1 Drone-imagery

264 Throughout the snow melt period (14 May - 02 June 2019) we used a fixed-wing drone
265 (eBeeX, Sensefly) to collect aerial images of the fine-scale study site. The drone was rigged
266 with a RGB camera (AeriaX, Sensefly). On two dates, we additionally flew with a pre-
267 calibrated (Cubero-Castan et al. 2018) multispectral camera (Sequoia+, Sensefly) to obtain
268 green, red, near-infrared, and red-edge images. We flew in perpendicular lines to the main
269 slope of the terrain and kept a constant height over the ground (between 50 and 100 m above
270 ground (depending on the camera and date) and speeds between 8–15 m/s. Image overlap was
271 75% or higher for the AeriaX camera, while for the Sequoia+, side overlap was 60% and
272 horizontal overlap 80%. We flew around noon and only on days with stable light and wind
273 conditions (max 7 m/s). We aimed to fly every fourth day but because of variable weather
274 conditions that was not always possible. We flew on the following dates 14 May, 18 May, 22
275 May and 02 June. We logged the GPS positions with a Leica GS10 (Leica Geosystems)
276 differential GPS base station in vicinity of the study site and used these for kinematic post-
277 processing (PPK) of the drone images. Through the PPK workflow, we obtained an accuracy

278 of 5 cm for the drone images and verified our results using ground control points (GCPs) as
279 checkpoints.

280

281 *2.4.1.2 Snow cover maps (drone images, fine scale)*

282 We generated orthomosaics from the drone imagery using structure for motion with Pix4D
283 mapper software (Pix4Dmapper 2021) to produce snow cover maps at the fine scale. To do
284 so, we generated RGB orthomosaics for all drone flight days, and additional multispectral
285 orthomosaics for the days we had those available (18 May, 02 June). To classify the images
286 into snow/no-snow, we generated a classification training dataset by drawing a minimum 50
287 of polygons (for snow and no-snow) and extracting the values for each RGB and multispectral
288 orthomosaic. Using rminer (Cortez 2020), we then used the training dataset to train random
289 forest (RF) models to predict the two classes (snow/no-snow) for the entire meso-scale study
290 site. This method is described in Eischeid et al. (2021) in more detail. We visually inspected
291 the snow classification results and used masks to manually fix some obvious
292 misclassifications that occurred in areas such as “dirty snow,” GCP targets, cable car pillars
293 and their shadows, and a stitching error on the 22 May that resulted in a thin black stripe.
294 Finally, we resampled each of the snow maps to the same extent and 5 cm resolution and
295 extracted the snow/no snow variables for each pixel cell.

296

297 *2.4.1.3 Vegetation class map (drone images, fine scale)*

298 We used a simplified version of the drone-imagery based ground-cover classification map of
299 (Eischeid et al. 2021) that overlapped with our fine-scale study site. We grouped the ground-
300 cover classes into three major vegetation classes: moss tundra, dwarf shrub heath and bare
301 ground/water. The moss tundra class included the ground-cover types (as described in
302 Eischeid et al. (2021)) *moss-graminoid*, *wet moss tundra*, *Carex subspathacea*, *brown moss*
303 and *moss-equisetum*. The dwarf shrub class included the classes *dryas*, *cassiope*, *heath-*
304 *graminoid* and *heath-moss*, the bare ground/water class included areas covered with *gravel*,
305 *rocks*, *bare ground*, *biological crust* or *water*.

306

307 *2.4.1.4 Satellite-imagery*

308 We created snow cover and vegetation cover maps of the valley-scale site using Google Earth
309 Engine (GEE) and Sentinel 2A images with the bands red, green, blue and near-infrared at 10

310 m resolution. We filtered for cloud free days within the timespan of the study by calculating a
311 cloud probability band (MSK_CLDPRB) and manually checking the quality of the images.

312

313 *2.4.1.5 Snow cover maps (satellite images, valley-scale)*

314 To generate snow cover maps from satellite images at the valley-scale we used GEE. For each
315 date we had a Sentinel 2A image available (n=6), we drew 30 snow/no snow training
316 polygons to train a classifier. We used the GEE integrated classification and regression trees
317 (CART) classifier (Breiman et al. 1984) to generate six snow cover maps. We had two larger
318 time data-gaps, therefore we used the images before and after the gaps, to interpolate
319 estimated snow cover maps for the dates 18 May and 30 May.

320

321 *2.4.1.6 Vegetation class map (satellite images, valley scale)*

322 We generated a vegetation class map for the valley using Sentinel 2A image (27 July 2019)
323 and a random forest (RF) classifier based on the red, green, blue and near-infrared (NIR)
324 bands. In the fine-scale vegetation map, we marked 50 points for each the three classes (moss
325 tundra, dwarf-shrub graminoid, bare ground/water) and extracted the values to use them for
326 training the RF classifier. To test classification robustness, we trained 30 RF with subsets of
327 the dataset and obtained an average macro-F1 score of 95% (same method as described in
328 Eischeid et al. (2021)). We generated a final RF with 100% of the training data (as variation
329 between the 30 subsets was small) and used the final RF to predict vegetation classes across
330 the valley-scale study area.

331 2.5 Data analysis

332 2.5.1. Extracting environmental predictors from drone and satellite imagery to assess habitat 333 selection and habitat use

334 Prior to analysis, we extracted the environmental predictors (vegetation class and date of
335 snowmelt) for each GPS location and field observation coordinate. GPS locations or
336 observations that occurred in an area before it became snow free or on bare ground/water
337 were removed from the analysis. To account for the absence of daily drone or satellite images,
338 and temporally uneven field observations, we included geese GPS positions that were
339 registered in an area that was snow free in an image up to one day later and goose
340 observations that were registered snow free in an image up to two days later. For the GPS
341 telemetry dataset, we only included a maximum of one location per hour (always choosing the
342 earliest observation within each hour) to reduce spatial-temporal autocorrelation. For the fine-

343 scale analysis we had a total of 609 goose locations available for analysis, while for valley-
344 scale there were 1981 observations/locations. Uncertainties in the estimation of the position of
345 the field-based goose observations and the 10 m resolution of the satellite map resulted in that
346 some observations, noted as snow-free habitat in the field, were assigned to snow covered
347 areas on map. In such cases, we assigned the observation to a snow-free patch of the same
348 vegetation class within a 20 m radius of the original location. In cases with multiple snow-free
349 patches within the 20 m radius, we selected the closest one and the one with the most similar
350 snow-free date compared to the original assigned location. If no snow-free patches were
351 within the 20 m radius, the observation was excluded. This resulted in a total of 630 field
352 observations of geese or goose groups (total number geese = 3655) that were used for habitat
353 selection and use analysis.

354

355 We grouped all GPS locations or goose observations together and treated each combination of
356 vegetation class (moss tundra and dwarf shrub heath) and snowmelt date (four dates - in the
357 fine scale analysis, eight dates- in the valley scale analyses) as its own habitat class. In the
358 fine-scale analysis, we therefore had a total of eight habitat classes, and for the valley-scale
359 analyses we had 16 habitat classes. Although time-specific maps of habitat availability and
360 snowmelt form the basis of the habitat selection analysis, the timing of the goose
361 observations/positions did not enter directly the analysis. We chose this approach of grouping
362 all goose positions because it allowed us to compensate for irregular drone and satellite image
363 availability. It made it also possible to compare habitat use with the vegetation disturbance
364 likelihoods that were calculated for the entire pre-breeding period and not a day-by day basis.

365

366 2.5.2 Analyzing the impact of snowmelt and vegetation class on habitat selection and habitat
367 use

368 We analyzed both geese habitat selection and habitat use. For both approaches, we adapted
369 the habitat selection estimation method by (Manly et al. 2002) and used the R package
370 adehabitatHS (Calenge 2006) to calculate habitat selection coefficients and confidence
371 intervals (95%) according to Manly's design 1, where there is no unique identification of
372 animals, but where the proportions of available habitat classes are known (Thomas and Taylor
373 2006). Habitat preference (positive selection) is indicated by values above one and has no
374 maximum limit. Habitat avoidance (negative selection) is indicated by habitat selection ratios
375 between one and zero. The metrics *habitat selection* and *habitat use* differed in how we
376 defined habitat availability (Figure 4). First, we calculated *habitat use* by dividing the

377 proportional number of geese per habitat class by the proportional area size of each habitat
378 class. We converted the resulting Manly habitat selection ratios into percentages by dividing
379 each ratio by the sum of all selection ratios. *Habitat use* thus represents the proportion of time
380 did geese spend in a habitat type. Second, we calculated *habitat selection* to assess which
381 habitats geese preferred, thus taking into account that habitat classes had different durations of
382 habitat availability. We determined Manly selection coefficients by calculating the percentage
383 of goose occurrences per habitat class and dividing it by the percentage of available habitat
384 class, which was defined by the area of each habitat class multiplied by the days the habitat
385 was available throughout the study period. With equal *habitat selection*, we would therefore
386 expect that *habitat use* is highest for the areas that are available the longest. Thus, the level of
387 habitat use should represent the level of vegetation disturbance.

388

389 2.5.3 Impact of vegetation and snow melt on vegetation disturbance

390 We assessed the impact of vegetation class and snow-free days on presence of goose
391 disturbance (i.e. beak holes or moss removal) using the data obtained from the field plots
392 (n=282). We applied a logistic regression model with a binomial (Bernoulli as observations
393 were binary, 0 not disturbed, 1 disturbed) distribution, but allowing for the asymptote to be
394 less than 1, as all plots do not necessarily reach 100% disturbance by the end of the pre-
395 breeding period. We treated goose disturbance as the response variable, vegetation class
396 (moss tundra and dwarf-shrub heath) as a categorical predictor variable and snow-free days as
397 a continuous predictor variable. We used the `drm()` function R package `drc` (Ritz et al. 2015).
398 We chose the LL2.3 parameterization to fit a logistic curve that starts at zero and reaches an
399 asymptote that is estimated as a separate parameter. The LL2.3 parameterization is defined as
400
$$(x) = \frac{d}{1 + \exp(b(\log(x) - e))}$$
, with d as the asymptote, b the logistic regression slope and we used
401 $x = \exp(\text{snow-free date})$ as a predictor in the function. Because the slope for dwarf-shrub heath
402 and moss tundra were similar, we simplified the model to a common slope for both vegetation
403 classes. We assessed the predictive power of the model by calculating the correlation between
404 the observed and predicted proportions (Zheng and Agresti 2000).

405

406 2.5.4 Vegetation disturbance likelihood maps

407 We used the disturbance likelihood model, developed with plot-scale data, to predict grubbing
408 likelihood across the fine-scale and valley-scale study extents. To do this, we used the `predict`
409 function of the R package `rminer` (Cortez 2020) and the raster layers of vegetation class and

410 snow-free days to generate disturbance likelihood maps. These were scaled from zero (no
411 likelihood of disturbance) to one (100% likelihood of disturbance). To estimate the total
412 amount of disturbed areas, we summed the frequencies of each habitat type (each vegetation
413 class and snow-free day combination) and multiplied it with its disturbance likelihood, i.e.,
414 habitat class area x disturbance likelihood = area disturbed (e.g., 200 m² habitat x 0.8
415 disturbance likelihood= 160 m² disturbed vegetation).

416

417 2.5.5 Habitat use and disturbance

418 Finally, we assessed the correspondence between the habitat use and vegetation disturbance
419 estimates by means of Spearman correlation coefficients (Figure 3).

420

421 3. Results

422 3.1 Weather characteristics and spring phenology of geese

423 In 2019, a late snowmelt year, temperatures were mostly sub-zero during the study period
424 with two warmer spells at Julian days 133-138 and 148-154 (13-18 May and 28 May – 03
425 June) (Figure 5a). During the first days of June, 50% of the valley extent was still covered in
426 snow (Figure 5b). Moss tundra and dwarf shrub heath within the study area became snow-free
427 at a similar speed throughout the season. The first geese were counted on day 130 (10 May)
428 and their numbers continued to increase until day 147 (27 May) (Figure 5c). At day 151 (31
429 May) goose numbers were lower than on day 147, as the geese started leaving the pre-
430 breeding areas. The first GPS collared goose arrived in the study area on day 136 (16 May)
431 (Figure 5c). The maximum of GPS collared geese (10 individuals) was reached at day 142 (22
432 May).

433 3.2 Habitat selection and habitat use

434 Geese showed positive habitat selection (preference) for moss tundra and negative selection
435 (avoidance) for dwarf-shrub heath (Figure 6). This was broadly consistent across both spatial
436 scales and goose census methods (GPS telemetry and field observation), with some
437 exceptions (Figure 6). Using GPS telemetry data, overall habitat selection was independent of
438 the snowmelt date. The field-based goose observations suggested that areas free of snow early
439 in the season were overall more selected for. Habitat was therefore generally highest for the
440 areas that became snow free early in the season (Figure S1), and most profound when
441 measured with goose field observations at valley scale (Figure S1c).

442 3.3 Impact of vegetation and snow melt on vegetation disturbance

443 For both habitats, the disturbance likelihood was lowest for the plots that became snow free
444 late in the season (Figure 7). Vegetation disturbance was highest (disturbance rates of above
445 80%) for moss tundra plots that became snow free relatively early, i.e., Julian date 142 (22
446 May), but dropped steeply after and reached 10% for the plots that became snow-free by the
447 end of the study period. For plots in the dwarf-shrub heath, disturbances were highest for
448 plots that became snow free before Julian date 146 (May 26) with disturbance rates around
449 50%. Disturbance likelihoods were continually above zero for both vegetation classes within
450 the pre-breeding period. The logistic regression model with habitat-specific asymptotes fitted
451 the data well (correlation between observed and predicted values: $R=0.92$). The slope (b) was
452 0.58 ($SE=0.17$) and asymptotes (d) of 0.44 (with $SE=0.071$) for dwarf-shrub heath and 0.89
453 ($SE=0.035$) for moss tundra. The value of date for which the proportion is half the asymptote
454 was 148 Julian days for dwarf-shrub heath and 150 Julian days for moss tundra.

455 3.4 Vegetation disturbance likelihood maps

456 At both study scales, disturbance likelihoods were unevenly distributed across the landscape
457 (Figure 8). In the fine-scale study site 21.4% (32.8% of moss tundra habitat and 11.5% of
458 dwarf-shrub heath) of the vegetated area was predicted to be disturbed by pink-footed geese.
459 At the fine-scale site, the highest disturbance (over 80%) was predicted to occur in the early
460 snow free moss tundra areas at low elevations. Within the extent of valley-scale area, the fine-
461 scale study site was one of the areas with most disturbance. In the valley-scale study area,
462 4.75% of the total area was predicted to be disturbed, 23.1% of moss tundra (0.5 km^2) and
463 10.1% of dwarf-shrub heath (0.94 km^2). Areas in the vicinity of roads were snow free early in
464 the season and therefore had high predicted disturbance rates for both vegetation classes. At
465 the end of the pre-breeding period, snow-free vegetated areas comprised 52.8% of the fine-
466 scale site and 37.6% of the valley-scale area. Areas that were predicted to have disturbance
467 likelihood of zero, were either in the class bare ground/water (excluded in the model) or were
468 still covered in snow by the end of the pre-breeding period.

469 3.5 Habitat use and vegetation disturbance

470 Habitat use was positively correlated to vegetation disturbance at both spatial scales and using
471 both methods (GPS telemetry and field observations) of measuring goose habitat use (Figure
472 9, Table 1). Habitat use values above 10% were generally associated with the highest
473 disturbance rates.

474 4. Discussion

475 Our analysis of habitat use and vegetation disturbance by pink-footed goose, showed that
476 habitat use was predicting vegetation disturbance during the pre-breeding period. This trend
477 was consistent across vegetation classes, spatial scales and methods of assessing habitat
478 selection (GPS telemetry and field observations). Moss tundra was preferred over dwarf-shrub
479 heath and more often disturbed by pink-footed geese. Both habitat use and vegetation
480 disturbance was highest for areas that were free of snow early in the season. Our disturbance
481 predictions showed that pink-footed geese had disturbed about 23% of moss tundra during a
482 single pre-breeding period at the Adventdalen valley site indicating that the role of geese in
483 modifying tundra vegetation is significant.

484

485 This study supports the findings of previous studies that have shown that pink-footed geese
486 prefer moist over dry habitats (Speed et al. 2009, Anderson et al. 2012, Pedersen et al. 2013a,
487 Pedersen et al. 2013b) and expands on knowledge of the role of snowmelt on habitat selection
488 and vegetation disturbance that has not been explicitly addressed earlier. Previous studies on
489 pink-footed goose disturbance were unable to include snow as a predictor (but see Anderson
490 et al. (2016)) due to the coarse temporal or spatial scales (Wisiz et al. 2008, Speed et al. 2009)
491 or had to rely on proxies for snowmelt timing, like air temperature (Fox et al. 2006) or slope
492 direction (Pedersen et al. 2013a). For example, a Svalbard-wide goose disturbance likelihood
493 model from 2006 and 2007 (Speed et al. 2009) predicted highest disturbance likelihood in
494 those areas in Adventdalen valley that were never free of snow in the pre-breeding period of
495 2019, a year with relatively late snowmelt. Our finding that areas being snow free during the
496 first two weeks of the pre-breeding period were used most and therefore had highest
497 vegetation disturbance intensities support the study of (Pedersen et al. 2013a) that suggests
498 elevated levels of goose disturbance in south-east facing slopes of dry habitats which were
499 thought to be free of snow early in the season. Our study documents the importance of
500 snowmelt for spring ecology of tundra vegetation and an avian herbivore, providing empirical
501 evidence to general notions about implications of climate change and snow season changes in
502 particular (Post and Forchhammer 2002, Rixen et al. 2002, John et al. 2020).

503

504 Our vegetation disturbance map predicted that 23.1% of moss tundra and 10.1% of the dwarf-
505 shrub heath habitats at the Adventdalen valley pre-breeding site had been disturbed by pink-
506 footed geese in a single season. The effects of grubbing on vegetation varies greatly, intensity

507 and frequency of the disturbance influences how quickly the habitat recovers or new plant
508 community structures evolve (Kerbes et al. 1990, Wal et al. 2020). Experimental studies have
509 shown that carbon loss due to (simulated) goose disturbance vary greatly between years,
510 habitats and plant functional group (Speed et al. 2010b, Petit Bon et al. 2021). In a simulated
511 goose disturbance experiment, (Speed et al. 2010b) estimated carbon loss of 343.47 g/m² for
512 dry habitats (low intensity) and 625.46 g/m² in mesic habitats (medium disturbance levels),
513 compared to controls without disturbance. If these numbers were to be extrapolated to our
514 predicted disturbed area in Adventdalen valley, they could result in approximately 300 tons
515 carbon lost for each of the two vegetation classes, i.e., a total of 600 tons carbon lost in the
516 time span of about three weeks. Higher carbon emissions per m² in moss tundra were
517 therefore outweighed by the larger spatial extent of the dwarf-shrub heath. Our study suggests
518 that disturbance estimates via satellite and drone images, given intensities of disturbance
519 experiments like that of (Speed et al. 2010b) and the actual disturbance documented in the
520 field are equivalent, could provide a useful tool to approximate carbon emissions as the result
521 of pink-footed goose disturbance.

522

523 The tight linkage between habitat use and vegetation disturbance that we observed indicates
524 that habitat use of geese nicely reflects the degree of disturbance. This means that GPS
525 telemetry derived estimates of habitat use can be a good predictor for pink-footed goose
526 disturbance extent and intensity and can be a promising alternative for extensive field
527 campaigns. In addition to snow cover, that we focused on in this study, soil and air
528 temperatures during snow melt can influence if habitats are available for feeding. In 2019, a
529 late snowmelt year, were habitats grubbed shortly after they were free from snow, whereas
530 early snowmelt but cold air and soil temperatures can prevent geese from grubbing (Fox et al.
531 2006, Anderson et al. 2012). Alternatively, persistent warm May temperatures and early
532 snowmelt can advance graminoid growth so that grazing can become more advantageous over
533 grubbing (Fox et al. 2006). Earlier timing of the switch from grubbing to grazing can thus
534 weaken the link between habitat use and predicted vegetation disturbances via grubbing,
535 hence snowmelt and preferably soil, or air temperatures (as a proxy), need to be taken into
536 account in future monitoring. Similar approaches of linking habitat use and vegetation
537 disturbance are likely applicable for other broad-billed geese, such as *Anser cygnoides* and
538 *Chen caerulescens* that show seasonally intensive grubbing (Gauthier et al. 2005, Fox et al.
539 2008) or avian herbivores in general, because they tend to feed large proportions of the day
540 (Gils et al. 2007).

541 Only few studies have combined aerial images from drones or planes to study animal habitat
542 selection via telemetry e.g., Stark et al. (2018) because the target species need to be confined
543 to a rather small area. Although pink-footed geese at the population level migrate long-
544 distance and inhabit areas that span from western Europe to Svalbard, Iceland and Russia
545 (Alisauskas 2009), drones and GPS telemetry were useful tools because we studied their
546 behavior in a very defined place in space and time. A similar approach may be valuable for
547 migratory animals that gather and feed intensively in confined spaces along their migration
548 route (e.g. Nolet et al. (2001)).

549

550 The high-resolution images and the associated predictors provided a good tool to capture
551 snowmelt progression in detail that earlier studies in the same region have not been able to
552 (see e.g. Anderson et al. (2016)). Drone images are promising tools to derive ecologically
553 relevant habitat variables to study animal habitat selection (Mangewa et al. 2019) or improve
554 the interpretation of satellite images (Assmann et al. 2020). The ten-meter resolution of the
555 Sentinel 2 image-based snow maps was too coarse to capture smaller snow-free patches, and
556 almost 50% of our field-based observations had to be excluded because we could not assign
557 them to a snow-free patch in vicinity. However, this could be alleviated by using drone
558 images that provided spatial resolutions that allow for more detailed ecological analyses.
559 Pink-footed goose habitat selection, habitat use, and vegetation disturbance estimates were
560 consistent at both spatial scales chosen for this study. This suggests that Sentinel 2 satellite
561 images could provide adequate estimates of pink-footed goose disturbances at a valley
562 (management relevant (Stark et al. 2018)) scale. Similarly, the same habitat selection and
563 habitat use trends were detected through both methods of locating the birds, with the
564 exception for the last week of the pre-breeding period where they showed contradicting
565 trends. The telemetry-based approach indicated positive habitat selection for vegetation that
566 became snow-free in the last week of the pre-breeding period whereas the field observation-
567 based method showed that they selected against these areas. An explanation to these opposing
568 trends can be that different groups of geese showed different behavior at this time of the
569 season and GPS collared geese – mainly birds that remained local – were not representative
570 for the entire goose population. The field-based observations included geese that gathered in
571 large flocks to leave the pre-breeding site and go elsewhere to breed or spend the summer.
572 The main gathering sites that we identified had already been free of snow for several days or
573 weeks. Several of the GPS collared geese stayed to breed in Adventdalen and continued
574 grubbing and expanding their habitat to newly snow-free areas. Thus, pending local

575 calibration with field assessments and drones, using satellite images and telemetry data is a
576 method that requires only minimal presence in the field and can provide a tool to detect
577 disturbance hotspots caused by herbivores.

578

579 There are several methodological considerations that arose from our results that can help
580 future successful detection of habitat selection, habitat use and prediction of vegetation
581 disturbance based on remote-sensed and telemetry data. Because goose numbers in the valley
582 site were not constant throughout the pre-breeding period, the method of grouping all
583 observations to evaluate habitat selection may skew results in favor for habitats that were
584 snow-free when most geese were present. We showed that our method of mapping at two
585 spatial scales worked well in a late snowmelt year with small, but highly disturbed, early
586 snow-free areas. In years of early snowmelt, geese may be more spread out in different parts
587 of the landscape (Anderson et al. 2016), and thus more difficult to capture through drone-
588 based, fine-scaled analyses. Cloud cover reduces the availability of optical satellite data, more
589 work would be needed to assess the minimum number of images needed to adequately predict
590 habitat use and vegetation disturbance in the future. By choosing a multi-data approach which
591 showed consistent results across methods and spatial scales, we were able to minimize the
592 effect of the limitations.

593

594 5. Conclusion

595 In this study we used an approach integrating multiple sources of data on habitat availability,
596 snow melt and pink-footed goose spring area use to study habitat selection, use and vegetation
597 disturbance. To our knowledge this is the first study in the Arctic that combines remote-
598 sensed snowmelt mapping with ecological habitat selection analysis, documenting that
599 snowmelt timing and vegetation were important drivers for both habitat selection, use and
600 vegetation disturbance. Our results, with an 80% vegetation disturbance likelihood in the most
601 used habitats, detail and document how abiotic conditions play a role in in how and where
602 biotic factors like herbivores can alter tundra ecosystems. Mapping where in the landscape
603 vegetation disturbances occur can initiate new studies that assess how vegetation, terrain, and
604 snowmelt over consecutive years influence vegetation recovery. We underline the importance
605 of detailed high temporal and spatial data on snow melt patters to understand the impacts of
606 goose grubbing on Arctic tundra ecosystems. And we encourage the integration of drone

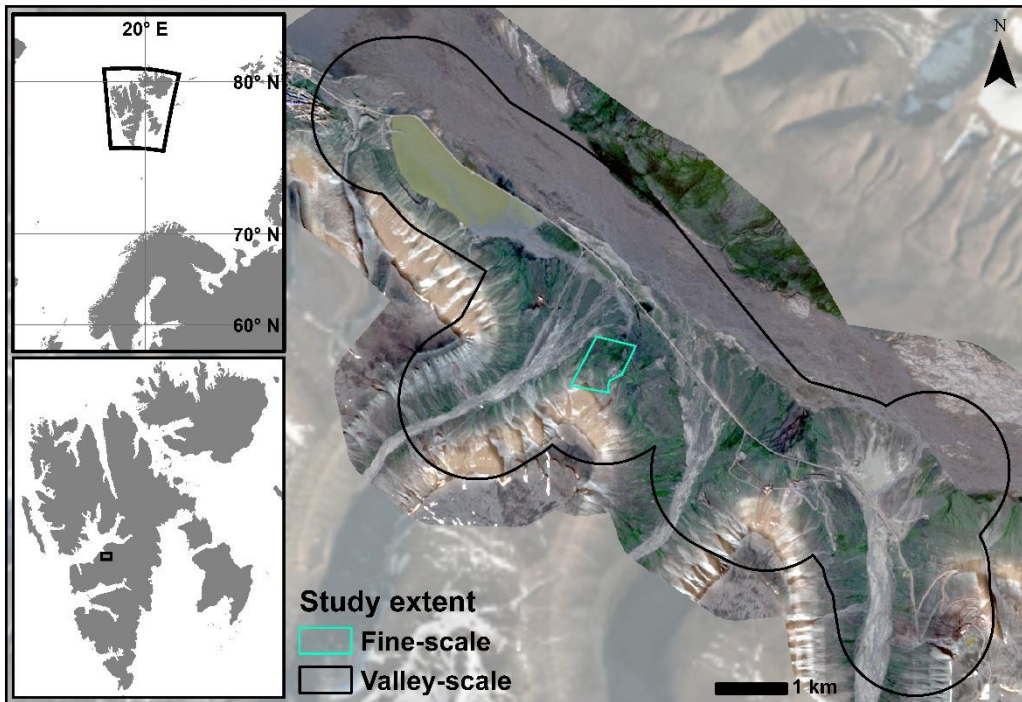
607 imagery as a tool to improve the information that can be gained from using satellite images
608 and GPS telemetry.

609

610 6. Acknowledgements

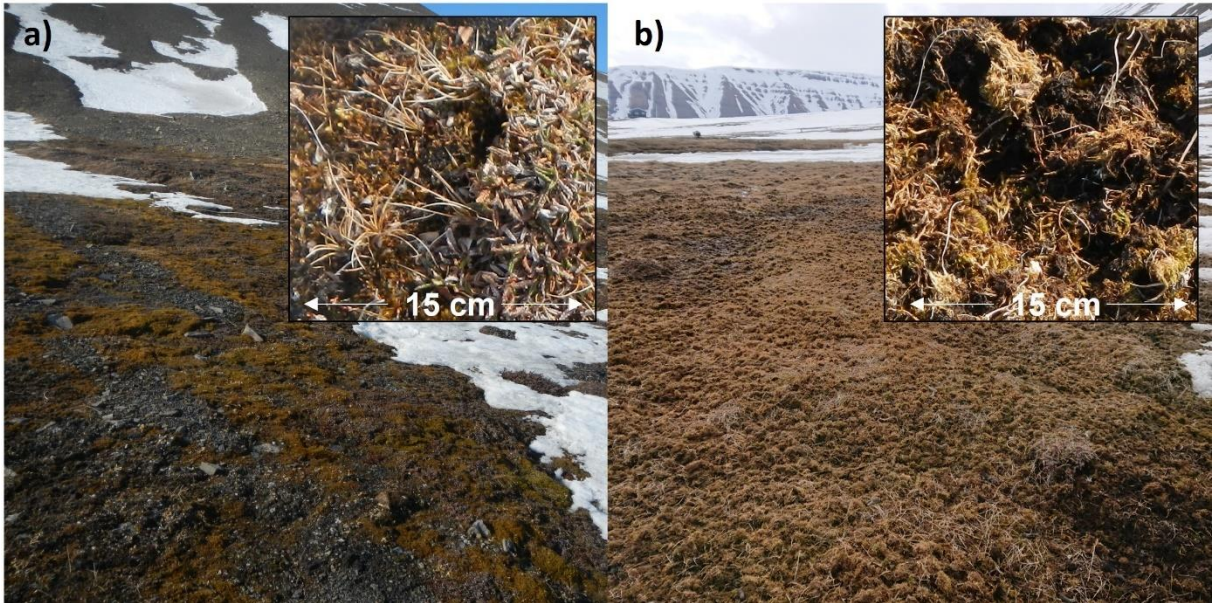
611 This research was funded by the Tromsø Research Foundation and made possible by support
612 from SIOS, a grant from the University of Aarhus to IE and a grant (ALWPP.2016.024) to
613 BAN. The Norwegian Polar Institute (NPI) provided personnel and field logistics. We thank
614 Linda Ársælsdóttir and Stein Tore Pedersen for support in the field and David Studer for the
615 help with image processing and classifications. Anne Urset and Harald Faste Aas at the NPI
616 mapping section provided valuable support with the GPS equipment. Furthermore, we thank
617 Rolf Andersen at the Arctic University of Norway (UiT) for providing us processing services
618 and support for using large datasets. This publication is a contribution from the Climate-
619 Ecological Observatory for Arctic Tundra (COAT).

620

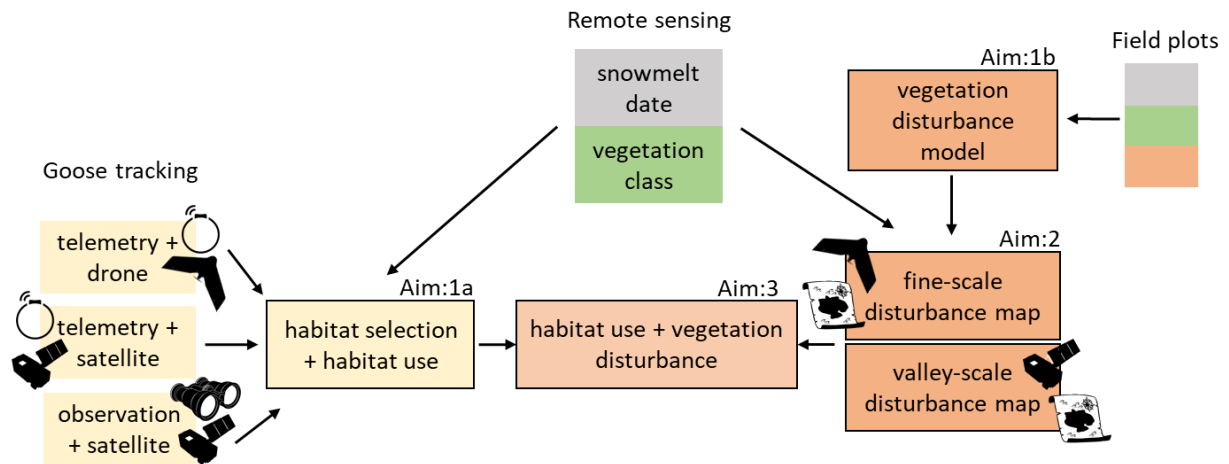


622
623 Figure 1: Location of this pink-footed goose habitat selection and vegetation disturbance
624 study, May-June 2019, in Adventdalen, Svalbard. Upper-left panel: Map of northern Europe,
625 showing the location of Svalbard. Lower-left panel: Map of Svalbard, showing the location of
626 the study area in the center of Nordenskiöld Land. Right panel: Satellite image (Sentinel 2A,
627 27.07.2019) of the study area showing the extent of the valley-scale and the fine-scale study
628 sites.

629
630



631
632 Figure 2: a) Dwarf-shrub heath and b) moss tundra vegetation class in late May 2019. Inserts
633 show the vegetation disturbances typical for the two vegetation classes: Single, isolated
634 grubbing holes in dwarf-shrub heath (left) and continuous grubbing removing the moss carpet
635 in moss tundra vegetation.
636



637

638

639

640

641

642

643

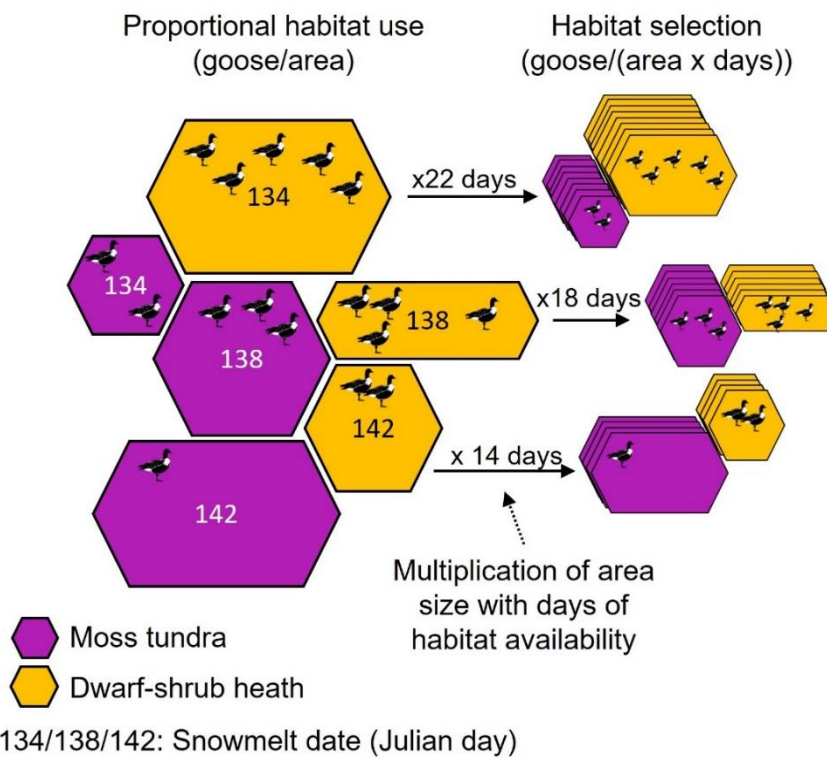
644

645

646

647

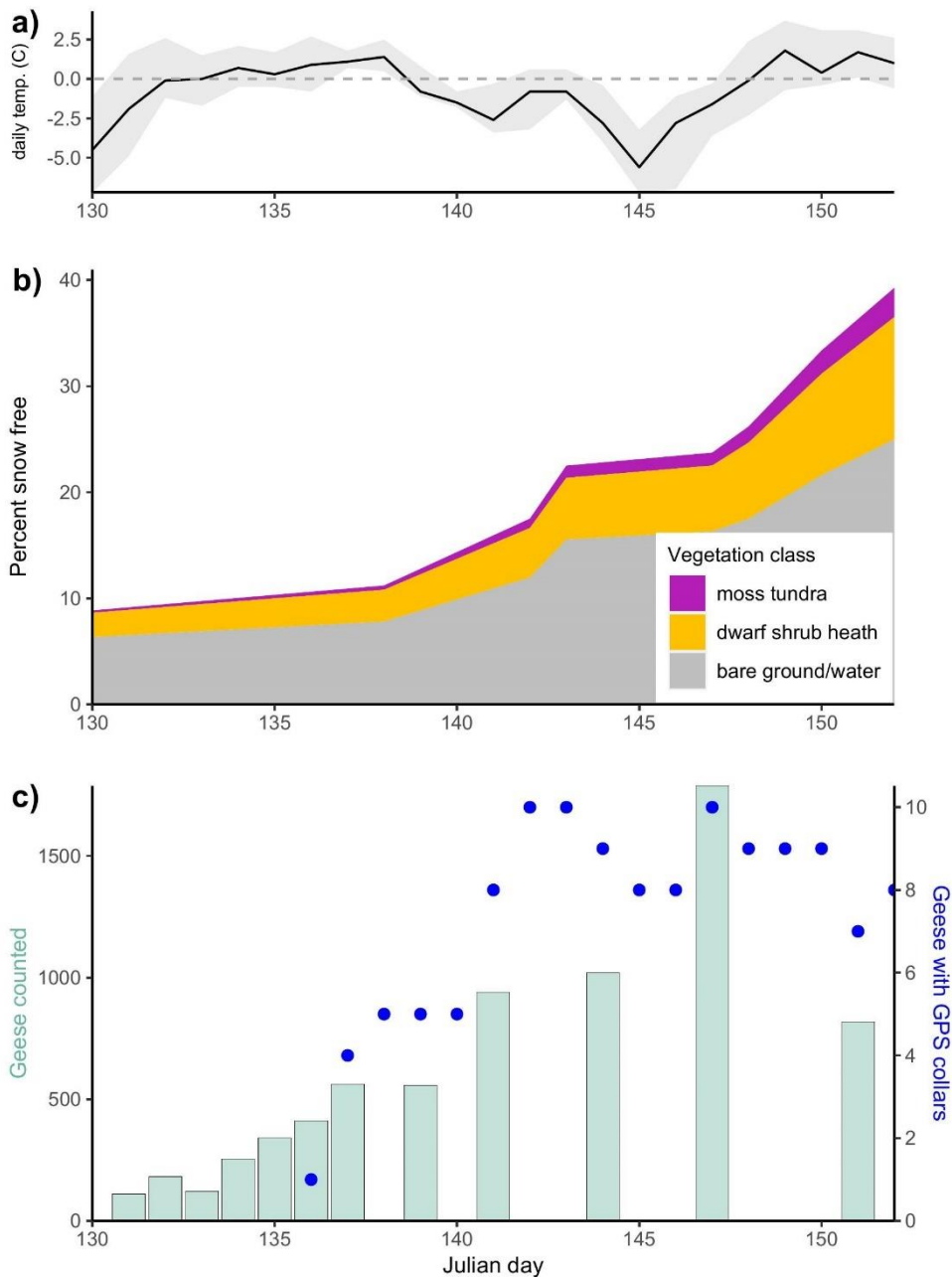
Figure 3: Study design for pink-footed goose habitat selection, use and vegetation disturbance survey during the pre-breeding season in Adventdalen Valley, Svalbard (2019). The study was conducted at two spatial scales, fine-scale (5 cm resolution) and valley-scale (10 m resolution). Drone and satellite images as well as field plots were used to obtain predictor variables on snowmelt date and vegetation class. 1a) Habitat selection and use were assessed using goose GPS telemetry or goose field observations and the remote sensed predictor variables. 1b) A vegetation disturbance model was generated from field plots assessments and 2) combined with the remote sensed predictor variables to generate vegetation disturbance maps at two spatial scales. 3) The results of the habitat use assessment and the vegetation disturbance maps were compared in the final step.



649

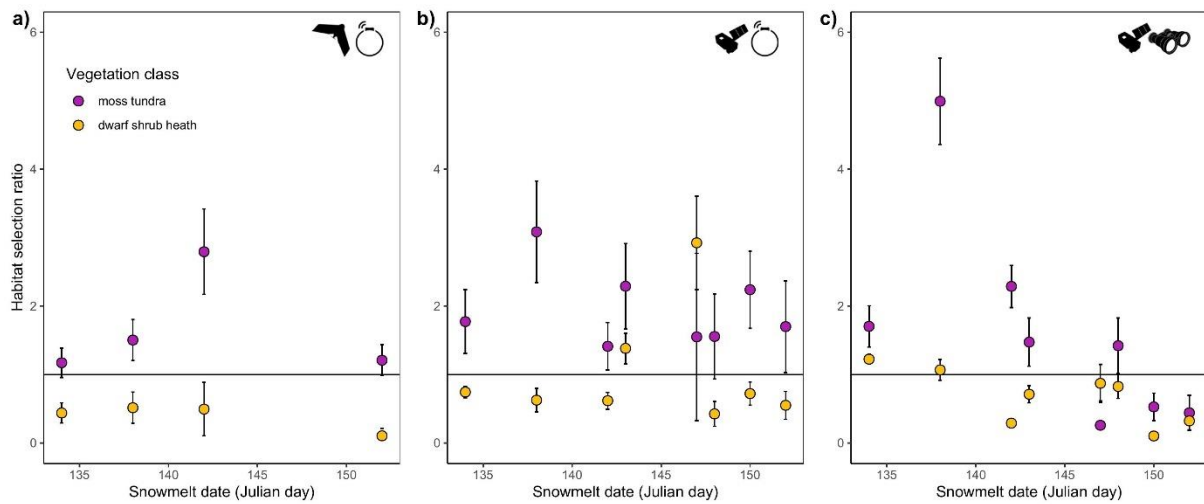
650 Figure 4: Schematic presentation of habitat use and habitat selection analysis. A habitat is
 651 defined by the two variables vegetation class and the snowmelt date. To calculate habitat use,
 652 the proportion of the number of goose positions was divided by the proportion of area size for
 653 each habitat class. The habitat selection assessment, as opposed to habitat use, considered
 654 differing duration of habitat availability. Habitat area sizes were therefore multiplied with the
 655 number of days they were available throughout the pre-breeding period. For example, the
 656 moss tundra and dwarf-shrub heath habitats that were free of snow earliest, were multiplied
 657 with 22 (days) and habitats that became available eight days later were multiplied by 14
 658 (days). Habitat selection was therefore calculated with the proportion of the number of goose
 659 positions divided by the proportion of area size of each habitat multiplied with the temporal
 660 availability of the habitat.

661



662
 663 Figure 5: Seasonal development in Adventdalen valley (10 May to 03 June, 2019. a) Daily
 664 mean temperature (C°, black line) at Longyearbyen airport (ca. 6 km from the study site). The
 665 gray field shows the min-max temperature range for each day. b) The proportion of snow-free
 666 area in the valley-scale study area, as measured from satellite imagery. c) The arrival of pink-
 667 footed geese to the Adventdalen valley. The turquoise bars show the number of geese counted
 668 during the field survey and the blue dots indicates the daily number of GPS collared geese
 669 that were within the spatial extent of the valley-scale study area.

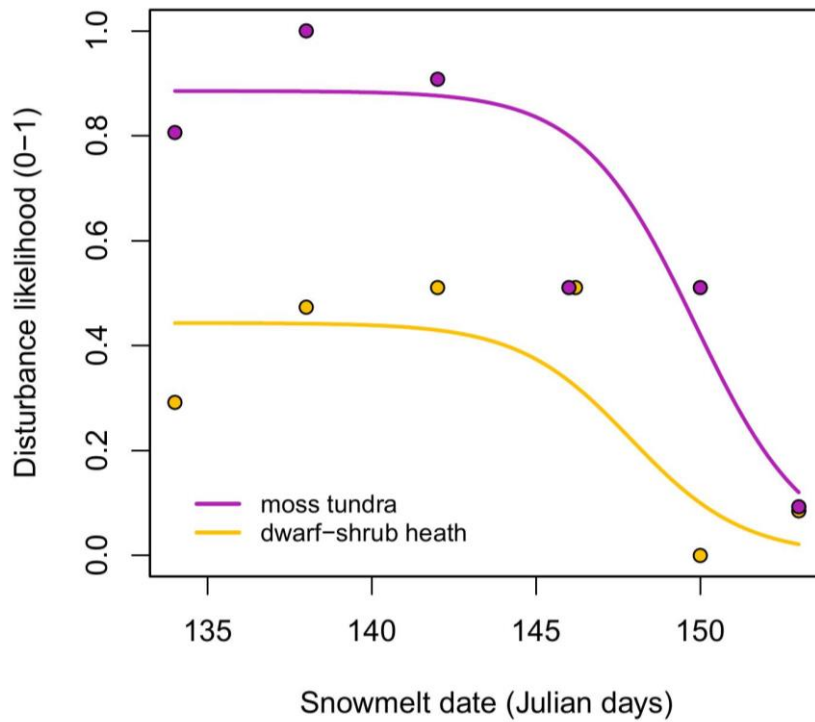
670



671

672 Figure 6: Manly's habitat selection ratios (w_i) and 95% confidence interval (CI) for pink-
 673 footed goose in the pre-breeding season (May-June 2019) in Adventdalen valley (Svalbard).
 674 Habitats are defined by vegetation class (moss tundra and dwarf shrub heath) and snowmelt
 675 date (Julian date: 134 -153). Positive selection (preference) is indicated by $CI > 1$, and
 676 negative selection (avoidance) is indicated by $CI < 1$. Habitat selection at a) fine-scale (5 cm
 677 resolution), based on predictors derived from drone images and goose GPS telemetry data, b)
 678 valley-scale (10 m resolution), based on predictors derived from satellite images and goose
 679 GPS telemetry data, c) valley-scale (10 m resolution), based on predictors derived from
 680 satellite images and field-based observations.

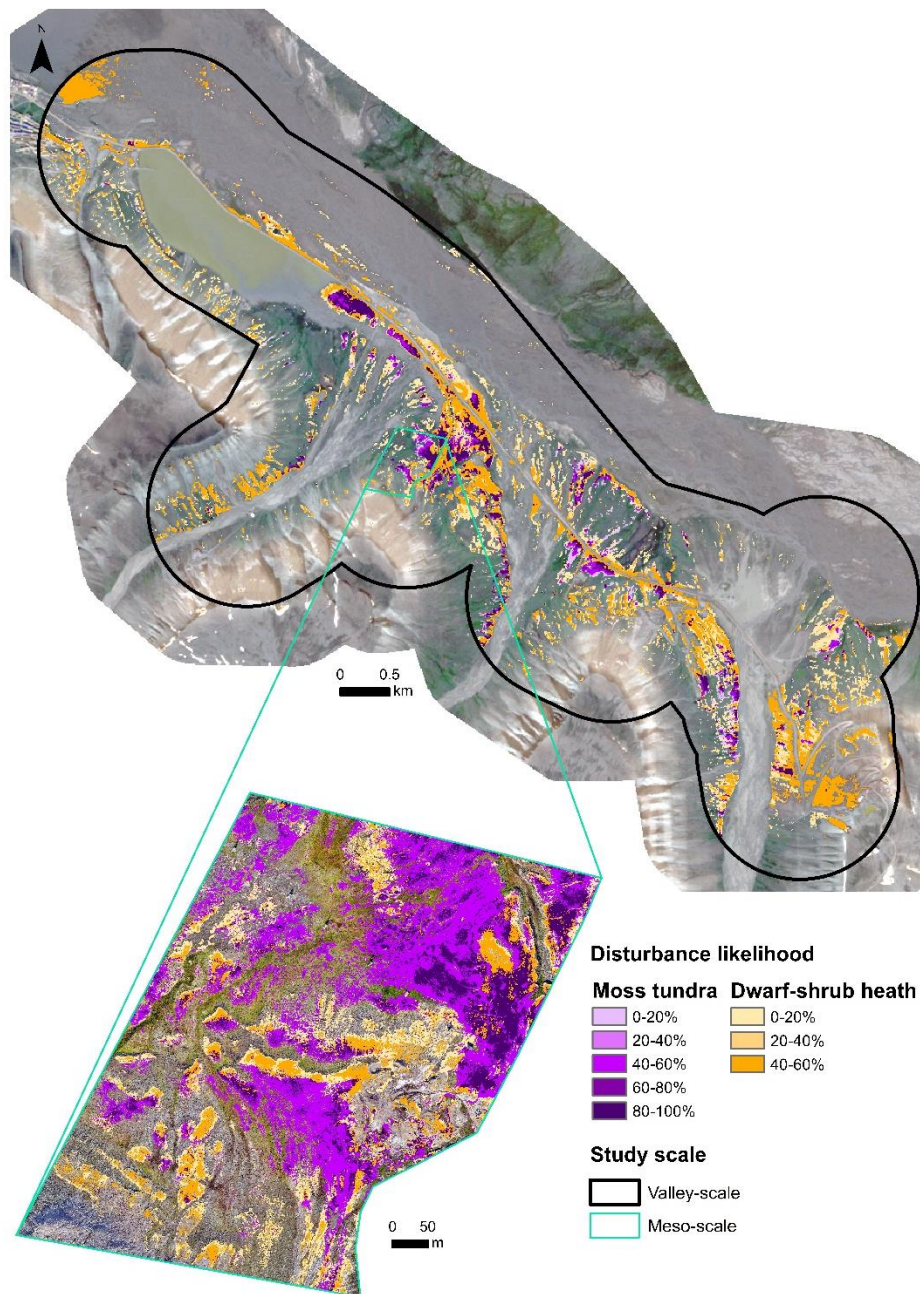
681



682

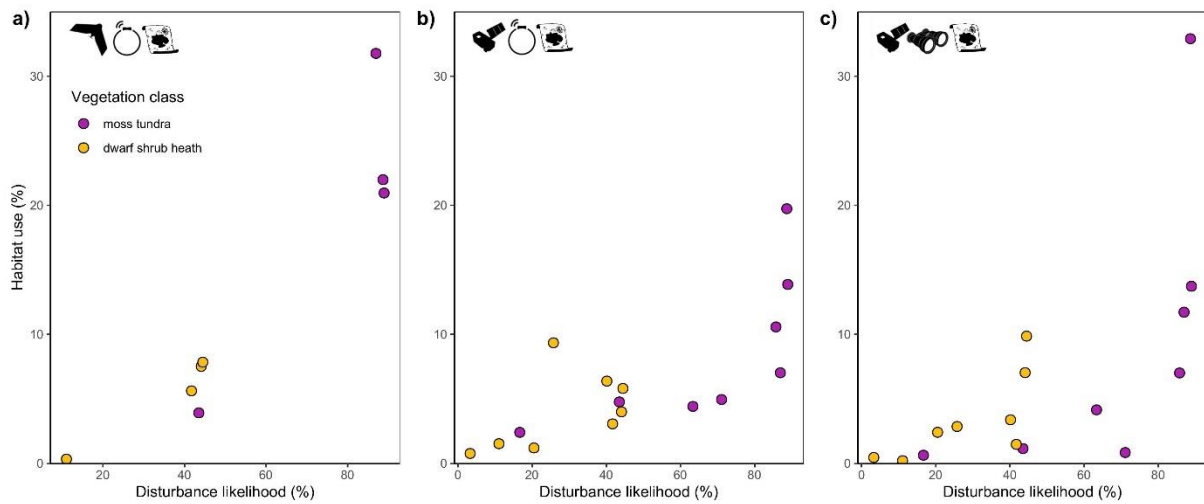
683 Figure 7: Field assessment (dots) and predicted (lines) vegetation disturbance likelihood,
 684 based on logistic regression model, in moss tundra and dwarf-shrub heath vegetation in
 685 Adventdalen valley, Svalbard as response to snowmelt (indicated by Julian day) between 14
 686 May and 03 June.

687



688

689 Figure 8: Pink-footed goose vegetation disturbance likelihood predictions, based on the
 690 logistic model (see Figure 7) and field surveys of snowmelt date and vegetation disturbance
 691 for moss tundra and dwarf-shrub heath vegetation at the fine-scale and valley-scale study
 692 areas site in Adventdalen valley (Svalbard) in May-June 2019.



693
 694 Figure 9: Pink-footed goose proportional habitat selection use and predicted disturbance
 695 likelihood during pink-footed goose pre-breeding season (May-June 2019) in Adventdalen
 696 valley (Svalbard). Habitat use and vegetation disturbance measured at a) fine-scale (5 cm
 697 resolution), based on predictors derived from drone images and GPS telemetry data, b) valley-
 698 scale (10 m resolution), based on predictors derived from satellite images and GPS telemetry
 699 data, c) valley-scale (10 m resolution), based on predictors derived from satellite images an
 700 field-based observations.

701

702

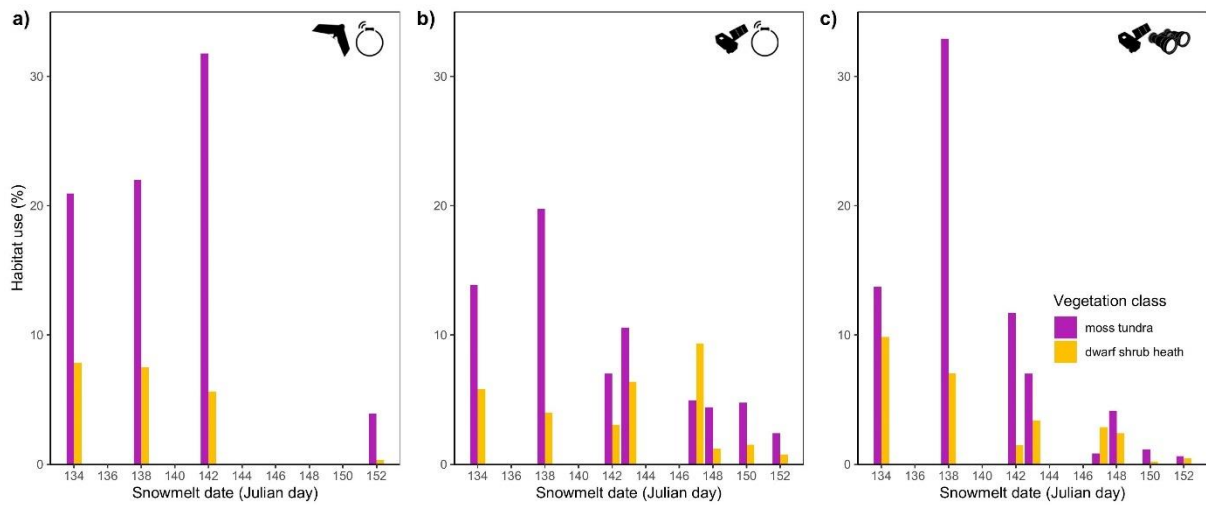
scale	observation	vegetation class	rho
fine-scale	GPS telemetry	all	0.88
fine-scale	GPS telemetry	moss tundra	0.20
fine-scale	GPS telemetry	dwarf-shrub heath	1.00
valley-scale	GPS telemetry	all	0.79
valley-scale	GPS telemetry	moss tundra	0.93
valley-scale	GPS telemetry	dwarf-shrub heath	0.60
valley-scale	field observation	all	0.81
valley-scale	field observation	moss tundra	0.90
valley-scale	field observation	dwarf-shrub heath	0.83

703

704 Table 1: Spearman rank correlation coefficients of pink-footed goose proportional habitat
705 selection use and predicted vegetation disturbance likelihood during pink-footed goose pre-
706 breeding season (May-June 2019) in Adventdalen valley (Svalbard). Habitat use and
707 vegetation disturbance measured at fine-scale (5 cm resolution), based on GPS telemetry data
708 and predictors derived from drone images, and valley-scale (10 m resolution), based on GPS
709 telemetry data or field observations and predictors derived from satellite images.

710

711



713
 714 Figure S1: Proportional habitat use (out of 100%) by pink-footed geese during pre-breeding
 715 season (May-June 2019) in Adventdalen valley (Svalbard). Habitat use at a) fine-scale (5 cm
 716 resolution), based on predictors derived from drone images and GPS telemetry data, b) valley-
 717 scale (10 m resolution), based on predictors derived from satellite images GPS telemetry data,
 718 c) valley-scale (10 m resolution), based on predictors derived from satellite images field-
 719 based observations.
 720

721 10. References

- 722 Abraham, K. F., R. L. Jefferies, and R. T. Alisauskas. 2005. The dynamics of landscape
723 change and snow geese in mid-continent north america. *Global Change Biology* 11:841–855.
724
- 725 Alisauskas, R. 2009. Goose populations of the western palearctic. A review of status and
726 distribution. *The Auk* 117:271–272.
727
- 728 Anderson, H. B., T. G. Godfrey, S. J. Woodin, and R. van der Wal. 2012. Finding food in a
729 highly seasonal landscape: Where and how pink footed geese *anser brachyrhynchus* forage
730 during the arctic spring. *Journal of Avian Biology* 43:415–422.
731
- 732 Anderson, H. B., C. E. Hübner, J. D. M. Speed, J. Madsen, and R. van der Wal. 2015. Biding
733 time before breeding: Flexible use of the arctic landscape by migratory geese during spring.
734 *Polar Research* 34.
735
- 736 Anderson, H. B., J. D. M. Speed, J. Madsen, Å. Ø. Pedersen, I. M. Tombre, and R. van der
737 Wal. 2016. Late snow melt moderates herbivore disturbance of the arctic tundra. *Écoscience*
738 23:29–39.
739
- 740 Assmann, J. J., I. H. Myers-Smith, J. T. Kerby, A. M. Cunliffe, and G. N. Daskalova. 2020.
741 Drone data reveal heterogeneity in tundra greenness and phenology not captured by satellites.
742 *Environmental Research Letters* 15:125002.
743
- 744 Barnas, A., B. Darby, G. Vandeberg, R. Rockwell, and S. Ellis-Felege. 2019. A comparison
745 of drone imagery and ground-based methods for estimating the extent of habitat destruction
746 by lesser snow geese (*anser caerulescens caerulescens*) in la pérouse bay. *PLOS ONE*
747 14:e0217049.
748
- 749 Bintanja, R. 2018. The impact of arctic warming on increased rainfall. *Scientific Reports* 8.
750
- 751 Bokhorst, S., S. Pedersen, L. Brucker, O. Anisimov, J. Bjerke, R. Brown, D. Ehrich, R.
752 Essery, A. Heilig, S. Ingvander, C. Johansson, M. Johansson, I. Jónsdóttir, N. Inga, K.
753 Luojus, G. Macelloni, H. Mariash, D. McLennan, G. Rosqvist, and T. Callaghan. 2016.
754 Changing arctic snow cover: A review of recent developments and assessment of future needs
755 for observations, modelling, and impacts. *Ambio* 45.
756
- 757 Breiman, L., J. Friedman, C. J. Stone, and R. A. Olshen. 1984. Classification and regression
758 trees. CRC press.
759
- 760 Calenge, C. 2006. The package adehabitat for the r software: Tool for the analysis of space
761 and habitat use by animals. *Ecological Modelling* 197:1035.
762
- 763 Clausen, K., K. Schreven, and J. Madsen. 2020. Effects of capture and marking on the
764 behaviour of moulting pink-footed geese *anser brachyrhynchus* on svalbard. *Wildfowl* 70:13–
765 29.
766
- 767 Cortez, P. 2020. Rminer: Data mining classification and regression methods.
768

769 Cubero-Castan, M., K. Schneider-Zapp, M. Bellomo, D. Shi, M. Rehak, and C. Strecha. 2018.
770 Assessment of the radiometric accuracy in a target less work flow using Pix4D software.
771 Pages 1–4 2018 9th workshop on hyperspectral image and signal processing: Evolution in
772 remote sensing (WHISPERS).
773

774 Dash, J. P., G. D. Pearse, and M. S. Watt. 2018. UAV multispectral imagery can complement
775 satellite data for monitoring forest health. *Remote Sensing* 10.
776

777 Descamps, S., J. Aars, E. Fuglei, K. M. Kovacs, C. Lydersen, O. Pavlova, Å. Ø. Pedersen, V.
778 Ravolainen, and H. Strøm. 2017. Climate change impacts on wildlife in a high arctic
779 archipelago–svalbard, norway. *Global Change Biology* 23:490–502.
780

781 Doiron, M., G. Gauthier, and E. Lévesque. 2015. Trophic mismatch and its effects on the
782 growth of young in an arctic herbivore. *Global Change Biology* 21:4364–4376.
783

784 Duriez, O., S. Bauer, A. Destin, J. Madsen, B. A. Nolet, R. A. Stillman, and M. Klaassen.
785 2009. What decision rules might pink-footed geese use to depart on migration? An individual-
786 based model. *Behavioral Ecology* 20:560–569.
787

788 Eischeid, I., E. M. Soininen, J. J. Assmann, R. A. Ims, J. Madsen, Å. Ø. Pedersen, F. Pirotti,
789 N. G. Yoccoz, and V. T. Ravolainen. 2021. Disturbance mapping in arctic tundra improved by
790 a planning workflow for drone studies: Advancing tools for future ecosystem monitoring.
791 *Remote Sensing* 13.
792

793 Elvebakk, A. 1994. A survey of plant associations and alliances from svalbard. *Journal of*
794 *Vegetation Science* 5:791–802.
795

796 Elvebakk, A. 2005. A vegetation map of svalbard on the scale 1:3.5 mill. *Phytocoenologia*
797 35:951–967.
798

799 Forbes, B. C., J. J. Ebersole, and B. Strandberg. 2001. Anthropogenic disturbance and patch
800 dynamics in circumpolar arctic ecosystems. *Conservation Biology* 15:954–969.
801

802 Fox, A. D., and E. Bergersen. 2005. Lack of competition between barnacle geese *branta*
803 *leucopsis* and pink-footed geese *anser brachyrhynchus* during the pre-breeding period in
804 svalbard. *Journal of Avian Biology* 36:173–178.
805

806 Fox, A. D., B. S. Ebbinge, C. Mitchell, T. Heinicke, T. Aarvak, K. Colhoun, P. Clausen, S.
807 Dereliev, S. Faragó, K. Koffijberg, H. Kruckenberg, M. J. J. E. Loonen, J. Madsen, J. Mooij,
808 P. Musil, L. Nilsson, S. Pihl, and H. van der Jeugd. 2010. Current estimates of goose
809 population sizes in western europe, a gap analysis and an assessment of trends. *Ornis Svecica*
810 20:115–127.
811

812 Fox, A. D., I. S. Francis, and E. Bergersen. 2006. Diet and habitat use of svalbard pink-footed
813 geese *anser brachyrhynchus* during arrival and pre-breeding periods in adventdalen. *Ardea*
814 94:691–699.
815

816 Fox, A. D., J. O. Leafloor, and others. 2018. A global audit of the status and trends of arctic
817 and northern hemisphere goose populations.
818

819 Fox, A., R. Hearn, L. Cao, P. Cong, X. Wang, Y. Zhang, S. Dou, X. Shao, M. Barter, and E.
820 Rees. 2008. Preliminary observations of diurnal feeding patterns of swan geese *anser*
821 *cygnoides* using two different habitats at shengjin lake, anhui province, china. *Wildfowl*
822 58:20–30.

823
824 Gauthier, G., J. Bêty, M.-C. Cadieux, P. Legagneux, M. Doiron, C. Chevallier, S. Lai, A.
825 Tarroux, and D. Berteaux. 2013. Long-term monitoring at multiple trophic levels suggests
826 heterogeneity in responses to climate change in the canadian arctic tundra. *Philosophical*
827 *Transactions of the Royal Society B: Biological Sciences* 368:20120482.

828
829 Gauthier, G., J.-F. Giroux, A. Reed, A. Béchet, and L. Bélanger. 2005. Interactions between
830 land use, habitat use, and population increase in greater snow geese: What are the
831 consequences for natural wetlands? *Global Change Biology* 11:856–868.

832
833 Gils, J. A. van, A. Gyimesi, and Bart. van Lith. 2007. AVIAN HERBIVORY: AN
834 EXPERIMENT, a FIELD TEST, AND AN ALLOMETRIC COMPARISON WITH
835 MAMMALS. *Ecology* 88:2926–2935.

836
837 Glahder, C., C. Hübner, J. Madsen, and I. Tombre. 2006. Pre-nesting site use of satellite
838 transmitter tagged svalbard pink-footed geese *anser brachyrhynchus*. *Ardea* 94.

839 Hastings, A., J. E. Byers, J. A. Crooks, K. Cuddington, C. G. Jones, J. G. Lambrinos, T. S.
840 Talley, and W. G. Wilson. 2007. Ecosystem engineering in space and time. *Ecology Letters*
841 10:153–164.

842
843 Heldbjerg, H., F. Johnson, K. Koffijberg, R. McKenzie, S. Nagy, G. Jensen, J. Madsen, and J.
844 Baveco. 2021. EGMP population status and assessment report. 6th meeting of the AEWA
845 european goose management international working group.

846
847 Holbrook, J. D., L. E. Olson, N. J. DeCesare, M. Hebblewhite, J. R. Squires, and R.
848 Steenweg. 2019. Functional responses in habitat selection: Clarifying hypotheses and
849 interpretations. *Ecological Applications* 29:e01852.

850
851 Hübner, C. E., I. M. Tombre, L. R. Griffin, M. J. Loonen, P. Shimmings, and I. S. Jónsdóttir.
852 2010. The connectivity of spring stopover sites for geese heading to arctic breeding grounds.
853 *Ardea* 98:145–154.

854 Ims, R. A., and E. Fuglei. 2005. Trophic Interaction Cycles in Tundra Ecosystems and the
855 Impact of Climate Change. *BioScience* 55:311–322.

856
857 Ims, R. A., and N. G. Yoccoz. 2017. Ecosystem-based monitoring in the age of rapid climate
858 change and new technologies. *Current Opinion in Environmental Sustainability* 29:170–176.

859
860 Ims, R. I., U. Jepsen J., A. Stien, and N. G. Yoccoz. 2013. Science plan for COAT: Climate-
861 ecological observatory for arctic tundra. Fram Centre, Norway.

862
863 IPCC - M., M., S. M., C. S., D. C., E. A., H. A., K. G., M. A., M.-T. J., M. M. M. C., O. G., P.
864 H., and S. E. A. G. 2019. Polar regions. Pages 203–320 in H.-O. Pörtner, D. C. Roberts, V.
865 Masson-Delmotte, P. Zhai, M. Tignor, E. Poloczanska, K. Mintenbeck, A. Alegría, M.
866 Nicolai, A. Okem, J. Petzold, B. Rama, and N. M. Weyer, editors. *The ocean and cryosphere*
867 *in a changing climate. A special report of the intergovernmental panel on climate change.*
868 Book Section, IPCC, Geneva.

869 Jefferies, R. L., R. F. Rockwell, and K. F. Abraham. 2003. The embarrassment of riches:
870 Agricultural food subsidies, high goose numbers, and loss of arctic wetlands – a continuing
871 saga. *Environmental Reviews* 11:193–232.

872

873 Jensen, G., J. Madsen, F. Johnson, and M. Tamstorf. 2014. Snow conditions as an estimator
874 of the breeding output in high-arctic pink-footed geese *anser brachyrhynchus*. *Polar Biology*
875 37.

876

877 John, C., D. Miller, and E. Post. 2020. Regional variation in green-up timing along a caribou
878 migratory corridor: Spatial associations with snowmelt and temperature. *Arctic, Antarctic,
879 and Alpine Research* 52:416–423.

880

881 Jones, C., J. Lawton, and M. Schachak. 1994. Organisms as ecosystem engineers. *Oikos* 69:
882 373–386. *Oikos* 69:373–386.

883

884 Kerbes, R. H., P. M. Kotanen, and R. L. Jefferies. 1990. Destruction of wetland habitats by
885 lesser snow geese: A keystone species on the west coast of hudson bay. *Journal of Applied
886 Ecology* 27:242–258.

887

888 Kölzsch, A., S. Bauer, R. de Boer, L. Griffin, D. Cabot, K.-M. Exo, H. P. van der Jeugd, and
889 B. A. Nolet. 2015. Forecasting spring from afar? Timing of migration and predictability of
890 phenology along different migration routes of an avian herbivore. *Journal of Animal Ecology*
891 84:272–283.

892

893 Lameris, T. K., I. Scholten, S. Bauer, M. M. P. Cobben, B. J. Ens, and B. A. Nolet. 2017.
894 Potential for an arctic-breeding migratory bird to adjust spring migration phenology to arctic
895 amplification. *Global Change Biology* 23:4058–4067.

896

897 Lawrimore, J., R. Ray, S. Applequist, B. Korzeniewski, and M. Menne. 2021. Global
898 summary of the month (GSOM), version 1. NOAA National Centers for Environmental
899 Information.

900

901 Madsen, J., M. Tamstorf, M. Klaassen, N. Eide, C. Glahder, F. Rigét, H. Nyegaard, and F.
902 Cottaar. 2007. Effects of snow cover on timing and success of reproduction in high-arctic
903 pink-footed geese *anser brachyrhynchus*. *Polar Biology* 30:1363–1372.

904

905 Mangewa, L. J., P. A. Ndakidemi, and L. K. Munishi. 2019. Integrating UAV technology in
906 an ecological monitoring system for community wildlife management areas in tanzania.
907 *Sustainability* 11.

908

909 Manly, B., L. McDonald, D. L. Thomas, T. L. McDonald, and W. P. Erickson. 2002.
910 *Resource selection by animals: Statistical design and analysis for field studies*. Springer
911 Science & Business Media.

912

913 Masný, M., K. Weis, and M. Biskupič. 2021. Application of fixed-wing UAV-based
914 photogrammetry data for snow depth mapping in alpine conditions. *Drones* 5.

915

916 Miranda, V., P. Pina, S. Heleno, G. Vieira, C. Mora, and C. E.G.R. Schaefer. 2020.
917 *Monitoring recent changes of vegetation in fildes peninsula (king george island, antarctica)*

918 through satellite imagery guided by UAV surveys. *Science of The Total Environment*
919 704:135295.

920

921 Mysterud, A., and R. A. Ims. 1998. Functional responses in habitat use: Availability
922 influences relative use in trade-off situations. *Ecology* 79:1435–1441.

923

924 Mysterud, A., and B.-E. Sæther. 2011. Climate change and implications for the future
925 distribution and management of ungulates in europe. Pages 349–375 in R. Putman, M.
926 Apollonio, and R. Andersen, editors. *Ungulate management in europe: Problems and*
927 *practices*. Cambridge University Press.

928

929 Niedzielski, T., W. Spallek, and M. Witek-Kasprzak. 2018. Automated snow extent mapping
930 based on orthophoto images from unmanned aerial vehicles. *Pure and Applied Geophysics*
931 175:3285–3302.

932

933 Nolet, B. A., V. A. Andreev, P. Clausen, M. J. M. Poot, and E. G. J. Wessel. 2001.
934 Significance of the white sea as a stopover for bewick’s swans *cygnus columbianus bewickii*
935 in spring. *Ibis* 143:63–71.

936

937 Pedersen, Å. Ø., I. Tombre, J. U. Jepsen, P. B. Eidesen, E. Fuglei, and A. Stien. 2013a.
938 Spatial patterns of goose grubbing suggest elevated grubbing in dry habitats linked to early
939 snowmelt. *Polar Research* 32:19719.

940

941 Pedersen, Åshild Ønvik, J. D. M. Speed, and I. M. Tombre. 2013b. Prevalence of pink-footed
942 goose grubbing in the arctic tundra increases with population expansion. *Polar Biology*
943 36:1569–1575.

944

945 Peterson, S. L., R. F. Rockwell, C. R. Witte, and D. N. Koons. 2013. The legacy of
946 destructive snow goose foraging on supratidal marsh habitat in the hudson bay lowlands.
947 *Arctic, Antarctic, and Alpine Research* 45:575–583.

948

949 Peth, S., and R. Horn. 2006. Consequences of grazing on soil physical and mechanical
950 properties in forest and tundra environments. Pages 217–243 *Reindeer management in*
951 *northernmost europe*. Springer.

952 Petit Bon, M., H. Böhner, K. A. BrÅthen, V. T. Ravolainen, and I. S. Jónsdóttir. 2021.
953 Variable responses of carbon and nitrogen contents in vegetation and soil to herbivory and
954 warming in high-arctic tundra. *Ecosphere* 12:e03746.

955

956 Pix4Dmapper. 2021. Pix4D SA. www.pix4d.com

957 Post, E., and M. C. Forchhammer. 2002. Synchronization of animal population dynamics by
958 large-scale climate. *Nature* 420:168–171.

959

960 Post, E., M. C. Forchhammer, M. S. Bret-Harte, T. V. Callaghan, T. R. Christensen, B.
961 Elberling, A. D. Fox, O. Gilg, D. S. Hik, T. T. Høye, R. A. Ims, E. Jeppesen, D. R. Klein, J.
962 Madsen, A. D. McGuire, S. Rysgaard, D. E. Schindler, I. Stirling, M. P. Tamstorf, N. J. C.
963 Tyler, R. van der Wal, J. Welker, P. A. Wookey, N. M. Schmidt, and P. Aastrup. 2009.
964 Ecological dynamics across the arctic associated with recent climate change. *Science*
965 325:1355–1358.

966

967 Ravolainen, V., E. M. Soininen, I. S. Jónsdóttir, I. Eischeid, M. Forchhammer, R. van der
968 Wal, and Å. Ø. Pedersen. 2020. High arctic ecosystem states: Conceptual models of
969 vegetation change to guide long-term monitoring and research. *Ambio* 49:666–677.
970

971 Ritz, C., F. Baty, J. C. Streibig, and D. Gerhard. 2015. Dose-response analysis using r. *PLOS*
972 *ONE* 10.
973

974 Rixen, C., T. T. Høye, P. Macek, R. Aerts, J. Alatalo, J. Andeson, P. Arnold, I. C. Barrio, J.
975 Bjerke, M. P. Björkman, D. Blok, G. Blume-Werry, J. Boike, S. Bokhorst, M. Carbognani, C.
976 Christiansen, P. Convey, E. J. Cooper, J. H. C. Cornelissen, S. Coulson, E. Dorrepaal, B.
977 Elberling, S. Elmendorf, C. Elphinstone, T. G. W. Forte, E. R. Frei, S. Geange, F. Gehrman,
978 C. Gibson, P. Grogan, A. Halbritter Rechsteiner, J. Harte, G. H. R. Henry, D. Inouye, R.
979 Irwin, G. Jespersen, I. S. Jónsdóttir, J. Y. Jung, D. Klinges, G. Kudo, J. Lämsä, H. Lee, J.
980 Lembrechts, S. Lett, J. S. Lynn, H. M. Mann, M. Mastepanov, J. Morse, I. Myers-Smith, J.
981 Olofsson, R. Paavola, A. Petraglia, G. Phoenix, P. Semenchuk, M. Siewert, R. Slatyer, M.
982 Spasojevic, K. Suding, P. Sullivan, K. Thompson, M. Väisänen, V. Vandvik, S. Venn, J.
983 Walz, R. Way, J. Welker, S. Wipf, and S. Zong. 2002. Winters are changing: Snow effects on
984 arctic and alpine tundra ecosystems. *Arctic Science Just_IN:AS-2020-0058*.
985

986 Schirmer, M., and J. W. Pomeroy. 2020. Processes governing snow ablation in alpine terrain –
987 detailed measurements from the canadian rockies. *Hydrology and Earth System Sciences*
988 24:143–157.
989

990 Schreven, K., C. Stolz, J. Madsen, and B. Nolet. 2021. Nesting attempts and success of arctic-
991 breeding geese can be derived with high precision from accelerometry and GPS-tracking.
992 *Animal Biotelemetry* 9.
993

994 Schweiger, A., M. Schuetz, P. Anderwald, M. Schaepman, M. Kneubuehler, R. Haller, and A.
995 Risch. 2015. Foraging ecology of three sympatric ungulate species – behavioural and resource
996 maps indicate differences between chamois, ibex and red deer. *Movement Ecology* 3:6.
997

998 Siewert, M., and J. Olofsson. 2021. UAV reveals substantial but heterogeneous effects of
999 herbivores on arctic vegetation. *Scientific Reports* 11.
1000

1001 Smit, C., and R. Putman. 2011. Large herbivores as “environmental engineers”. Pages 260–
1002 283 in R. Putman, M. Apollonio, and R. Andersen, editors. *Ungulate management in europe:*
1003 *Problems and practices*. Cambridge University Press.
1004

1005 Speed, J. D. M., E. J. Cooper, I. S. Jónsdóttir, R. Van Der Wal, and S. J. Woodin. 2010a.
1006 Plant community properties predict vegetation resilience to herbivore disturbance in the
1007 arctic. *Journal of Ecology* 98:1002–1013.
1008

1009 Speed, J. D. M., S. J. Woodin, H. Tømmervik, M. P. Tamstorf, and R. van der Wal. 2009.
1010 Predicting habitat utilization and extent of ecosystem disturbance by an increasing herbivore
1011 population. *Ecosystems* 12:349–359.
1012

1013 Speed, J., S. Woodin, H. Tømmervik, and R. van der Wal. 2010b. Extrapolating herbivore-
1014 induced carbon loss across an arctic landscape. *Polar Biology* 33:789–797.
1015

1016 Stark, D. J., I. P. Vaughan, L. J. Evans, H. Kler, and B. Goossens. 2018. Combining drones
1017 and satellite tracking as an effective tool for informing policy change in riparian habitats: A
1018 proboscis monkey case study. *Remote Sensing in Ecology and Conservation* 4:44–52.

1019 Stark, S., and D. Grellmann. 2002. Soil microbial responses to herbivory in an arctic tundra
1020 heath at two levels of nutrient availability. *Ecology* 83:2736–2744.

1021

1022 Thomas, D. L., and E. J. Taylor. 2006. Study designs and tests for comparing resource use
1023 and availability II. *The Journal of Wildlife Management* 70:324–336.

1024

1025 Tuomi, M., M. Väisänen, H. Yläne, F. Q. Brearley, I. C. Barrio, K. Anne Bråthen, I.
1026 Eischeid, B. C. Forbes, I. S. Jónsdóttir, A. L. Kolstad, and others. 2021. Stomping in silence:
1027 Conceptualizing trampling effects on soils in polar tundra. *Functional Ecology* 35:306–317.

1028

1029 Tveraa, T., A. Stien, B.-J. Bårdsen, and P. Fauchald. 2013. Population densities, vegetation
1030 green-up, and plant productivity: Impacts on reproductive success and juvenile body mass in
1031 reindeer. *PloS one* 8:e56450.

1032

1033 Wal, R. van der. 2006. Do herbivores cause habitat degradation or vegetation state transition?
1034 Evidence from the tundra. *Oikos* 114:177–186.

1035

1036 Wal, R. van der, H. Anderson, A. Stien, L. E. Loe, and J. Speed. 2020. Disturbance, recovery
1037 and tundra vegetation change final report project 17/92 -to svalbard environmental protection
1038 fund. Svalbard Environmental Protection Fund.

1039

1040 Wilby, A., M. Shachak, and B. Boeken. 2001. Integration of ecosystem engineering and
1041 trophic effects of herbivores. *Oikos* 92:436–444.

1042

1043 Wisz, M., M. Tamstorf, J. Madsen, and M. Jespersen. 2008. Where might the western
1044 svalbard tundra be vulnerable to pink-footed goose (*anser brachyrhynchus*) population
1045 expansion? Clues from species distribution models. *Diversity and Distributions* 14:26–37.

1046

1047 Zheng, B., and A. Agresti. 2000. Summarizing the predictive power of a generalized linear
1048 model. *Statistics in medicine* 19:1771–1781.

Paper IV

MACHINE LEARNING FOR CLASSIFICATION OF AN ERODING SCARP SURFACE USING TERRESTRIAL PHOTOGRAMMETRY WITH NIR AND RGB IMAGERY

H. Bernsteiner¹, N. Brožová², I. Eischeid³, A. Hamer⁴, S. Haselberger⁵, M. Huber⁶, A. Kollert⁷, T. M. Vandyk⁸, F. Pirotti⁹

¹ University of Bayreuth, Chair of Geomorphology, 95447 Bayreuth, Germany - Heidemarie.Bernsteiner@uni-bayreuth.de

² WSL Institute for Snow and Avalanche Research SLF, Flüelastrasse 11, 7260 Davos Dorf, Switzerland - natalie.brozova@slf.ch

³ Department of Arctic and Marine Biology, UiT The Arctic University of Norway, 9037 Tromsø, Norwegian Polar Institute, Fram Center, Hjalmar Johansens gate 14, 9007 Tromsø, Norway, Aarhus University, Department of Bioscience, Denmark - isabell.eischeid@uit.no

⁴ University of Manchester, Geography, School of Environment Education & Development, Manchester M13 9PL, UK - alexandra.hamer@manchester.ac.uk

⁵ University of Vienna, Institute of Geography and Regional Research, 1010 Vienna, Austria. stefan.haselberger@univie.ac.at

⁶ Centre de Recherches Pétrographiques et Géo-chimiques, 15 rue Notre Dame des Pauvres, 54500 Vandœuvre les Nancy, France - marius.huber@univ-lorraine.fr

⁷ Institute for Interdisciplinary Mountain Research, Austrian Academy of Sciences, Technikerstr. 21a, 6020 Innsbruck, Austria - andreas.kollert@oew.ac.at

⁸ Department of Geography, Royal Holloway University of London, Egham, Surrey, TW200EX, UK - thomas.vandyk.17@ucl.ac.uk

⁹ CIRGEO Interdepartmental Research Center in Geomatics, TeSAF Department, University of Padova, 35020 Legnaro (PD), Italy - francesco.pirotti@unipd.it

Commission III, III/10

KEY WORDS: Terrestrial Photogrammetry, Structure from Motion, Surface Classification, Machine Learning, High Mountain Environment

ABSTRACT:

Increasingly advanced and affordable close-range sensing techniques are employed by an ever-broadening range of users, with varying competence and experience. In this context a method was tested that uses photogrammetry and classification by machine learning to divide a point cloud into different surface type classes. The study site is a peat scarp 20 metres long in the actively eroding river bank of the Rotmoos valley near Obergurgl, Austria. Imagery from near-infra red (NIR) and conventional (RGB) sensors, georeferenced with coordinates of targets surveyed with a total station, was used to create a point cloud using structure from motion and dense image matching. NIR and RGB information were merged into a single point cloud and 18 geometric features were extracted using three different radii (0.02 m, 0.05 m and 0.1 m) totalling 58 variables on which to apply the machine learning classification. Segments representing six classes, dry grass, green grass, peat, rock, snow and target, were extracted from the point cloud and split into a training set and a testing set. A Random Forest machine learning model was trained using machine learning packages in the R-CRAN environment. The overall classification accuracy and Kappa Index were 98% and 97% respectively. Rock, snow and target classes had the highest producer and user accuracies. Dry and green grass had the highest omission (1.9% and 5.6% respectively) and commission errors (3.3% and 3.4% respectively). Analysis of feature importance revealed that the spectral descriptors (NIR, R, G, B) were by far the most important determinants followed by verticality at 0.1 m radius.

1. INTRODUCTION

In the past decades a step change in close range remote sensing technologies has allowed techniques such as photogrammetry to be employed by an increasingly diverse range of users, not only the specialist (Eltner et al., 2016; Westoby et al., 2012). The inevitable result of this proliferation has been an abundance of high-quality data for which automated processes of classification have become a practical necessity (Grilli et al., 2017), since manual labelling and classification are cost- and time-demanding and unfeasible for large datasets. In this context, at the 2019 Innsbruck Summer School, Obergurgl (Rutzinger et al., 2018, 2016), a team of researchers applied machine learning (ML) to a point cloud derived from dense image matching of a terrestrial photogrammetric survey. This came as part of a larger survey in a mountain environment with also a remotely piloted aircraft system (RPAS) over the whole valley (Scaioni et al., 2018). Near infrared and RGB information was collected from both RPAS and terrestrial surveys, as previous literature has largely proven

that any vegetation component can validly be labelled with spectral features (Alba et al., 2011).

The fields of interest of the participants comprise a diversity of applications that can benefit from close-range sensing: from primary colonisation of recently deglaciated ground, through slope stability and evolution, to the surveying and interpretation of rarely preserved 700-million-year-old landforms. These users represent some of the numerous examples that may benefit from common data manipulation techniques, allowing statistical data to be derived from classifications within point cloud data.

Within this study the aim was to i) classify relevant surface types within a small section of a mountain valley floor, ii) compare the efficacy of optical and geometric properties in distinguishing between key surface types and finally iii) to evaluate photogrammetric methods and machine learning approaches with respect to the group members' research interests.

A terrestrial photogrammetry survey was undertaken on a partially snow-covered river bank comprising peat, loose soil, rock and vegetation and these different components were each assigned a class. Point cloud segments representative of each were used for training a machine learning model, subsequently used to classify areas within the entire point cloud with a degree of reliability.

2. STUDY SITE

The study area is located at the main alpine divide of the Austrian Alps at the border between the State of Tyrol (Austria) and the Province of South Tyrol (Italy). The Rotmoos valley ($46^{\circ} 50' 24''$ N, $11^{\circ} 01' 59''$ E) extends c. 6 km from SE to NW and covers an area of c. 1 km² with an altitudinal range from c. 2240 m to c. 3400 m. The area is characterised by an inner alpine climate and surrounded and protected by mountains. The nearby weather station (Obergurgl, 1938 m) shows a low mean annual precipitation of c. 819 mm, with maxima from June to August. Mean annual air temperature is + 2.2 °C, with the highest monthly means of around + 16 °C in July and the lowest mean of -8.3 °C in February (data period 1971-2000; ZAMG - Austria's national weather service 2018).

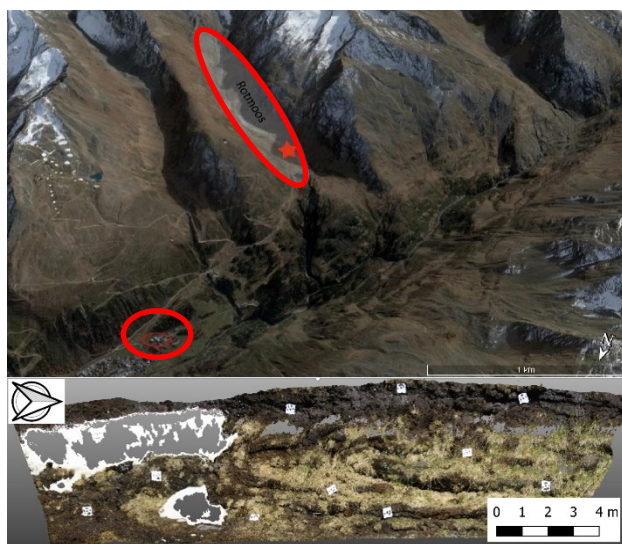
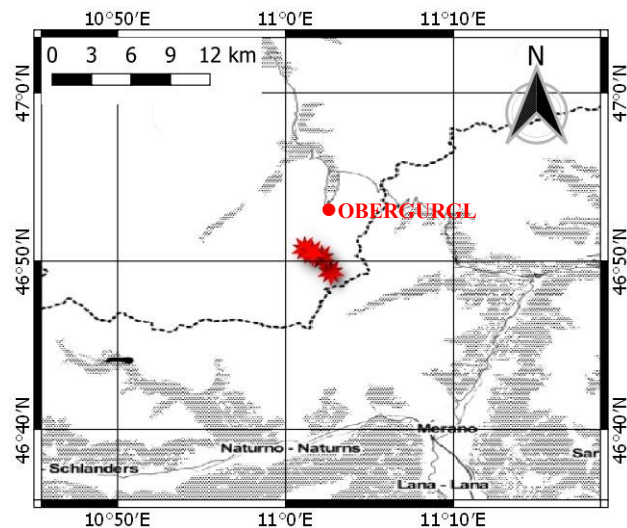


Figure 1. Location of study area (red star) and Obergurgl (circle on middle image). The bottom image shows a close-up of the erosion feature surveyed for this study.

During the last glacial, the valley was shaped by glacial erosion through multiple advances of the Rotmoos glacier. The last glaciation of the valley floor was during the Younger Dryas period. After the retreat of the Younger Dryas glacier, the valley was filled with up to 40 m of sediment (Patzelt, 1995) and remained ice free during the last re-advance of the Rotmoos glacier during the Little Ice age. The attributed prominent terminal moraine complex is located c. 1 km up valley from the study site. In the distal and central part of the valley, a peat bog developed that covers an area of c. 800 by 120 m. The peat deposits are up to 2.65 m thick and radiocarbon dates from the base and top of the peat are c. 5994 and 1629 years before present respectively (Bortenschlager, 2010). Today, the peat bog is dissected and eroded by the river Rotmoosache, a tributary of the river Ötztaler Ache. A c. 20 m stretch of its bank is the object of this study (for location see Figure 1, red star). The study section comprises steep peat faces, which are highly water saturated and partly covered by snow and vegetation (Figure 1 bottom).

3. METHODS

Data acquisition was planned together with a team that acquired UAV imagery. Three of their ground control points (GCPs) were measured with differential GNSS (Global Navigation Satellite System) in order to georeference the final product in a projected coordinate system. A control measurement between points revealed sub-centimetre accuracy of the GCPs. In the study area for this investigation eleven GCPs were placed on the eroding scarp (Figure 1 bottom) and georeferenced using a total station positioned on one of the measured UAV GCPs.

Terrestrial photogrammetry was used to survey the eroding scarp surface. Images were acquired using a consumer-grade RGB camera Canon EOS 450D (27mm) and a NIKON D-200 with HOYA R72 filter, modified to operate in the Near-Infrared region (NIR) of the electromagnetic spectrum (750 – 1,500 nm). The modification allowed the CCD sensor to record reflected radiation above 720 nm. As shown in Figure 2, the natural sensitivity of the CCD sensor includes wavelengths up to 950 nm, but these are filtered out by the camera filter. By removing this filter and adopting an external filter, NIR information can be recorded in the image.

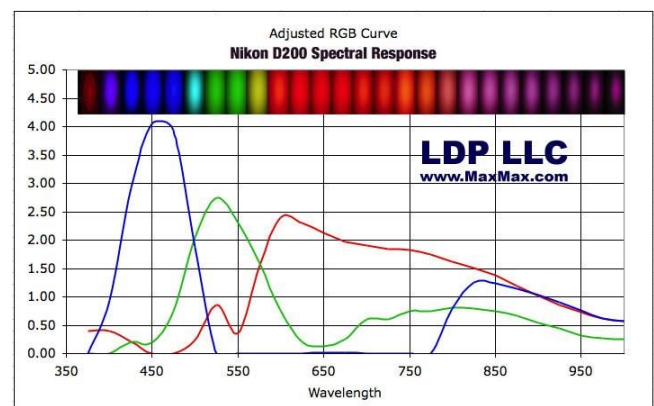


Figure 2. CCD sensitivity of Nikon D200.

3.1 Pre-processing

In total 24 images were imported to Agisoft Metashape (AM). The GCPs were automatically detected and located by the

software. The coordinates of the GCPs that were measured using the total station in the field, were loaded into AM. After camera alignment, dense image matching was performed in order to obtain a dense point cloud. The same workflow was applied to the NIR imagery acquired with the modified camera.

The point clouds from the RGB and NIR imagery were imported to CloudCompare software. First, NIR information was merged to the RGB point cloud using three nearest neighbours. The software finds, for each point in the RGB cloud, the three closest points in the NIR cloud, and appends the average from the three NIR values to the RGB point. Additionally, 18 geometric features were calculated within CloudCompare (see Table 1). A description on the computation of the eigenvalue and vector based features is given by Hackel et al. (2016).

1. Roughness	2. Mean curvature
3. Gaussian curvature	4. Normal change rate
5. Number of neighbours	6. Surface density
7. Volume density	8. Eigenvalues sum
9. Omnivariance	10. Eigenentropy
11. Anisotropy	12. Planarity
13. Linearity	14. PCA1
15. PCA2	16. Surface variation
17. Sphericity	18. Verticality

Table 1. List of geometric features calculated from the point cloud.

The geometric features are calculated by considering a number of neighbours. In CloudCompare the neighbours are identified using a user-defined radius. In this work three radii were tested: 0.02 m, 0.05 m and 0.1 m. Respectively each distance had the following number of neighbouring points – average (standard deviation): 4.8(3.1), 12(8), 24.12(16). The final cloud had ~2.16 million points. The final cloud was exported as a text file with information on the coordinates (x, y, z), RGB and NIR values and the 18 geometric features for each radius. The final feature count was therefore 54 geometric features and four spectral features (NIR, R, G, B), for a total of 58 descriptive features that can be used for classification. Further analysis was carried out using the statistical software R and R Studio.

3.2 Classification

The final cloud was imported in a text file format as a table (data.frame) in R 3.6 (R Core Team, 2018). A random forest classifier was used as previous tests have shown positive results (Pirotti et al., 2016; Pirotti and Tonion, 2019) and initial tests run on the data of this study supported the use of this classifier. This choice is however debatable as many factors must be taken into consideration and the issue is expanded upon in the Discussion Section. For the random forest model, the number of trees in the ensemble was set to 200 and the number of variables to split a node was set to 16, after tuning the model trying a grid of 6x6 reasonable values of number of trees and number of variables. Six surface classes were defined, *dry grass*, *green grass*, *peat*, *rock*, *snow* and *target* (Table 2). This last class is represented by the 11 black and white targets used for GCPs.

For classification with machine learning (ML), manually labelled (classified) points were used for training and testing. Manual labelling was a crucial task. For this study, subsets for each of the six classes were extracted from the original point cloud by manually clipping regions with points having a defined unique class. Table 2 shows that the number of labelled points per class is quite balanced, except for the “rock” class. The rock class is under-represented in the study area, as the surveyed area is

mostly covered with grass, peat or snow. It was nevertheless included as it does represent a class of its own and cannot be reasonably merged in the other classes.






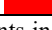
ID	Class	N. Points	
1	dry grass	10932	
2	green grass	6494	
3	peat	13344	
4	rock	1621	
5	snow	5476	
6	target	12198	

Table 2. List of classes with number of points in the labelled subset and colour related to Figure 4.

The labelled point set was further split into training (50%) and testing (50%) subsets. Random Forest was used to create a classification model based on the training data. The efficacy of each variable in creating the model was reported as Mean Decrease Accuracy (MDA). To assess accuracy of the model, the points in the test dataset were classified and the predicted classes compared to the labelled classes using a confusion matrix and accuracy metrics. Finally, the fitted Random Forest model was used to classify the entire point cloud, to generate a labelled 3D model of the study area (Figure 4).

4. RESULTS

The machine learning approach provided a very high overall classification accuracy of 98% across all classes, with a Kappa index of 97%. These figures are related to the independent testing dataset. Predictor accuracy was highest for the following classes: target, peat and snow, followed by rock and dry vegetation. Green and dry vegetation had both highest commission and omission errors, thus showing a likely mutual misclassification. Accuracy was high for snow, rock, peat and targets (> 98%). However, when dividing vegetation into dry and green, the observer's accuracy drops to below 98.1% and 94.4% respectively (Table 3).

	1	2	3	4	5	6	Σ	
1	4183	72	4	1	0	2	4262	1.9%
2	132	2384	9	0	0	0	2525	5.6%
3	5	11	5119	0	0	4	5139	0.4%
4	0	0	0	633	0	0	633	0.0%
5	0	0	0	0	2139	2	2141	0.1%
6	6	1	6	0	9	4806	4828	0.5%
Σ	4326	2468	5138	634	2148	4814	19528	
	3.3%	3.4%	0.4%	0.2%	0.4%	0.1%		

Table 3. Confusion matrix: columns=IDs of predicted classes, rows=IDs of real classes, commission errors (red) and omission errors (green) for each class. Class names are listed in Table 2.

Feature importance over the whole classification process was also analysed (Figure 3). Figure 3 revealed that spectral descriptors were the most influential in classification. Within these, NIR ranked highest followed by red and then overall RGB. The next most-important non-spectral descriptor was the verticality at 0.1 m radius.

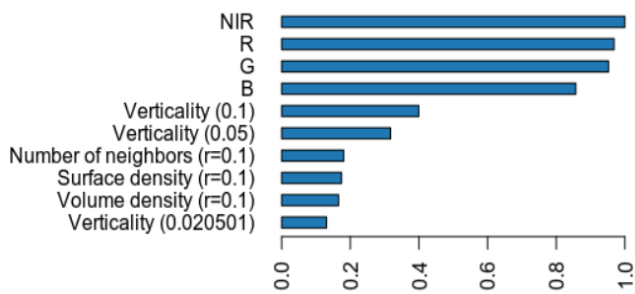


Figure 3. Overall variable importance of first ten most important features.

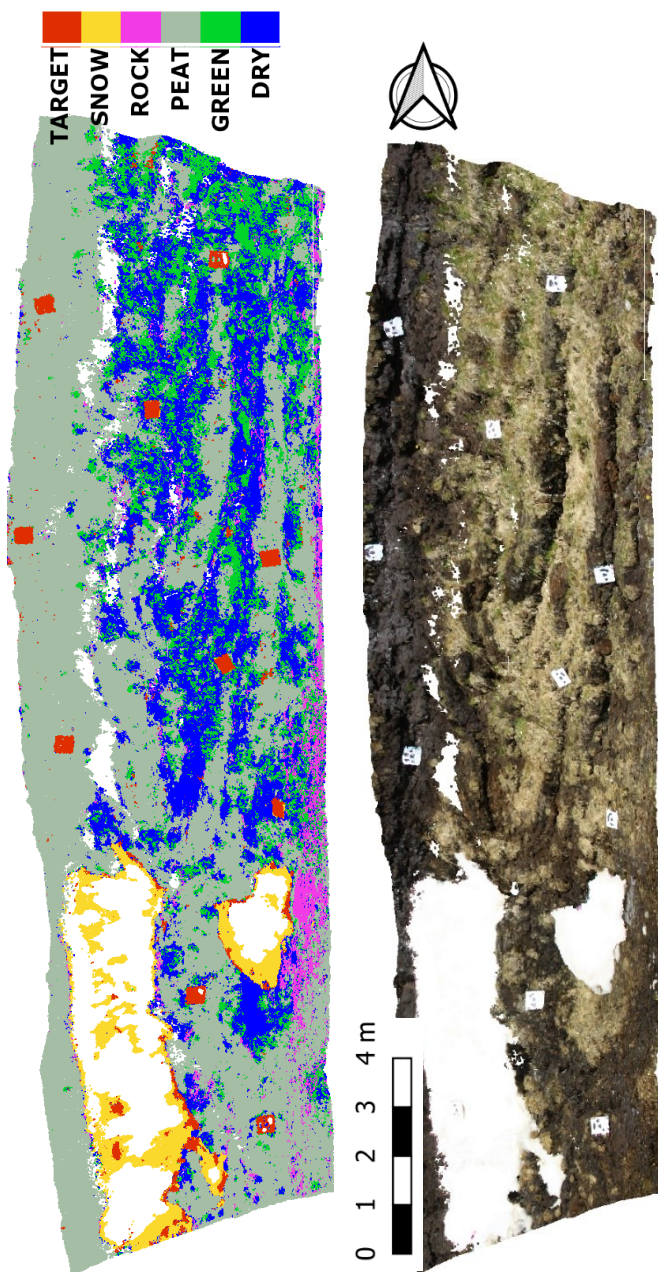


Figure 4. Classified results over the full point cloud (left) and RGB point cloud (right).

Looking at importance of each feature for class scale (Table 4) shows that verticality at the highest radius size (0.1 m) was particularly important for the “target” and “green grass” classes, along with point density features (features 5, 6 and 7 - i.e. number of neighbours, surface and volume density – see Table 1). Surface variation (16) and sphericity (17) at 0.1 m showed a moderate, but relatively constant importance over all classes.

Feature	dry		green		rock	snow	target
	grass	grass	peat	grass			
R	1,00	0,85	1,00	0,87	0,97	1,00	1,00
G	1,00	0,83	1,00	0,89	0,97	1,00	1,00
B	0,98	0,87	1,00	0,95	0,87	0,98	0,98
NIR	1,00	0,92	0,91	0,81	1,00	1,00	1,00
1 (0.05)	0,59	0,59	0,67	0,59	0,59	0,57	0,57
2 (0.05)	0,60	0,60	0,64	0,60	0,60	0,58	0,58
3 (0.05)	0,65	0,65	0,76	0,65	0,65	0,59	0,59
4 (0.05)	0,69	0,69	0,82	0,69	0,69	0,62	0,62
5 (0.05)	0,60	0,83	0,82	0,60	0,60	0,83	0,83
6 (0.05)	0,60	0,83	0,82	0,60	0,60	0,83	0,83
7 (0.05)	0,60	0,83	0,82	0,60	0,60	0,83	0,83
8 (0.05)	0,51	0,54	0,52	0,51	0,51	0,54	0,54
9 (0.05)	0,58	0,58	0,81	0,64	0,58	0,54	0,54
10 (0.05)	0,51	0,54	0,51	0,52	0,52	0,54	0,54
11 (0.05)	0,70	0,70	0,83	0,70	0,70	0,62	0,62
12 (0.05)	0,59	0,59	0,59	0,59	0,59	0,59	0,59
13 (0.05)	0,54	0,59	0,54	0,56	0,54	0,59	0,59
14 (0.05)	0,54	0,57	0,60	0,54	0,54	0,57	0,57
15 (0.05)	0,58	0,59	0,58	0,58	0,58	0,59	0,59
16 (0.05)	0,69	0,69	0,82	0,69	0,69	0,62	0,62
17 (0.05)	0,70	0,70	0,83	0,70	0,70	0,62	0,62
18 (0.05)	0,82	0,94	0,77	0,70	0,71	0,94	0,94
1 (0.02)	0,53	0,53	0,64	0,56	0,53	0,53	0,53
2 (0.02)	0,58	0,58	0,72	0,58	0,58	0,55	0,55
3 (0.02)	0,59	0,59	0,70	0,59	0,59	0,56	0,56
4 (0.02)	0,58	0,58	0,81	0,63	0,58	0,55	0,55
5 (0.02)	0,55	0,82	0,74	0,55	0,55	0,82	0,82
6 (0.02)	0,55	0,82	0,74	0,55	0,55	0,82	0,82
7 (0.02)	0,55	0,82	0,74	0,55	0,55	0,82	0,82
8 (0.02)	0,51	0,54	0,52	0,51	0,51	0,54	0,54
9 (0.02)	0,58	0,58	0,81	0,64	0,58	0,54	0,54
10 (0.02)	0,51	0,54	0,51	0,52	0,52	0,54	0,54
11 (0.02)	0,58	0,58	0,82	0,63	0,58	0,54	0,54
12 (0.02)	0,62	0,66	0,52	0,52	0,61	0,66	0,66
13 (0.02)	0,61	0,65	0,56	0,51	0,62	0,65	0,65
14 (0.02)	0,60	0,60	0,60	0,53	0,62	0,60	0,60
15 (0.02)	0,62	0,66	0,53	0,51	0,61	0,66	0,66
16 (0.02)	0,58	0,58	0,81	0,63	0,58	0,55	0,55
17 (0.02)	0,58	0,58	0,82	0,63	0,58	0,54	0,54
18 (0.02)	0,76	0,87	0,75	0,66	0,65	0,87	0,87
1 (0.1)	0,62	0,62	0,62	0,62	0,62	0,60	0,60
2 (0.1)	0,63	0,61	0,61	0,61	0,61	0,63	0,63
3 (0.1)	0,69	0,71	0,69	0,69	0,69	0,71	0,71
4 (0.1)	0,77	0,77	0,80	0,77	0,77	0,70	0,70
5 (0.1)	0,67	0,92	0,89	0,67	0,67	0,92	0,92
6 (0.1)	0,67	0,92	0,89	0,67	0,67	0,92	0,92
7 (0.1)	0,67	0,92	0,89	0,67	0,67	0,92	0,92
8 (0.1)	0,54	0,57	0,54	0,60	0,56	0,57	0,57
9 (0.1)	0,76	0,76	0,80	0,76	0,76	0,71	0,71
10 (0.1)	0,57	0,60	0,55	0,59	0,56	0,60	0,60
11 (0.1)	0,77	0,77	0,80	0,77	0,77	0,71	0,71
12 (0.1)	0,57	0,57	0,57	0,60	0,57	0,57	0,57
13 (0.1)	0,53	0,54	0,52	0,62	0,53	0,54	0,54
14 (0.1)	0,63	0,60	0,60	0,64	0,60	0,63	0,63
15 (0.1)	0,56	0,57	0,56	0,60	0,56	0,57	0,57
16 (0.1)	0,77	0,77	0,80	0,77	0,77	0,70	0,70
17 (0.1)	0,77	0,77	0,80	0,77	0,77	0,71	0,71
18 (0.1)	0,85	0,98	0,80	0,73	0,79	0,98	0,98

Table 4. Variable importance for each class and feature. Numbers in first column are related to Table 1, values in parenthesis in first column is radius for neighbourhood definition.

5. DISCUSSION

The primary objective of this investigation was to test the performance of a well-known machine learning algorithm, Random Forest, for classification of point clouds from a terrestrial photogrammetric survey. The following discussion will focus on the strengths and weaknesses of the techniques applied and their resulting outputs, allowing suggestions for future improvements. Moreover, consideration will be given to the replicability of the method used herein, to address the respective research questions of other fields of research.

5.1 Effectiveness of methods and outputs

Visual comparison of the classified point cloud and original images immediately reveals a striking qualitative similarity, (Figure 4) which is supported by the confusion matrix and the Kappa index of agreement and other accuracy metrics which have high values. It must be noted that the accuracy metrics are calculated over an independent set, but still over a small number of points, i.e. ~50 thousand labelled points from a total of a point cloud with ~2 million points (~2.5%). The points have been chosen from across the dataset, to avoid spatial autocorrelation (see Figure 5), and further splitting into training and testing datasets have been done with stratified random sampling (strata according to classes), thus keeping independency, but still training and testing data are limited to a small dataset. This implies that classification accuracy metrics can be very high, but not necessarily reflect the performance over all the area. A visual analysis from the classified set (Figure 4) shows that some points of snow patches are erroneously classified as targets. This is probably due to similarity in colour (white target and white snow) and in shape of the object, as a snow patch around a 10 cm radius will appear close to flat, just like a target. Since colour and verticality are the most important features (Figure 3), a similarity in these features will result in class mixing.

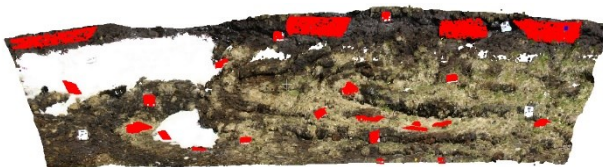


Figure 5. Red points represent labelled points used for training on the whole dataset.

Moreover, there is a lack of point cloud data within the snow patches (Figure 4); a more quantitative approach reveals that, whereas discrimination between rock, snow, soil and vegetation was reliable, the distinction between wet and dry vegetation was more problematic (Table 3).

The weakness discriminating between the two classes of vegetation (green and dry vegetation) is likely due to the gradational boundaries between the two classes, where one blends into the other. This is exacerbated by their physical proximity, as they do not occur in discrete areas of dry and wet vegetation. In any case this distinction between wet and dry is somewhat arbitrary, using qualitative colour choices within the image for the selection of training data. Future workers should consider the ground truthing of wet and dry areas by touch or using a more quantitative approach with moisture detection equipment.

The lack of data cloud points within the snow areas results from the high snow albedo in contrast to the relatively dark remainder of the images, resulting in over-exposure of the former. This

could be overcome by multiple images from the same position using different exposure settings (i.e. ISO, shutter speed, F-stop), or by using a camera with greater bit depth. The former is potentially labour intensive if images require merging by hand before construction of the point cloud, whereas the latter solution is limited by the available camera. Other options might be taking images in the RAW format and using post-processing in order to fix the over-exposed spots or using a polarizing filter, which increases contrasts and the overall colour saturation. These solutions may however be equally labour or cost intensive and have their limitations.

5.2 Descriptors

The importance of NIR and red descriptors suggests that the Normalized Difference Vegetation Index (NDVI) could be used as a proxy for changes along the eroding riverbank. Although generally much less important than spectral features, verticality was the highest non-spectral descriptor and especially useful in dividing rocks from other classes.

5.2.1 Geometric descriptors: as seen in Table 4, verticality and density-based descriptors like surface and volume density and number of neighbours do have importance for the Random Forest method. It must be noted that correlation does not necessarily indicate causation and therefore importance might not be related to class-intrinsic information, but to a coincidental relationship. For example most targets were placed vertically thus verticality might support classification, yet this would not be useful in a scenario where targets were placed at different angles. An important rule is that machine learning and artificial intelligence in general work as well as the similarity to trained data. Care must be taken when applying a model trained with a dataset which has different characteristics than the dataset to be classified.

5.2.2 Neighbourhood size: The questions of ideal radius size and ideal number of neighbours are important when considering descriptors that use neighbours to describe shape and morphology (Pirotti and Tonion, 2019; Weinmann et al., 2015). The ideal method would involve finding the best number of neighbours for each point from a range by adopting a minimal entropy approach. Although effective this requires very intensive calculation as entropy has to be determined for a range of neighbours for each point. For this study therefore three radii were tested, instead of adopting the minimal entropy method. As a compromise, considering that a number of geometric features, including verticality, showed highest importance at the largest chosen radius, (0.1) the study could be extended to test if even larger radii could give better results.

5.3 Class definition

In general, the choice of classes within any point cloud will be guided by the research question at hand. However practical limitations of the data may restrict what can be distinguished by the machine learning process. With this in mind it is suggested that future work could attempt unsupervised classification of the point cloud data. On the one hand this may provide insights into the type of further classifications that could reliably be made and on the other it may reveal patterns that are not otherwise obvious. This would overcome a limitation of the technique employed herein. Specifically, spectral attributes (i.e. examination of the photographs) were used to select classes and training segments therefore it is unsurprising that spectral descriptors are the most influential.

5.4 Data acquisition

In terms of practicalities two potential obstacles were encountered, both relating to time. First the terrestrial photography of the survey team took place within the UAV flying area of another team, allowing our data to be placed into a broader context. However, both teams worked on the area at the same time, resulting in significant waiting time during which the area could not be accessed whilst imaged from the air. Improved coordination would significantly reduce time in the field improving efficiency. Second, although only a small area was imaged for terrestrial photogrammetry, it was time consuming in terms of processing time. Caution must be applied in similar surveys in determining the ideal scale for surveying the area of interest as a function of required detail and objects to be classified.

5.5 Future work

Several aspects can be further investigated. An interesting aspect is the impact of point density on results. As mentioned in the previous section, the processing time does impact significantly on the method. Depending on the study area size and types of classes it is very likely that there is an ideal density below which the classification accuracy drops unacceptably. Addressing this is relatively simple, as the method can be applied to gradually decimated point clouds. The presented workflow could also be preceded by a point cloud segmentation to enable an object-based classification. As outlined by Vosselman, (2013), this would allow for the computation of additional features such as shape, which could be well suited for discriminating targets from other classes. If rocks have a common morphological appearance in the study area due to their transport history, descriptors of size and shape could also improve the classification.

As outlined in Section, 5.2.1, the importance of some features is likely related to peculiarities of the research area. Therefore, future work should also assess the transferability of the proposed method. This could for example include alteration of class definitions, size of the research area and environmental characteristics. Additionally, the study design should be tested for robustness under different weather conditions. At the day of the study most surfaces were relatively dry. Moist weather could change the surfaces reflectance, making it harder to distinguish certain classes (for example dry and green vegetation or rocks and peat).

5.6 Relevance to the research interests

The potential applications of these methods are diverse, in terms of both scale and classification type. At the metre to ten-metre scale, classification techniques can distinguish categories of surface features upon boulders, to help elucidate their transport history. At the kilometre scale this method may be used to classify bedrock surfaces using UAV data, that may be host to subglacially striated areas. The advantage of machine learning in this approach is that these surfaces have distinct geomorphological characteristics, of roughness and curvature, but are often in remote areas. The resulting classification could allow targeting of the most likely areas for ground examination. Machine learning techniques based on the Random Forest algorithm are used to detect landslides and to assess landslide susceptibility maps for large regions e.g. Catani et al., 2013; Kim et al., 2018; Stumpf and Kerle, 2011; Taalab et al., 2018). In terms of monitoring and predicting landslide movements, these methods can be of great help for civil protection and risk mitigation.

Distinguishing between biotic and abiotic classes to better understand their relative influences on a recently deglaciated landscape could also be a target for a classification framework of point cloud data. Moreover, integration of the classification with spatial data can be used to investigate the relationship between primary succession and relief. More environmental applications can be distinguishing between healthy and damaged vegetation, for example due to icing events in Arctic tundra environments.

6. CONCLUSIONS

During the course of the Summer School the participants captured, constructed and merged geo-referenced point clouds that contained NIR and RGB data respectively and used these to train a machine learning process that segregated the merged cloud into six classes. The target, snow, rock and peat classes were reliable whereas distinguishing between wet and dry vegetation classes was more problematic, likely due to ambiguous training segments. Optical descriptors were far the most important attributes in classification, although, this is pre-determined by the selection of training areas based on visible light properties. Shape features from 3D points clouds bring some improvement over the overall classification results, and this can be further addressed including the laser scanning data (Pirotti, 2019) from the RPAS survey of the area. During data acquisition, processing and analyses each of the participants learned new skills and identified practical applications of those skills in their own study areas.

ACKNOWLEDGEMENTS

The study at hand was carried out during the Innsbruck Summer School of Alpine Research 2019 (Rutzinger et al., 2018, 2016). The coordinates of the ground control points for the UAV as well as the terrestrial targets were processed and provided by Prof. Marco Scaioni. The use of open source project R-CRAN and the software CloudCompare is acknowledged.

REFERENCES

- Alba, M., Barazzetti, L., Fabio, F., Scaioni, M., 2011. Filtering vegetation from terrestrial point clouds with low-cost near infrared cameras. *Ital. J. Remote Sens.* 55–75. <https://doi.org/10.5721/ItJRS20114325>
- Bortenschlager, S., 2010. Age determination of sediment core HASENM, Hasenmoos, Austria. <https://doi.org/10.1594/PANGAEA.740396>
- Catani, F., Lagomarsino, D., Segoni, S., Tofani, V., 2013. Landslide susceptibility estimation by random forests technique: Sensitivity and scaling issues. *Nat. Hazards Earth Syst. Sci.* <https://doi.org/10.5194/nhess-13-2815-2013>
- Eltner, A., Kaiser, A., Castillo, C., Rock, G., Neugirg, F., Abellán, A., 2016. Image-based surface reconstruction in geomorphometry-merits, limits and developments. *Earth Surf. Dyn.* <https://doi.org/10.5194/esurf-4-359-2016>
- Grilli, E., Menna, F., Remondino, F., Scanning, L., Scanner, L., 2017. A review of point clouds segmentation and classification algorithms. *Int. Arch. Photogramm. Remote Sens. Spat. Inf. Sci.*

- XLII, 1–3. <https://doi.org/10.5194/isprs-archives-XLII-2-W3-339-2017>
- Hackel, T., Wegner, J.D., Schindler, K., 2016. Fast Semantic Segmentation of 3D Point Clouds with Strongly Varying Density, in: ISPRS Annals of the Photogrammetry, Remote Sensing and Spatial Information Sciences. <https://doi.org/10.5194/isprs-annals-III-3-177-2016>
- Kim, J.C., Lee, Sunmin, Jung, H.S., Lee, Saro, 2018. Landslide susceptibility mapping using random forest and boosted tree models in Pyeong-Chang, Korea. *Geocarto Int.* <https://doi.org/10.1080/10106049.2017.1323964>
- Patzelt, G., 1995. The clay pit of Baumkirchen, in: *Quaternary Field Trips in Central Europe INQUA*. p. 394.
- Pirotti, F., 2019. Open software and standards in the realm of laser scanning technology. *Open Geospatial Data, Softw. Stand.* 4, 14. <https://doi.org/10.1186/s40965-019-0073-z>
- Pirotti, F., Sunar, F., Piragnolo, M., 2016. Benchmark of Machine Learning Methods for Classification of a Sentinel-2 Image. *ISPRS - Int. Arch. Photogramm. Remote Sens. Spat. Inf. Sci.* XLI-B7, 335–340. <https://doi.org/10.5194/isprs-archives-XLI-B7-335-2016>
- Pirotti, F., Tonion, F., 2019. Classification of Aerial Laser Scanning Point Clouds Using Machine Learning: A Comparison Between Random Forest and Tensorflow. *ISPRS - Int. Arch. Photogramm. Remote Sens. Spat. Inf. Sci.* XLII-2/W13, 1105–1111. <https://doi.org/10.5194/isprs-archives-XLII-2-W13-1105-2019>
- Rutzinger, M., Bremer, M., Höfle, B., Hämmerle, M., Lindenbergh, R., Oude Elberink, S., Pirotti, F., Scaioni, M., Wujanz, D., Zieher, T., 2018. Training in Innovative Technologies for Close-Range Sensing in Alpine Terrain. *ISPRS Ann. Photogramm. Remote Sens. Spat. Inf. Sci.* IV–2, 239–246. <https://doi.org/10.5194/isprs-annals-IV-2-239-2018>
- Rutzinger, M., Höfle, B., Lindenbergh, R., Oude Elberink, S., Pirotti, F., Sailer, R., Scaioni, M., Stötter, J., Wujanz, D., 2016. Close-Range Sensing Techniques in Alpine Terrain. *ISPRS Ann. Photogramm. Remote Sens. Spat. Inf. Sci.* III–6, 15–22. <https://doi.org/10.5194/isprs-annals-III-6-15-2016>
- Scaioni, M., Crippa, J., Corti, M., Barazzetti, L., Fugazza, D., Azzoni, R., Cernuschi, M., Diolaiuti, G.A., 2018. Technical aspects related to the application of SfM photogrammetry in high mountain. *ISPRS - Int. Arch. Photogramm. Remote Sens. Spat. Inf. Sci.* XLII–2, 1029–1036. <https://doi.org/10.5194/isprs-archives-XLII-2-1029-2018>
- Stumpf, A., Kerle, N., 2011. Combining Random Forests and object-oriented analysis for landslide mapping from very high resolution imagery, in: *Procedia Environmental Sciences*. <https://doi.org/10.1016/j.proenv.2011.02.022>
- Taalab, K., Cheng, T., Zhang, Y., 2018. Mapping landslide susceptibility and types using Random Forest. *Big Earth Data*. <https://doi.org/10.1080/20964471.2018.1472392>
- Vosselman, G., 2013. Point cloud segmentation for urban scene classification. *ISPRS - Int. Arch. Photogramm. Remote Sens. Spat. Inf. Sci.* XL-7/W2, 257–262. <https://doi.org/10.5194/isprsarchives-XL-7-W2-257-2013>
- Weinmann, M., Jutzi, B., Hinz, S., Mallet, C., 2015. Semantic point cloud interpretation based on optimal neighborhoods, relevant features and efficient classifiers. *ISPRS J. Photogramm. Remote Sens.* 105, 286–304. <https://doi.org/10.1016/j.isprsjprs.2015.01.016>
- Westoby, M.J., Brasington, J., Glasser, N.F., Hambrey, M.J., Reynolds, J.M., 2012. ‘Structure-from-Motion’ photogrammetry: A low-cost, effective tool for geoscience applications. *Geomorphology* 179, 300–314. <https://doi.org/10.1016/j.geomorph.2012.08.021>

